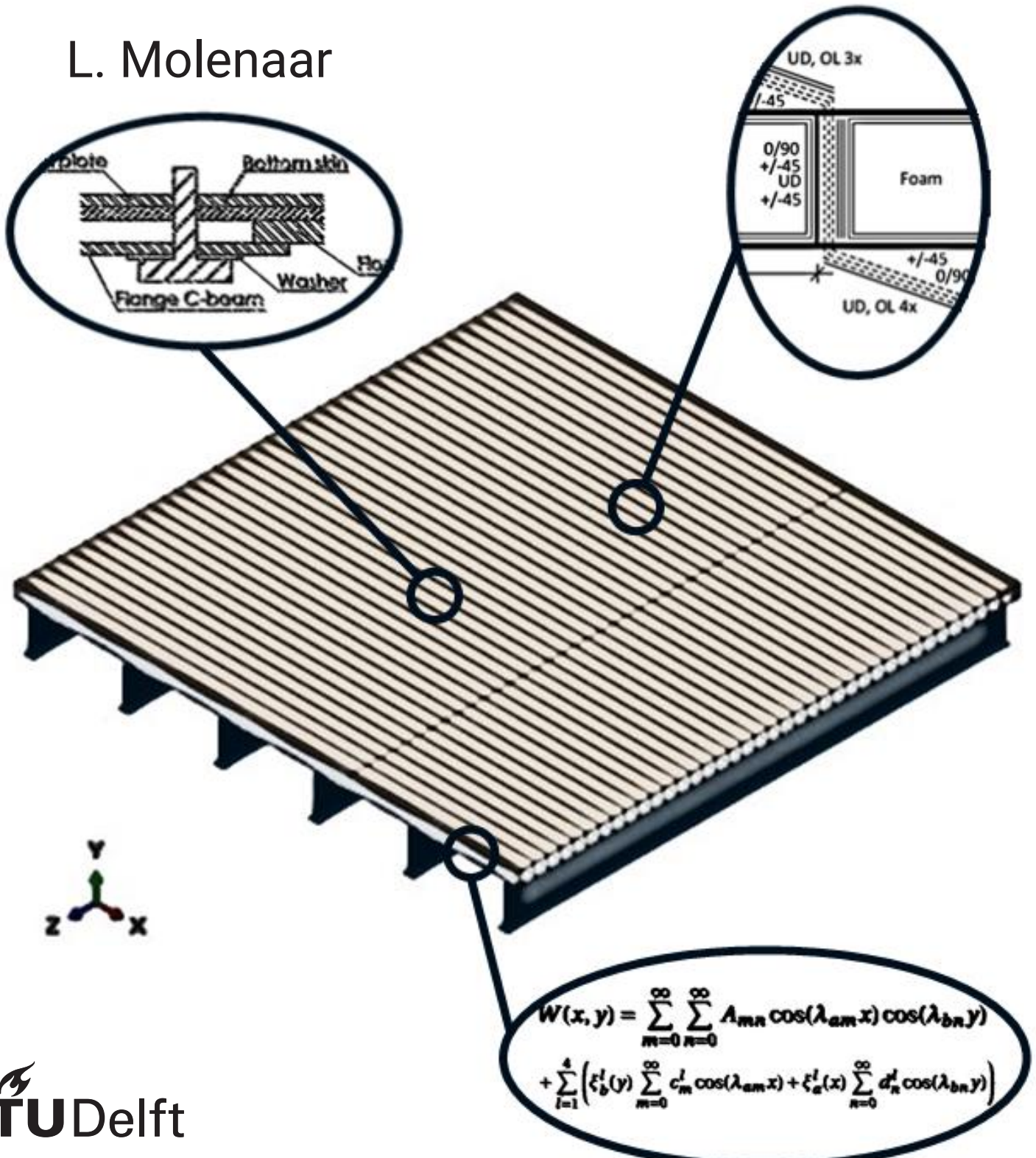# Design and optimization of FRP traffic decks considering uplift bolt forces

## Based on analytical and numerical approaches

## L. Molenaar

$$W(x,y) = \sum_{m=0}^{\infty} \sum_{n=0}^{\infty} A_{mn} \cos(\lambda_{am}x)\cos(\lambda_{bn}y)$$
$$+ \sum_{l=1}^{4}\left(\xi_b^l(y)\sum_{m=0}^{\infty} c_m^l \cos(\lambda_{am}x) + \xi_a^l(x)\sum_{n=0}^{\infty} d_n^l \cos(\lambda_{bn}y)\right)$$

**TU**Delft

# Design and optimization of FRP traffic decks considering uplift bolt forces

## Based on analytical and numerical approaches

by

# L. Molenaar

to obtain the degree of Master of Science
at the Delft University of Technology,
to be defended publicly on Thursday July 21, 2022 at 13:30.

| | | |
|---|---|---|
| Student number: | 4717880 | |
| Project duration: | November 18, 2021 – July 21, 2022 | |
| Thesis committee: | Dr. Ir. M. Pavlovic, | TU Delft, Chairman |
| | Ir. A. Christoforidou, | TU Delft |
| | Dr. Ir. A. A. Mehrotra, | TU Delft |
| | Ir. R. Grefhorst, | FiberCore Europe |
| | Ir. T. Sharma, | FiberCore Europe |

An electronic version of this thesis is available at `http://repository.tudelft.nl/`.

# Preface

Dear reader,

In front of you, you can find my graduation work. It was written to complete the Master of Structural Engineering at the Faculty of Civil Engineering and Geoscience at the Technical University of Delft and to obtain the degree of Master of Science. The research was carried out in collaboration with the company FiberCore Europe which is an international company specialized in fiber-reinforced polymer structures in the infra industry.

At the cover of the report, a fiber-reinforced bridge deck is shown. This model was used as a reference model during this research. In the image, several parts have been enlarged for which research has been performed. In the left ellipse, the considered connection is shown. For this type of connection, the uplift bolt forces were calculated. In the lower right ellipse, a formula is shown that was used to calculate the deformation of the deck. Lastly, the most optimal design found for the deck is shown in the upper right ellipse.

For the performed research, all steps are described in this report and the results are shown. However, not all data has been provided due to the property rights of the company, but this does not affect the traceability of the research. Enjoy reading the report and hopefully, it will contribute to (your) follow-up research.

*L. Molenaar*
*Delft, July 2022*

# Abstract

In the infra industry, FRP (Fiber Reinforced Polymer) is more and more used to produce (parts of) bridges. The company FiberCore Europe produces, among other things, relatively thin FRP traffic decks (slabs) which can be placed on an existing steel structure. In this way, the lifetime of an existing road bridge that is at the end of its lifespan can be extended. To be able to make their product competitive in the FRP market, the company wants to optimize and standardize the design of the bridge slabs. Before this optimization can be performed, more knowledge about the uplift forces in the connections between the FRP slabs and the supporting structure is needed since this will have an influence on the design.

Therefore, this graduation work is about which geometry of FRP slabs is the most optimal, in terms of costs, to use for a given load and boundary conditions taking the occurring uplift bolt forces into account. As a reference case, a detailed numerical model is used to represent reality since no experimental work is performed yet and tests cannot be performed within the scope of this thesis either. For the calculation of the uplift forces, it is assumed that the bolts can only take tension forces since shear studs are used to transfer the shear forces. The considered load models are limited to the first two load models from the Eurocode for bridge design (EN1991-2). Next to this, limits on the design are taken into account based on the experience of the company FiberCore Europe. For the calculations of the bolt forces, a reference project of the company is used.

The first part of the graduation work focuses on the calculation of the uplift forces in the bolted connections caused by the moving loads. For this, first a detailed numerical model, based on a Python script, is made in Abaqus. Using this python code to make the model, gives the opportunity to adapt the dimensions of the slab, the bolt pattern and the laminate layups. Based on this most detailed numerical model, different simplifications are made to make the calculations easier and less time-consuming. Numerical models with linear bolts instead of non-linear bolts and with load superposition using a one-wheel load instead of a complete vehicle are considered. Next to this, equivalent material properties are calculated to make a model with an orthotropic deck plate instead of modeled geometry of skins and webs. For the numerical model with this orthotropic deck, the same simplifications of linear bolts and/or load superposition are applied.

Next to the numerical models, different analytical models are considered. Beam models with and without springs and different plate models are made. All different numerical and analytical models made, are compared on possibilities, calculation and modeling time and accuracy. Based on the comparison between the models and the capacity of the connections, it is concluded that the uplift design of the bolted connections does not need to be taken into account in the optimization of the slabs.

The second part of the graduation work is about the optimization of the FRP slabs considering the global behavior of the deck, for which a genetic algorithm is used to detect the most optimal geometry. The most important parameters for the design are the height of the deck, the spacing of the webs and the layup of the topskin, bottomskin and webs. The layup of the different elements is dependent on the number of plies, the ply orientation and the overlapping length.

During the optimization process, design and initial (global) strength, stability and stiffness checks are performed. First, optimization is done for the same deck that is considered in part one of the research. Next to this case, different cases for the distance between the supports are considered for which standardization is done with respect to engineering and production of the slabs.

Based on the performed research it can be concluded that the uplift bolt forces are in a range of 0.5 to 5.5 $kN$ when calculated with numerical models and in a range of 8.5 to 21.5 $kN$ when calculated with analytical (beam) models. For analytical plate models, it is up till now not possible to calculate the bolt forces. Simplifications can be done by the use of an orthotropic deck with equivalent material properties. The maximum difference using this simplification is 2.9 kN while the calculation time needed is reduced by a factor of 4-5. Other simplifications that can be done are the use of linear bolts and/or load superposition. Using linear bolts gives a maximum difference of 0.5 kN and load superposition a maximum difference of 0.3 kN, both without an improvement of the calculation time. The optimal geometry for different boundary conditions is given as

a standard design with a variable number of plies for the topskin and a variable height based on intervals for the distance between the supports.

Based on the performed research it is recommended to calculate the bolt forces with a (detailed) numerical model. Since all other models are compared to this detailed model, it is needed to validate the model with experiments. For the optimization of the design of FRP bridge slabs, a genetic algorithm can be used for its effectiveness without taking the uplift design of the bolted connections into account. Optimization taking the global behavior into account is covered in this research. It is recommended to add checks for local bending of the topskin and local buckling of the webs in the procedure to cover the local behavior of the slabs as well.

# Acknowledgements

I would like to thank my committee for the guidance throughout my research. First of all, my main supervisor Dr. Marko Pavlovic, who guided me with his experience along the unfeasible options to the best result. He always asked critical questions so that I could look with the right critical view at my own work. I would like to thank Ir. Angeliki Christoforidou for her time and help with Abaqus and next to this, her never-ending enthusiasm which motivated me to go on. Furthermore, I want to thank Ir. Anjali Mehrotra for her help with the plate models in Python, although I, unfortunately, didn't manage to get it to work, and for her unbiased view on the project.

In addition to the university supervisors, I would like to thank my company supervisors. Ir. Ronald Grefhorst for setting up the project and his always creative ideas and Ir. Tushar Sharma for his weekly help in progress and arranging the necessary dates for the project. Next to my supervisors, I would also like to thank my colleagues from FiberCore Europe for the conversations we had from which I was able to get new ideas. I would like to thank two (former) colleagues in particular, Ir. Floris Zaaijer and Dr. Ir. Amin Hosseini, for their help with programming and formalizing the research.

I also would like to express my deepest gratitude to my family. My parents for their support throughout my whole study and next to them my sister and brother. I want to thank my friends for their encouragement and help with my thesis in particular but also during the rest of my study. And last but not least I want to thank Leonie for her never-ending encouragement and her support in my dream to become an engineer.

# Contents

# List of Symbols

**Roman upper case letters**

| | |
|---|---|
| $A$ | Area |
| $A$ | Stiffness matrix |
| $B$ | Stiffness matrix |
| $D$ | Stiffness matrix |
| $E$ | E-modulus |
| $EI$ | Bending stiffness |
| $F$ | Vertical point load |
| $F$ | Bolt force |
| $G$ | Shear modulus |
| $H$ | Horizontal point load |
| $I$ | Moment of inertia |
| $K$ | Correction factor |
| $L$ | Span of a plate or beam |
| $L_0$ | Span between two steel girders |
| $L_e$ | Buckling length |
| $L_y$ | With of the plate for local buckling |
| $M$ | Mass |
| $M$ | Moment |
| $N_{cr}$ | Buckling force |
| $P$ | Point load |
| $S$ | Shear strength |
| $W$ | Section modulus |
| $W_b$ | Coefficient for bending deformation |
| $W_s$ | Coefficient for shear deformation |
| $V$ | Shear force |
| $V$ | Volume |
| $Q$ | Costs |
| $Q$ | Wheel load |
| $X$ | Strength in the fiber direction |
| $Y$ | Strength in direction perpendicular to the fibers |

**Roman lower case letters**

| | |
|---|---|
| $a$ | Length of the slab |
| $a_{mn}$ | Coefficient for analytical solution |
| $b$ | Width of the slab |
| $c$ | Distance between the webs |
| $c_m$ | Coefficient of the analytical solution for boundary conditions |
| $d$ | Diameter of the bolt |
| $d_n$ | Coefficient of the analytical solution for boundary conditions |
| $e$ | Distance between the bolt and the edge of the plate |
| $f$ | Eigenfrequency |
| $f$ | Height of the slab |
| $f$ | Steel strength |
| $g$ | Gravity constant |
| $h$ | Height of slab |

| | |
|---|---|
| $k_e$ | Equivalent shear stiffness |
| $m$ | Number of sines and/or cosines involved in x direction |
| $m_b$ | Geometry factor for buckling |
| $n$ | Number of sines and/or cosines involved in y direction |
| $n$ | Number of webs/foam blocks |
| $np$ | Number of plies |
| $p$ | Distance between the webs |
| $p$ | Price |
| $q$ | Uniformly distributed load |
| $r$ | Radius of the bolts |
| $s$ | Coordinate along a line |
| $s$ | Speed |
| $t$ | Thickness of the laminate |
| $u$ | Deformation |
| $w$ | Deformation |
| $w$ | Web spacing |
| $w_b$ | Bending deformation |
| $w_s$ | Shear deformation |
| $x$ | Coordinate main direction |
| $y$ | Coordinate main direction |
| $z$ | Coordinate main direction |

**Greek letters**

| | |
|---|---|
| $\alpha$ | Angle |
| $\alpha_m$ | Ratio cosines and sines with different amplitude |
| $\overline{\alpha}_n$ | Ratio cosines and sines with different amplitude |
| $\overline{\overline{\alpha}}_n$ | Ratio cosines and sines with different amplitude |
| $\beta_n$ | Ratio cosines and sines with different amplitude |
| $\overline{\beta}_n$ | Ratio cosines and sines with different amplitude |
| $\overline{\overline{\beta}}_n$ | Ratio cosines and sines with different amplitude |
| $\gamma$ | Safety factor |
| $\Delta$ | Length of one cell |
| $\delta_A$ | Summation of work |
| $\eta$ | Ratio of the shear deformation |
| $\eta$ | Conversion factor |
| $\lambda$ | Slenderness factor |
| $\lambda_{am}$ | Amplitude of the analytical solution |
| $\lambda_{bn}$ | Amplitude of the analytical solution |
| $\nu$ | Poisson's ratio |
| $\xi_a$ | Function to correct solution for boundary conditions |
| $\xi_b$ | Function to correct solution for boundary conditions |
| $\rho$ | Density |
| $\sigma$ | Axial or bending stress |
| $\tau$ | Shear stress |
| $\phi$ | Rotation angle |
| $\omega$ | Frequency plate |

# List of Abbreviations & Definitions

**Abbreviations**

| | |
|---|---|
| ACO | Ant Colony Optimization |
| CLT | Classical Laminate Theory |
| DSA | Design Sensitivity Analysis |
| FCE | FiberCore Europe |
| FEA | Finite Element Analysis |
| FEM | Finite Element Method |
| FRP | Fiber Reinforced Polymer |
| FSDT | First-order Shear Deformation Theory |
| GA | Genetic Algorithm |
| GFRP | Glass Fiber Reinforced Polymer |
| HSDT | Higher-order Shear Deformation Theory |
| iSRR | injected Steel Reinforced Resin |
| LM1 | Load Model 1 |
| LM2 | Load Model 2 |
| LP | Linear Programming |
| LW | Layer Wise theory |
| MF | Matrix Frame |
| MRDO | Multi-objective Robust Design Optimization |
| NR | Newton-Rapshon |
| PL | Point Load |
| PSOA | Particle Swarm Optimization Algorithm |
| REDUCE | Reuse and Demountability using Steel Structures and the Circular Economy |
| RBDO | ReliaBilty Design Optimization |
| SA | Simulating Annealing method |
| UD | UniDirectional |
| UDL | Uniform Distributed Load |
| ZZT | Zig-Zag Theory |

**Definitions** [1]

| | |
|---|---|
| Analytical method | An analytical method is the framing of a problem in a well-understood form and the solving of the exact solution using logical reasoning. |
| Finite element method | A finite element method (FEM) is a method for numerically solving differential equations arising in engineering and mathematical modeling. |
| Numerical method | A numerical method is an approximate method used for solving a mathematical problem that often has no analytical solution. |
| Optimization | Optimization is the action of making or detecting the best or most effective use of a situation or resource. |
| Plate | A plate is a structural element used in engineering characterized by a three-dimensional object whose thickness is small compared with the other dimensions. |
| Slab | Slab is the engineering name for a relatively thin structural element used to create flat horizontal surfaces like a plate. |
| Standardization | Standardization is the process of making something conform to a standard such that it can be used efficiently. |
| Uplift force | An uplift force is a tension force in a bolted connection caused by the uplifting of the deck at the location of the bolt due to a (local) load in an adjacent span. |

# List of Figures

# List of Tables

# 1

# Introduction

## 1.1. Project motivation

Fiber-reinforced polymers (FRP) are increasingly used in the building and infra industries. One of the companies that are using FRP is FiberCore Europe (FCE). FCE designs and manufactures pedestrian bridges (self-supporting), traffic bridge decks (placed at an existing structure) and lock gates using glass fiber reinforced polymer (GFRP). Since the bridge decks are relatively thin (100 - 200 mm) compared to the length and width, the bridge decks behave like a slab. When it comes to the behavior of the slab or a part of the bridge deck, the word slab is often used. When more clarity is needed or the complete deck is intended, the words bridge deck or deck plate will be used. At the moment there is no special Eurocode for FRP structures like it is the case, for example, for steel. Design calculations for the slabs are partly done analytically, and partly with finite element analysis (FEA). Most of the finite element (FE) calculations are checked with beam models. The code that is used the most at the company is the CUR96 and therefore this code is used in the research as well.

To be competitive in the market of FRP bridges, FCE wishes to (further) standardize the design of the bridge slabs to reduce the costs involved in design and manufacturing. In this way, the FRP decks can compete with bridge decks from other materials. From this detection, the question came to make a set of optimized FRP bridge slabs. The idea is that a limited number of well-designed slabs are listed, which can be used to design an FRP bridge deck. Using this method, the costs and time can be reduced which makes it possible to make the FRP bridges competitive with the designs of other companies.

Another interest of FCE is the optimization of the number and design of the connections between the FRP slabs and the steel structure underneath. The steel structure consists of main girders with secondary girders with an I-profile. These secondary girders are the main girders supporting the FRP slabs. Between these main supporting girders for the slabs, secondary girders with a C-profile are placed on which the connections are made with the FRP slabs. Next to the interests of the company, at the Technical University of Delft research is done on a new type of connector to connect the FRP decks to existing steel structures. The connector that is developed is the iSRR (injected steel reinforced resin) connector. For this, the two fields come together. From both the company and the university, there is interest in the forces which occur in the connections due to the uplift effect of multiple spans of the slabs. For projects calculated by FCE, they use beam models to calculate the uplift forces in the bolts. In reality, the slabs will work as a plate instead of a beam. The question has raised what the difference is between the plate and beam behavior of the slabs. Simple finite element (FE) models are made by the company which gives values for the uplift forces in the bolts which are twice as low compared to the beam models [2]. Another type of analytical and/or numerical calculation is needed to verify the FE models and gain confidence that the used methods to calculate the forces are reliable enough. To be able to optimize the FRP slabs and the number of connections, a better (analytical) understanding of the behavior of the slabs is needed. Next to this, there is interest from both the university and the company in the fatigue forces in the connections. Based on the magnitude of the obtained uplift forces based on the standard load models from the Eurocode, an indication can be given about the importance of the fatigue checks of the connection.

Given the need for optimization and standardization of the slabs, a model has to be made which is reliable and for which it is easy to adapt parameters. An analytical method is more suitable for this because no mesh is made, which is the case for the finite element method (FEM) when parameters are changed. The

results are depending on the mesh size and when the process is automatized, the mesh is not checked and bad results can occur if the mesh contains disturbing elements. Using analytical and FE methods, both models can be used to verify each other and a comparison can be made on which model is more suitable for the optimization. To make it able to use the best model for each application, different levels of complexity have to be investigated. This means that for both methods, simple and more complex models have to be made.

The main goal for the company is to get a set of optimized slabs, which can be used for the design of FRP bridge decks. Next to this, they want to have models calculating connector forces and a framework that can be used for optimization. In the first part of the thesis, the main focus will be on different numerical models and analytical models based on beam and plate theories. The second part will focus on the optimization and standardization of the slabs. For the optimization part, the best geometry of a bridge deck is investigated with regard to costs. In addition, the weight of the slabs in combination with the occurring stresses in the laminates is considered. These are compared with a reference design from the company. The devised optimization technique is used to calculate results for different boundary conditions in the context of standardization.

## 1.2. Problem statement

To make it able to optimize the procedure of design and manufacturing of FRP bridge slabs, a standard set of slabs is needed, which is not available at the moment. A standard design can be used to give direct information to the client and reduce the engineering time and therefore the costs considerably. The standardized slabs have to be optimized to guarantee a safe and economical design.

An optimal design can only be made when the behavior of the slabs can be described well enough. At the moment this is not the case for the uplift forces in the connectors between the deck and the steel beams. Calculation of these forces with FE models and analytical beam models gives a difference of around 50% [3]. Based on this, there is a need for a better analytical and/or numerical model which describes the force distribution throughout the slabs to the steel structure underneath. There is not enough confidence in the current calculation of the bolt forces due to the large difference between the analytical and FE models.

## 1.3. Aim and objectives

The goal is a set of standardized and optimized FRP slabs. This can be a table or graph for example. From this, a slab can be selected for a specific range of free span of the slab and an occurring load class. For this optimization, a framework needs to be developed based on the parameters that are important for the design of the slabs. Since the FRP structure is made of an integer number of plies, the optimization procedure needs to handle discontinuous and continuous parameters at the same time. There is a high degree of freedom of design for FRP constructions, which makes many variants possible. Therefore, the goal is an optimization procedure that can quickly reach an optimum based on intelligent choices.

However, before optimization can be done a better understanding of the uplift forces in the connections between FRP slabs and a steel structure is needed. Different analytical and (simplified) numerical models need to be investigated and compared to each other. The goal of these different models is to explore models which are accurate enough and are at the same time easier to model and/or have a shorter calculation time. The difference in results and calculation time needs to be determined for linear and non-linear numerical calculations, analytical and numerical calculations, and simplified and detailed numerical calculations.

Based on the scientific research on the different models, a model has to be selected to use during the optimization procedure. To be useful, this model needs to be fast and accurate enough at the same time. Next to this, it needs to be possible to (easily) adapt the parameters of the model. When the forces in the bolted connections are in a critical region, the fatigue load and the fatigue performance of the bolted connection have to be determined. The difference between the investigated models and the reference model has to be lower than 10% to make sure the selected modeling approach is accurate enough. Using different methods makes it able to verify them with each other. The different investigated models will not be able to match exactly with the detailed numerical model. However, when the results are in the same order of magnitude, enough confidence is gained to be able to use these models for optimization.

To achieve these goals, the following research question is considered:

*Which geometry of FRP slabs is optimal to use for a given load and boundary conditions calculated by analytical and (simplified) numerical models taking the uplift forces in the connectors between these slabs and a steel supporting structure into account?*

The different sub-questions used to answer this main question are:

1. Which analytical and (simplified) numerical methods can be used to describe the behavior of FRP bridge slabs, and which one suited best for the calculation of uplift forces in bolted connections?

2. What is the magnitude of the uplift forces in the connections, that connect the FRP traffic decks with a steel structure, calculated with analytical and numerical models for a given load?

3. How can a numerical model, used for calculation of the uplift forces, be simplified and what is the difference in uplift forces between a detailed and simplified numerical calculation?

4. Which are the (main) parameters that influence the design of the FRP slabs and how can the slabs be optimized based on these parameters?

5. Which method can be used to standardize the FRP bridge slabs and which slabs are optimal to use for a given load and boundary conditions?

## 1.4. Methodology

Two types of calculation methods are used and compared to each other. The first method is a numerical method, for which Abaqus is used, and the second method is the use of analytical formulas. For the analytical method, MatrixFrame (MF), Python and hand calculations are used. Different levels of detailing of both methods are used to search for an optimum in terms of accuracy and calculation and modeling time for specific applications.

## 1.5. Scope

The research is limited to thin FRP slabs that are placed on an existing steel structure. It is assumed that the detailed numerical model represents reality and therefore, this model is used as a reference model. To validate this reference model, experiments are needed. However, no tests are available in the literature and within the scope of this graduation work, it is not possible to perform these tests. Therefore, it is assumed that the reference model is right but the validation has to be done in follow-up research.

The bolted connections that are investigated are only used for the transfer of tension forces and therefore shear forces are not considered. The load models that are considered are limited to the ones described at the Eurocode EN1991-2 [4] and special vehicles are not taken into account. For the dimensions of the deck, limits are given for a maximum free span by 1.5 $m$ and the other limits are given in Section 7.5.1. For the optimization of the slabs, only global behavior is considered and therefore, local behavior of the slab, like local buckling and delamination are out of scope for this research.

## 1.6. Outline

In this thesis, first a literature review has been done for which the results are described in the second chapter. Next to the literature review, the research consists of two main parts. The first part is about the calculation of uplift forces in bolts between an FRP deck and a steel structure. This part is described in chapters three to five. In the third chapter, a detailed numerical model is described which is used as a representation of reality. Chapter four describes different simplified numerical models which are investigated. After the numerical models, the analytical models are described in chapter five. Each chapter contains the results of the different models that are described and a discussion of these results. A comparison of the different models that are investigated is described in chapter six. Based on the comparison and the capacity of the connections, conclusions are made as input for the second part of the graduation work.

The second part of the graduation work is about the optimization of FRP decks, which is described in chapter seven. First, the optimization procedure is described and shown for the same case as considered in part one of the thesis. Standardization is done using the optimization procedure and is described at the end of the seventh chapter. The last chapter gives the conclusions and recommendations of the research. In the attached appendices extra information and results which support the research can be found. A schematic overview of the complete research is shown in Figure 1.1. The main steps are shown in the blue boxes and the chapters in which these parts are described are shown in the green boxes.
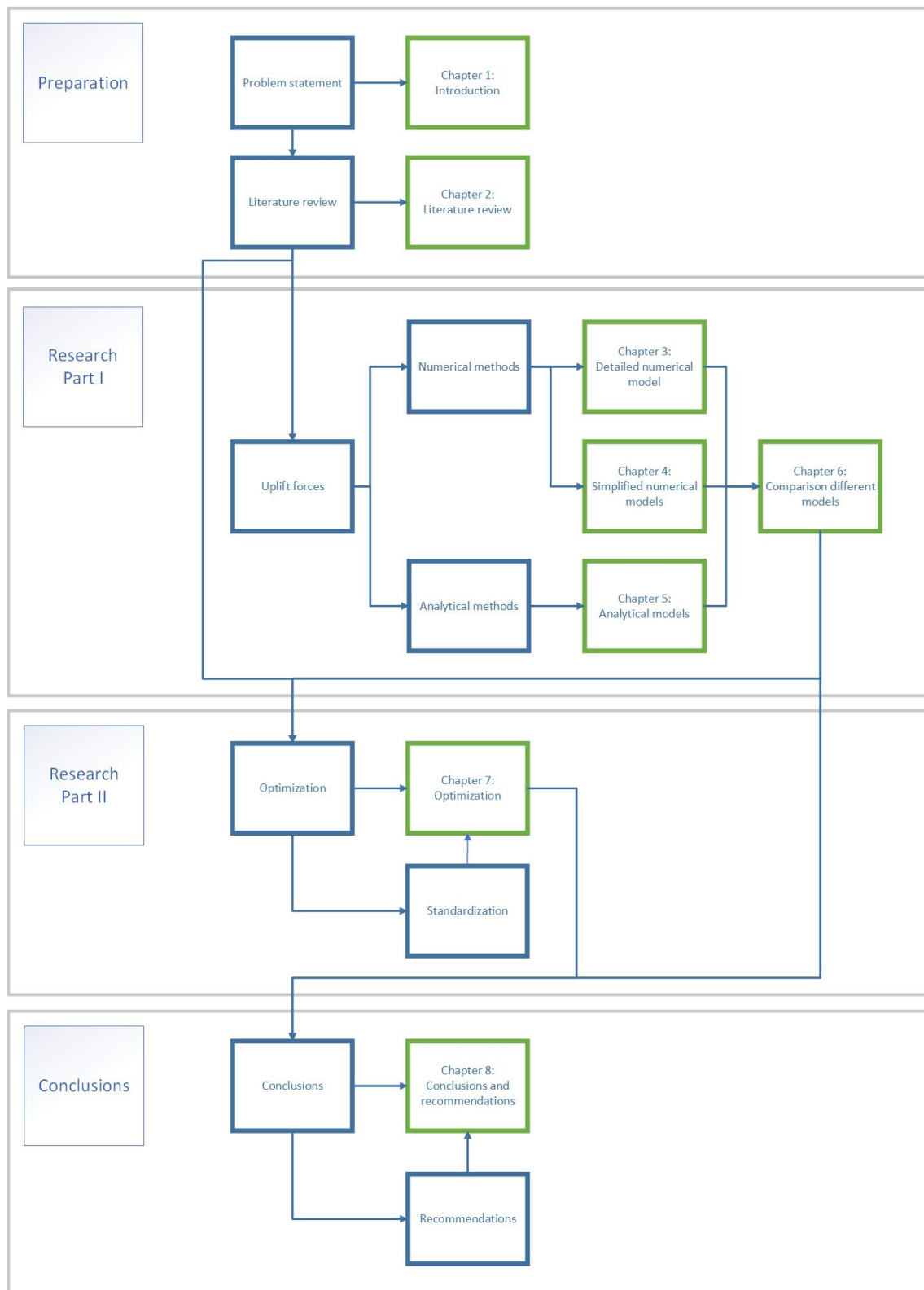
Figure 1.1: Outline thesis

<div style="text-align: right">

# 2

</div>

<div style="text-align: right">

# Literature review

</div>

The information in this chapter is given to be able to understand the research that has been performed and shows where in the field of scientific research this graduation work belongs. It is the basis on which the research is performed. In the first section, some general information about FRP in bridges is given and next to this a short discussion about the material characteristics that are important for the optimization. The second and third sections show different numerical and analytical models and how they can be modeled. After this, an overview of the different types of connections that can be used and the forces occurring in these connections are described in section four of this chapter. The last sections give an overview of the different optimization techniques that are available in the literature and a short discussion of the presented literature.

## 2.1. FRP used in bridges

Basic knowledge of fiber-reinforced polymers like the type of fibers, material composition and different production techniques is assumed to be known and essential for the understanding of this thesis. When this is not the case or for more information, the book about composites of R.P.L. Nijssen [5] and the CUR96 [6] can be consulted. In the two upcoming sub-sections information about the FRP slabs made at the company FiberCore Europe and information about the material concerning the fiber orientation are given.

### 2.1.1. FRP slabs made by FiberCore Europe

At the company FiberCore Europe, an unique type of layup is used to build the FRP bridge decks. This is called the InfraCore technology, which is a patented technology [7].

Figure 2.1: Principle of InfraCore Inside [8]
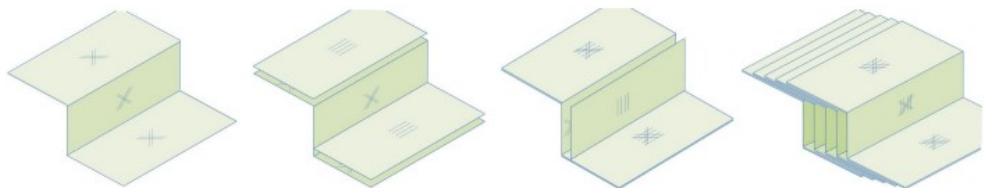
Figure 2.2: InfraCore Inside fabric stacking sequence [8]

5

The decks are made with vacuum infusion, which is a production method based on a mould in which the glass fibers and foam blocks are placed. The mould is vacuumed and in this way, the bridge part can be filled with resin. The advantage of this type of production technique is the freedom in shape and the low production costs when (part of) the mould can be reused. For a detailed description of the production process, a paper written by Peeters can be consulted [8].

An overview of the InfraCore technology is shown in the Figures 2.1 and 2.2 [7]. The principle of the InfraCore decks is based on the load transfer of an I-shaped beam. The shear forces are taken mainly by the webs and therefore most fibers are oriented in the vertical direction. The top part of the deck, which is called the topskin, and the bottom part, which is called the bottomskin of the deck, are taking the bending forces. The layers of the webs are continuing for a distance of about five times the web spacing to connect the webs to the top and bottomskins, shown in Figure 2.1. Due to this technique, the problem of delamination is prevented [8].

Different traffic bridge decks are made according to this same principle at FiberCore Europe. Therefore, these bridge decks can be standardized and optimized. In this report, one of the traffic decks made is considered as a representation. A 3D view of the types of decks is shown in Figure 2.3.
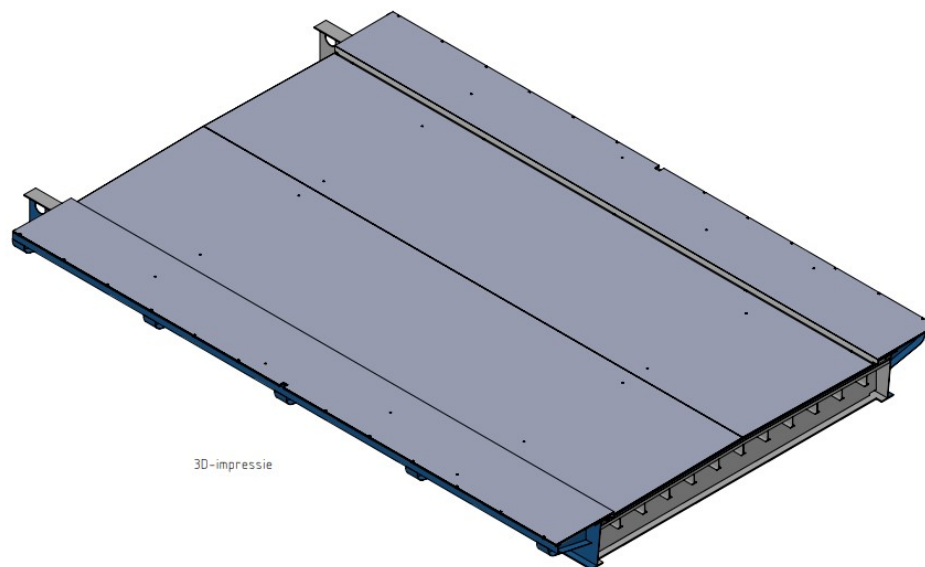


Figure 2.3: 3D view FiberCore Europe deck [9]

## 2.1.2. Fiber orientation and laminate strength

One of the main characteristics of fiber-reinforced materials is the difference in characteristics in different directions due to the difference in the amount of fibers in each direction. Since FRP laminates are made of different layers, the strength of the laminates is depended on the type of plies that are used to build the laminate. The (normalized) laminate strength of fibers with different orientations is shown in Figure 2.4 [10]. In this figure, it is shown that the strength in the fiber direction, $\sigma_{11}$, is maximum when all fibers are placed in the 0° direction. Placing all fibers perpendicular to this direction gives zero strength. For the strength in the perpendicular direction, $\sigma_{22}$, the opposite holds. The shear strength, $\sigma_{12}$, shows the highest value for the $+/-45°$ orientation.

Based on the different characteristics, the different plies can be used for different purposes. Placing more fibers in one of the directions makes the laminate stronger in that direction. The plies with most fibers in 0° direction can be used to transfer the normal stresses and the plies with fibers in the $+/-45°$ direction can be used for the transfer of shear stresses. Since the stacking of the plies with different fiber orientations is free to choose, optimization can be performed on how much fibers are used in each direction compared to the application.
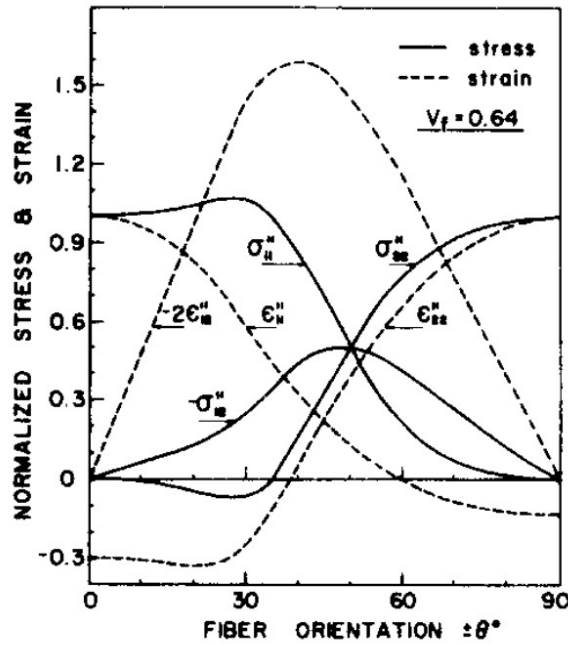
Figure 2.4: Lamina stress and strain vs fiber orientation [10]

The same as what applies to the strength properties, applies to the stiffness of the laminates. The stiffness of a ply laminate compared to the initial stiffness value is shown for different fiber orientations in Figure 2.5. In this graph it is shown that the stiffness is the highest when the fibers are placed in the zero direction. The lowest stiffness is obtained for the ply laminate with the fibers in 90° direction.
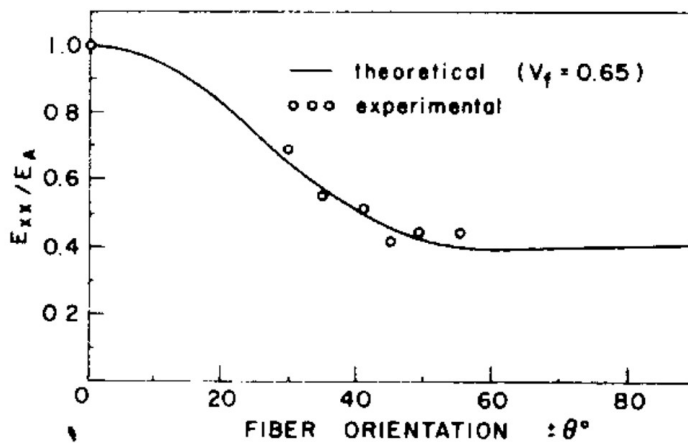


Figure 2.5: Stiffness relative to initial stiffness of ply laminates vs fiber orientation [10]

## 2.2. Modeling of FRP bridge slabs

Modeling of FRP bridge slabs can be done in different ways. Except for modeling the detailed geometry of the webs and skins, an orthotropic slab can be modeled with equivalent material properties. The biggest advantage of this type of modeling is the fact that less time is needed to make the model and the calculation time reduces significantly as well. In this section, a short overview of the different research that is performed on the equivalent material properties of FRP slabs is given.
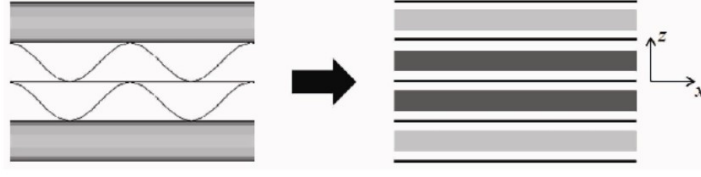
Figure 2.6: Model corrugated-core sandwich panels [11]

Y.J. Cheon and H.G. Kim performed research on the equivalent material properties of corrugated-core sandwich panels. The model that is used in the research is shown in Figure 2.6. As a result of the research adapted stiffness terms are found as follows [11]:

$$
\begin{aligned}
\overline{A_{11}} &= \frac{2c}{\frac{I_1}{A_{11}} + \frac{I_2}{D_{11}}} \\
\overline{A_{12}} &= \frac{A_{12}}{A_{11}} \overline{A_{11}} \\
\overline{A_{22}} &= \frac{A_{12}}{A_{11}} \overline{A_{12}} + \frac{l}{c} \frac{A_{11} A_{22} - A_{12}^2}{A_{11}} \\
\overline{A_{66}} &= \frac{c}{l} A_{66} \\
\overline{D_{11}} &= \frac{c}{l} D_{11} \\
\overline{D_{12}} &= \frac{D_{12}}{D_{11}} \overline{D_{11}} \\
\overline{D_{22}} &= \frac{1}{2c} (I_2 A_{22} + I_1 D_{22}) \\
\overline{D_{66}} &= \frac{c}{l} D_{66}
\end{aligned}
\tag{2.1}
$$

The different parts of the stiffness matrix are denoted by $A$ and $D$ with in the subscripts the location of the parameter in the matrix. The stiffness terms without a bar denotes the original values, the ones with a bar the adapted ones. The height of the core is denoted by $c$, the length of one repetitive unit in the core by $l$ and the equivalent stiffness in the two main directions by $I$. The stiffness parameters of the case with a sin-wave geometry are given as

$$
\begin{aligned}
I_1 &= \int_0^{2l} \left(\frac{dx}{ds}\right)^2 ds \\
I_2 &= \int_0^{2l} z^2 ds
\end{aligned}
\tag{2.2}
$$

With $x$ and $z$ denoting the coordinates in the main directions and $s$ the coordinate along the webs. Considering a trapezoidal geometry of the core, the stiffness parameters can be calculated with the formulas below. In these formulas the angle between the horizontal and the inclined parts of the core is denoted by $\alpha$, the height of the core by $f$ and the width by $c$.

$$
\begin{aligned}
I_1 &= \frac{4f \cos \alpha}{3 \sin \alpha} + 2c - \frac{4f}{\tan \alpha} \\
I_2 &= \frac{4f^3}{3 \sin \alpha} + 2f^2 \left(c - \frac{2f}{\tan \alpha}\right)
\end{aligned}
\tag{2.3}
$$

Taking these adapted stiffnesses into account, the rest of the procedure uses the (adapted) classical laminate theory (CLT) to calculate the deformations. In the paper, a comparison is made between calculations for a plate with these equivalent orthotropic properties and calculations for a plate with the corrugated core

sandwich geometry. For different thicknesses of the plates, it is concluded that the maximum relative error is 3.7% [11].

Another research that takes multiple configurations into account is performed by A. Pydah and R.C. Batra. In this research, the different configurations shown in Figure 2.7 are considered. For these configurations, different analytical solutions are found to represent the behavior of the web core sandwich panels. In the conclusion of the research, the difference between the deformation of the web plates in the corrugated and web core panels is described. The webs in the corrugated core deform in compression while the webs in the web core panels deform in bending [12].
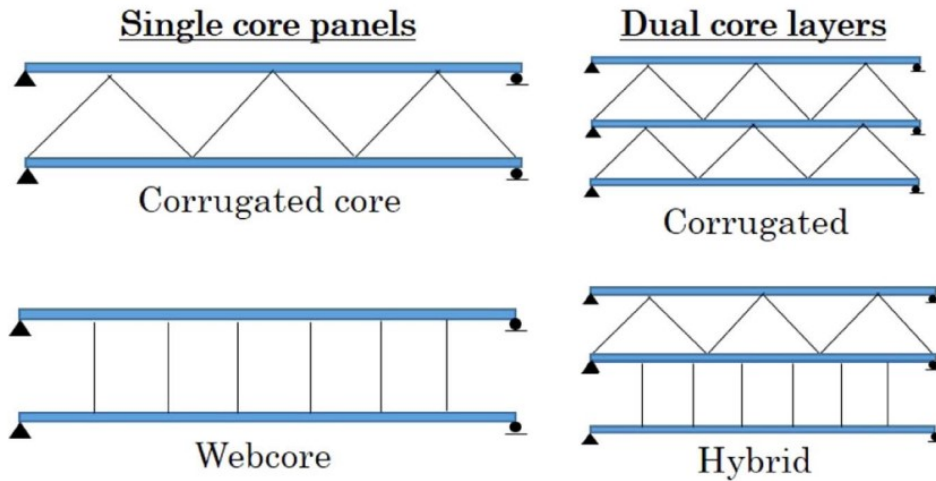


Figure 2.7: Models different configurations webcore sandwich panels [12]
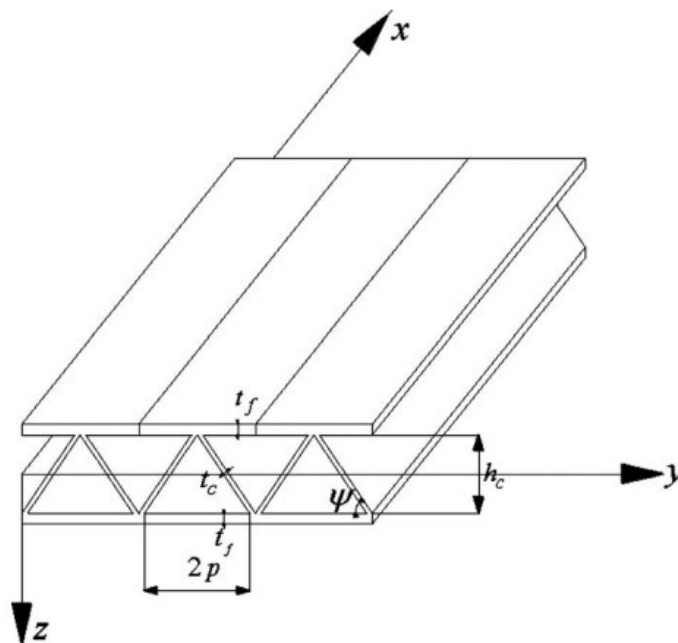


Figure 2.8: Model equivalent elastic constants of truss core sandwich panels [13]

Another research that describes the equivalent material properties with analytical formulas is performed by H.X. Wang and S.W. Chung. In the paper based on this research equivalent material properties for the model shown in Figure 2.8 are given by [13]:

$$E_x = E \frac{t_c}{p \sin \phi}$$

$$E_y = E \frac{t_c^3 \cos \phi}{(h_c^2 - t_c^2 \cos^2 \phi) h_c}$$

$$E_z = E \frac{t_c^3 \sin \phi}{p^3 - p t_c^2 \sin^2 \phi}$$

$$G_{xy} = G \frac{p t_c \sin \phi}{h_c^2} \tag{2.4}$$

$$G_{yz} = E \frac{t_c \sin \phi \cos^2 \phi}{p}$$

$$G_{zx} = G \frac{t_c \sin \phi}{p}$$

In these formulas, the height of the plate is denoted by $h_c$, the thickness of the skins and the webs by $t_f$ and $t_c$ respectively. The angle of the webs is given by $\phi$ and the horizontal distance between the webs by $2p$. $E$ is the general bending modulus and $G$ the shear modulus. In the paper, a comparison is made for detailed and simplified models by the examination of two cases. The maximum difference found for the different methods is 2.5%. As the main conclusion, the difference in the number of elements needed and therefore the reduction in computational time is mentioned [13]. Next to this, equivalent Poisson's ratios are given.

A more general analytical approach is developed by G. Bartolozzi et al. In the described research formulas for the equivalent properties are given which are shown below based on the model shown in Figure 2.9. In these formulas, the main dimensions of one repetitive unit of the core are denoted by $P_0$ for the width and $H_0$ for the height. $\delta_H$ denotes the horizontal displacement due to a horizontal load applied. The thickness of the arbitrary shaped core is given by $t_c$ and the general bending stiffness and shear stiffness respectively by $E$ and $G$. The stiffness of one repetitive core unit in the different main directions is described by Formula 2.6. This formula use the derivative of the function $f(x)$ that describes the shape of the core. Based on a comparison with results from other papers, a maximum relative error of about 2.6% is claimed for the generally applicable formulas. However, further research on the influence of the different shear stiffnesses is needed [14].

$$E_x = \frac{P_0}{H_0} \frac{1}{\delta_H}$$

$$E_y = E \frac{t_c(l_1 + l_2)}{H_0 P_0}$$

$$G_{xy} = G \frac{(l_1 + l_2) t_c}{H_0 P_0} \tag{2.5}$$

$$G_{yz} = G \frac{H_0 t_c}{P_0} \left( \frac{1}{l_1} + \frac{1}{l_2} \right)$$

With

$$l_i = \int_0^{p_i} \sqrt{1 + |f_i{}'(x)|^2} \, dx \tag{2.6}$$
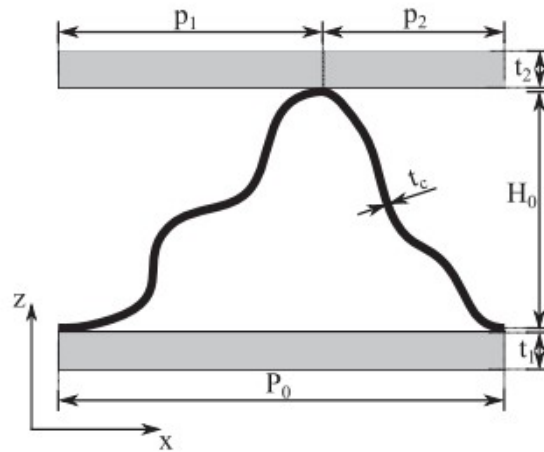
Figure 2.9: Model general analytical method for equivalent properties of corrugated cores [14]

Next to the analytical description of the equivalent properties, numerical modeling is used. Research performed by D. Tumino describes equivalent in-plane stiffness properties for the model shown in Figure 2.10 by the formulas stated below. In these formulas, the geometry is described by the height, $h$, and the thickness, $t_s$. The properties in the main directions $x$ and $y$ that are used are the bending stiffness $E$, the shear stiffness $G$, the moment of inertia $I$ and the viscosity $v$. With subscripts, the direction for the properties is denoted. In the research, the implementation into a shell element from ANSYS is described. The validity of the method is tested with experiment work [15].

$$D_x = \frac{1}{2} E_x t_s h^2 + E_x I_c$$

$$D_y = \frac{\frac{1}{2}(t_s h^2 + 2I_c) E_x E_y t_s h^2}{E_x(t_s h^2 + 2I_c - v_{xy} v_{yx} t_s h^2 - 2 v_{xy} v yx I_c) + v_{xy}^2 E_y t_s h^2}$$

$$D_{xy} = G_{mxy} t_s h^2$$

(2.7)
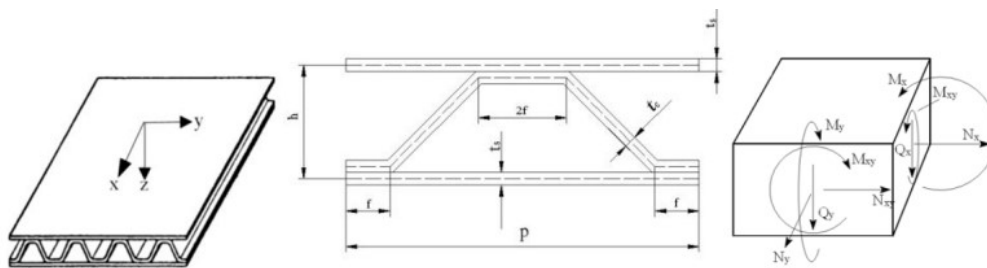


Figure 2.10: Model mechanical behavior of core sandwich panels for numerical modeling [15]

## 2.3. Analytical methods

Different analytical models can be used to model the FRP slabs to be able to calculate the deformations. Some models are even suitable to calculate strains and/or stresses. In the following sub-sections, different theories are given in order of increasing complexity.

### 2.3.1. Beam theories

A simplification of the analytical model that can be done for a slab is the use of a beam model. Instead of considering a two-dimensional plate, only one dimension is stated as superior to the other ones. Modeling a plate as a series of beams reduces the computational time. Two main theories existing are the Euler-Bernoulli theory and the Timoshenko theory. The Euler-Bernoulli theory is described by

$$EI \frac{d^4 w}{dx^4} = q \tag{2.8}$$

in which $w$ denotes the deformation of the beam, $E$ the bending stiffness, $I$ the moment of inertia and $x$ the coordinate along the beam. The applied load is described by $q$. The Timoshenko theory is described by the two formulas shown below in which the same parameters are used as for the Euler-Bernoulli theory. Next to these parameters, the rotation of the beam is given by $\phi$, the shear modulus by $G$ and the effective width that may taken into account for the shear resistance by $A_{eff}$.

$$EI \frac{d^2 \phi}{dx^2} - GA_{eff} \left( \frac{dw}{dx} + \phi \right) = 0$$
$$GA_{eff} \left( \frac{d^2 w}{dx^2} + \frac{d\phi}{dx} \right) = q \tag{2.9}$$

The Euler-Bernoulli theory does not take shear deformation into account. For FRP structures, shear deformation has to be taken into account since the stiffness is quite low compared to the strength of the material.

**CUR96**
Based on the beam theories, two special cases are given in the CUR96 [6] to calculate the deformation at the middle of the beam. One equation for a point load

$$w_{tot} = \frac{1}{48} \frac{F \cdot L^3}{\sum_i E_i I_i} + \eta \frac{1}{4} \frac{F \cdot L}{\sum_i G_i A_i} \tag{2.10}$$

In which $L$ denotes the length of the beam, $F$, the applied point load and $\sum_i E_i I_i$ and $\sum_i G_i A_i$ the summation of the bending stiffness and shear stiffness respectively. The ratio of shear deformation that hase to be taken into account is denoted by $\eta$. The other case is for a distributed load denoted by $q$.

$$w_{tot} = \frac{5}{384} \frac{q \cdot L^4}{\sum_i E_i I_i} + \eta \frac{1}{8} \frac{q \cdot L^2}{\sum_i G_i A_i} \tag{2.11}$$

### 2.3.2. Plate theories
Plate theories can mainly divided in five groups of theories listed underneath in increasing order of complexity [16].

1. Classical laminated plate theory (CLPT)

2. First-order shear deformation theory (FSDT)

3. Higher order shear deformation theories (HSDT)

4. Zig-zag theories (ZZT)

5. Layer wise theories (LW)

For this research only the first order shear deformation theories are used. Some examples of this theory are discussed in more detail. The CLT is used to calculate the laminate properties.

**CUR96**
A special closed formed solution for a simply supported plate with an uniform distributed load is provided by the CUR96. This solution is described by [6]

$$w(x, y) = \sum_{m=1,3,5,\dots}^{\infty} \sum_{n=1,3,5,\dots}^{\infty} a_{mn} \sin \frac{m \cdot \pi \cdot x}{a} \sin \frac{n \cdot \pi \cdot y}{b} \tag{2.12}$$

with

$$a_{mn} = \frac{16 \cdot q \cdot a^2 \cdot b^2}{\pi^6 \cdot m \cdot n \cdot D_{abmn}} \tag{2.13}$$

$$D_{abmn} = m^4 \left(\frac{b}{a}\right)^2 \cdot D_{11} + 2m^2 n^2 (D_{12} + 2D_{66}) + n^4 \left(\frac{a}{b}\right)^2 \cdot D_{22} \tag{2.14}$$

In these formulas, the number of sines taken into account in $x$ and $y$ direction, is denoted by $m$ and $n$ respectively. The length of the plate in $x$ direction is given by $a$ and in $y$ direction by $b$. The different stiffness parameters from the stiffness matrix are denoted by $D$, with in the subscript the location in the stiffness matrix. The applied distributed load is denoted by $q$.

**First-order shear deformation theory**
One of the used plate theories is the theory developed by R.P. Shimpi [17]. This theory is based on the following equations

$$D_{11}\frac{\partial^4 w_b}{\partial x^4} + 2(D_{12} + 2D_{66})\frac{\partial^4 w_b}{\partial x^2 \partial y^2} + D_{22}\frac{\partial^4 w_b}{\partial y^4} = q_0 \tag{2.15}$$

$$-\left[A_{55}\frac{\partial^2 w_s}{\partial x^2} + A_{44}\frac{\partial^2 w_s}{\partial y^2}\right] + \frac{1}{84}\left[D_{11}\frac{\partial^4 w_s}{\partial x^4} + 2(D_{12} + 2D_{66})\frac{\partial^4 w_s}{\partial x^2 \partial y^2} + D_{22}\frac{\partial^4 w_s}{\partial y^4}\right] = q_0 \tag{2.16}$$

$D$ describes the different stiffness terms, $q_0$ the applied load and $w_b$ and $w_s$ the bending and shear deformation. The coordinates used are $x$ and $y$. The solution for the bending deformation and shear deformation are searched in the form of

$$w_b = \sum_{m=1,3,\dots}^{\infty} \sum_{n=1,3,\dots}^{\infty} W_{b_{mn}} \sin\left(\frac{m\pi x}{a}\right)\sin\left(\frac{n\pi y}{b}\right) \tag{2.17}$$

$$w_s = \sum_{m=1,3,\dots}^{\infty} \sum_{n=1,3,\dots}^{\infty} W_{s_{mn}} \sin\left(\frac{m\pi x}{a}\right)\sin\left(\frac{n\pi y}{b}\right) \tag{2.18}$$

In which $m$ sines are used in x-direction and $n$ sines in y-direction. The dimensions of the plate are given by $a$ and $b$ for the $x$ and $y$ direction respectively. $W_b$ and $W_s$ are two constants used for solving the equations. Based on the comparison with other theories, it is concluded in the research that the theory is the simplest yet accurate shear deformable theory with the use of only two variables [17].

**Plate theory with general boundary conditions**
Another plate theory which can be applied to all type of boundary conditions, is based on the following governing equation [18]

$$D_{11}\frac{\partial^4 W}{\partial x^4} + 4D_{16}\frac{\partial^4}{\partial x^3 \partial y} + 2(D_{12} + 2D_{66})\frac{\partial^4 W}{\partial x^2 \partial y^2} + 4D_{26}\frac{\partial^4 W}{\partial x \partial y^3} + D_{22}\frac{\partial^4}{\partial y^4} = q(x,y) \tag{2.19}$$

In this formula, $D$ denotes the different stiffness terms of the stiffness matrix, $x$ and $y$ the coordinates in the main direction, $q(x,y)$ the function of the applied load and $W$ the deformation of the plate. To solve this partial differential equation, a solution is assumed with a summation of cosines. In these solution the parameters $A_{mn}$ are used to solve for, $\lambda_{am}$ and $\lambda_{bn}$ are the amplitudes in $x$ and $y$ direction and $xi_a$ and $\xi_b$ are functions to compensate for the applied boundary conditions.

$$W(x,y) = \sum_{m=0}^{\infty}\sum_{n=0}^{\infty} A_{mn}\cos(\lambda_{am}x)\cos(\lambda_{bn}y) + \sum_{l=1}^{4}\left(\xi_b^l(y)\sum_{m=0}^{\infty}c_m^l\cos(\lambda_{am}x) + \xi_a^l(x)\sum_{n=0}^{\infty}d_n^l\cos(\lambda_{bn}y)\right) \tag{2.20}$$

The constants $A_{mn}$ can be solve with the following set of equations in which $\alpha_m$, $\overline{\alpha}_m$, $\overline{\overline{\alpha}}_m$, $\beta_n$, $\overline{\beta}_n$ and $\overline{\overline{\beta}}_n$ give different ratios of sines and cosines with different amplitudes.

$$(D_{11}\lambda_{am}^4 + D_{22}\lambda_{bn}^4 + 2(D_{12} + 2D_{66}\lambda_{am}^2\lambda_{bn}^2)A_{mn} + \sum_{l=1}^{4}\left(D_{11}\beta_n^l\lambda_{am}^4 - 2(D_{12} + 2D_{66}\lambda_{am}^2\overline{\beta}_n^l + D_{22}\overline{\overline{\beta}}_n^l\right)c_m^l$$

$$+ \sum_{l=1}^{4}\left(D_{22}\alpha_m^l\lambda_{bn}^4 - 2(D_{12} + 2D_{66}\lambda_{bn}^2\overline{\alpha}_m^l + D_{11}\overline{\overline{\alpha}}_m^l\right)d_n^l - \rho h\omega^2\left(A_{mn} + \sum_{l=1}^{4}\left(\beta_n^l c_m^l + \alpha_m^l d_n^l\right)\right) = q_{mn} \tag{2.21}$$

Furthermore, $\rho$ describes the density, $h$ the height of the plate and $\omega$ the eigenfrequency. The equation can be solved in terms of the unknown constants $c_m^l$ and $d_n^l$ by setting the eigenfrequency $\omega$ to zero. The other constants can be solved by the use of boundary conditions. With these solved constants the deformation of the plate is given by the assumed solution. In the research, the analytically obtained results are compared to finite element models made with Abaqus. Showing the results for cases with different static loads and boundary conditions with less than 1% difference makes the theory generally applicable [18].

## 2.4. Connections in composite FRP-steel bridges

This section first gives information about the different connections in composite bridges. Different types of bolted connections are displayed and the results of the tests performed on these connections are shown. Next to this, some additional explanation about the origin of the forces is given. This information can be used to compare and verify the results obtained in this study.

### 2.4.1. Type of connections

The connection between an FRP deck and an existing steel structure can be made in different ways. To connect FRP slabs with a steel structure two main types of connections exist namely (adhesive) bonded joints and mechanical joints. For more information about adhesive connections and their performance, the research of T. Keller and M. Schollmayer can be considered [19]. A comparison between these two types of connections is made by listing the most important advantages and disadvantages which are shown in Table 2.1. Since the focus of this thesis is on bolt forces, only the mechanical joints will be considered in more detail. These types of connectors have two main tasks. The first task is the transfer of shear forces and the second one is the transfer of axial (tension) forces. Most of the connectors are developed mainly for the first task. Due to these two main tasks, two types of mechanical joints can be distinguished, shear studs and connectors. Shear studs are designed to transfer only the shear forces between the deck and steel structure. Connectors can be used for both types of load transfer. The different types of connectors, which are available at the moment, are explained shortly and compared to each other based on performance.

Table 2.1: Comparison of different connection techniques [20]

| Type of connection | Advantages | Disadvantages |
|---|---|---|
| Bolted connection | Requires no special surface preparation | Low strength to stress concentrations |
| | Can be disassembled | Special practices required in assembly |
| | Ease of inspection | Fluid and weather tightness normally requires special gaskets or sealants |
| | Quasi-ductivle behavior | Corrosion |
| Adhesive connection | High joint strength can be achieved | Cannot be disassembled |
| | Low part count | Requires special surface preparation |
| | Fluid and weather tightness | Difficulty of inspection |
| | Potential corrosion problems are minimized | Temperature and high humidity can affect joint strength |
| | Smooth external surfaces | Brittle |
| | Stiffness | |

**Bolts with and without embedded nut**

The most simple type of connector is a bolt that is embedded in the FRP deck during the construction of the deck. This type of connector is shown in Figure 2.11. The same figure shows the options of one or two embedded nuts to increase the capacity of the connection. These types of connectors are developed initially for concrete steel connections as an alternative option for studs. Different push-out tests are performed in the research of M. Pavlovíc for M16 and M24 bolts with a grade of 8.8. As a result, the research concludes that the shear resistance is about 95% of the resistance of welded headed studs which will have the same geometry [21].
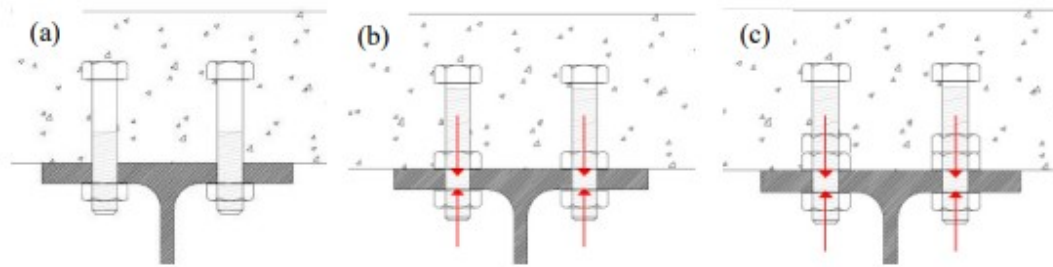
Figure 2.11: (a) bolt without nut, (b) bolt with single embedded nut, (c) bolt with double embedded nut [22]

**Blind bolts**

A comparable type of connection is made with blind bolts. These types of bolts are shown in Figure 2.12 and can be with and without anchors. An advantage of this type of connection is that the bolts can be placed after the bridge deck is made, at the construction site. However, the holes in the steel beams have to be pre-drilled and therefore, slotted holes have to be used otherwise the deck cannot be installed due to small deviations.

Two often used types of blind bolts are Ajax connector and Lindapter connector. These two types of connectors are tested in multiple studies performed at the technical university of Delft [23] [24] [25] and are shown in Figure 2.14. The test set-up for these tests is shown in Figure 2.13 and the results are given in Table 2.2. For the experiments, four connectors of M20 are used on each side. Conclusions are drawn based on this research with respect to the maximum shear and axial resistance. Next to this, it is concluded that due to the rotation of the bolts an extra axial force of 10-20% of the shear load can occur [25].
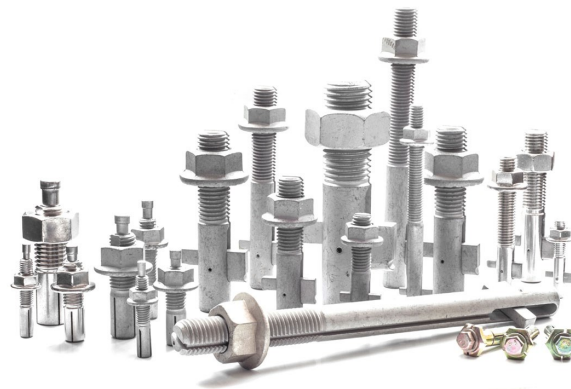


Figure 2.12: Blind bolts [26]



Figure 2.13: Test set-up push-out tests [25]

**Injection bolt**

Injection bolts are developed for a better fatigue behavior compared to other bolted connections and reduce

the slip in the connection. Reducing the slip in the connection increases the hybrid interaction between the steel structure and the FRP deck plate, and therefore the capacity [22]. An example is the iSRR (injected Steel Reinforced Resin) connector, which is shown in Figure 2.14c. A study performed by G. Olivier et al. describes different tests performed on M20 bolts of grade 10.9 [23]. The test set-up for these different static, cyclic and creep tests are shown in Figure 2.15. Based on the performed tests a maximum shear capacity of 160 $kN$ is found. Next to this, different conclusions about fatigue behavior are made [23].
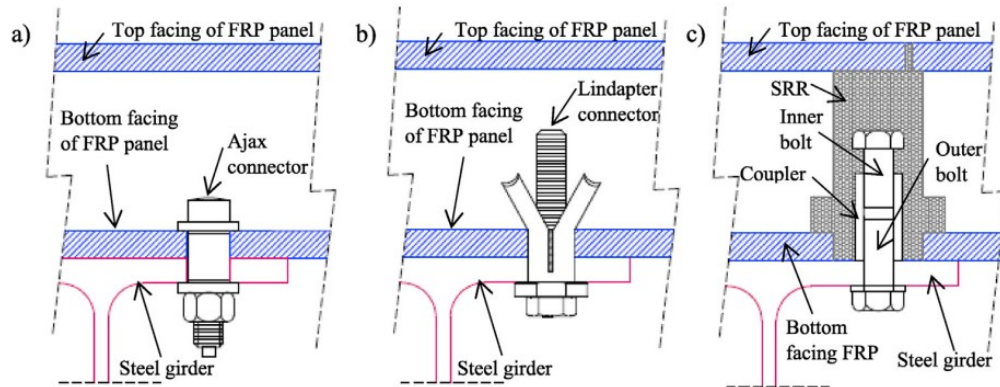


Figure 2.14: (a) Ajax connector, (b) Lindapter connector, (c) iSRR connector [25]
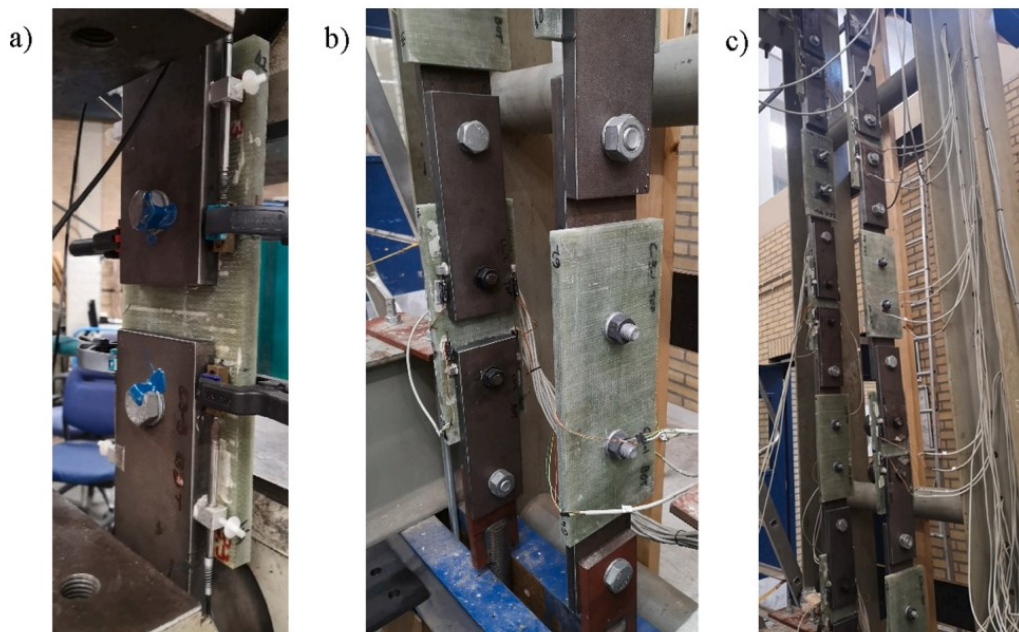


Figure 2.15: Test set-up: (a) Static and cyclic loading, (b) sustained loading, (c) creep tower [23]

**Embedded mechanical connector REDUCE project**

The REDUCE (Reuse and Demountability using Steel Structures and the Circular Economy) project is a research project from the steel construction institute in the UK, the University of Luxembourg together with the technical university of Delft and some other parties involved [27]. During this project, a shear connector, shown in Figure 2.16 [22], is developed and tested, which is originally meant for a steel-concrete connection but can be used for steel-FRP connections as well. Different tests are performed for both shear and axial behavior.
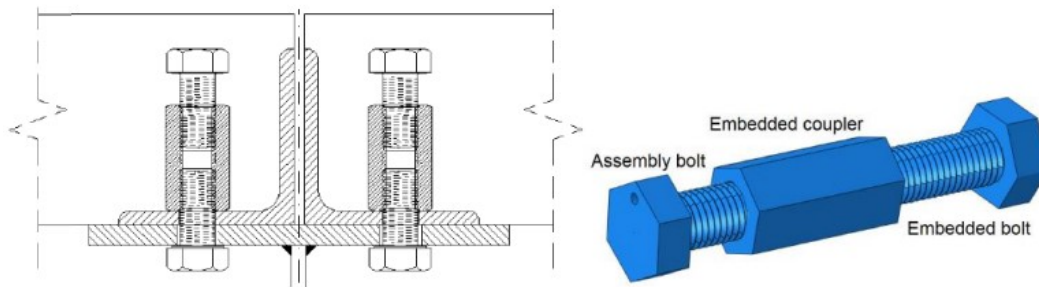
Figure 2.16: Embedded mechanical connector REDUCE project [22]

**Bolt with embedded plate**

At the company FiberCore Europe, a rather simple connector is used. This connector is made of a steel plate which is embedded in the slab during production. After production, a hole is drilled into the slab and a bolt can be used to connect the girder with the steel plate. In this way, a steel-to-steel connection is made. This connection is only used for the transfer of tensile forces and shear studs are used for the same deck to transfer the shear forces due to the traffic load. A schematic overview of this type of connection is shown in Figure 2.17 based on the technical drawings of FCE [9].
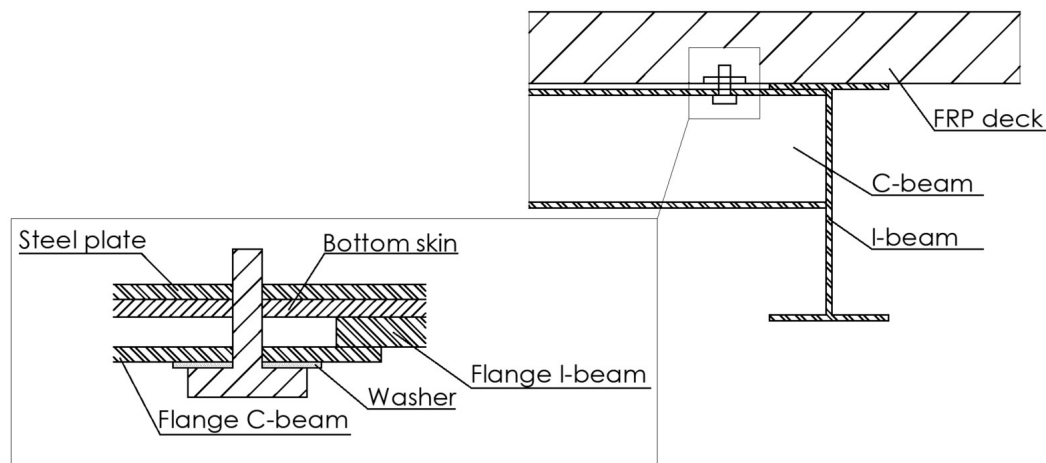


Figure 2.17: Connector FCE: bolt with embedded plate

**Comparison of connectors**

The different types of connections are compared to each other based on the research that is performed and described above[25] [22] [23] [24]. Results of this comparison are shown in Table 2.2 for bolts of size M20 and grade 10.9.

Table 2.2: Comparison of different type of mechanical connectors

| Type of connector | Shear capacity [$kN$] | Tensile capacity [$kN$] | Dynamic Behavior [$cycles$] |
|---|---|---|---|
| Ajax connector [25] | - | 207.4 | - |
| Lindapter connector [25] [24] | 154 | 164.3 | $2.2 \cdot 10^4$ |
| iSRR connector [25] [23] | 153.9 | 120.0 | $2.31 \cdot 10^6$ |
| Embedded mechanical connector REDUCE project [22] | 131 | - | - |

Based on the comparison between the different connectors, it is shown that for the fatigue resistance the iSRR connector has the best performance. This connector shows the same shear capacity as the blind bolt

connectors. However, the blind bolt connectors, Ajax and Lindapter, show a better axial behavior due to the design of these connectors. Therefore, the choice of the best connector is dependent on the main task. Next to this costs and installation time can be considered. The costs of the blind bolts are higher compared to the iSRR connector. For the blind bolt connections, the construction time is less than the iSRR connection, which reduces the costs in this way [22].

## 2.4.2. Forces in the connections

FRP bridge decks have in general a lower stiffness compared to other types of decks, like orthotropic steel decks. Due to this low stiffness, the distance between the steel girders underneath the deck cannot be large and the FRP deck plate has to span multiple spans. Loading a multiple span slab with a wheel load, causes tension forces in some of the supports, which is shown in 2D in Figure 2.18. These tension forces are called uplift forces since they are caused by the uplifting of the deck due to a load in an adjacent span. In most cases, the bridge decks are placed on top of the steel beams without connecting the deck directly to the girders. To prevent the deck from uplifting, several bolted connections are placed to take these uplift forces. At FiberCore Europe, the bolted connections are designed in such a way that only tension forces can occur. This means that compression and shear forces have to be transferred in another way. Shear studs are installed at the end of the same deck and used to transfer the shear forces due to the moving vehicles. However, several other types of connections exist as well.
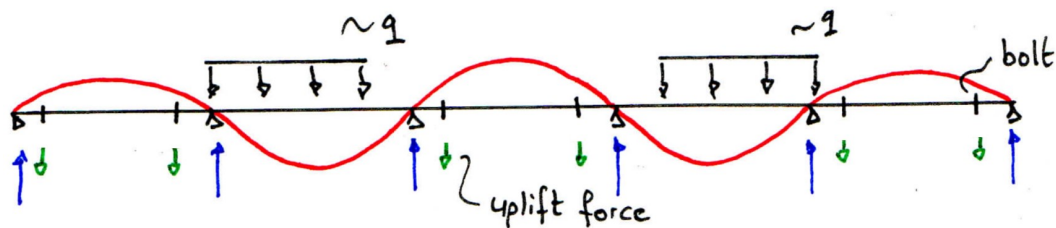


Figure 2.18: Uplift forces occurring in the connections

Considering performed research about the magnitude of the forces two types of research can be done. Most of the research is done on the shear forces in the connectors and only a limited amount of research is done on tension forces. A case study performed by J. ter Kuile shows that the shear force in connections between FRP slabs and a steel structure is in the range of -22.5 $kN$ and 22.5 $kN$ [28]. The same type of research is performed by K. Gribnau. In his master's thesis, he shows that the magnitude of the shear force in the bolted connections due to traffic loads is in the range of 10 to 110 $kN$ [29].

T. Peeters performed a case study about fatigue compressive forces in bolted connections. At his research, he found a force range of 10 to 65 $kN$ [30]. For the research, springs are used which can take compression forces at the locations of the supports. Research on tensile stress in adhesive joints due to uplift forces is performed by T. Keller and M. Schollmayer according to the principle shown in Figure 2.19. The test set-up that is used for the experiments is shown in Figure 2.20. As a result of the experiments, an average stress of 0.79 $MPa$ is found in the adhesive joints for a load of 119 $kN$. Taking the stress concentration factor into account, they concluded in the research that the failure stress becomes 9.8 $MPa$ [19]. Except for these researches, there is no information available at the moment about uplift forces in FRP bridge decks. This means that a knowledge gap exists on this topic in the literature.

Regarding other types of decks, the connections are made in a different way. For orthotropic steel decks, most of the connections are made with welds and therefore the force distribution will be different. For timber bridge decks, the connection to the main load-bearing structure of steel or timber is made right above the main girders. Therefore, the bolt forces can be calculated in a more straightforward way.
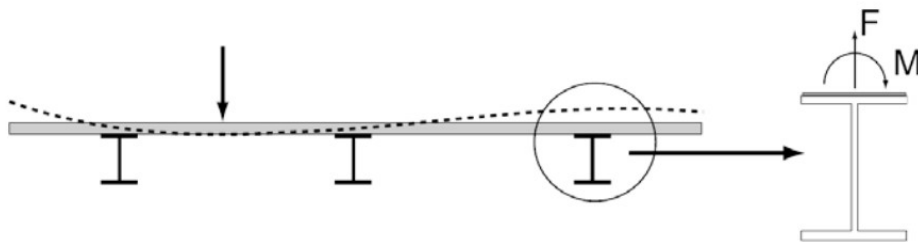
Figure 2.19: Principle tensile stress adhesive joints [19]
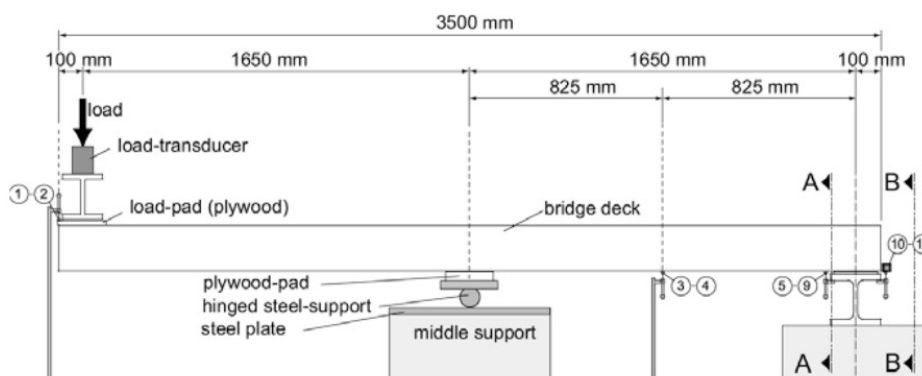


Figure 2.20: Test set-up for experiments on tensile stress adhesive joints [19]

## 2.5. Optimization theories

Different optimization theories exist. An overview of the techniques that are already used in civil engineering for FRP structures is given by a paper from Awad et all. [31]. In this section different possible optimization techniques are mentioned and explained shortly.

**Design sensitivity analysis (DSA)**
Design sensitivity analysis is an optimization technique that is based on a reference model. For this model, the change in target variables is calculated for a change in the other variables. In this way, the sensitivity of the target variables can be determined. These sensitivity values are used to modify the variables to calculate the optimal values. Furthermore, these sensitivity values can be used to calculate the errors made in different cases. The design sensitivity analysis can be performed based on analytical calculations, and next to this finite element and finite difference methods can be used [32].

**Genetic algorithm (GA)**
The optimization techniques of genetic algorithms are a family of methods inspired by the evolution principle. An overview of the essence of this optimization technique is shown in Figure 2.21. In general, the optimization technique works as follows; First, an initial population is created based on the different parameters that are available in the optimization process. As a result of modifications to these populations, a new population is created. For each individual in this new population, a fitness value is calculated. The next generation is created based on the individuals in the previous generation with the highest score. Proceeding with this process gives the most ideal options after multiple iterations [33].
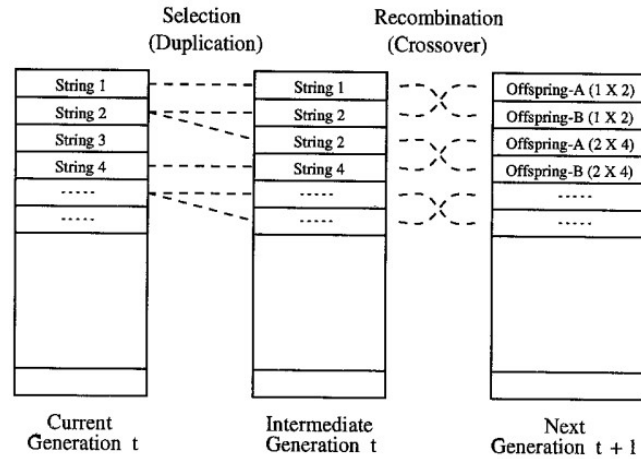
Figure 2.21: Overview genetic algorithm [33]

**Simulating annealing method (SA)**

Simulating annealing method is a probabilistic optimization method developed in the metal industry. The optimization procedure is based on a continuous cost function. At this function, an initial starting point is chosen for which the value is calculated. The next value is chosen (close to the initial value) and evaluated as well. Comparing this value to the initial value gives a probability that the chosen value is better or not. When the chosen option is less preferable than the initial value it is rejected and when the new chosen option is better, it is set to the reference value. Performing multiple iterations gives a convergence to the (local) optimum option [34].

**Reliability design optimization (RBDO)**

This optimization method search for the optimum design for both safety and costs. Based on several limits and/or constraints of the different variables the optimum possible design is calculated. For each possibility, the failure probability is calculated even as the costs. The optimization process starts at a chosen point and the optimum design depends on this starting point since the method is sensitive to local minima [31].
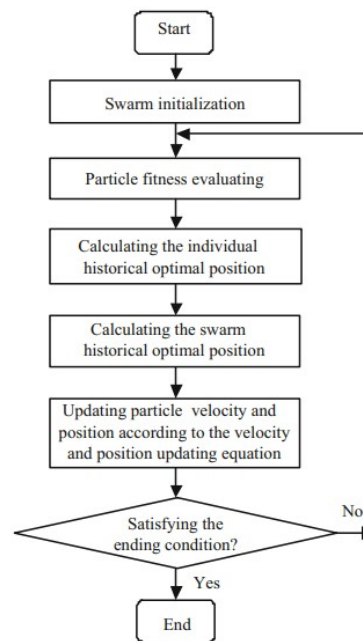


Figure 2.22: Overview particle swarm optimization algorithm [35]

**Particle swarm optimization algorithm (PSOA)**
Based on the social behavior of the swarm, the PSOA was developed. The optimization procedure is based on two parts. The first part is the evolutionary algorithm and the second one is the artificial life. The last one is based on five principles; Proximity, quality, diverse response, stability and adaptability. The process starts with an initial swarm for which the fitness values are calculated. In each iteration, the optimization variables are changed after which the fitness values are calculated again. The process is stopped when the end conditions are satisfied. A schematic overview of the process is shown in Figure 2.22 [35].

**Ant colony optimization (ACO)**
Ant colony optimization is an iterative optimization technique based on the behavior of ant colonies. The process that is optimized is divided into different options that can be chosen after each other. In the first iteration different ants, which represents an option, are following the line of the process and make their own choices. During the evaluation of this step, the choices are given a score based on the outcome. These scores are used in the next step to bias the new ants for making their choices. Repeating these steps gives a convergence to the optimal path that can be chosen which gives the most optimal design [36].

**Multi-objective robust design optimization (MRDO)**
This type of optimization technique is a collection of different optimization techniques based on mathematical optimization procedures. For a mathematical description of the problem, the minimum value of a vector is calculated. Probabilities are used to detect the optimum global value which makes the method robust compared to other methods [37].

Based on a comparison of the possibilities of each method and the results of different studies Awad et all. conclude that the MRDO method is the most suitable for design optimization [31]. Next to this, several mathematical optimization theories exist. These types of optimization theories are able to find a (local) optimum for a given function. For example, a function that is calculating the costs based on different parameters for the design of a structure. Different of these types of theories are described below.

**Newton-Raphson (NR) optimization**
Newton-Raphson method is a mathematical procedure to calculate the minimum and/or maximum values of a (multi variable) function. The method uses the first and second derivative of the function for which an optimum has to be found [38].

**Linear programming (LP) optimization**
Linear programming optimization is an optimization technique based on a linear cost function. This function in space has several boundary conditions based on the boundary conditions of the optimization problem. These boundary conditions are linear inequalities of the optimization variables. Within these boundaries, the minimum value for the cost function is calculated [39].

A more elaborate overview of optimization techniques used for structures is given by the research of Song et all. [40]. Next to this optimization with Abaqus is possible, in this program a special optimization module exists.

**Abaqus**
The optimization process that can be used in Abaqus is shown in Figure 2.23. Optimization can be done for topology, shape, size and bead based on an objective function, constraints and restrictions. Abaqus is searching for a given amount of cycles for the optimal design which satisfied the given constraints and restrictions [41].
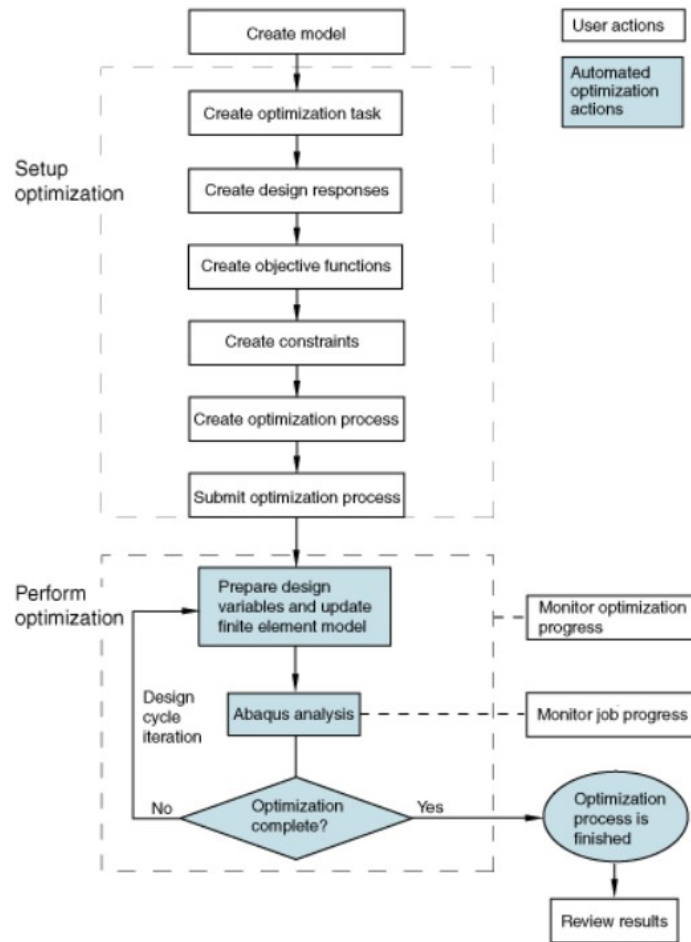
Figure 2.23: Overview optimization process Abaqus [41]

## 2.6. Discussion literature review

In the performed literature study it is shown that different types of connectors exist to connect an FRP deck to a steel structure, with a known performance based on tests and models. However, the forces which occur in these connectors are not well known at the moment. Different types of calculation methods that are available were described in this chapter and are used to calculate these forces in a more accurate way. Different investigations are described which can be used for simplification in the modeling of the sandwich bridge deck as an orthotropic plate. In this thesis, information is tried to deliver to close up the knowledge gap for the magnitude of the uplift forces in the bolted connections between FRP slabs and a steel structure.

For the second part of this research different optimization techniques are described. Next to the described techniques, different other (sub-) techniques exist. However, these techniques are less useful for the optimization of FRP structures or not used at the moment in this research field.

# PART I
## Uplift bolt forces

# 3

# Detailed numerical model

During the performed research, different models are made to calculate the uplift bolt forces. Chapter 3 describes the detailed numerical model that is used as a reference model throughout the research. Figure 3.1 shows an overview of the different models that are made with the model that is described in this chapter highlighted by the use of green boxes. The numerical model is made as detailed as possible, with modeling real geometry of the considered traffic decks. The numerical model is made with the FE software Abaqus. In the first section, the modeling steps are explained in the same order as the model is built in Abaqus. The second section contains the verification of the detailed numerical model. As a part of this, a small study is performed in which the model assumptions are verified. This study can be found in Appendix B. In the third section, the results obtained with this numerical model are given. The last section contains the discussion on these obtained results.
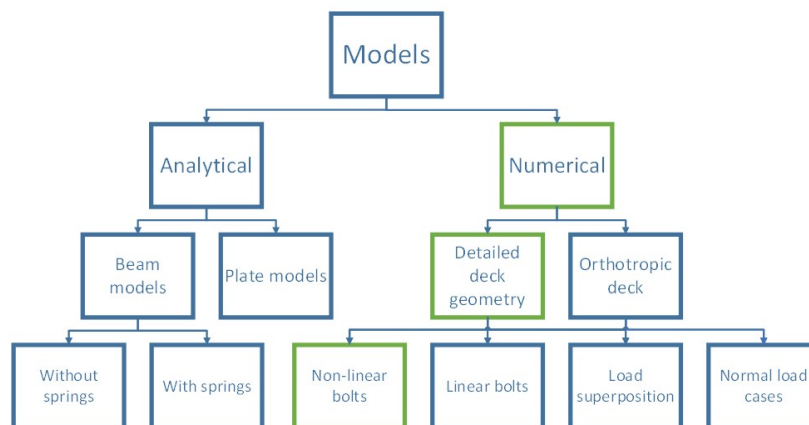
Figure 3.1: Detailed numerical model in overview models

## 3.1. Description of the detailed numerical model

This section describes the modeling steps and input values for Abaqus. The same order is presented as the order in which the model has to be built in the finite element software. For building the model, Python code is used which directs the CAE module of Abaqus. Using this modeling technique gives the opportunity to adapt the dimensions of the deck plates, locations of the bolts and the dimensions of the steel structure underneath. The layup orientation of the FRP can be changed as well, which is used in the optimization procedure as described in the second part of the thesis.

While building the model, different options are used and compared to each other to obtain the best suitable option for the given application. Three different types of elements are considered namely, solid, shell and continuum shell elements. The last elements were the most suitable given calculation time and accuracy and used therefore in this thesis. One element through thickness can be used for the skins and webs for the continuum shell elements. For the steel structure underneath, options are considered with fixed surfaces,

beam elements and modeling the geometry with the use of (continuum) shell elements. The results of this study are shown in Appendix B. Based on this study the beam elements are used to model the steel structure since they give the best performance compared to the calculation time needed. Bolts can be modeled in two ways. The first option is to model the geometry of the bolt, shank, head and nut, and make a hole in the steel structure and the deck plate at the locations where the bolts are placed. The behavior of the bolts can be modeled using contact definitions. Another option is to use wires, which is a connection option in Abaqus [41]. To this wire, a bolt section has to be assigned which represents the behavior of the bolts. For the detailed model, the wires are used since these give directly the forces in the bolts and it is a more stable option compared to the one with interaction properties for the modeled bolts, which gives often convergence errors. A comparison of the two modeling techniques is given in Section 3.2.1.

### 3.1.1. Limits and Assumptions
For the detailed numerical model, different assumptions are made. The shear forces are taken by shear studs, which are placed at the end of the deck plates. The shear studs are not modeled since the horizontal forces are not considered. Therefore, it is assumed that the bolts only take tension forces. This assumption is allowed since the bolted connections are designed to take only tension force. Next to this, the dimensions of the steel structure underneath are assumed as average values, based on reference projects of FCE since in most cases these dimensions will be different [2]. It is also assumed that the considered load models are the only ones or are governing and no special vehicles need to be taken into account. Some limits are given for the model which is made as well, which are given by limits from FCE (for example from the production). The model is only suitable for deck plates made with the InfraCore technology. Only traffic decks are considered and not bicycle and pedestrian bridges. For the traffic decks, only the mid part of the deck is considered, the edges, flanges and possible bicycle and/or pedestrian lanes are out of the scope.

### 3.1.2. Geometry
The dimensions of the deck are chosen to be large enough to be able to consider the uplift forces in the bolts. However, the dimensions may not be too large otherwise the calculation time needed will be too long. At FiberCore Europe, there is earlier research done on the forces in the bolts, using an orthotropic plate for modeling the deck [3]. To be able to compare the results with the results obtained from the research of Fiber-Core Europe, the same dimensions are used. These dimensions are shown in Figure 3.2 and Table 3.1, which are standard dimensions used in projects of FiberCore Europe as described in the section about the traffic decks in Chapter 2.

Table 3.1: Dimensions Abaqus model

| Dimension | Value | Unit |
|---|---|---|
| Length | 4500 | mm |
| Width | 4500 | mm |
| Height ot the deck | 120 | mm |
| Number of webs | 38 | - |
| Spacing webs | 116 | mm |
| Number of I-beams | 6 | - |
| Number of C-beams | 9 | - |
| Width I-beams | 100 | mm |
| Width C-beams | 50 | mm |
| Number of bolts | 18 | - |
| Diameter bolts | 20 | mm |

Underneath the FRP deck, a steel structure is modeled which consists of I-beams with a spacing of 850 $mm$ and a height of 400 $mm$ acting as the main girders. The I-beams are modeled with beam elements in Abaqus, using the profile of an IPE beam. For secondary beams, C-beams are used with a height of 200 $mm$. The C-beams are modeled with beam elements as well, with the shape of a C-profile. The distance and other dimensions of the beams are shown in Figure 3.2. Modeling the I- and C-beams with beam elements gives the opportunity to reduce the complexity of the model and at the same time, the deformation of the beams can be calculated, which has an influence on the total deformation of the deck.

(a) Top view geometry modeled deck [*mm*]

(b) Bolt numbers and bolt rows

(c) Side view geometry modeled deck [*mm*]

(d) Intersection A-A geometry modeled deck [*mm*]

Figure 3.2: Geometry of the modeled deck

The bolts are modeled as wire connectors with an influence radius of the radius of the bolts that are used in the projects as shown in Figure 3.3. Due to the fact that the bolts only work for tension, the nonlinear behavior of the bolts is modeled. For a positive displacement, which means elongation of the bolt, a high stiffness value of $10^6$ $N/mm$ is given. Using a high value for the stiffness guarantees that the bolt will take all the force which can occur. For a negative displacement, which means a shortage of the bolt, a small stiffness value of $10^{-6}$ $N/mm$ is given and the bolt does not transfer forces bigger than this applied value, which means that the compression forces can be neglected. The distance between the bolts in the longitudinal direction is 1740 $mm$ and in the transverse direction 498 $mm$. The complete bolt pattern is shown in Figure 3.2a.
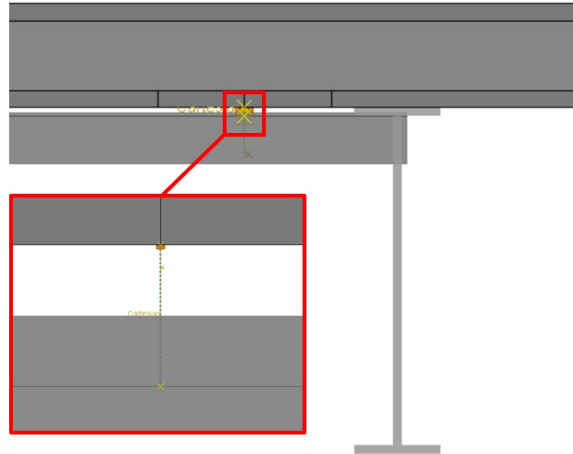


Figure 3.3: Wire connection Abaqus

### 3.1.3. Material properties

The main load-bearing structure is made out of steel and has steel properties as shown in Appendix A, Table A.2. Ply orientation and ply thickness for each of the skins of the deck and the web are given in the appendix as well, in Tables A.3 and A.4. These layups are used from a reference project of FiberCore Europe as described in Section 7.2.2.

### 3.1.4. Boundary conditions

Boundary conditions for the deck are modeled as for the worst-case scenario. Since it is unknown if the plate is a separate produced plate or part of a bigger plate, boundary conditions are used for the case of one separate plate. In Figure 3.2a, a part of the rest of the structure is drawn to visualize where the boundary conditions come from. The deck edges are free in all directions representing a free plate. The I-beams are restricted in all displacement directions at both ends, representing continuous beams. The choice of boundary conditions will have an effect on the results. When the modeled deck is part of a bigger plate, the deformations will be lower, due to the difference in boundary conditions, and therefore the forces in the connectors as well. The modeling of the boundary conditions in Abaqus is shown for one side of the deck in Figure 3.4. For the other side of the slab, the boundary conditions are the same.

### 3.1.5. Interaction properties

To connect the I-beams with the C-beams, tie constraints are used to fix all displacement degrees of freedom, since in practice the connection is made by welding. The same type of tie constraints are used to connect the deck on the I-beams. In reality, this connection is made by simply placing the deck on top of the beams. This means that the connection can only transform compressive forces and no tension forces. The influence of this type of modeling only occurs when the deck gets free from the beams. However, this will not happen due to the own weight and the fact that in real cases pre-loading of the bolts is applied. Therefore, this type of modeling can be used without influencing the results.

### 3.1.6. Loads

Different load cases are considered which are described in the Eurocode EN-1991-2 [4].
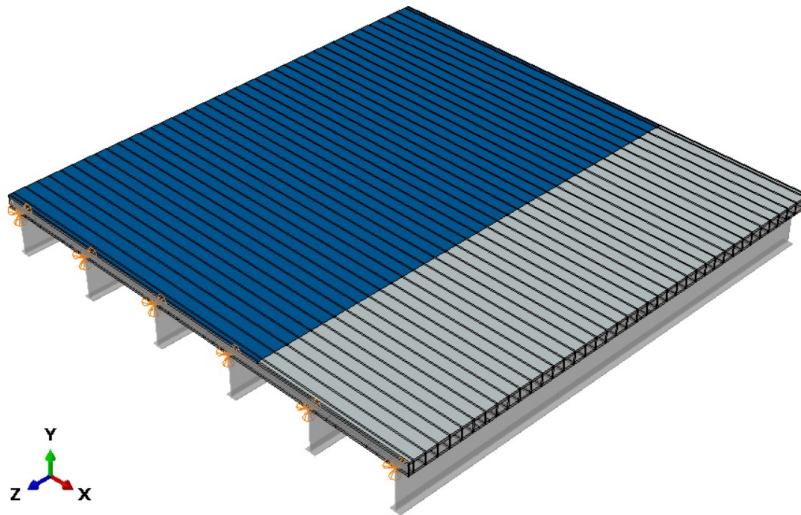
Figure 3.4: Overview boundary conditions and lanes detailed numerical model

**Load model 1**

According to the Eurocode, the deck has to be separated into lanes. Each lane is three meters wide. The first lane has the highest load, which has to be chosen at the most unfavorable position. The two axles at the first lane have a load of 300 $kN$, at the second line 200 $kN$ and at the third lane 100 $kN$. For the other lanes, no extra axle has to be considered. At the same time, an uniformly distributed load has to be considered. At the first lane 9 $kN/m^2$ and at the other lanes 2.5 $kN/m^2$. The geometry of the axles is given in Figure 3.5a.

Due to the small width of the deck that is considered, namely 4.5 $m$, only the axle load of 300 $kN$ is considered in this case. At this lane, the uniformly distributed load of 9 $kN/m^2$ is taken into account. The rest of the deck is loaded with an uniformly distributed load of 2.5 $kN/m^2$. The lane which is considered in the research is highlighted in blue in Figure 3.4 [4].
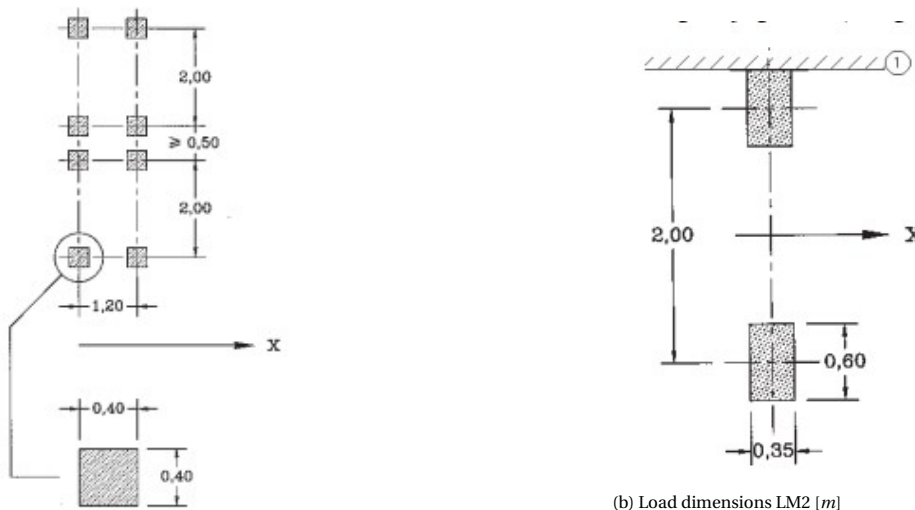


(a) Load dimensions LM1 [$m$]



(b) Load dimensions LM2 [$m$]

Figure 3.5: Dimensions load models [4]

**Load model 2**

For each location on the deck one axle load of 400 $kN$ has to be considered. The dimensions and distance between the two wheels are given in Figure 3.5b. Since the load has to be place at each location of the deck, the lanes on the deck, indicated in Figure 3.4 are not considered [4].

**Load model 3**
Special vehicle: This load case is not considered because in general it is not known which special vehicle has to be considered. For specific projects this load case has to be added.

**Load model 4**
Load model 4 is about a crowd on a bridge. For this load case a uniformly distributed load of 5 $kN/m^2$ has to be used for the whole deck. This load has to be applied as a static load in a separate load case [4].

**Considered load cases**
For the performed calculations, three different load cases are considered based on the models of the Eurocode. Load model one is considered at one location on the deck as is stated in the Eurocode, half a meter from the side of the deck. This load case is visualized in Figure 3.6. Load model two has to be placed at any location on the deck, therefore two locations are considered. One location directly at the side of the deck to be able to obtain the behavior in the moving direction of the load. The other one is at the middle of the deck, which will give the highest forces in the bolts. These load cases are shown respectively in the Figures 3.7 and 3.8.
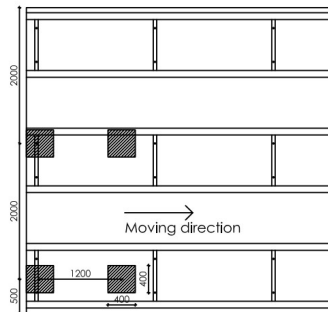


(b) Load model 1 side view



(a) Load model 1 top view

Figure 3.6: Load model 1
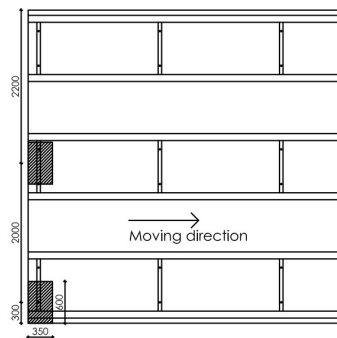


(b) Load model 2 case 1 side view



(a) Load model 2 case 1 top view

Figure 3.7: Load model 2 case 1
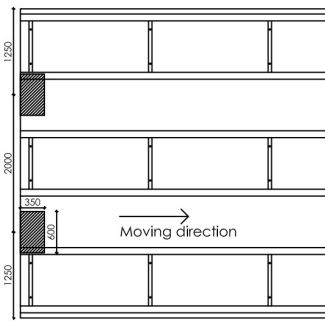
Load model 2 case 2

(a) Load model 2 case 2 top view
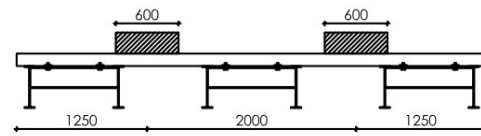


Load model 2 case 2

(b) Load model 2 case 2 side view

Figure 3.8: Load model 2 case 2

### 3.1.7. Mesh

The type of elements that are used for the deck is the continuum shell elements SC8R. This is an 8-node quadrilateral in-plane general-purpose continuum shell element with reduced integration and hourglass control. The I-beams are modeled with beam element B31, a 2-node linear beam element in space. For the C-beams, the same type of elements as for the I-beams are used.

The mesh size for the deck is considered as 30 mm and the mesh size for the I- and C-beams is considered as 30 mm as well to prevent discontinuities. This means that one element through-thickness is used for the skins and webs, which is enough for continuum shell elements. However, at the location of the bolts (wires) for the deck, locally the mesh size is reduced to see the influence of the bolts and bolt forces which is shown in Figure 3.10. The justification of the chosen mesh size is shown in 3.1.8. A 3D view of (part of) the mesh for the slab, with a mesh size of 30 mm, is shown in Figure 3.9.
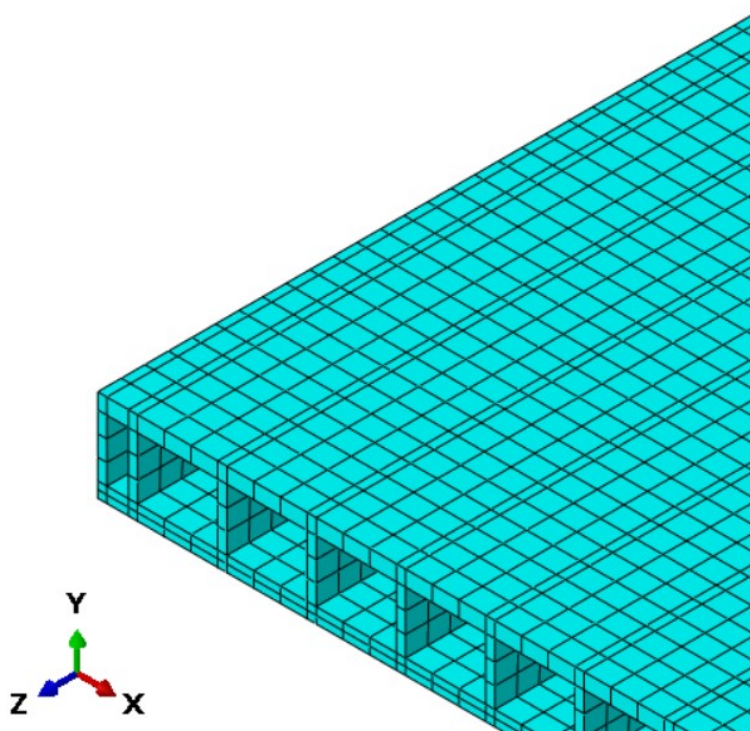


Figure 3.9: 3D view mesh (30 mm)
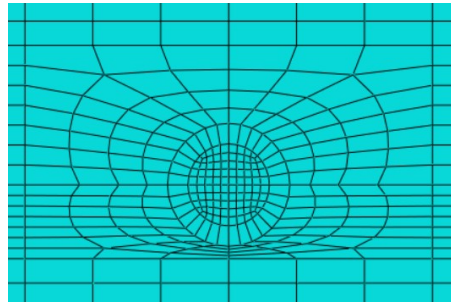
Figure 3.10: Mesh around bolts
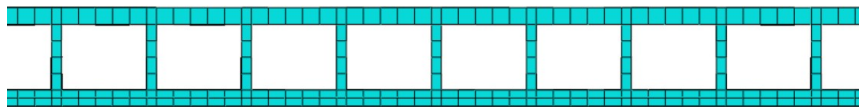


(a) Side view mesh 20 $mm$
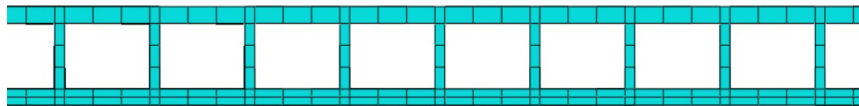


(b) Side view mesh 30 $mm$
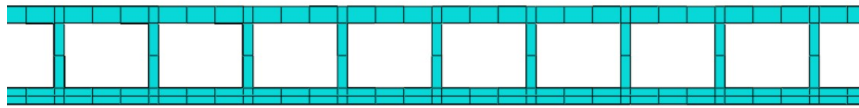


(c) Side view mesh 40 $mm$
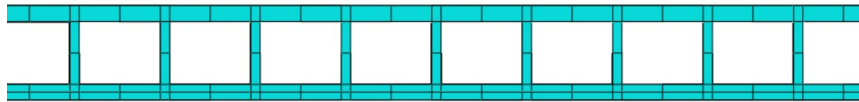


(d) Side view mesh 50 $mm$

Figure 3.11: Side views different mesh sizes

### 3.1.8. Mesh refinement study

To be able to know which element size is small enough to obtain accurate enough results, a mesh refinement study is performed. For this study, load model 2 case 2 is used. The study is started with a mesh size of 50 $mm$ and the mesh size is reduced by 10 $mm$ each step. The maximum bolt forces for each bolt are shown in Figure 3.12 for all obtained mesh sizes.
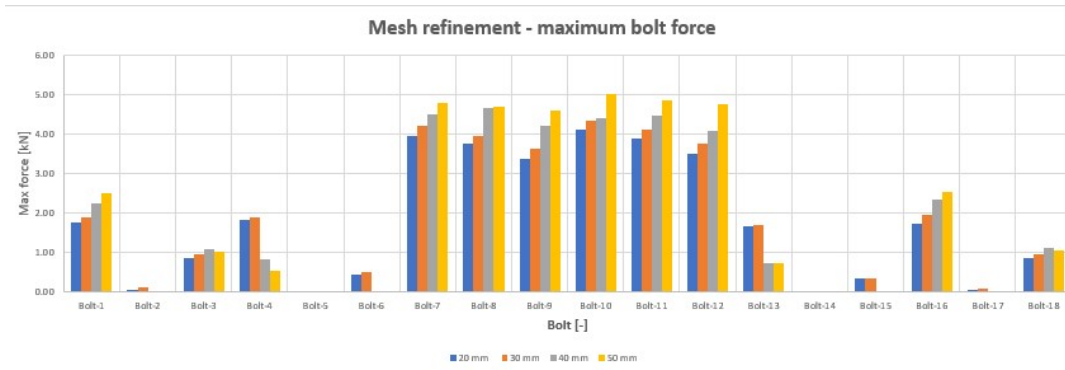
Figure 3.12: Results of the mesh refinement study for the maximum bolt forces per bolt [$kN$]

The deck is partitioned in Abaqus to obtain a good mesh with cubic shaped elements, which is shown in Figure 3.11 for the different mesh sizes obtained. In the bottomskin, two elements through-thickness are used by Abaqus. This is not desirable for continuum shell elements but due to the location of the bolts and the refined mesh in these places, it is not possible to make a mesh with only one element through-thickness.

Since the bolt forces are related to the deformation of the slabs, the deformation is considered in the mesh refinement study as well. Figure 3.13 shows the maximum deformation of the deck for the different mesh sizes. In Figure 3.14, the absolute difference is shown relative to the deformation of the model with a mesh size of 20 $mm$.
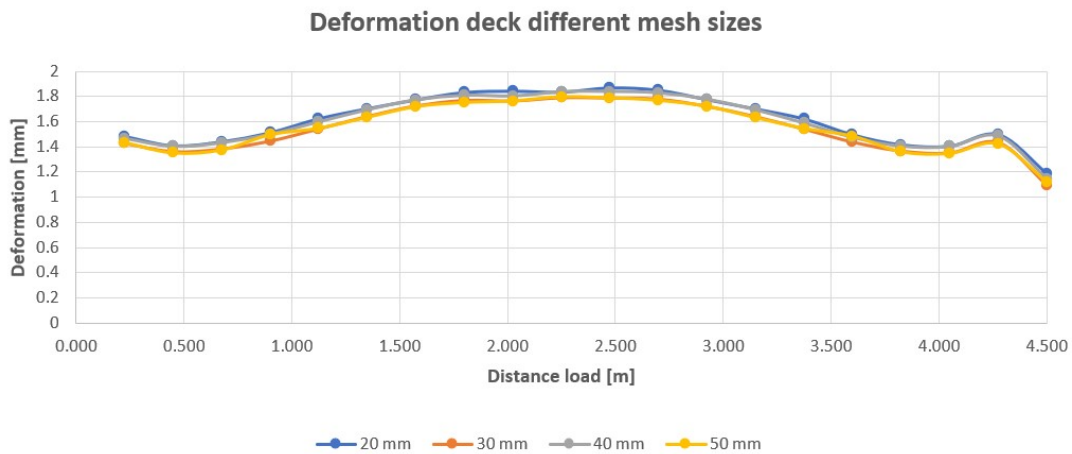


Figure 3.13: Results of the mesh refinement study for the deformation of the deck deck for load model 2 case 2
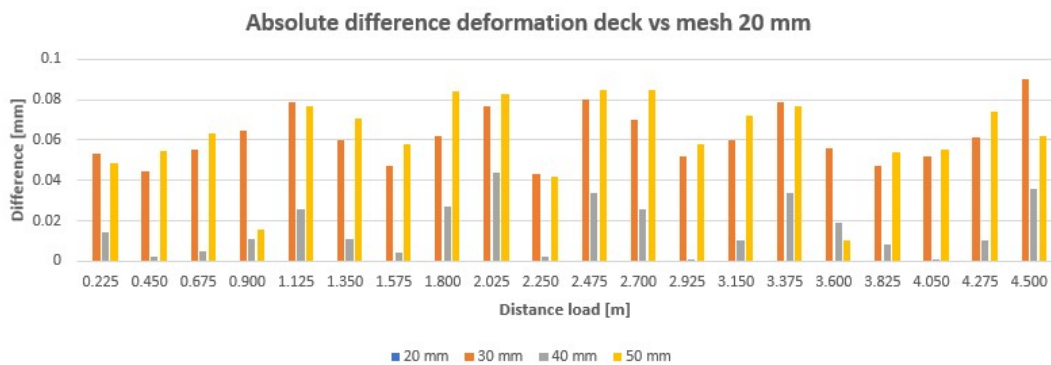


Figure 3.14: Results of the mesh refinement study for the absolute difference of the deformation of the deck for load model 2 case 2

**Discussion and conclusion on mesh refinement study**

Observing the results of the mesh refinement study for the bolt forces, it is shown that the magnitude of the forces decreases with decreasing mesh size. This is due to the influence of asymmetric results and disturbing elements. Since both the applied load case, load model 2 case 2, and the used deck are symmetric, the obtained results must also be symmetric. Considering the bolt forces shown in Figure 3.12 while taking the locations of the bolts, shown in Figure 3.2b, into account, it is shown that the smaller the mesh size, the more symmetric the results become. For asymmetric results, some of the bolt forces will be higher and therefore a coarser mesh will result in higher bolt forces.

Next to this, a coarser mesh will increase the change on (some) disturbed elements. The smaller the elements, the more ideal shapes can be made. Since different partitions have to be done and the webs are connected to the skins, less ideal-shaped elements will be made when increasing the element size. As a result of this, unequal load transfer can take place which means that more load is transferred to one side of the element than to the other side. This result in higher maximum forces in some bolts. Apart from these project dependent issues, in general, the results become more accurate for smaller mesh sizes [41].

Figure 3.13 shows the maximum deformation for the different observed mesh sizes. In this graph, a similar shape and magnitude of the results are shown for the different mesh sizes. Figure 3.14 shows the maximum absolute difference for each distance of the load on the deck. For the considered mesh sizes, a discontinuous behavior is observed without convergence. This is due to the same reasons as for the bolt forces. One element size will fit better for a certain web spacing compared to another element size due to the mesh size compared to the web spacing. For example, a web spacing of 100 mm will have good elements with a size of 20 mm or 50 mm but less ideal shaped elements when a mesh size of 30 mm or 40 mm is used.

As a result of the mesh refinement study, it can be concluded that a mesh size of $30mm$ gives accurate enough results for the bolt forces. Using a smaller mesh size the computation time needed for the model will increase even more while the results do not become more accurate. However, the mesh refinement study on the deformation shows a discontinuous behavior. This makes it difficult to base a good conclusion on this. However, the deformations are not considered the main objective in this study and therefore the conclusion is based on the study of the bolt forces.

### 3.1.9. Overview model Abaqus

Figure 3.15 shows the detailed numerical model which is made in Abaqus with the dimensions that are considered.
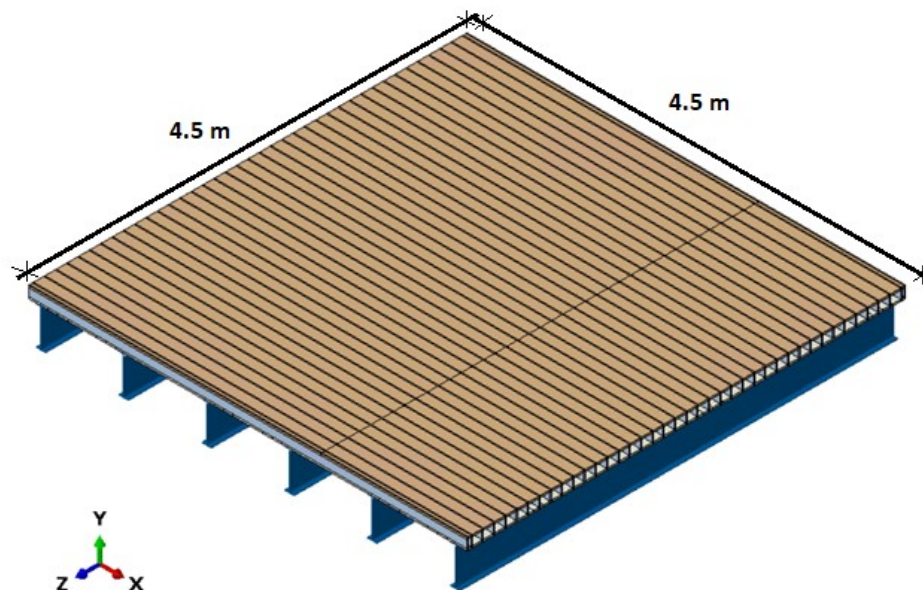


Figure 3.15: 3D view detailed numerical model Abaqus

## 3.2. Verification of the detailed numerical model

To be able to trust the model, a verification study is done. First, the modeling assumptions are verified with smaller models after which, the deformations are checked with other types of (analytical) models. This study is given in Appendix B. Next to this, a comparison is made between the modeling with different bolt options and a comparison between different types of models which are described in Chapter 4 and 5

### 3.2.1. Comparison models with bolts and with wires

Another type of modeling the bolts is by the use of solid elements to model the geometry of the bolts and making (oversized) holes in the different elements. The interaction between the head of the bolt and the steel beam can be modeled with interaction properties in Abaqus and the same has to be done for the interaction between the nut or plate at the end of the bolt and the deck plate. Two types of behavior have to be specified for this namely tangential and normal behavior. The tangential behavior is described with a friction coefficient. This takes the friction between the bolt and the beam or slab into account. The other behavior is the normal behavior which can be specified with hard contact between the different elements. In this way, the nut or head of the bolt cannot go through the deck plate or steel beam.

Using this type of modeling, the stresses in the bolts can be determined. Multiplying the stresses with the area of the bolt gives the force in the bolt. Bending can be taken into account when a small enough element size is used. The bolts can be pre-loaded as well. This can be done by adapting the length of the bolt or by the use of thermal behavior [41]. The main disadvantage of this type of modeling is the difficult behavior of the contact definitions. Abaqus cannot always find a solution and the solid elements will enlarge the calculation time needed. For this reason, wires are used in this research.

### 3.2.2. Comparison deformations calculated with different models

Due to the fact that rigid supports at the place of the I-beams are considered in the analytical beam model, the deformation of the I-beams in the Abaqus model is subtracted from the total deformation of the deck. The results and comparison are given in Table 3.2 for the maximum deformation of the plate for the different load cases. It is shown that the maximum deformation calculated with ElamX, is a bit lower compared to the one calculated with Abaqus. This will be due to the fact that in ElamX a massive plate is assumed, which is not the case in Abaqus. In general, the deformations calculated with a plate model are lower than the beam models. The comparison indicates that the deformations are in the right order of magnitude.

Table 3.2: Comparison of deformation for different models

| deformation [mm] | Load model 1 | Load model 2 case 1 | Load model 2 case 2 |
|---|---|---|---|
| MatrixFrame | 1.7 | 1.9 | 1.8 |
| ElamX | - | - | 1.74 |
| Abaqus total | 6.220 | 2.113 | 5.087 |
| Abaqus I-beams | 4.609 | 0.700 | 3.254 |
| Abaqus deck | 1.611 | 1.413 | 1.833 |
| Difference MF [%] | 5.5 | 34 | 1.8 |
| Difference ElamX [%] | - | - | 5.1 |

## 3.3. Results detailed numerical model

The model is run with load models 1 and 2 as described in section 3.1.6. Load model 4 is not used because this load model does not give uplift forces due to the uniformly distributed load. For load model 2, two cases are considered. For case one the axle is placed at the same location as for load model 1. The second case has the axle placed in such a way the wheels are placed at the spans where no bolts are placed, which gives the highest uplift forces for this load model. In the sub-sections, first the deformations are shown since the obtained bolt forces are related to the deformations. Considering the deformations gives an extra check for the magnitude of the forces. Next to the deformations, the actual bolt forces are given and discussed.

### 3.3.1. Deformations

Deformations caused by the considered load models are given in Table 3.3. For each load model, the total observed deformation is shown which is including the deformation of the steel structure underneath. Next to this, the deformation of only the slab is shown which is called the deformation of the deck. This deformation

is calculated as the total deformation minus the deformation of the steel supporting structure. For load model one an example of the results is shown in Figure 3.17. Figure 3.16 shows the maximum deformation of the deck for the considered load models for different distances of the vehicle placed on the deck.

Table 3.3: Deformation of the deck for different load models

| Deformation [mm] Distance [m] | Load model 1 | | Load model 2 case 1 | | Load model 2 case 2 | |
|---|---|---|---|---|---|---|
| | Total | Deck | Total | Deck | Total | Deck |
| 0.225 | 1.803 | 1.416 | 2.064 | 1.405 | 1.906 | 1.460 |
| 0.450 | 2.122 | 1.329 | 2.435 | 1.096 | 2.296 | 1.389 |
| 0.675 | 2.583 | 1.344 | 2.889 | 0.872 | 2.782 | 1.419 |
| 0.900 | 2.922 | 1.347 | 3.327 | 0.688 | 3.260 | 1.484 |
| 1.125 | 3.432 | 1.417 | 3.927 | 0.667 | 3.769 | 1.584 |
| 1.350 | 4.021 | 1.477 | 4.528 | 0.723 | 4.230 | 1.687 |
| 1.575 | 4.694 | 1.527 | 4.990 | 0.757 | 4.588 | 1.763 |
| 1.800 | 5.285 | 1.521 | 5.359 | 0.766 | 4.874 | 1.809 |
| 2.025 | 5.776 | 1.480 | 5.562 | 0.758 | 5.014 | 1.806 |
| 2.250 | 6.281 | 1.540 | 5.665 | 0.790 | 5.087 | 1.833 |
| 2.475 | 6.424 | 1.456 | 5.592 | 0.799 | 5.028 | 1.829 |
| 2.700 | 6.330 | 1.302 | 5.366 | 0.777 | 4.882 | 1.819 |
| 2.925 | 6.288 | 1.197 | 5.001 | 0.756 | 4.600 | 1.766 |
| 3.150 | 6.494 | 1.360 | 4.545 | 0.718 | 4.245 | 1.686 |
| 3.375 | 6.365 | 1.497 | 3.945 | 0.656 | 3.785 | 1.582 |
| 3.600 | 6.220 | 1.611 | 3.308 | 0.632 | 3.270 | 1.475 |
| 3.825 | 5.816 | 1.599 | 2.859 | 0.798 | 2.784 | 1.401 |
| 4.050 | 5.223 | 1.564 | 2.456 | 1.076 | 2.314 | 1.385 |
| 4.275 | 4.608 | 1.523 | 2.113 | 1.413 | 1.942 | 1.469 |
| 4.500 | 3.966 | 1.424 | 1.357 | 1.208 | 1.239 | 1.118 |
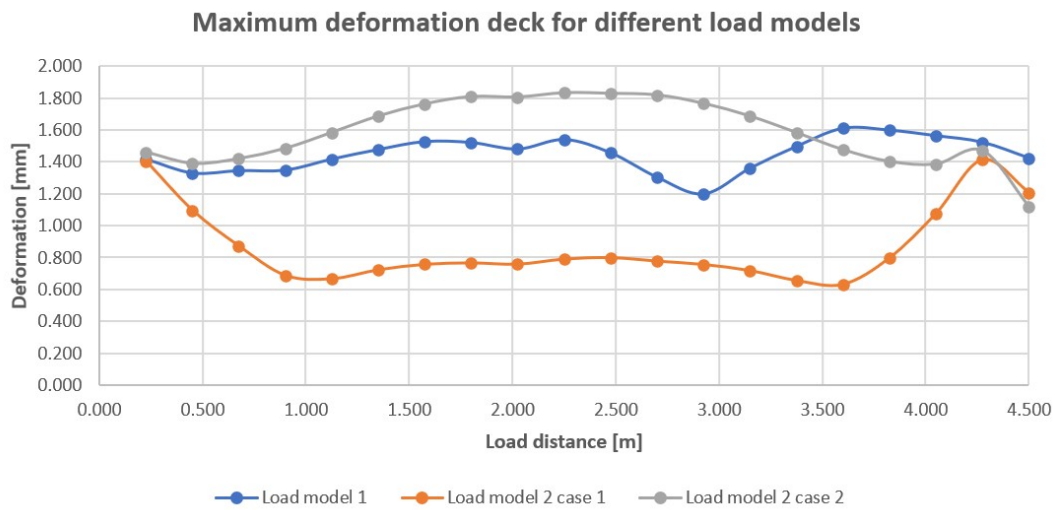


Figure 3.16: Deformation of the deck for different load models
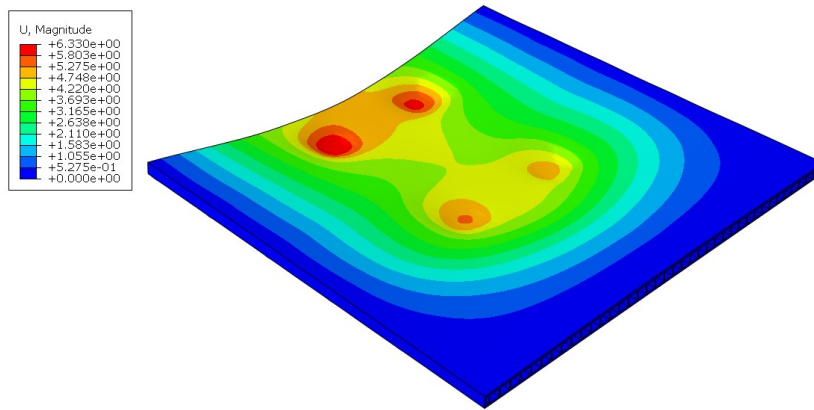
Figure 3.17: Deformation of the deck for load model 1 with vehicle at t=2.70 [$mm$]

### 3.3.2. Bolt forces

With the model made in Abaqus and the described load models, the bolt forces are calculated. The Figures 3.18 up to and including 3.21 show the obtained results for the time when the axle is passing. The chosen speed is 1 $m/s$, which means that the time is equivalent to the distance the axle has moved over the deck. For the first load model, two calculations are done to see the difference between the case with and without the uniformly distributed load as described in the Eurocode.

In the graphs the highest calculated force is added. Next to the graph, the critical load position is shown for the relevant load model. The bolt(s) where the maximum force occurs is/are highlighted with a red circle. Considering the graph in Figure 3.18, it is shown that the maximum load is 0.49 $kN$ which occurs in bolt 14. At the same time, the second-highest force is 0.32 $kN$ which occurs in bolt 17 which is located in the same row. This force is about 35 % lower compared to the force in bolt 14 since the upwards deformation at that location is lower. Next to the forces in row 2, (smaller) forces occur in the bolts 13 and 16 in span 5 of the first row. A more in-depth discussion of the bolt forces is described in Section 3.4.1 where the bolt forces are separated for the different bolt rows.
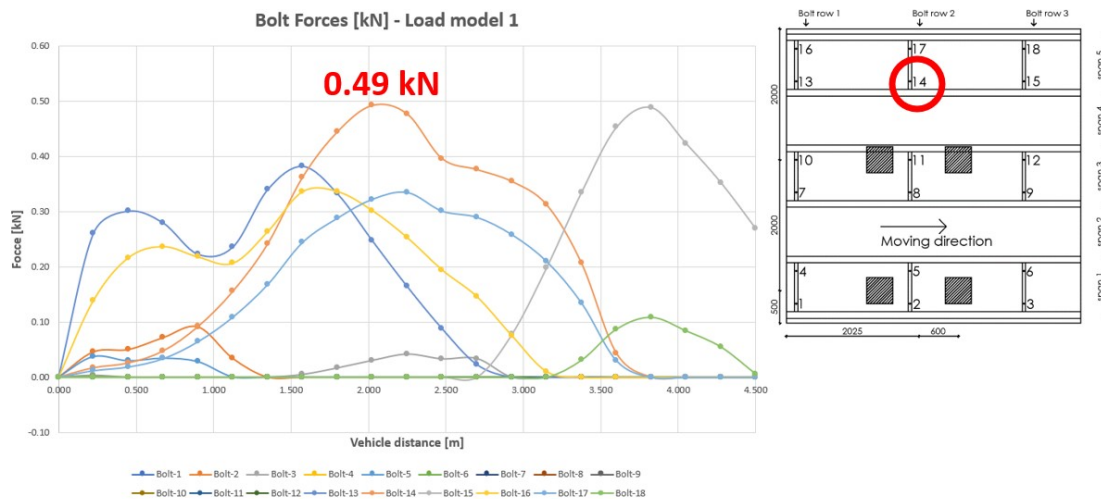


Figure 3.18: Bolt forces load model 1 including UDL

When the uniform distributed load is excluded from the calculation, it is shown that the magnitude of the forces obtained is higher. The maximum force, 0.75 $kN$ in bolt 15 shown in Figure 3.19, is obtained in the same span but in a different bolt row. At the same loading position, the second-highest force is 0.36 $kN$, approximately 50 % lower, occurring in bolt 18. Next to these forces, there are some smaller forces in bolts in the other rows. When the UDL (uniform distributed load) is excluded, forces in the bolts placed in the loaded

spans one and three are visible when the vehicle is not placed above these bolts.
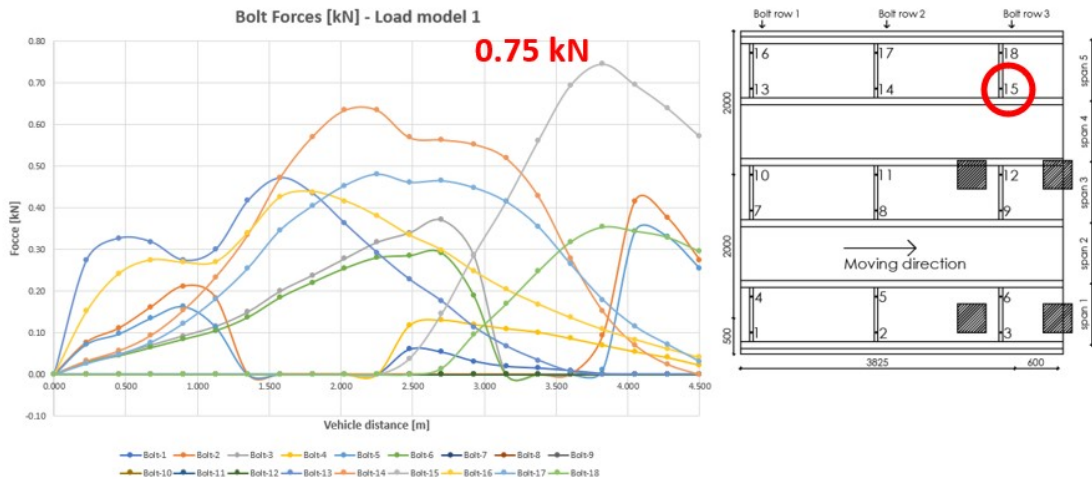


Figure 3.19: Bolt forces load model 1 excluding UDL

Figure 3.20 shows the results for load model 2 case 1. The maximum bolt force of 2.02 $kN$ occurs in bolt 5. For the same load location forces between 1 and 1.5 $kN$ occurring in the bolts 2, 3 and 6. These bolts are all located around the location where the wheel is placed in span 1. This indicates that the bending in the direction of the moving load is higher than the bending in the direction perpendicular to the load. A more in-depth investigation of this observation is given in Section 3.4.1. Next to these forces, smaller forces are obtained for the bolts in span 5.
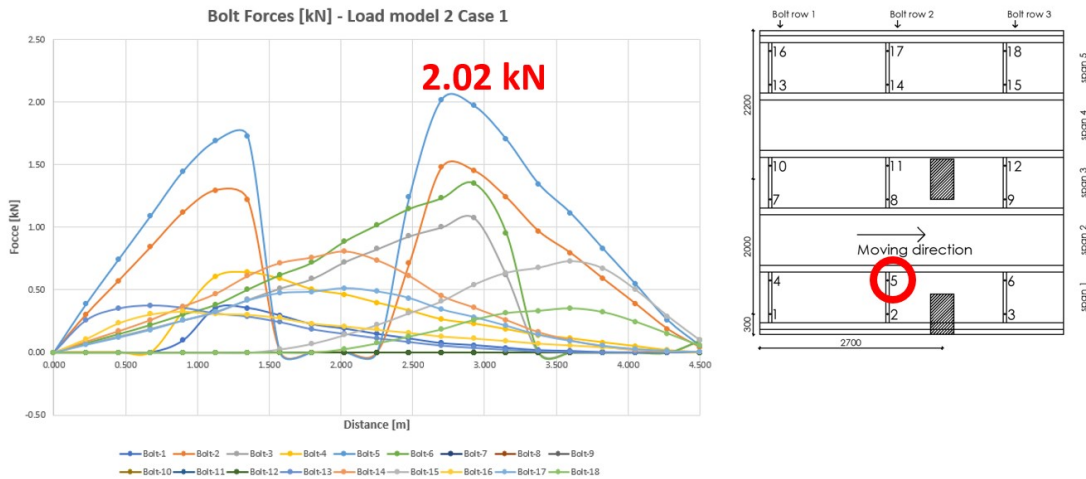


Figure 3.20: Bolt forces load model 2 case 1

Since the considered deck is symmetric in the width direction, symmetric bolt forces are obtained in one direction when placing the load in the middle of the deck as shown in Figure 3.21. The maximum force of 4.2 $kN$ is obtained in the bolts 7 and 10. The second-highest forces, with a magnitude of about 2 $kN$, are obtained in bolts 4 and 13. The lowest forces are obtained in the bolts 1 and 16 since the upwards deformation is smaller at that location. As shown in the graph, only the bolts in one row are active for this load case. This indicates that the effective width is lower than the distance between the bolts.
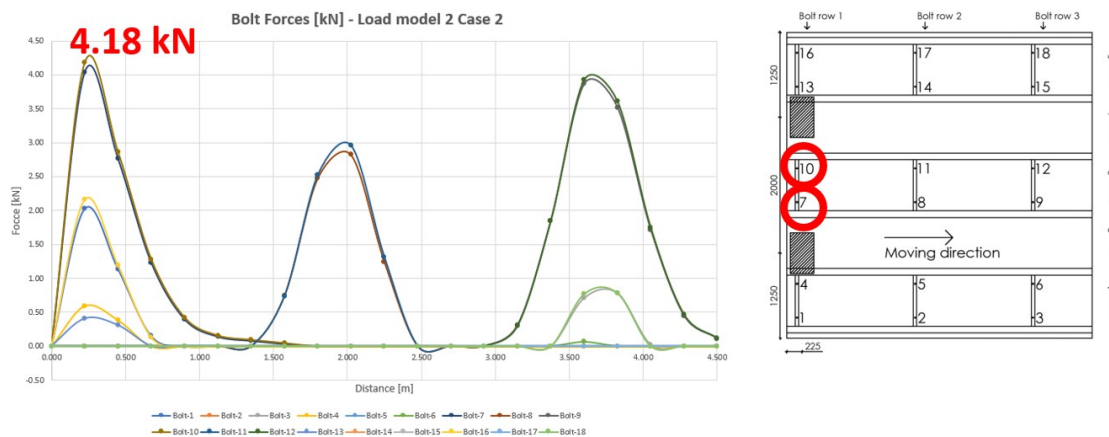
Figure 3.21: Bolt forces load model 2 case 2

## 3.4. Discussion detailed numerical model

To be able to trust the results, a verification needs to be performed. First, a mesh refinement study is done to be able to choose the appropriate mesh size which is described in Section 3.1.8. Next to this, the forces are subtracted for different bolt rows to observe patterns and an extra beam model is made with Abaqus to obtain the differences in results for plate models and beam models which are described in Section 5.1.

### 3.4.1. Discussion bolt forces

Between the I-beams, five spans are made with the FRP deck as shown in Figure 3.2. For load model 2 case 2, the second and fourth spans are loaded due to the wheel loads, wherefore uplift forces are expected in all the bolts in a row. Based on the deformations, the highest forces will occur in the bolts in the mid-span (span 3) when the axle is passing the row of bolts. Figure 3.21 shows this is the case. Lower forces occur in the bolt rows of the outer spans (spans 1 and 5) close to loaded spans. Bolt forces are lower in the bolts close to the middle of the deck which is due to the effect on the global deformation of the deck by the deformation of the steel structure underneath.

Considering the other load cases that are used, the force in the bolts in the third span has to be zero due to the type of loading. In Figures 3.19 and 3.20 it is shown that this is the case. Next to this, the forces in the bolts in the first span have to be zero as well when the axle is passing by. The drop of the lines for the bolt forces shows a clear drop at these locations which indicates that this is correct.

Next to these global checks, a comparison between the bolt rows is made for each load model. For load model one, this is shown in the Figures 3.22 until 3.24. On the left side of these figures, the forces in the bolts are plotted against the position of the center of the vehicle at the deck. On the right side, the critical loading condition for this specific bolt row is shown. Each of the three graphs shows the same pattern for the forces in the bolts, however, this pattern is shifted with the distance between the bolt rows. The biggest forces occur in the unloaded span and two peaks are shown with an internal distance of approximately 1.2 $m$ which is the distance between the two axles of the load model. The forces are lower for the first bolt row, at the edge of the deck, since only at one side of the bolt row the load is placed.
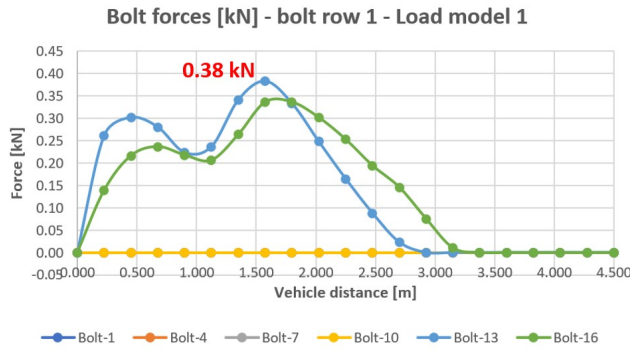
(a) Bolt forces LM1 including UDL bolt row 1 [kN]
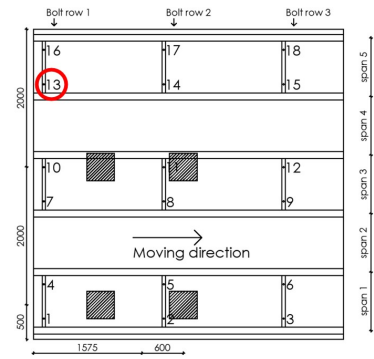
(b) Load position maximum forces bolt row 1 LM1

Figure 3.22: Bolt forces LM1 including UDL row 1
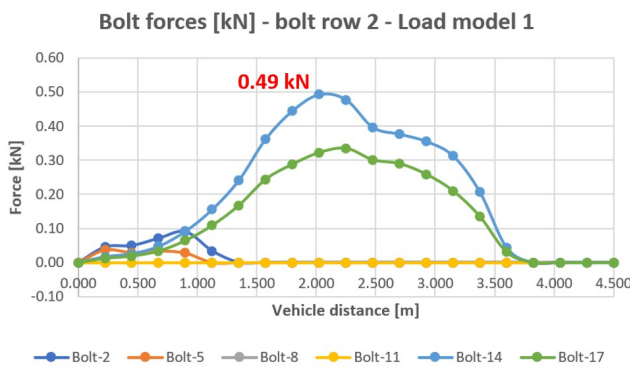


(a) Bolt forces LM1 including UDL bolt row 2 [kN]
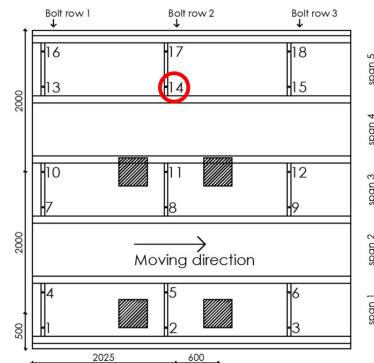
(b) Load position maximum forces bolt row 2 LM1

Figure 3.23: Bolt forces LM1 including UDL row 2
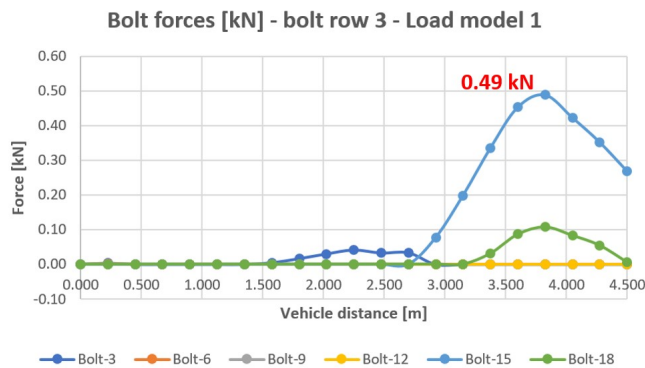


(a) Bolt forces LM1 including UDL bolt row 3 [kN]
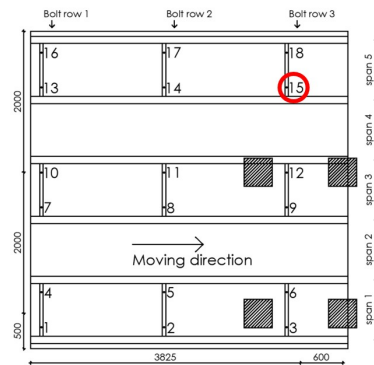
(b) Load position maximum forces bolt row 3 LM1

Figure 3.24: Bolt forces LM1 including UDL row 3

The same distinction between the bolt rows is made for the case with load model 1 without the uniform distributed load. By comparing these graphs, Figure 3.25 until 3.27, to the graphs with the uniform distributed load, it can be seen that the forces are higher. The distributed load gives a downwards deformation of the deck and therefore, the total upward deformation due to the wheel load is lower and so are the forces.

(a) Bolt forces LM1 excluding UDL bolt row 1 [kN]
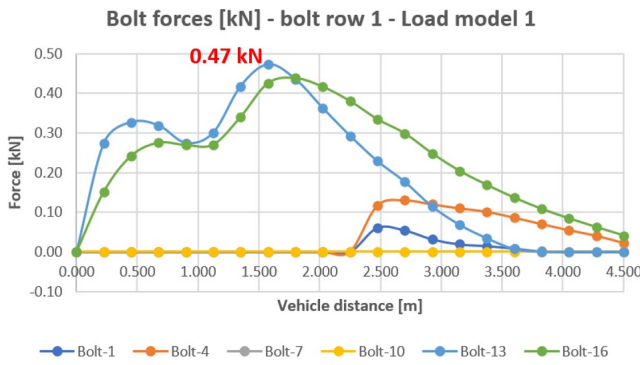
(b) Load position maximum forces bolt row 1 LM1

Figure 3.25: Bolt forces LM1 excluding UDL row 1
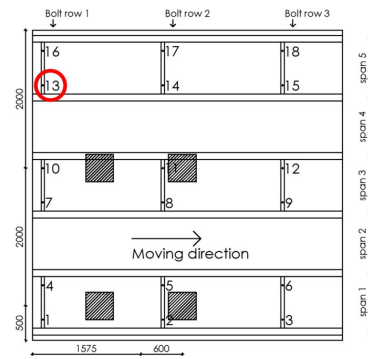


(a) Bolt forces LM1 excluding UDL bolt row 2 [kN]
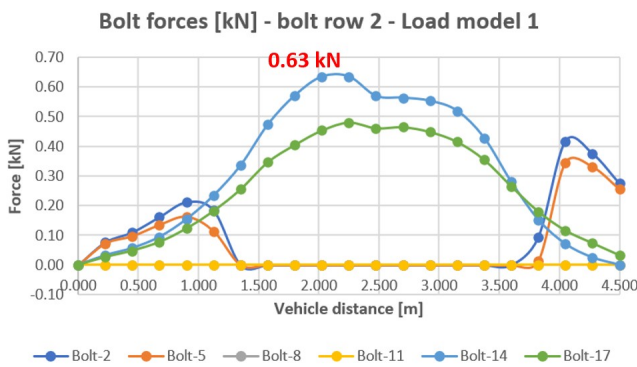
(b) Load position maximum forces bolt row 2 LM1

Figure 3.26: Bolt forces LM1 excluding UDL row 2
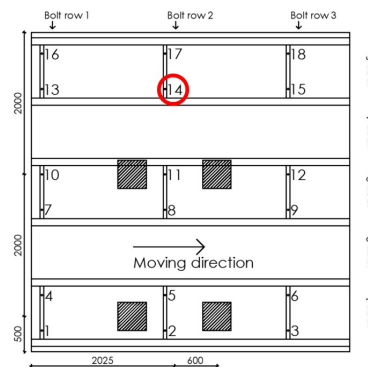


(a) Bolt forces LM1 excluding UDL bolt row 3 [kN]
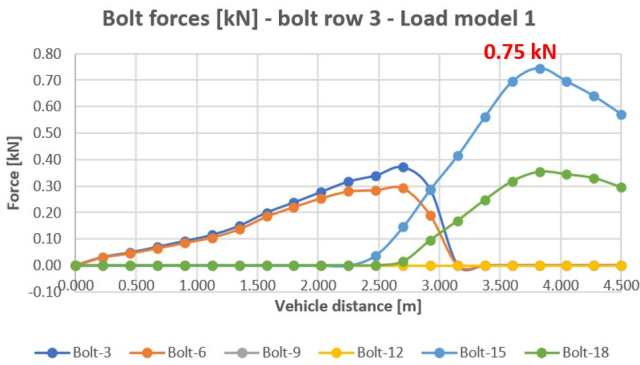
(b) Load position maximum forces bolt row 3 LM1

Figure 3.27: Bolt forces LM1 excluding UDL row 3
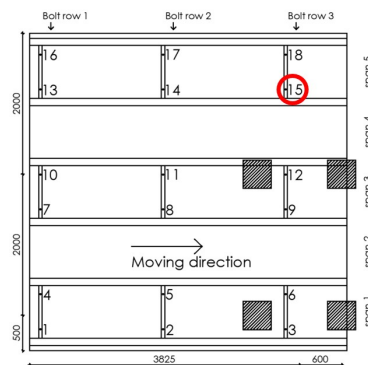
The same type of visualization of the results for load model 2 is done which is shown in Figures 3.28 until 3.30 for the first case of load model two and in Figures 3.31 until 3.33 for the second case of load model two. For the second case, it shows the clear pattern as described earlier and it gives the maximum load positions at the location of the bolt rows. For the first case of load model 2, the three graphs show the same pattern for the maximum forces in the fifth span, which is unloaded at the location of the bolt rows.

Next to this, another pattern is observed which gives even higher forces. In the bolts in the first span, which is a loaded span for this case, forces occur as well. When the axle is at the location of the bolt row, these forces are zero and at all other locations, uplift forces are detected. This has to be the case due to bending in

the direction of the load which explains the difference in plate and beam behavior. A more in depth discussion about the difference in behavior is given in Section 3.4.2.
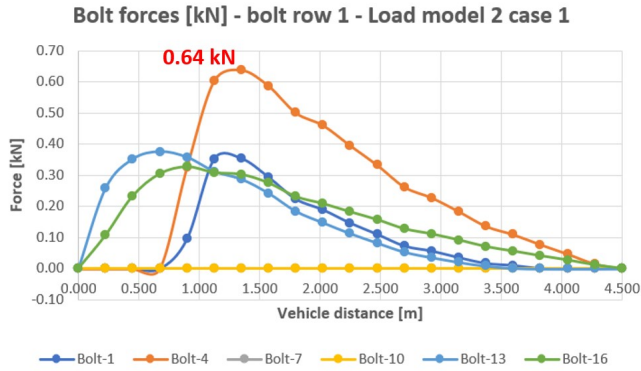


(a) Bolt forces LM2 case 1 bolt row 1 [kN]

(b) Load position maximum forces bolt row 1 LM2 case 1

Figure 3.28: Bolt forces LM2 case 1 row 1
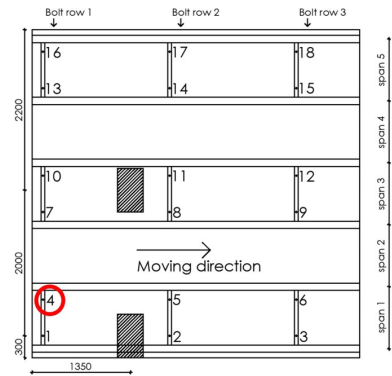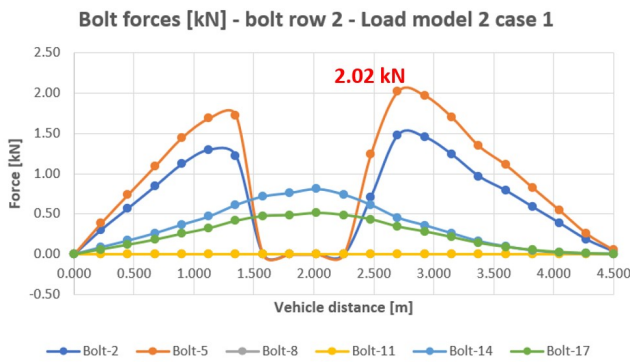


(a) Bolt forces LM2 case 1 bolt row 2 [kN]

(b) Load position maximum forces bolt row 2 LM2 case 1

Figure 3.29: Bolt forces LM2 case 1 row 2
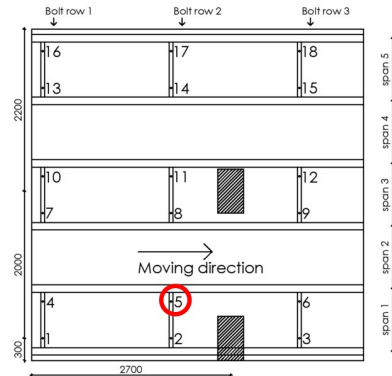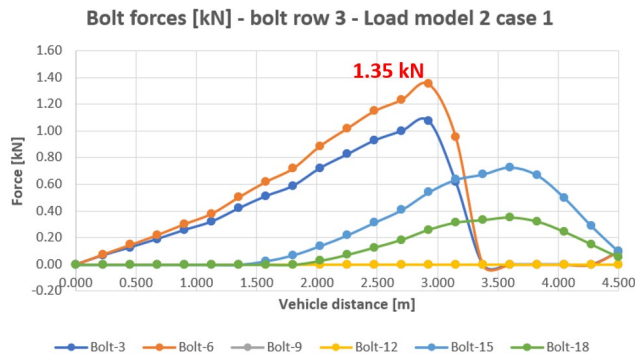


(a) Bolt forces LM2 case 1 bolt row 3 [kN]

(b) Load position maximum forces bolt row 3 LM2 case 1

Figure 3.30: Bolt forces LM2 case 1 row 3
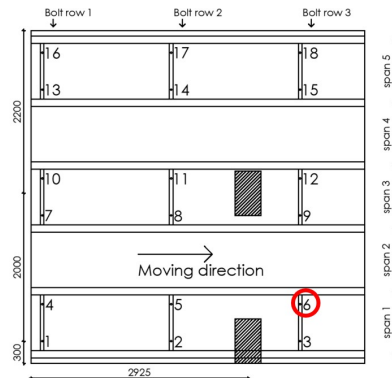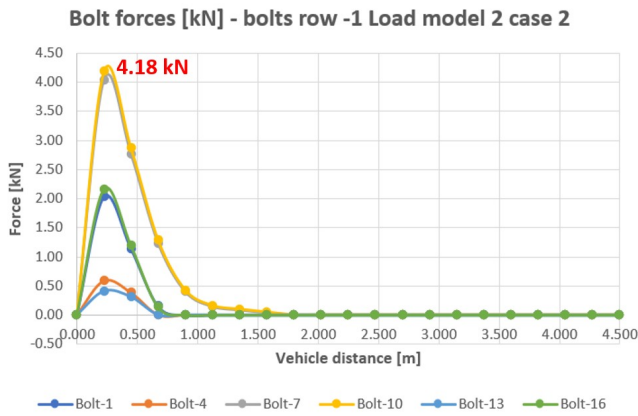
(a) Bolt forces LM2 case 2 bolt row 1 [kN]

(b) Load position maximum forces bolt row 1 LM2 case 2

Figure 3.31: Bolt forces LM2 case 2 row 1
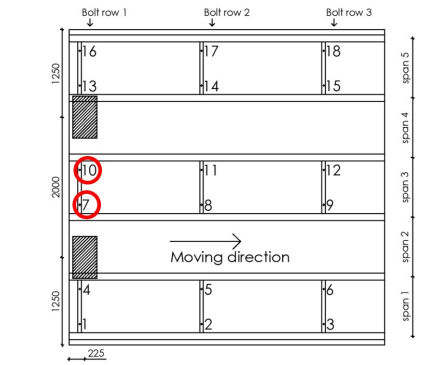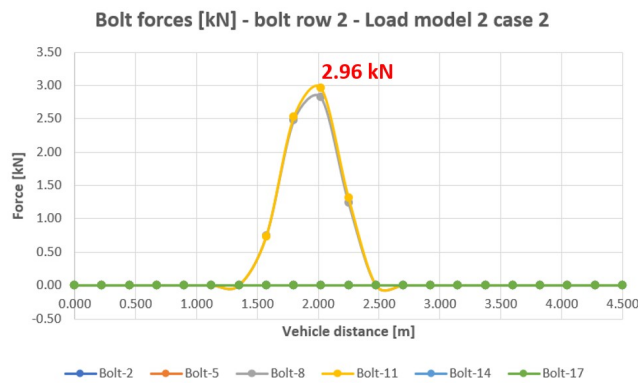


(a) Bolt forces LM2 case 2 bolt row 2 [kN]

(b) Load position maximum forces bolt row 2 LM2 case 2

Figure 3.32: Bolt forces LM2 case 2 row 2
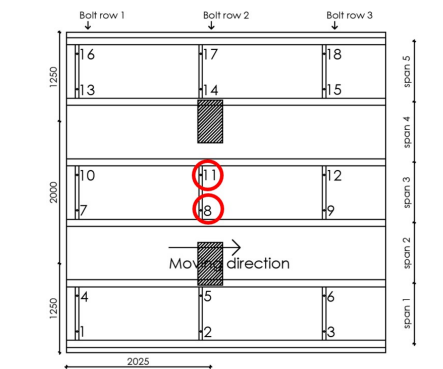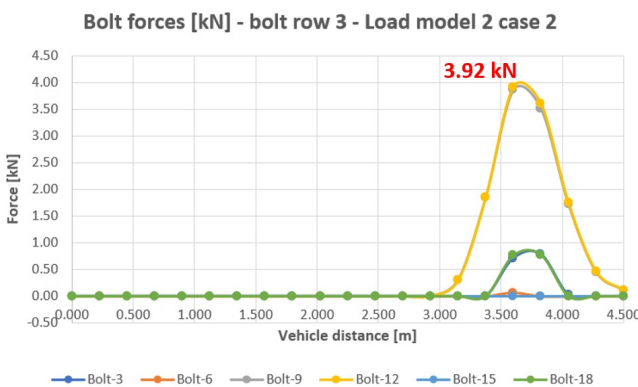


(a) Bolt forces LM2 case 2 bolt row 3 [kN]

(b) Load position maximum forces bolt row 3 LM2 case 2

Figure 3.33: Bolt forces LM2 case 2 row 3
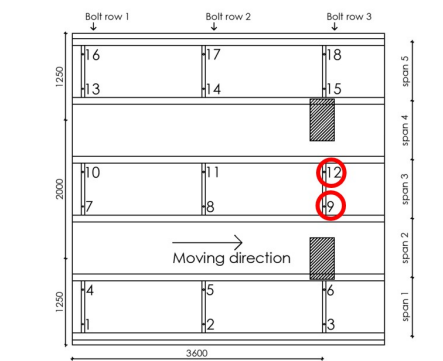
### 3.4.2. Plate vs beam behavior

Compared to the bolt forces, which are calculated with the analytical beam models as described in Section 5.1, the forces obtained with the numerical plate model are much lower. This is due to the different behavior of a plate compared to a beam. When looking at the behavior of a beam model which is described in Section 5.1, it shows a different behavior as for the plate. The obtained deformation with the beam model shown in

Section 5.1.2 is higher than the obtained deformation of the plate model, about 1.8  *mm*, given in Table 3.3, for the same load case. Comparing the results for the bolt forces to the ones of the analytical beam models, shown in Figure 5.3 and 5.6, a significant difference in magnitude is shown. The beam model gives higher forces for all cases. The load distribution of a plate is done in two directions. For the beam model, all load is transferred to the supports along the length direction of the beam, which results in higher forces at the supports.

To investigate the difference in behavior in more detail, a beam model is made in Abaqus with the width of 350 *mm*, which is the width of the wheel for load model 2. This model contains three webs and a top and bottomskin. The deformation of this model is shown in Figure 3.34 and is compared to the maximum deformation obtained for the same load model, load model 2 case 2, stated in Table 3.3. It is shown that the deformation of 2.7 *mm* obtained with the numerical beam model is larger than the maximum deformation of 1.8 *mm* given for the numerical plate model.
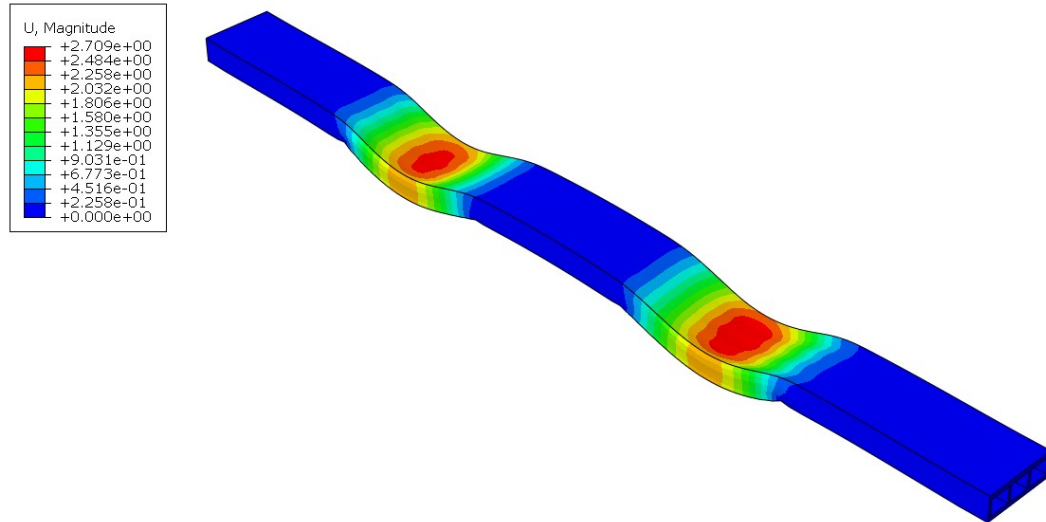


Figure 3.34: Deformation of the beam model made in Abaqus

With the same model, the bolt forces are calculated for the row of six bolts for which the results are shown in Table 3.4. The bolts are numbered the same as in the detailed numerical model. Comparing the results to the results obtained with the plate model given in Figure 3.32a shows that the obtained forces are in the same order of magnitude but lower. Forces obtained with this beam model with a width of the wheel size, are higher. This shows that the difference in bolt force between a beam model and a plate model can (partially) be explained by the difference in behavior. The ratio between the deformation is 2/3 for the beam vs plate model and more or less the same ratio in bolt forces is found.

Table 3.4: Bolt forces obtained by numerical beam and plate model Abaqus

| Bolt | Bolt-2 | Bolt-5 | Bolt-8 | Bolt-11 | Bolt-14 | Bolt-17 |
|------|--------|--------|--------|---------|---------|---------|
| **Force beam model [kN]** | 2.00 | 0.90 | 4.20 | 4.24 | 0.76 | 2.08 |
| **Force plate model [kN]** | 0.00 | 0.00 | 2.82 | 2.96 | 0.00 | 0.00 |

### 3.4.3. Critical load model and critical bolt forces

The critical bolts can be found at the locations of the deck with the highest upward deformation. These will always be the bolts in the mid-span for the considered deck plate because these are the only bolts for which wheels can be placed on both sides. Since both the deformation of the I-beams and the deformation of the deck plate are considered, the highest bolt forces will occur at the edge of the plate where the deformation of the I-beams is the lowest. Assuming the I-beams are rigid, which means no deformation will take place, the forces in the bolts in the same line will be the same.

Two phenomena are describing the deformation of the deck plate. Bending in the moving direction of the vehicle and bending in the direction perpendicular to this direction. Due to the second axle of a load model with two axles, the first type of bending is smaller since the wheel of the second axle gives a downwards

deformation which counteracts the upwards deformation of the wheel from the first axle. The contribution of the second axle to the bolt forces is rather low depending on the distance between the two axles. As shown in the comparison between beam and plate behavior in the previous section, the effective width which is transferring the load is rather small compared to the distance between the axles. Therefore, multiple axles with a distance that is more than twice the width of the wheel will not cause larger bolt forces compared to one axle. This can also be concluded by comparing the graphs in Figure 3.35 and 3.36 where it is shown the behavior and the magnitude for two and one axles respectively.

For the considered load cases this means that load model 2 will always be critical because there is no uniformly distributed load and the axle load is the highest. The highest bolt forces for load model 1 will occur in the case that the vehicle with two axles is placed at the middle of the deck, for which the results are shown in Figure 3.35. The total load on the bolts in the mid-span will be higher than load model two, however, due to the plate behavior, some of the load is already transferred to the I-beams close to the wheels. Therefore, load model 2 will always be governing.
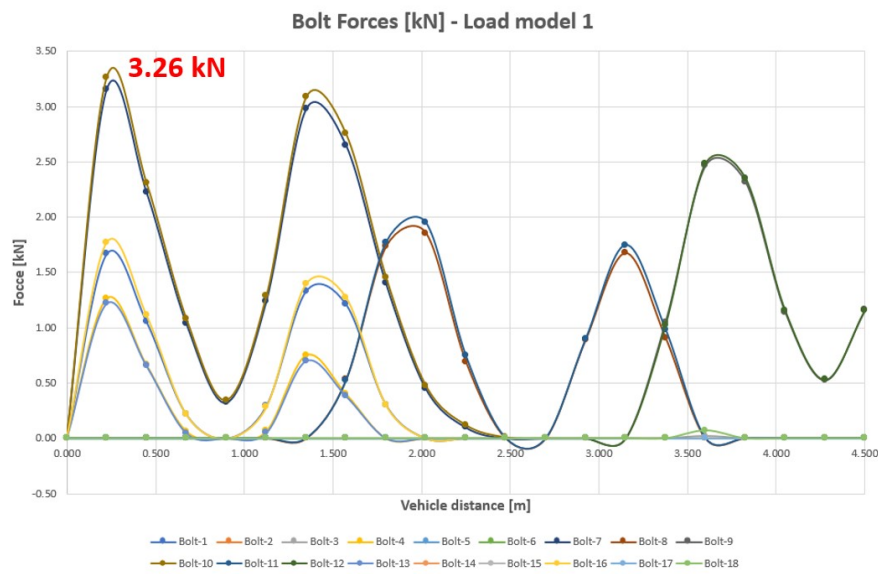


Figure 3.35: Bolt forces for load model 1 placed at the middle of the deck [$kN$]
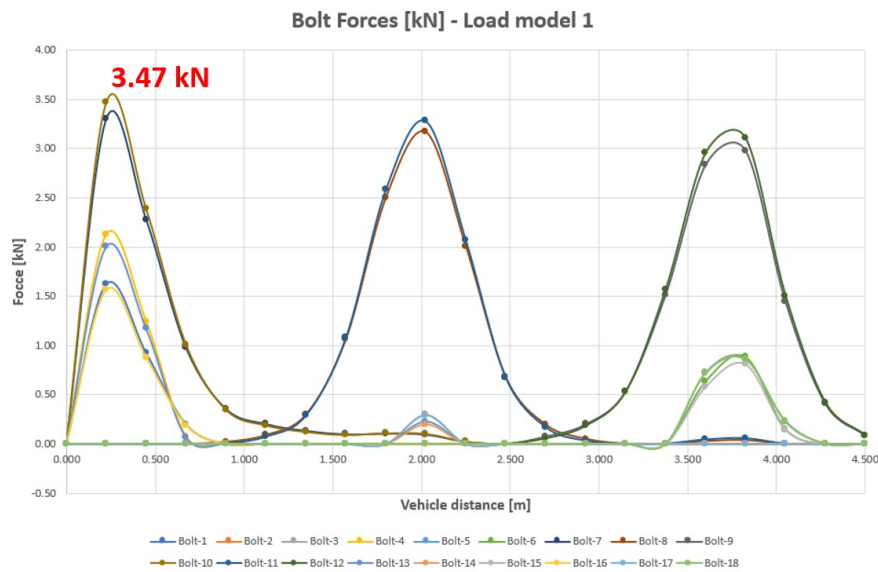


Figure 3.36: Bolt forces for load model 1 with one axle placed at the middle of the deck [$kN$]

### 3.4.4. Discussion detailed model

Based on the detailed numerical model it can be concluded that the maximum occurring bolt force for the considered load models from the Eurocode is between 4 and $4.5kN$ as shown in Figure 3.37. This means that such a force is needed to prevent the deck from (large) upwards deformation. Therefore, a minimum pre-tensioning of the bolts with this force has to be applied. Compared to the forces calculate with analytical beam models, the numerical plate model gives lower results. The main causes for this are the modeling assumptions made by calculating the deck as a beam model. The supports of the beam model are at the locations of the I-beams whereas for the plate model the bolts are modeled inside the spans. Using springs for modeling the bolts at the proper locations shows a more comparable behavior to the forces obtained with the plate theory.

The other differences can be explained by the difference in theory, plate vs beam, and the influence of the shear deformation. A part of the load is transferred by shear deformation. This type of deformation has no influence on the next span and therefore it does not cause uplift forces. The bending deformation does influence the deformation of the adjacent span and will cause the forces in the bolts. The plate theory includes the shear deformation and will give slightly lower results.

**Critical loading condition**
The critical loading condition is load model 2 with the case where the axle is placed at the spans without bolts. The position of the axle is shown in Figure 3.37 together with the occurring forces in each bolt for this case.
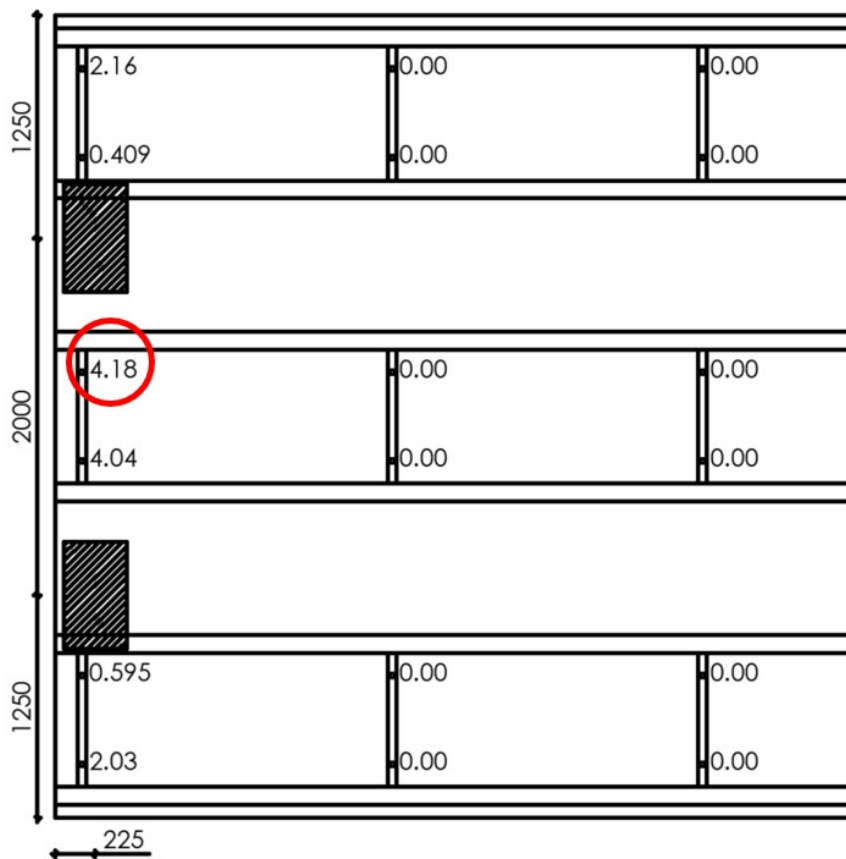


Figure 3.37: Critical loading condition

# 4

# Simplified numerical models

Chapter 3 describes a detailed numerical model which is used to represent reality. In this chapter, different simplified numerical models are made and compared to the reference model. These models are used to search for simplifications that can be done to make calculations easier and faster without losing too much accuracy or information. Since the bridge decks that are considered have large dimensions, simplifications are needed to reduce the time that is needed for the modeling of the slabs and the time needed for a calculation. The following models are made and described in this chapter:

- Model with detailed deck geometry and load superposition

- Model with detailed deck geometry and linear bolts

- Model with detailed deck geometry, linear bolts and load superposition

- Model with orthotropic deck

- Model with orthotropic deck and load superposition

- Model with orthotropic deck and linear bolts

- Model with orthotropic deck, linear bolts and load superposition
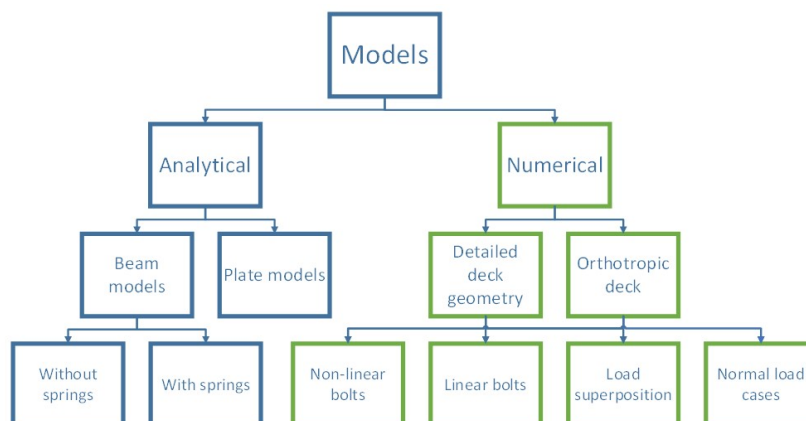


Figure 4.1: Simplified numerical models in overview models

Figure 4.1 shows an overview of all models made during the research. The models that are described in this chapter are shown in the green boxes. In the first sections (Section 4.1 - 4.3), the models are described that are based on the detailed model with one simplification. After this, a description of the material properties for the simplified models with an orthotropic deck is given in Section 4.4. In the fifth section, a comparison

between the models with a detailed deck and the ones with a simplified deck is described. The models with an orthotropic deck and different simplifications are described in the Sections 4.6 - 4.9. In the end, a discussion is given based on the different models that are considered. In this chapter, only the results for one load case, load model 2 case 2, are given to be able to compare the results to each other and to the reference model. Results for the other load models, if applied, are shown in Appendix D.

## 4.1. Model with detailed deck geometry and load superposition

In this section first a description of the model that is considered is given. After this, the results obtained with this model are given and discussed. A comparison between the model and the other models is shown in Section 4.10.

### 4.1.1. Description of the model

For this simplified model, the detailed model in Abaqus described in Section 3.1 is used. Instead of using the different load models from the Eurocode, a load of one wheel is applied to the model. Using the DLOAD function of Abaqus, the wheel is applied at all locations of the deck. The loading path is described with Fortran code and called during the calculation. From this calculation, the bolt forces can be obtained for a wheel load at each location of the deck. For a loading case with an axle with two wheels, the forces in each bolt can be added together using superposition of the results for a wheel at one location and the results from a wheel at another location to get the total result. The same can be done for loading cases with multiple axles.

The result will not be exact due to the fact that the bolts are modeled with non-linear behavior since the bolts can only take tension. Due to the fact that the superposition principle may only be used for linear calculations, an error will occur. However, the tension forces in the bolts will always be equal or higher compared to a calculation with multiple wheels. Higher tension forces are calculated since the downward deformations, which result in a negative contribution to the bolt forces are not taken into account. This means that the outcome is on the safe side.

Figure 4.2 show the loading path of the wheel over the deck. For this, the deck is divided into different lanes. Lanes with a width of the wheel can be used for example. A continuous time is used and the wheel starts at the beginning of the first lane. After reaching the end of the first lane, the wheel is placed at the beginning of the second lane. This procedure is repeated until the complete deck is covered.
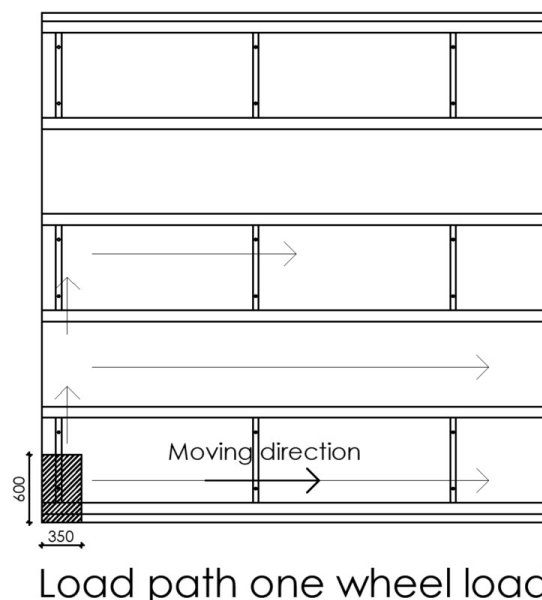


Figure 4.2: Overview load path one wheel loading

### 4.1.2. Results

To be able to compare the results with the results obtained with the detailed model given in Section 3.3, the results are filtered for the load cases considered for the detailed model. The graph in Figure 4.4 shows the

results for the loading case of load model 2 case 2 based on the superposition of the results of two separate wheels. Comparing the graph to the results obtained for the detailed model, the same pattern and ratio of the forces in the different bolt rows are shown. The main difference is the low forces in the bolts in row 2 span 3 which are occurring when the wheels are placed above bolt row 1 and 3. In the detailed model, these forces are canceled due to the influence of the other wheel.

The bolt forces are consisting of the bolt forces for the calculations of two separate wheels. The results from the separate wheels are shown in Figure 4.3. It is shown that both graphs have the same pattern and magnitude for the bolt forces. This has to be the case since the model is symmetric in the width direction. Therefore, it can be concluded that the pattern and magnitude results are accurate enough for this model.
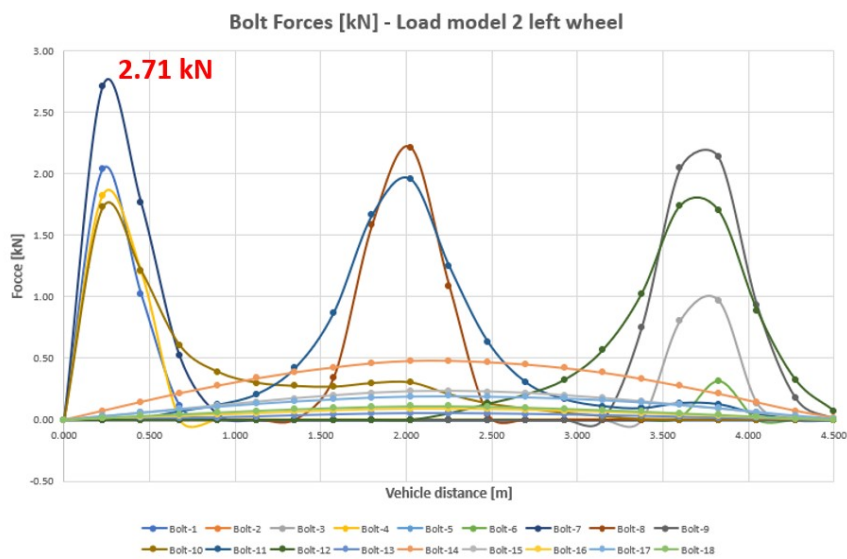


(a) Bolt forces LM2 case 2 left wheel [$kN$]
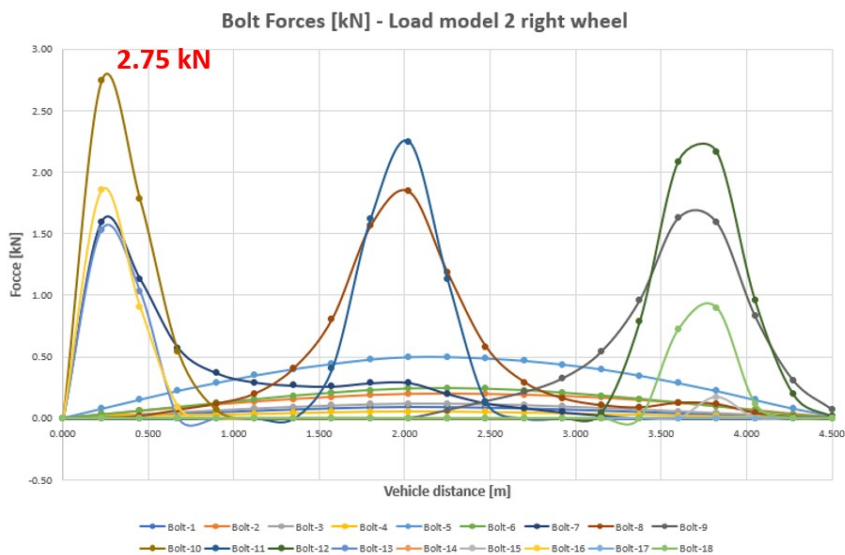


(b) Bolt forces LM2 case 2 right wheel [$kN$]

Figure 4.3: Bolt forces LM2 case 2 different wheels [$kN$]
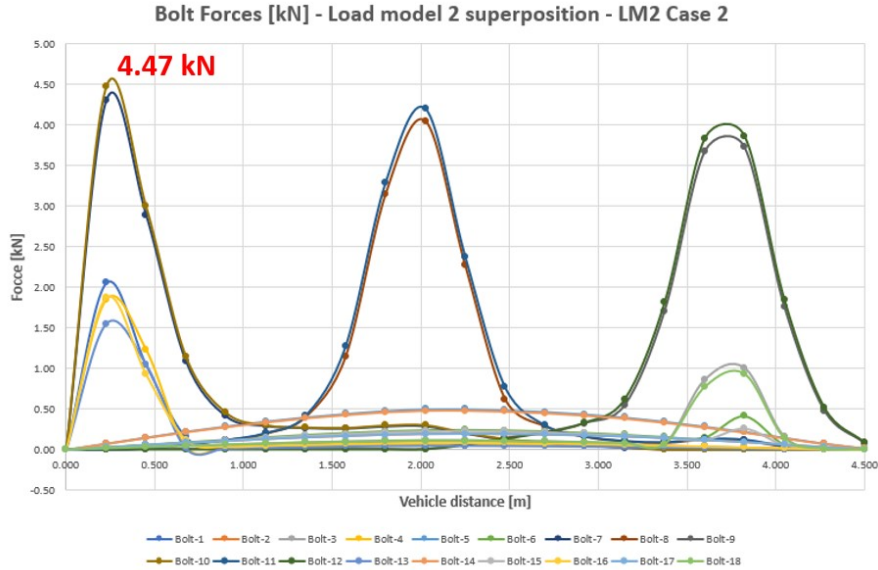
Figure 4.4: Bolt forces LM2 case 2 based on superposition [$kN$]

The difference in bolt force between the detailed model and this simplified model is calculated relative to the detailed numerical model and shown in Figure 4.5. The absolute difference is calculated by

$$absolute\ difference = bolt\ force\ detailed\ model - bolt\ force\ simplified\ model \qquad (4.1)$$

The relative difference is calculated as

$$relative\ difference = \frac{bolt\ force\ simplified\ model - bolt\ force\ detailed\ model}{bolt\ force\ detailed\ model} \cdot 100\% \qquad (4.2)$$

Calculating the differences using these formulas for the maximum bolt forces stays that a negative difference means that the simplified model gives larger forces and a positive difference means that the simplified model gives smaller forces. Therefore, a negative difference indicates that the model is on the safe side. For the cases where the bolt forces are zero in the detailed model, the difference is given as zero % since otherwise, the difference becomes infinity. The relative difference can be extremely high for cases where the force obtained with the detailed calculation is almost zero. These percentages are not useful to compare the two different calculations. As shown for the case with load superposition in Figure 4.5 the biggest differences occurring are negative and therefore an overestimation of the bolt forces. However, also small underestimations up to 0.3 $kN$ are calculated. Since this underestimation is not caused by the simplification, it is caused by a calculation error or difference in the used mesh.
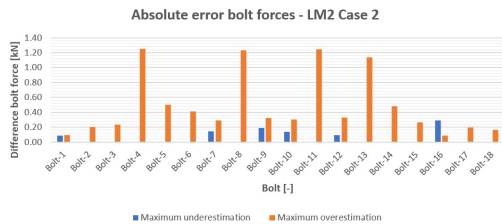


(a) Absolute error bolt forces load model 2 case 2 [$kN$]
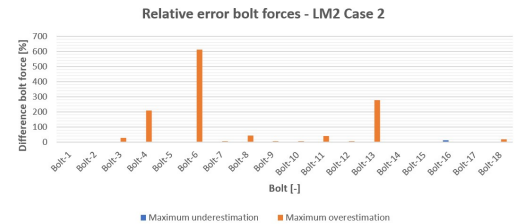


(b) Relative error bolt forces load model 2 case 2 [%]

Figure 4.5: Difference in bolt forces for model with detailed deck geometry and load superposition with respect to reference model for load model 2 case 2

## 4.2. Model with detailed deck geometry and linear bolts
In this section first a description of the model that is considered is given. After this, the results obtained with this model are given and discussed. A comparison between the model and the other models is shown in

Section 4.10.

### 4.2.1. Description of the model

The previous model encountered the problem of superposition of non-linear results. Therefore, this model uses linear bolts which means that compression in the bolts is allowed. Except for the linear bolts, the same detailed model is used as described in Section 3.1.

### 4.2.2. Results

As a result of the calculation with linear bolts, both tension and compression forces are obtained. To be able to compare the results with the detailed model with non-linear bolts, the compression forces are removed. For load model 2 case 2, the results are shown in Figure 4.6. Results for the other load models are shown in Appendix D Section D.1. The maximum force obtained is the same as for the detailed model and the force pattern is also the same.
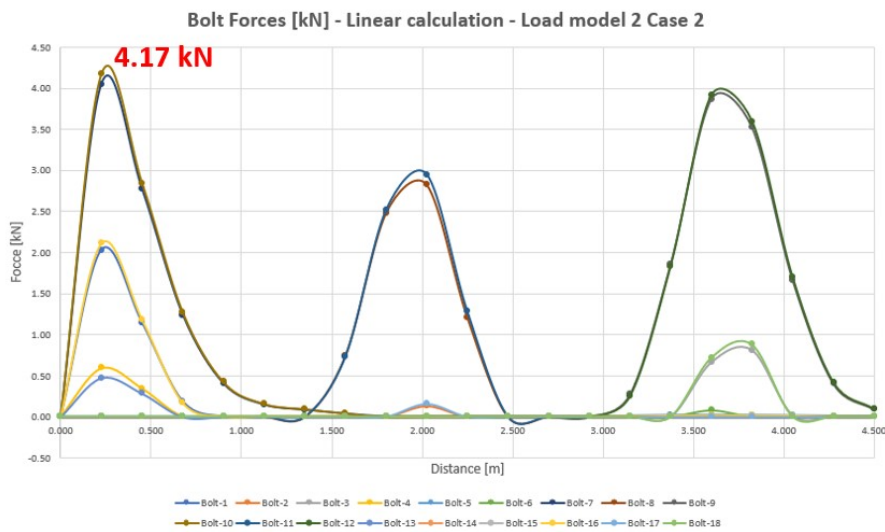


Figure 4.6: Bolt forces linear calculation LM2 case 2 [$kN$]

The results from the linear calculation show the same patterns as the non-linear calculation. For the difference between the two types of calculations, the results of the linear calculation are subtracted from the ones of the non-linear calculation. These results are shown in the graphs in Figure 4.7 and in Appendix D Section D.1. A negative difference means that the result of the linear calculation is higher and vice versa. It is shown that the maximum underestimation is 0.05 $kN$ (6%). The maximum overestimation is 0.16 $kN$ (24%).
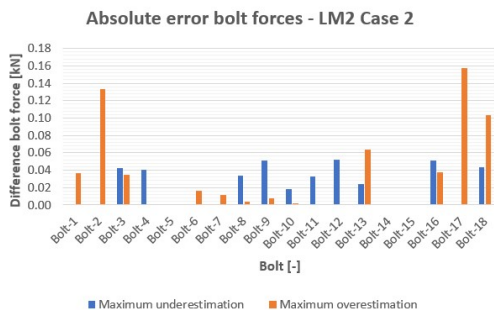


(a) Absolute error bolt forces load model 2 case 2 [$kN$]
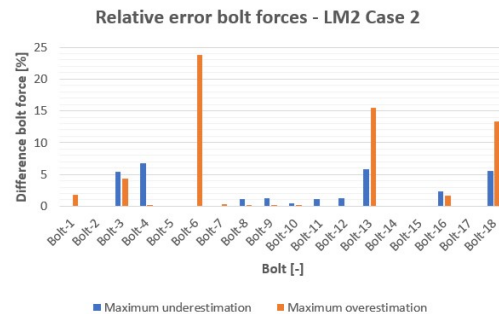
(b) Relative error bolt forces load model 2 case 2 [%]

Figure 4.7: Difference in bolt forces for model with detailed deck geometry and linear bolts with respect to reference model for load model 2 case 2

## 4.3. Model with detailed deck geometry, linear bolts and load superposition

### 4.3.1. Description of the model

In this section first a description of the model that is considered is given. After this, the results obtained with this model are given and discussed. A comparison between the model and the other models is shown in Section 4.10.

### 4.3.1. Description of the model

With the same model as described in Section 4.2, the loading condition with one wheel is considered. How the load superposition is applied is explained in Section 4.1. In contrast with the model with non-linear bolts, superposition is possible in this case. The same loading path is used as for the model with non-linear bolts as visualized in Figure 4.2.

### 4.3.2. Results

Results for this calculation for the same load model 2 case 2 are shown in Figure 4.8. The bolt forces are obtained from a superposition of the bolt forces for the two separate wheels. Comparing the results shows that a slightly larger maximum bolt force is obtained, 4.42 $kN$ instead of 4.18 $kN$. The force pattern is the same and the same magnitude of forces is obtained in the different bolts. It is noticed that the maximum forces of each bolt row are slightly higher and the most other bolts in the spans 1 and 5 are higher.
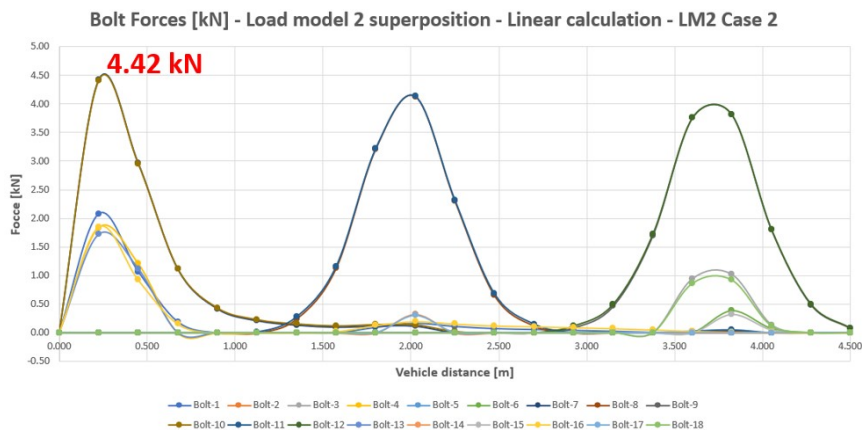


Figure 4.8: Bolt forces linear calculation LM2 case 2 based on superposition [$kN$]

The difference, for the maximum force occurring at the bolt, between the non-linear detailed calculation and the linear calculation based on superposition calculated with respect to the non-linear model is given in Figure 4.9 calculated the same way as the other simplified models. From the observations, it can be concluded that the biggest differences occur in the bolts in spans 1 and 5. These differences are an overestimation of the bolt forces of around 1.0 $kN$.
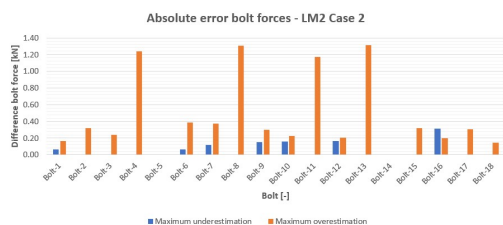


(a) Absolute error bolt forces load model 2 case 2 [$kN$]
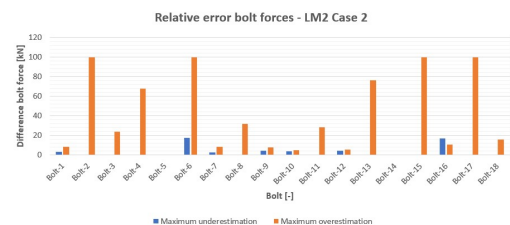
(b) Relative error bolt forces load model 2 case 2 [%]

Figure 4.9: Difference in bolt forces for model with detailed deck geometry, linear bolts and load superposition with respect to reference model for load model 2 case 2

## 4.4. Description modeling of the orthotropic deck

To make the calculations simpler, the deck can be represented by an orthotropic plate instead of modeling the geometry of skins and webs. For this, equivalent properties are needed which represent the skins and core (webs). Different options are tried and the results of this study can be found in Appendix C. Below a description of the modeling and the used equivalent properties is given.

**Geometry**

The deck is modeled with one orthotropic plate instead of the real geometry of skins and webs. An overview of the geometry of the simplified models with an orthotropic deck is shown in Figure 4.11. The I-beams are modeled with beam elements and the deck itself is modeled with continuum shell elements. Except for the deck plate, the model is the same as the detailed model described in Section 3.1.

**Boundary conditions, interaction properties and loads**

The same boundary conditions and loads are applied to the simplified model as to the detailed one. The interaction between the deck and the I-beams is modeled with tie constraints. For a detailed description of how this is performed, see Section 3.1.5. The same load models are used for the calculations, therefore the deck has to be separated into lanes. Figure 4.10 shows in blue the lane that is used for load model 1.
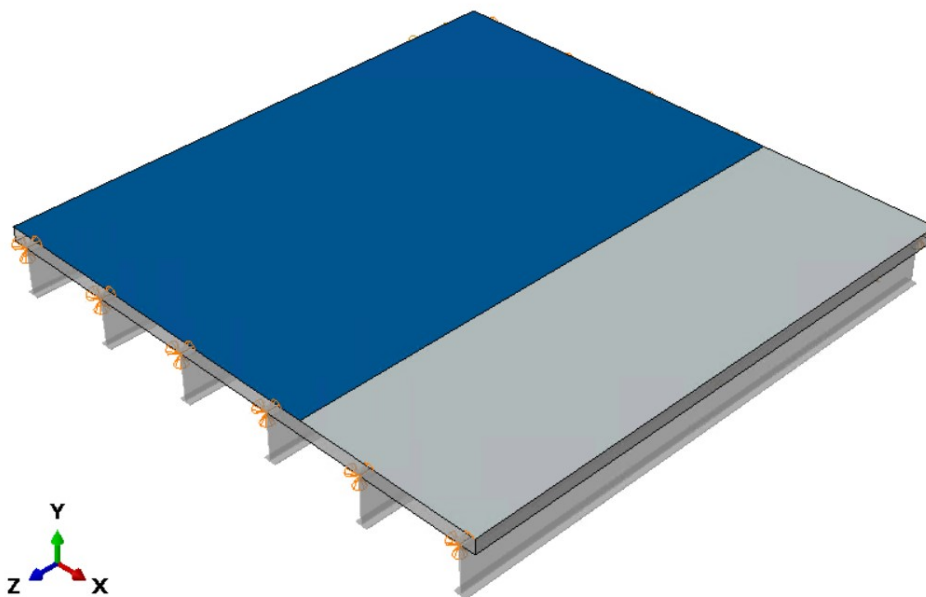


Figure 4.10: Overview boundary conditions and lanes simplified numerical model
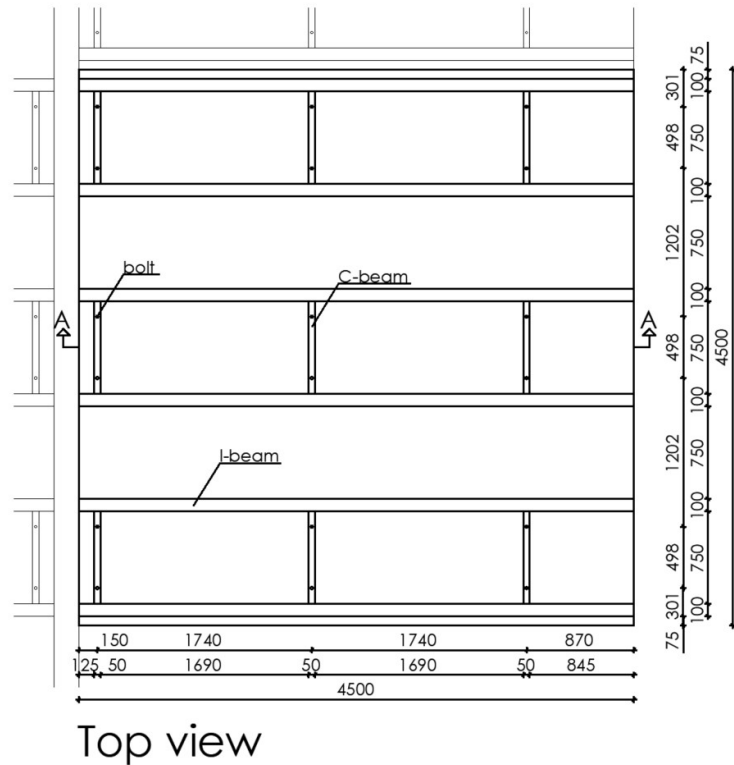
(a) Top view geometry orthotropic modeled deck [*mm*]
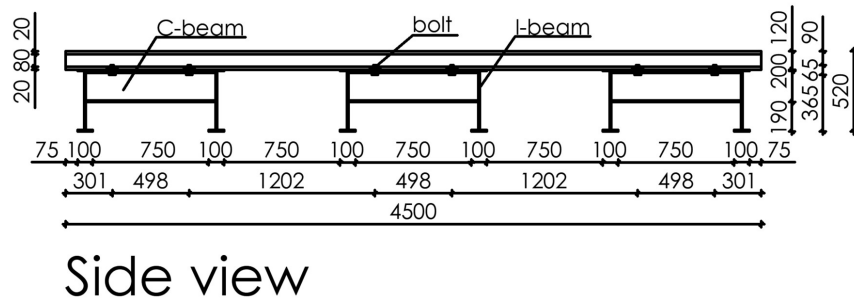


(b) Side view geometry orthotropic modeled deck [*mm*]
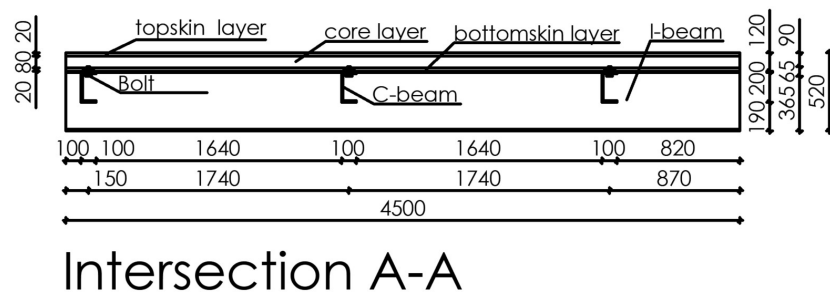


(c) Intersection A-A geometry orthotropic modeled deck [*mm*]

Figure 4.11: Geometry orthotropic modeled deck

**Mesh**

For the simplified numerical model, the same type of elements is used namely the continuum shell elements. One element through-thickness is used for each modeled layer because otherwise the modeled elements are stacked over the height. In the directions of the width and length of the plate, the mesh size is 30 *mm*, the same as for the detailed numerical model. For the beam elements of the I-beams, the same size of 30 *mm* is

used.

**Equivalent material properties one layer model**

Equivalent material properties can be used instead of modeling the layups. A study about these equivalent material properties can be found in Appendix C. Here, the formulas used for the plate model with one layer representing the complete slab are given. After that, the formulas for a model with three equivalent layers are given. Which are the formulas that are used for the models in this chapter. The equivalent material properties for one layer models are used for the analytical models as described in Chapter 5. Different numerical models are made with only one layer representing the slab. However, these results are less accurate than the ones of the three-layer models. The results of the different models with one layer that are considered are given in Appendix C.

The first formula is for the bending modulus in the main (longitudinal) direction. 10% of the material is taken into account for the webs since the plate model uses a solid layer instead of webs with empty space in between. In the detailed model about 10% of the area is filled with webs and therefore only this amount of the modulus is considered.

$$E_1 = \frac{E_{1.tf} \cdot t_{tf} + 0.1 \cdot E_{1.web} \cdot h_{web} + E_{1.bf} \cdot t_{bf}}{h} \tag{4.3}$$

In this formula, $h$ denotes the height and $t$ the thickness. With the different subscripts, the considered element is denoted. The topskin is denoted by $_{tf}$, the bottomskin by $_{bf}$ and the webs by $_{web}$. The same type of formula is applied for the bending modulus in the transverse direction. For the bending stiffness of the webs, a value of 1.0 is used since the stiffness in this direction is almost zero.

$$E_2 = \frac{E_{2.tf} \cdot t_{tf} + 0.1 \cdot E_{2.w} \cdot h_{web} + E_{2.bf} \cdot t_{bf}}{h} \tag{4.4}$$

The equivalent Poisson's ratio is calculated as

$$\nu_{12} = \frac{\nu_{12.tf} \cdot t_{tf} + \nu_{12.w} \cdot h_{web} + \nu_{12.bf} \cdot t_{bf}}{h} \tag{4.5}$$

The shear modulus is calculated in the two in-plane directions $G_{12}$ and $G_{13}$ and in the out-of-plane direction $G_{23}$. The different formulas used are shown below. For the shear stiffness of the two in-plane directions, the same type of formulas is used as for the bending stiffness. The out-of-plane shear modulus is calculated using a model from Welleman [42]. This is explained by the description of the equivalent material properties for the three-layer model.

$$G_{12} = \frac{G_{12.tf} \cdot t_{tf} + 0.1 \cdot G_{12.w} \cdot h_{web} + G_{12.bf} \cdot t_{bf}}{h} \tag{4.6}$$

$$G_{13} = \frac{G_{13.tf} \cdot t_{tf} + 0.0 \cdot G_{13.w} \cdot h_{web} + G_{13.bf} \cdot t_{bf}}{h} \tag{4.7}$$

$$G_{23} = k_e \tag{4.8}$$

An overview of the material properties used for one layer models is given in Table 4.1.

Table 4.1: Equivalent material properties one layer model

| Parameter | Value |
|---|---|
| $E_1$ [MPa] | 9398 |
| $E_2$ [MPa] | 4854 |
| $\nu_{12}$ [-] | 0.214 |
| $G_{12}$ [MPa] | 1348 |
| $G_{13}$ [MPa] | 989 |
| $G_{23}$ [MPa] | 339 |

**Equivalent material properties three layer model**

An overview of the equivalent material properties used for the three layer models is shown in Table 4.2. Most

of the values for the material parameters are calculated by averaging the values obtained with the classical laminate theory for the topskin, core and bottomskin. As a weight factor, the height of each part is used. For the E modulus perpendicular to the webs ($E_2$), a value of 1.0 is assumed since the forces cannot be distributed in this direction due to the absence of material. Also the shear modulus $G_{23}$ is calculated in a different way since this stiffness depends on the contribution of bending of the webs to the stiffness of the skins. Therefore, the stiffness cannot be calculated based on averaging the values for the different layers.

Table 4.2: Equivalent material properties three layer model

| Material Parameter | Topskin | Core | Bottomskin |
|---|---|---|---|
| $E_1$ [MPa] | 25466 | 1108.1 | 26576 |
| $E_2$ [MPa] | 14276 | 1.0 | 14899 |
| $v_{12}$ [-] | 0.143 | 0.250 | 0.143 |
| $G_{12}$ [Mpa] | 2910 | 538 | 3037 |
| $G_{13}$ [Mpa] | 2910 | 538 | 3037 |
| $G_{23}$ [MPa] | 339 | 339 | 339 |

The shear stiffness $G_{23}$ is calculated using a model of H. Welleman [42] which is adapted to the behavior of the FRP deck. The model is shown in Figure 4.12.
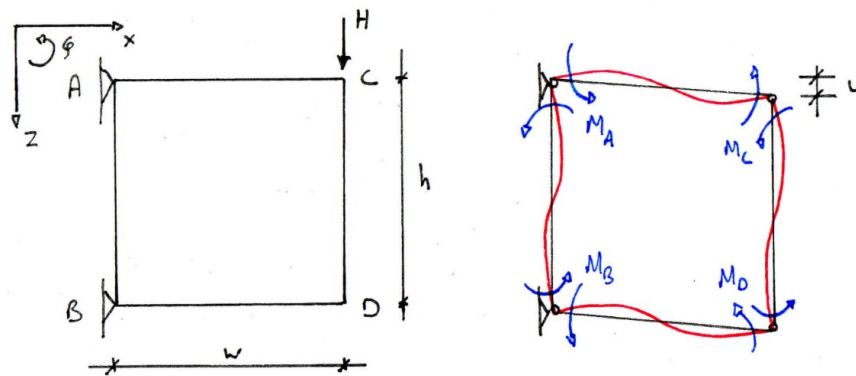


Figure 4.12: Sketch of the model for the shear stiffness

Based on this model the following equations can be determined to solve for the moments and displacement of the model:

$$
\begin{aligned}
\phi_A^{AB} &= \phi_A^{AC} \\
\phi_B^{BA} &= \phi_B^{BD} \\
\phi_C^{CA} &= \phi_C^{CD} \\
\phi_D^{DB} &= \phi_D^{DC} \\
\delta A &= 0
\end{aligned}
\tag{4.9}
$$

$\phi$ is the rotation of the different elements. Which element is meant is given by the subscript. The total work perfomed by the system is denoted by $A$. Based on these equations, the matrix equation below is governing the system. In this matrix, the stiffness of the different elements is described by $EI$, the dimensions by $w$ for the width and $h$ for the height. $H$ is the applied load and $M$ the moments at the different locations denoted by the subscripts. The vertical displacement is denoted as $u$.

$$
\begin{bmatrix}
\frac{h}{3EI_w} - \frac{w}{3EI_{tf}} & -\frac{h}{6EI_w} & \frac{w}{6EI_{tf}} & 0 & \frac{1}{w} \\
-\frac{h}{6EI_w} & \frac{h}{3EI_w} - \frac{w}{EI_{bf}} & 0 & \frac{w}{6EI_{bf}} & \frac{1}{w} \\
-\frac{w}{6EI_{tf}} & 0 & \frac{w}{3EI_{tf}} - \frac{h}{3EI_w} & \frac{h}{6EI_w} & -\frac{1}{w} \\
0 & -\frac{w}{6EI_{bf}} & \frac{h}{6EI_w} & \frac{w}{3EI_{bf}} - \frac{h}{3EI_w} & -\frac{1}{w} \\
-1 & -1 & -1 & -1 & 0
\end{bmatrix}
\begin{bmatrix}
M_A \\ M_B \\ M_C \\ M_D \\ u
\end{bmatrix}
=
\begin{bmatrix}
0 \\ 0 \\ 0 \\ 0 \\ Hw
\end{bmatrix}
\tag{4.10}
$$

Due to the known moment distribution in the model, the contribution of the shear stiffness due to the bending of the vertical members can be obtained. The shear stiffness of the model is given based on the deformation caused by the applied load.

$$
k_e = \frac{Hh}{u} = \frac{12(6hEI_{tf}EI_{bf} - wEI_{bf}EI_W - wEI_{tf}EI_w)EI_w}{w(3EI_{bf}EI_{tf}h^2 - 2EI_{bf}EI_whw - 2EI_{tf}EI_whw + EI_w^2 w^2)}
\tag{4.11}
$$

Figure 4.12 shows one cell, which contains a part of the top and bottomskin and two (half) webs. Since the deck is made out of different cells next to each other, an extended model is made which is shown in Figure 4.13. This model gives a more realistic approach to the force distribution in the cells. However, calculating the stiffness based on this model gives a higher stiffness. This is the case due to the extra constrain at the connection by the next cell. In the model, fixed corners are assumed which is the case due to the continuing fibers in the skins and webs. However, in reality, the corners can deviate a bit from the right angle. To be on the safe side, the stiffness calculated with the one cell model is used.
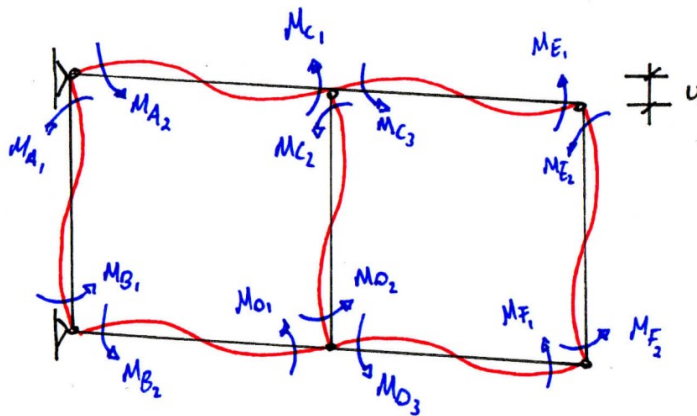


Figure 4.13: Sketch of the model for the shear stiffness using multiple cells

A 3D view of the simplified numerical model modeled in Abaqus with a deck plate modeled as an orthotropic plate is shown in Figure 4.14. With this model, different calculations are performed and also the same simplifications are considered as for the detailed numerical model as described in the previous sections.
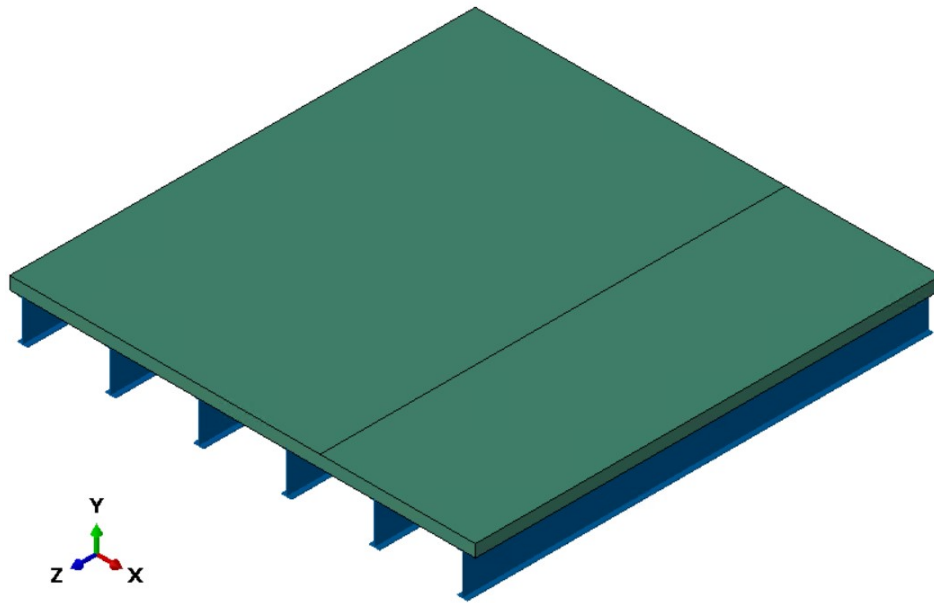
Figure 4.14: 3D view simplified numerical model Abaqus

## 4.5. Comparison of models with detailed and simplified deck

To be able to observe the behavior of the different models, two small models are made. These models have dimensions as shown in Figure 4.15 for the small detailed model and in Figure 4.16 for the small simplified model. The results are compared on the deformation in the two main directions.
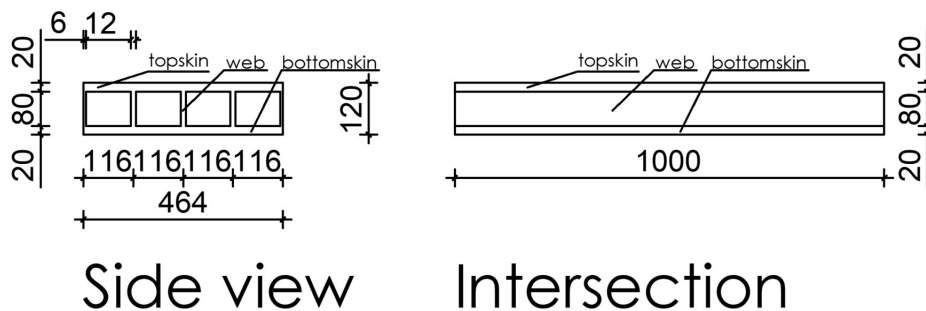


Figure 4.15: Geometry small detailed model [$mm$]
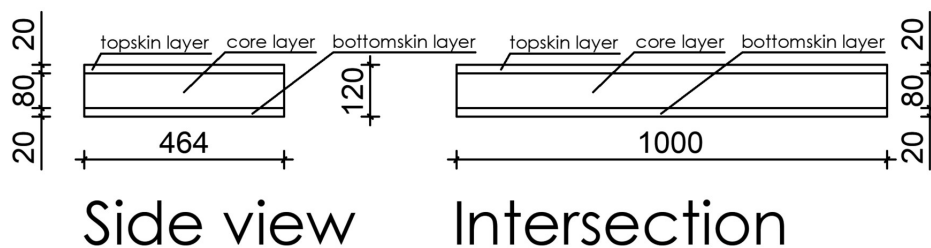


Figure 4.16: Geometry small simplified model [$mm$]

Figure 4.17 shows the boundary conditions applied for these models. Two loading conditions are considered. First, an uniformly distributed load of 0.05 $N/mm^2$ is applied. The results for these load cases are shown in Figure 4.18 and Figure 4.19. The second load case that is applied is a point load of 100 $kN$ that is applied over an area of 100 $mm$ by 100 $mm$. The results for this load case are shown in Figure 4.20 for the detailed model and in Figure 4.21 for the simplified model.

(a) Boundary conditions small detailed model

(b) Boundary conditions small simplified model
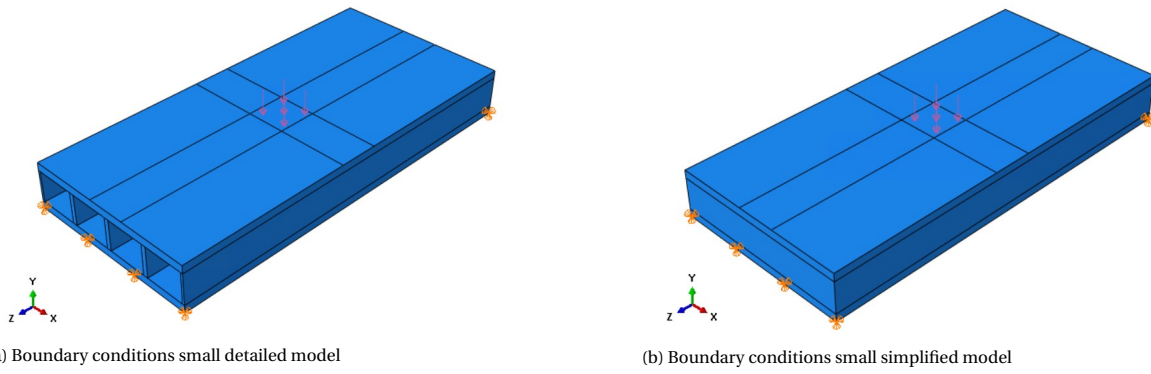
Figure 4.17: Boundary conditions small models
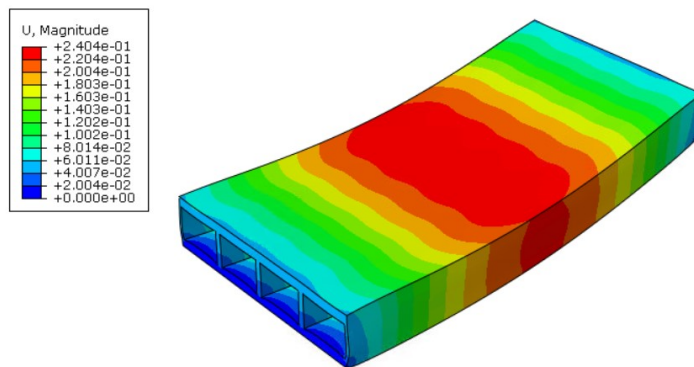


Figure 4.18: Deformation small detailed model with UDL [*mm*]
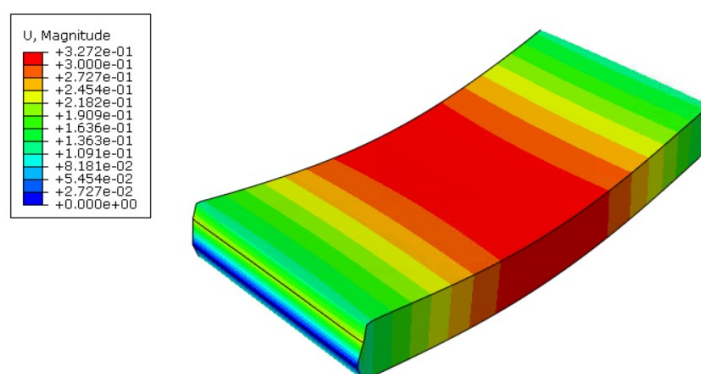


Figure 4.19: Deformation small simplified model with UDL [*mm*]
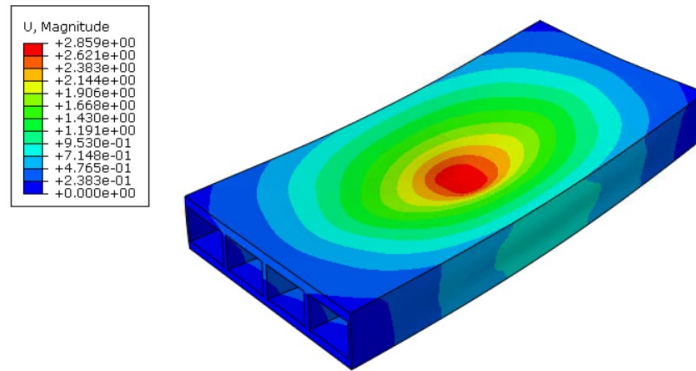
Figure 4.20: Deformation small detailed model with PL [$mm$]
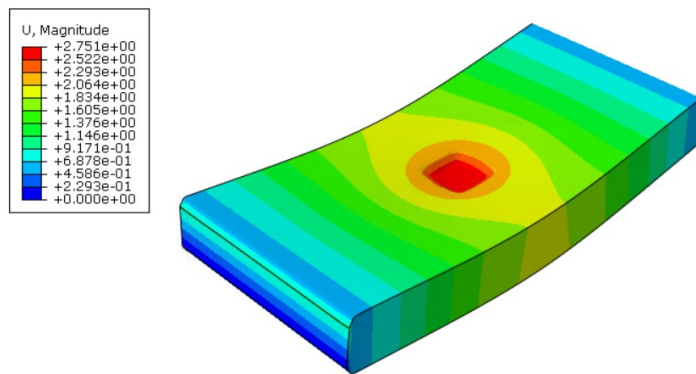


Figure 4.21: Deformation small simplified model with PL [$mm$]

Observing the results, it is shown that the load transfer throughout the plates is the same for both models when a UDL is applied. Both plates work as a wide beam to transfer the applied load to the supports. It is shown that the maximum deformation is about 0.9 $mm$ higher for the simplified model which indicates that the equivalent stiffness properties are too low.

Comparing the two cases with a point load applied shown in the Figures 4.20 and 4.21, a difference in behavior is observed. For the simplified model, it is shown that the load is transferred in two directions. Underneath the area where the point load is applied, a local deformation occurs. Next to this, an almost equal global deformation is shown in the transverse direction due to the low stiffness of the core layer. This behavior is different from what can be observed for the detailed model in Figure 4.20. For the detailed model, the width of the plate is not used equally to transfer the point load to the supports. Instead, a smaller width is used of only the middle three webs.

One of the explanations in behavior that can be expected is buckling of the webs or a small out-of-plane deformation. This will explain a reduction in stiffness. The deformation of the webs for the case with a point load is shown in Figure 4.22. In this figure, it is shown that no buckling or large out-of-plane deformation occurs.

The difference in behavior can be explained by the difference in models. In the case of the simplified model, the complete topskin is supported by the solid core which has equal properties over the width of the plate. The detailed model has only a certain amount of webs supporting the topskin with empty space in between. Considering the uniformly distributed load, no real difference is observed except from a small deviation at the locations of the webs. Since the point load is applied at only one web, the core difference gives a difference in load transfer.

Based on the comparison of the small models that are made, it can be concluded that the equivalent material properties are not accurate enough to calculate the deformation of the plates. However, due to the larger load spreading, the bolt forces will be higher and therefore on the safe side. Therefore, the material properties as given in Table 4.2 are used for the rest of the simplified numerical models that are considered.
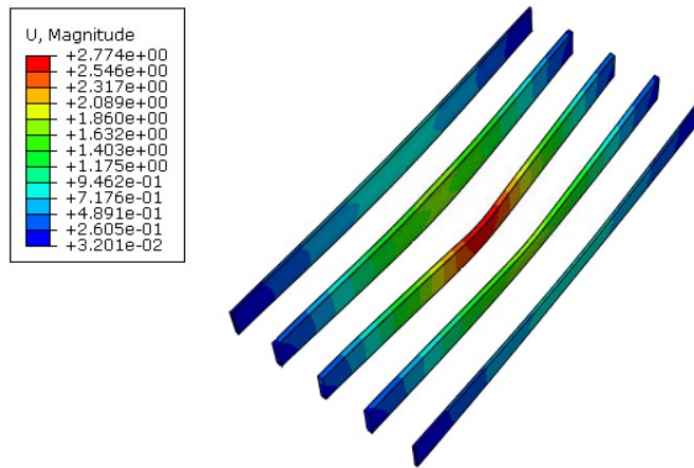
Figure 4.22: Deformation webs small detailed model with PL [$mm$]

## 4.6. Model with orthotropic deck

In this section first a description of the model that is considered is given. After this, the results obtained with this model are given and discussed. A comparison between the model and the other models is shown in Section 4.10.

### 4.6.1. Description of the model

The first model made with an orthotropic deck is excepting the deck, the same as the detailed model described in Chapter 3. Replacing the detailed deck with an orthotropic one does have an influence on the global behavior and therefore on the bolt forces obtained. For this model, the same load models are run as for the detailed model.

### 4.6.2. Results

Results of the model with an orthotropic deck for load model 2 case 2 are shown in Figure 4.23. For the other load models, the results are shown in Appendix D Section D.2. Observing the results shows a slightly larger deviation from the symmetric case than for the detailed model. The maximum obtained force is about 1.0 $kN$ higher in this case. The force pattern is the same but the maximum forces obtained are higher.
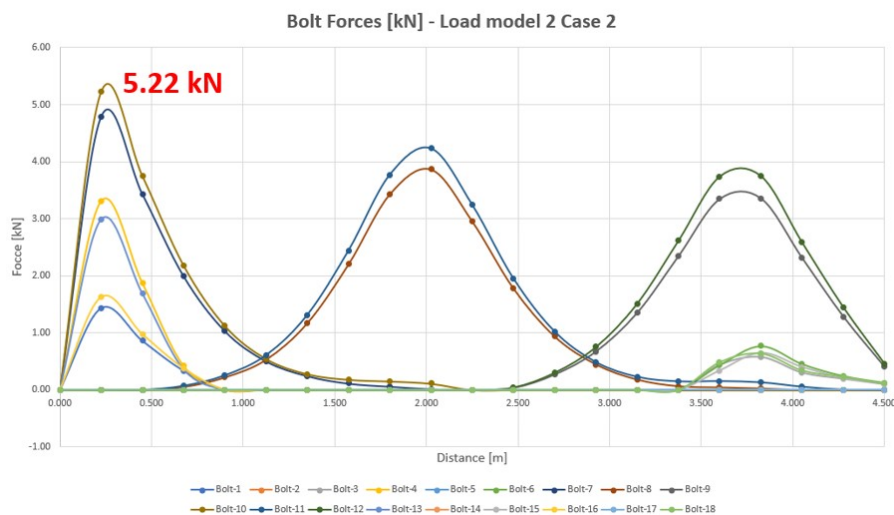


Figure 4.23: Bolt forces simplified numerical calculation LM2 case 2 [$kN$]

The obtained results are compared to the ones calculated with the detailed model and the difference in bolt forces is shown in Figure 4.24. The maximum difference occurs in bolts 4 and 13. This is due to the difference

in the type of slabs. The orthotropic plate spreads the load more than the detailed model which gives higher forces in spans 1 and 5.
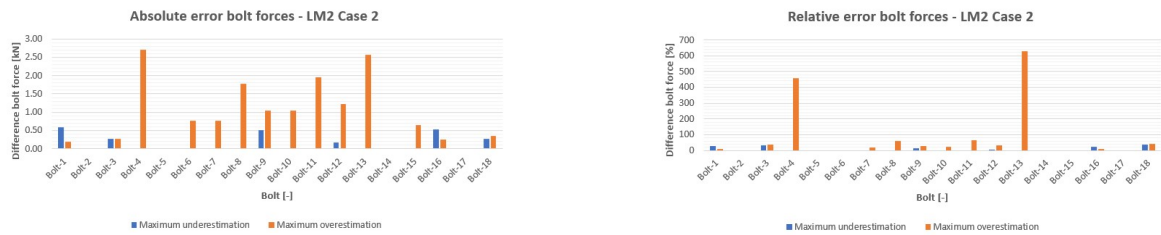


(a) Absolute error bolt forces load model 2 case 2 [*kN*]



(b) Relative error bolt forces load model 2 case 2 [%]

Figure 4.24: Difference in bolt forces for model with orthotropic deck with respect to reference model for load model 2 case 2

## 4.7. Model with orthotropic deck and load superposition

In this section first a description of the model that is considered is given. After this, the results obtained with this model are given and discussed. A comparison between the model and the other models is shown in Section 4.10.

### 4.7.1. Description of the model

To be able to consider different load models with one calculation, load superposition can be used. The same as for the simplification of the detailed numerical model, load superposition is considered for the simplified numerical model with an orthotropic deck. A description of the load superposition is given in Section 4.1.

### 4.7.2. Results

Adding the results from two wheels at the right locations gives the results for load model 2 case 2 as shown in Figure 4.25. Just like the other simplified model with non-linear bolts, this model gives a bit asymmetric results. Comparing the pattern to the one from the model without an orthotropic deck but with the load superposition as described in Section 4.1, it is shown that the same forces are obtained in the bolts in row 2 span 3. These forces are also occurring when the wheels are placed above bolt rows one and three.
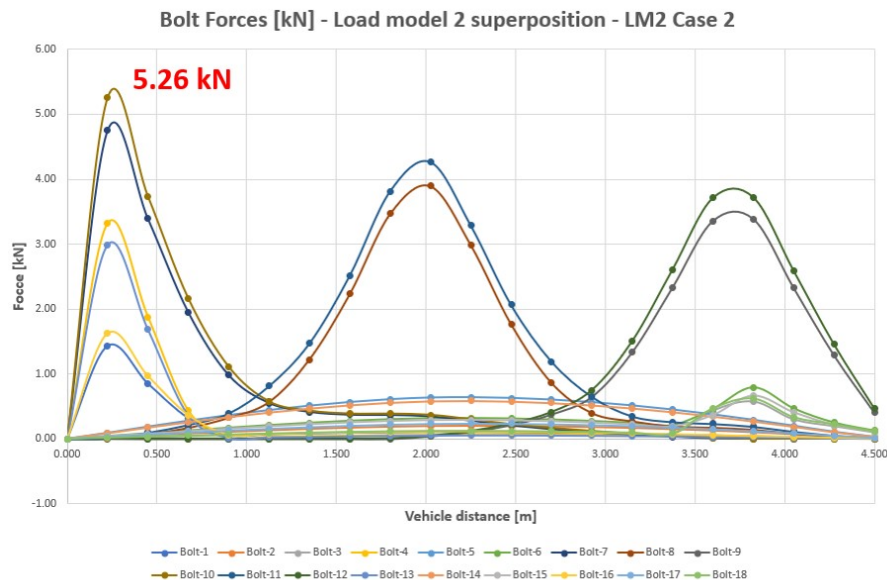


Figure 4.25: Bolt forces simplified calculation LM2 case 2 based on superposition [*kN*]

The error which is made compared to the detailed model is shown in the graphs in Figure 4.26. The largest error occurs for the same bolts as for the other simplified models with an orthotropic modeled deck. For this

simplified model, bolt forces occur in the bolts 6 and 13 as shown in Figure 4.25. In the detailed numerical model, the forces in these bolts are almost zero. Calculating the error base on Formula 4.2, gives a relative difference of more than 1000% since the difference is divided by almost zero as shown in Figure 4.26.
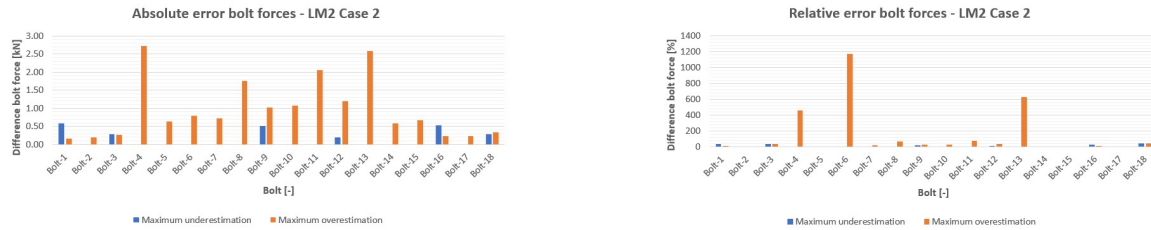


(a) Absolute error bolt forces load model 2 case 2 [$kN$]



(b) Relative error bolt forces load model 2 case 2 [%]

Figure 4.26: Difference in bolt forces for model with orthotropic deck and load superposition with respect to reference model for load model 2 case 2

## 4.8. Model with orthotropic deck and linear bolts

In this section first a description of the model that is considered is given. After this, the results obtained with this model are given and discussed. A comparison between the model and the other models is shown in Section 4.10.

### 4.8.1. Description of the model

The same as for the detailed model, the linear behavior of the bolts can be used as a simplification. With this model, the influence of the two simplifications, an orthotropic deck plate and linear bolts, is researched.

### 4.8.2. Results

The results for load model 2 case 2 are shown in Figure 4.27 to be able to compare this model to the other ones considered. Results for other load models considered are shown in Appendix D Section D.3. Unlike the previous model, the observed pattern is almost completely symmetric in the width direction. In general, higher forces are obtained compared to the reference model and the maximum obtained force is also higher.
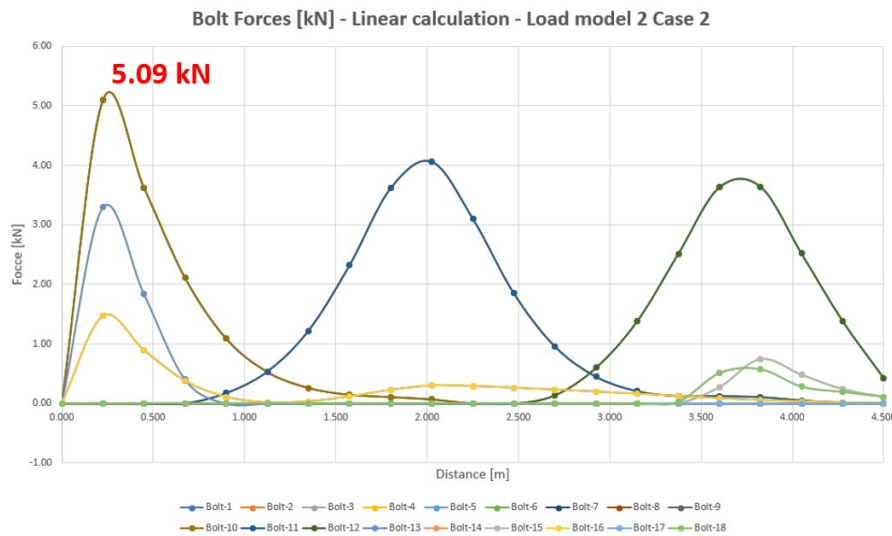


Figure 4.27: Bolt forces linear simplified numerical calculation LM2 case 2 [$kN$]

The difference between this simplified model and the detailed model is shown in Figure 4.28. Just like the previous model, the maximum difference is obtained at the bolts 4 and 13 which is due to the difference in properties in the transverse direction.
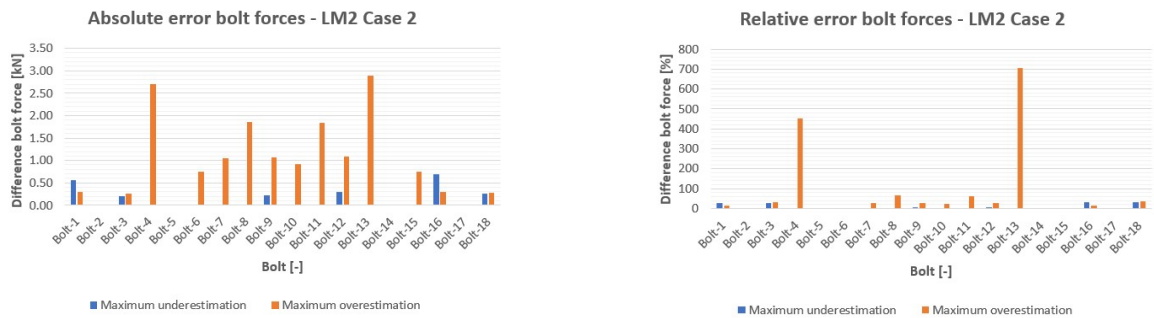
(a) Absolute error bolt forces load model 2 case 2 [*kN*]



(b) Relative error bolt forces load model 2 case 2 [%]

Figure 4.28: Difference in bolt forces for model with orthotropic deck and linear bolts with respect to reference model for load model 2 case 2

## 4.9. Model with orthotropic deck, linear bolts and load superposition

In this section first a description of the model that is considered is given. After this, the results obtained with this model are given and discussed. A comparison between the model and the other models is shown in Section 4.10.

### 4.9.1. Description of the model

This model has the most simplifications, all the ones which are considered in different other models are included in this model. These simplifications are an orthotropic deck, linear bolts and load superposition.

### 4.9.2. Results

Performing calculations with this model gives the results for load model 2 case 2 as shown in Figure 4.29. The difference that is made in the results compared to the reference detailed model is given in Figure 4.30. The load pattern shows an almost perfect symmetric result with higher forces compared to the detailed numerical model. The pattern is more or less the same as for the simplified model with an orthotropic deck and linear bolts.
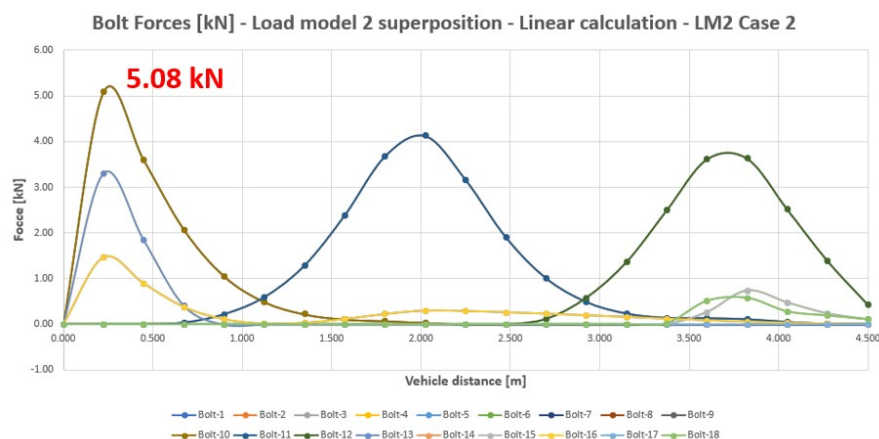


Figure 4.29: Bolt forces simplified linear calculation LM2 case 2 based on superposition [*kN*]

The same as for almost all other simplified models, the largest error is found in bolts 4 and 13. However, next to these overestimations, some underestimation is given for the bolts 1 and 16 which are in the same spans 1 and 5.
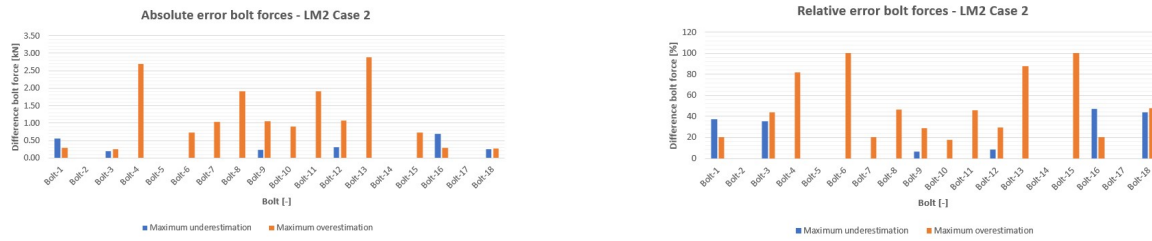
(a) Absolute error bolt forces load model 2 case 2 [*kN*]



(b) Relative error bolt forces load model 2 case 2 [%]

Figure 4.30: Difference in bolt forces for model with orthotropic deck, linear bolts and load superposition with respect to reference model for load model 2 case 2

## 4.10. Discussion simplified numerical models

Table 4.3 gives an overview of the maximum bolt forces obtained with the calculations with the different numerical models. The maximum error that is made compared to the detailed numerical model is given in Table 4.4.

Table 4.3: Overview maximum bolt forces different numerical models

| Type of model | Load model 1 Including UDL Max Force [kN] | Load model 1 Excluding UDL Max Force [kN] | Load model 2 Case 1 Max Force [kN] | Load model 2 Case 2 Max Force [kN] |
|---|---|---|---|---|
| **Detailed model** | 0.49 | 0.75 | 2.02 | 4.18 |
| **Load superposition** | | | | 4.47 |
| **Linear bolts** | 0.52 | 0.68 | 1.61 | 4.17 |
| **Linear bolts & Load superposition** | | | | 4.41 |
| **Orthotropic deck** | 1.36 | 1.42 | 1.58 | 5.22 |
| **Orthotropic deck & Load superposition** | | | | 5.26 |
| **Orthotropic deck & Linear bolts** | 1.42 | 1.49 | 1.52 | 5.09 |
| **Orthotropic deck & Linear bolts & Load superposition** | | | | 5.08 |

Table 4.4: Overview difference in bolt forces different numerical models

| Type of model | Load model 1 Including UDL Max Difference [kN] | Load model 1 Excluding UDL Max Difference [kN] | Load model 2 Case 1 Max Difference [kN] | Load model 2 Case 2 Max Difference [kN] |
|---|---|---|---|---|
| **Detailed model Load superposition** | | | | 1.25 |
| **Linear bolts** | 0.19 | 0.27 | 0.44 | 0.16 |
| **Linear bolts & Load superposition** | | | | 1.31 |
| **Orthotropic deck** | 0.98 | 0.86 | 1.40 | 2.71 |
| **Orthotropic deck & Load superposition** | | | | 2.72 |
| **Orthotropic deck & Linear bolts** | 1.04 | 0.92 | 1.32 | 2.89 |
| **Orthotropic deck & Linear bolts & Load superposition** | | | | 2.89 |

Since the different models are made based on the detailed numerical model, the models don't need to be verified themselves. Each simplified model contains one simplification compared with the detailed model or other simplified models. Comparing the different models with each other shows the error that is introduced due to the simplification. After considering different simplified models and comparing them with the detailed model and with each other the following observations are made.

- Superposition of the bolt forces for non-linear calculation gives higher bolt forces than non-linear calculation with the complete vehicle. This is due to the fact that the downwards deformations are not taken into account. For load model 2 case 2, one wheel gives an upwards deformation at certain locations and the other wheel gives a downwards deformation. Considering both wheels in one calculation takes this into account. This is due to the non-linear behavior of the model with non-linear bolts. Comparing the different models with linear bolts and with and without load superposition, it is shown that the results are more or less similar. Since the load superposition principle neglect the negative contribution to the bolt forces, the results with load superposition will always be higher and therefore on the safe side.

- Linear calculations give both an overestimation and an underestimation of the bolt forces depending on the load case which is considered. As shown in Table 4.3, the difference between the different linear and non-linear calculations is a maximum of 0.5 $kN$. However, since also lower results occur, unsafe results can be obtained. To solve for this an extra safety factor needs to be introduced based on the error that is made. Using this safety factor made it possible to use linear calculations.

- Calculating the relative errors, it is observed that some errors that are made are more than 100 %. This is because small (or almost zero) forces are obtained for the detailed model which is used as a reference model. Dividing the difference in force between a simplified numerical model and the detailed model by this small number gives a high value while the occurring forces remain low. The forces obtained by the models with an orthotropic deck are larger since more load is spread in the direction perpendicular to the moving direction of the load. These differences in forces are not relevant for the uplift design of the connections since the error is not made on the largest bolt force.

- The largest errors that have an influence on the maximum bolt force, are occurring due to the use of an orthotropic plate instead of a deck plate with modeled geometry of skins and webs. This is due to the difference in load distribution throughout the plate. In Section 4.5, the difference in load distribution is shown with smaller models. Based on the deformations it can be concluded that the load is spread more in the direction of the moving load for the plate model compared to the detailed model. Since the bolt forces are related to the deformations, the model gives in general higher bolt forces due to a larger spreading. Therefore, it has to be concluded that models with an orthotropic deck plate cannot be used to calculate the bolt forces accurately enough unless better equivalent properties are used.

- The most trustful simplified model is the one with the linear bolts. To improve the results for the other models, a better description of the equivalent properties has to be found. This can be done by the use of a thicker equivalent core which is a part of the topskin and bottomskin and the complete webs. On both sides of this core, thin layers with equivalent properties based on the ones from the skins have to be modeled. Using this type of model will give a more similar load spreading as for the detailed model.

A more extensive comparison of all the different models that have been made is described in Section 6.1.

# 5

# Analytical models

Different levels of complexity can be used to calculate analytically the deformation of a bridge deck. In this chapter, the different analytical models that are considered are described. Figure 5.1 shows in the green boxes which models are described in this chapter. The models are ranged in order of complexity and start with the most simple ones, the beam models which are described in the first section. Sections two and three describe the plate models that are considered in ElamX and Python respectively. After the description and the presentation of the results in the different sections, Section 5.4 gives a comparison of the different analytical models. In the end, a discussion on the analytical models is given in the last section.
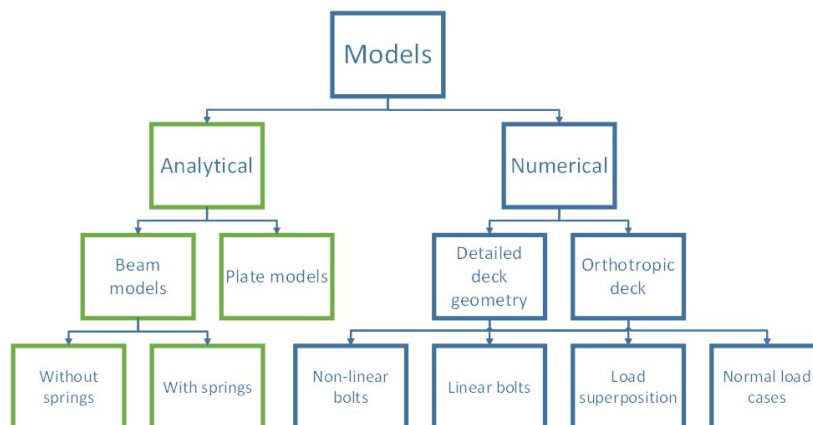


Figure 5.1: Analytical models in overview models

## 5.1. Beam models - MatrixFrame

The easiest method to calculate the bolt forces is the use of a beam model. A beam model is a model for which one of the dimensions is significantly more important than the other two. Therefore, the deformation in the other directions is neglected. This makes the models easier to make and reduces the calculation time compared to plate models. However, the accuracy and the possibilities will be less due to this simplification.

Two types of beam models are used in this research. The first model which is described in Section 5.1.1, uses only supports at the location of the supporting beams. This is a large simplification however, it makes it possible to implement the model in almost all engineering software packages. The second beam model has next to the supports at the locations of the supporting beams, springs at the locations of the bolts. This makes the behavior of this model closer to the plate models. A more elaborate explanation of this second model is given in Section 5.1.3.

### 5.1.1. Description model 1 - without springs

A beam model is made with MatrixFrame to be able to compare the obtained deformations with the numerical models. This is done for three different load cases as described in Section 3.1.6. Material properties for the

beam are given in Table 5.1. The area, moment of inertia and elasticity modulus of the beam are calculated for a massive beam consisting out of three parts. These parts are the topskin, webs and bottomskin. A description of the equivalent material properties is given in Section 4.4. For the simplification of the plate as a model, a width of 400 $mm$ is used. This width is assumed based on the width of the wheels from the load. The beams are supported with rigid supports at the locations of the I-beams. Distance between the supports is the same as for the numerical model described in Section 3.1.2 and for the beam model, it is shown in Figure 5.2. In short, the beam model is a 2D representation of the plate model.
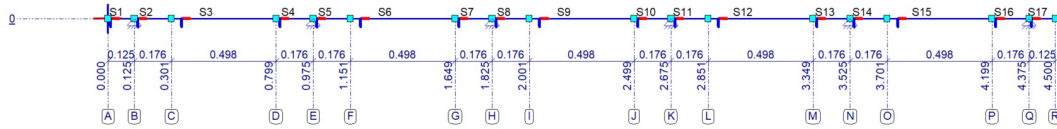


Figure 5.2: Geometry of the model 1 made in MatrixFrame [$m$]

Table 5.1: Material parameters used for the models made in MatrixFrame

| Parameter | Value |
|---|---|
| Area [$m^2$] | 1.2000e-01 |
| Moment of inertia [$m^4$] | 5.760e-05 |
| E-modulus [$kN/m^2$] | 9.398e+06 |

## 5.1.2. Results model 1 - without springs

Using a linear calculation based on equilibrium conditions, the forces in the supports can be calculated by MatrixFrame. The calculation gives the results as shown in Figure 5.3 for the different load cases.



(a) Bolt forces MatrixFrame load model 1 [$kN$]



(b) Bolt forces MatrixFrame load model 2 case 1 [$kN$]



(c) Bolt forces MatrixFrame load model 2 case 2 [$kN$]
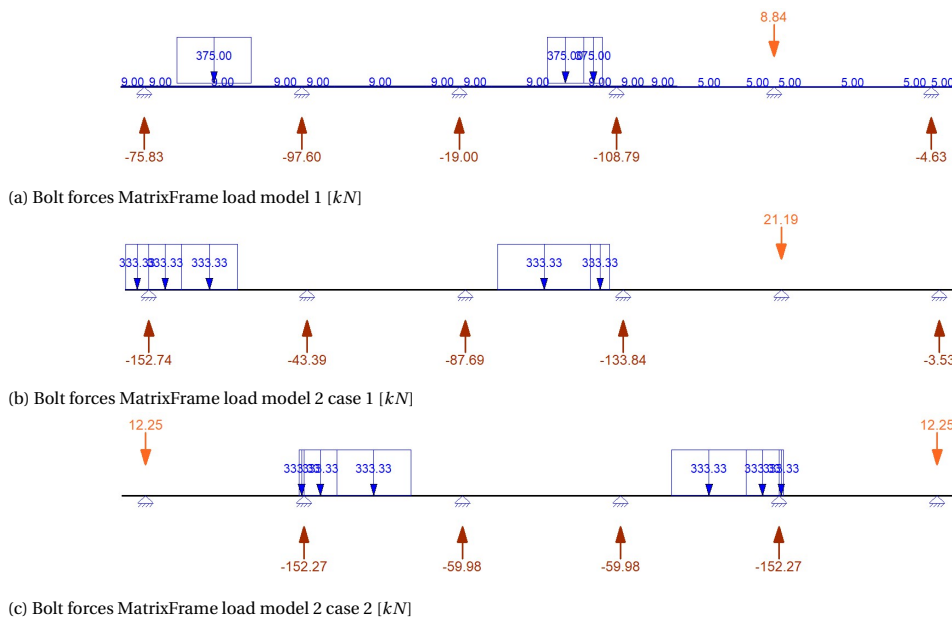
Figure 5.3: Bolt forces MatrixFrame model 1

Figure 5.3 shows that tension forces occur in the different supports depending on the load case. The uplift forces occur at the support from the unloaded span next to the loaded span due to the upwards deformation in the unloaded span. Comparing the magnitude of the forces to the ones obtained with the numerical models as shown in Section 4.10, it is shown that the obtained forces are higher. The deformations obtained with beam model 1 for the different load cases are shown in Figure 5.4.

(a) Deformations MatrixFrame load model 1 [$m$]



(b) Deformations MatrixFrame load model 2 case 1 [$m$]



(c) Deformations MatrixFrame load model 2 case 2 [$m$]
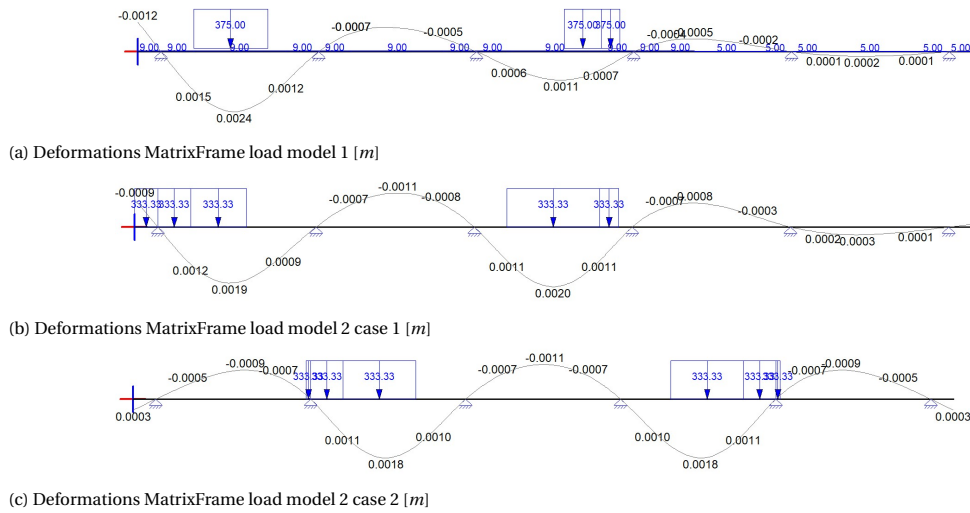
Figure 5.4: Deformations MatrixFrame model 1

### 5.1.3. Description model 2 - with springs

Model 1 excludes the bolts in the model. However, this is an important part because calculating the bolt forces is one of the main tasks of the research. To add the bolts to the beam model, springs are used to represent the behavior of the bolts. A spring constant of 5000 [$kN/m$] is used, which means a force of 5 $kN$ for every $mm$ elongation or shrinkage of the bolt. This model is shown in Figure 5.5.
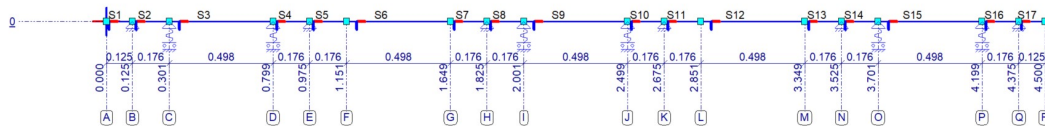


Figure 5.5: Geometry of the model 2 made in MatrixFrame [$m$]

### 5.1.4. Results model 2 - with springs

The main issue with this type of calculation is the need for non-linear springs to represent the real behavior of the bolts. In practice, the bolts only work in tension and the I-beams can only take compression. The results with the linear springs are visualized in Figure 5.6, which shows that, depending on the load case, compression in the bolts and/or tension in the supports occur. This problem can be solved with non-linear springs and supports. However, the student edition of MatrixFrame does not include this option and therefore these calculations are not performed. It endorses the need for a numerical model in which the non-linear behavior of the bolts can be handled in a proper way. Next to the forces in the springs, the deformations are shown in Figure 5.7. Comparing these deformations with the deformations found in model one, without the springs, it can be seen that the deformations are lower in the case with the springs. This is due to the restriction of the movement of the deck due to the bolts.

(a) Bolt forces MatrixFrame load model 1 [$kN$]



(b) Bolt forces MatrixFrame load model 2 case 1 [$kN$]



(c) Bolt forces MatrixFrame load model 2 case 2 [$kN$]
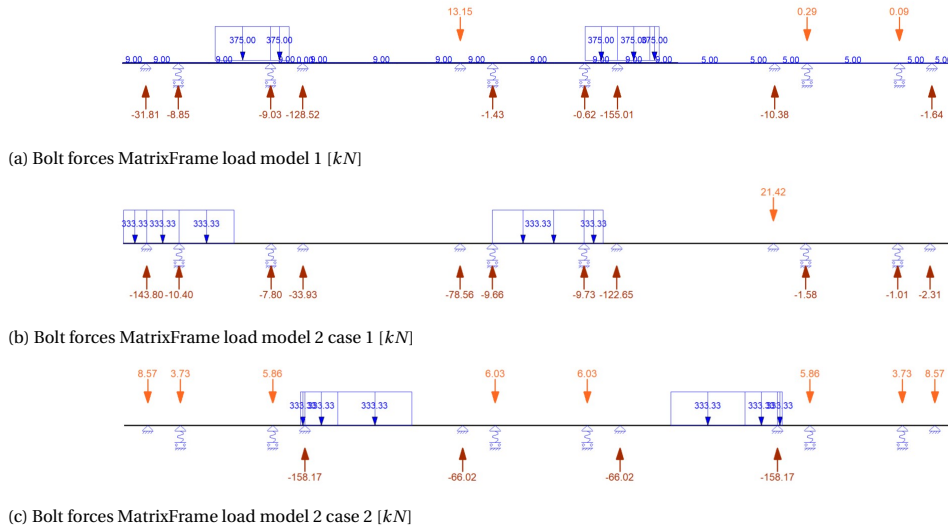
Figure 5.6: Bolt forces MatrixFrame model 2



(a) Deformations MatrixFrame load model 1 [$m$]



(b) Deformations MatrixFrame load model 2 case 1 [$m$]



(c) Deformations MatrixFrame load model 2 case 2 [$m$]
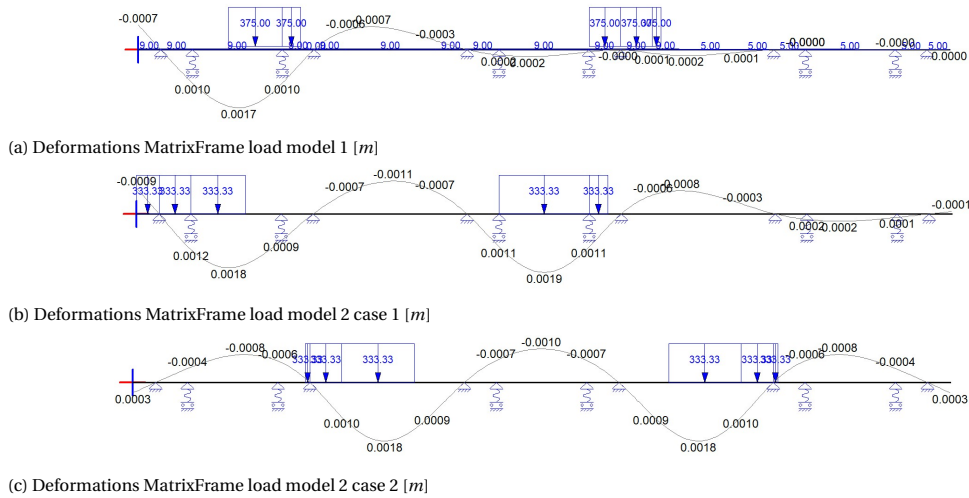
Figure 5.7: Deformations MatrixFrame model 2

## 5.2. Plate models - ElamX

Another type of analytical calculation can be performed with a plate theory-based software called ElamX. ElemX is a free software developed at the University of Dresden [43] that can be used to calculate the maximum deformation of an FRP plate. However, there are some limitations to the software with respect to the loads that can be applied and the boundary conditions that can be used. The main limitations are listed below.

- Results are only shown for the maximum and minimum value.

- Plate has to be symmetric in through-thickness direction.

- Only a point loads and/or uniform distributed loads over the complete area of the plate can be applied

- There is a limit in the type of supports that can be applied at the edges of the plate. Internal or point supports cannot be used.

Due to the limitations of the software, ElamX cannot be used to calculate all the load cases which are considered in this research. The software is used to check the models that are made with simpler load cases and boundary conditions.

### 5.2.1. Description of the model

In ElamX, a plate model is made with the same dimensions as the numerical models for which the dimensions are shown in Figure 3.2. The plate is 4.5 $m$ by 4.5 $m$ and has a thickness of 120 $mm$. Even as for the simplified numerical models with an orthotropic deck plate, described in Section 4.4, the plate is made by the use of equivalent material properties. However, in this case, only one layer is used for the complete plate. Therefore, all material properties are calculated based on the volume ratio of each original layer. Stiffeners are added to the model at the location of the supporting beams to represent the girders underneath the plate. The stiffeners do have the properties of the applied I-beams in the numerical models.

### 5.2.2. Results

Since the uniformly distributed loads can only be applied over the complete plate, it is not possible to calculate load model 1 in ElamX. For load model 2, the wheel loads are simplified to point loads which makes it able to perform the calculation. The results are shown in Figure 5.8 for load model 2 case 2, however, the results are not exact due to the fact that the plate is not symmetric in thickness direction.
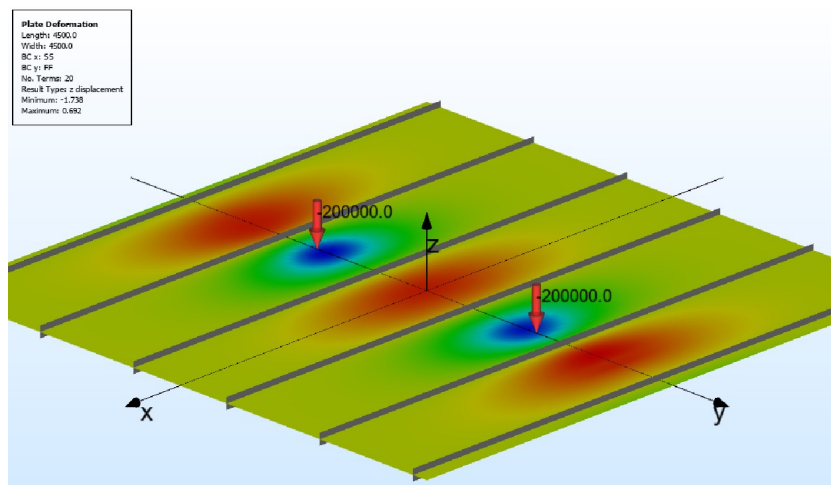


Figure 5.8: Deformations obtained with the model made in ElamX for load model 2 case 2

Next to the calculation of one of the applied load models, a calculation is done with a UDL load of $5kN/m^2$ to compare to other plate theories that are made in Python as described in Section 5.3. The dimensions of this plate are smaller as explained in Section 5.3 because only the part between two I-beams is modeled. The results from this calculation are shown in Figure 5.9.
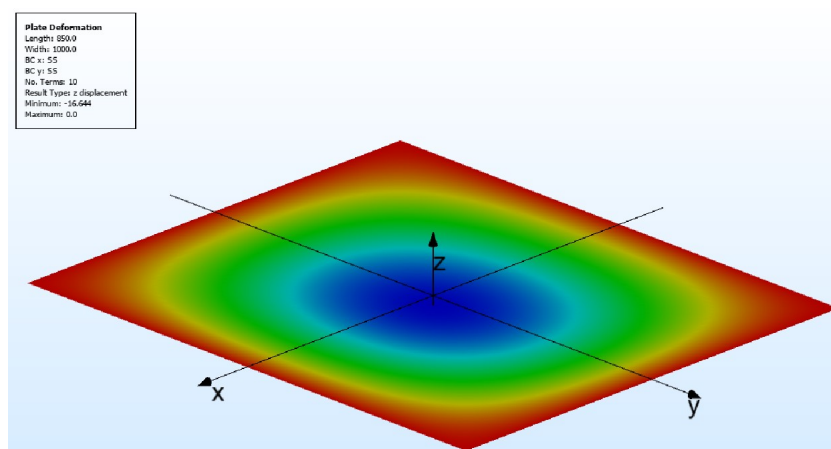


Figure 5.9: Deformations obtained with the model made in ElamX for UDL

## 5.3. Plate models - Python

Next to the beam models, different types of plate theories can be used to calculate deformations of orthotropic FRP decks. In the previous section, a model made with ElamX was described. Next to this, it is possible to model plate theories in Python, or another software, to be able to calculate stresses, strains and deformations. Different types of plate theories are given in Section 2.3.2 of the literature review. Theories that are used in this research are described more in detail in this section, including the results that are obtained.

The properties used for the different plate models are given in Table 5.2. The material properties are the same as the ones used for the orthotropic plate in the simplified numerical model as described in Section 4.4 for the one-layer model. Different dimensions are used compared to the other models. Since the plate theories do not offer the opportunity to implement internal supports or stiffeners, only one span of the plate can be modeled. Therefore, the width of the plate is set to the distance between two I-beams, which is 850 $mm$. For the length, a value of 1000 $mm$ is used to be sure that the model will work as a plate. The different models are modeled in Python based on found literature as described in Section 2.3.2. A short description of each model used with the results obtained for the models is given in the following sub-sections.

Table 5.2: Dimensions and material properties for analytical plate models

| Parameter | Value |
|---|---|
| Height [$mm$] | 120 |
| Length [$mm$] | 1000 |
| Width [$mm$] | 850 |
| Ex [$MPa$] | 9398 |
| Ey [$MPa$] | 4854 |
| Gxy [$MPa$] | 1348 |
| Gxz [$MPa$] | 989 |
| Gyz [$MPa$] | 339 |
| $\nu_{xy}$ [$-$] | 0.214 |
| $\nu_{xz}$ [$-$] | 0.193 |
| $\nu_{yz}$ [$-$] | 0.193 |

### 5.3.1. Description model CUR96

The model from the CUR96 is shown in Figure 5.10 [6]. Formulas describing the model are given in Section 2.3.2 and will therefore not be repeated here. Restrictions for this model are given by the boundary conditions and loading type. The CUR96 only gives a solution for simply supported boundary conditions at all sides of the plate and a uniformly distributed load. Therefore, the model cannot be used for calculations of wheel loads on multiple span decks. However, it can be used as a check for other models since the model is easy to make and the calculation time is low (less than one minute) for the considered load case, dimensions and number of sines used.
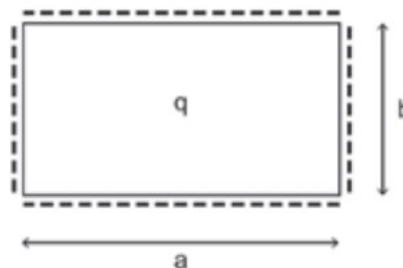


Figure 5.10: Overview model of the CUR96 [6]

### 5.3.2. Results model CUR96

To be able to compare all analytical plate models with each other, the same load case of an uniformly distributed load of 5 $kN/m^2$ is applied. The results of the calculation with the UDL load are shown in Figure 5.11. In this figure, the x-coordinate represents the width of the plate and the y-coordinate the length. It

is shown that the deformation is zero at the edges of the model, which is correct since simply supported boundary conditions are applied on all edges. A parabolic deformation is observed which corresponds to the applied load. The maximum deformation, 16.4 $mm$, is reached in the middle of the plate.
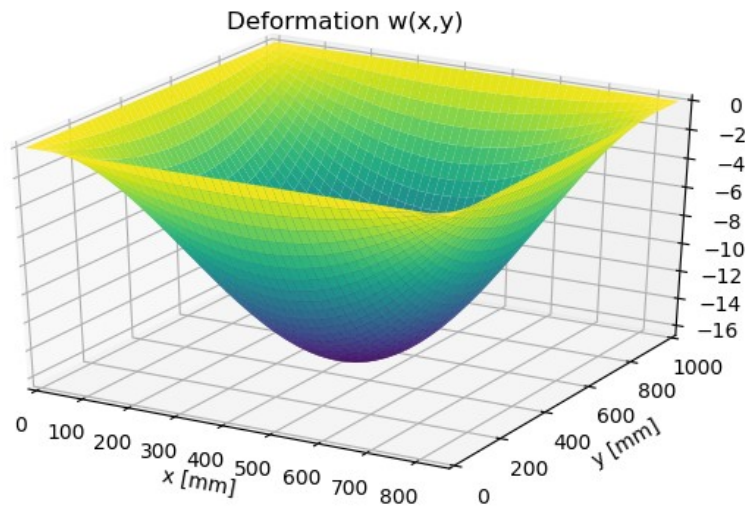


Figure 5.11: Deformation plate calculated with CUR96 model [$mm$]

### 5.3.3. Description of the model based on an orthotropic plate theory

A theory that takes both shear and bending deformation into account is the two-variable refined plate theory for orthotropic plate analysis as described by Shimpi and Patel [17]. The used model in this theory is shown in Figure 5.12 and the formulas are given in the literature review in Section 2.3.2. Since for FRP structures, shear deformation has a significant contribution, this theory can be useful to calculate deformations for a given load. However, this theory has the same limitations as the CUR solutions concerning the boundary conditions and loads which are described in the previous sub-section. Therefore, simply supported boundary conditions are used at all edges of the model. The dimensions and material properties are given in Table 5.2.
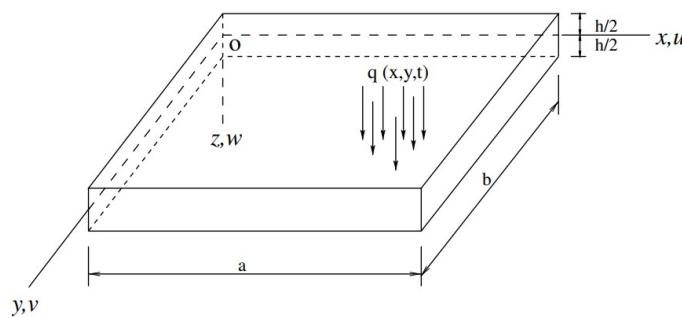


Figure 5.12: Overview model orthotropic plate theory [17]

### 5.3.4. Results of the model based on an orthotropic plate theory

The results for a calculation with the same UDL load of 5 $kN/m^2$ as for the calculation with the model of the CUR96 are shown in Figure 5.14. The same shape for the deformation is shown as for the previous plate model. A maximum total deformation of 21.9 $mm$ occurs at the middle of the plate. The different contributions of bending and shear deformation are shown in Figure 5.13. About 20% of the total deformation is caused by shear deformation and the other 80% is caused by bending deformation.
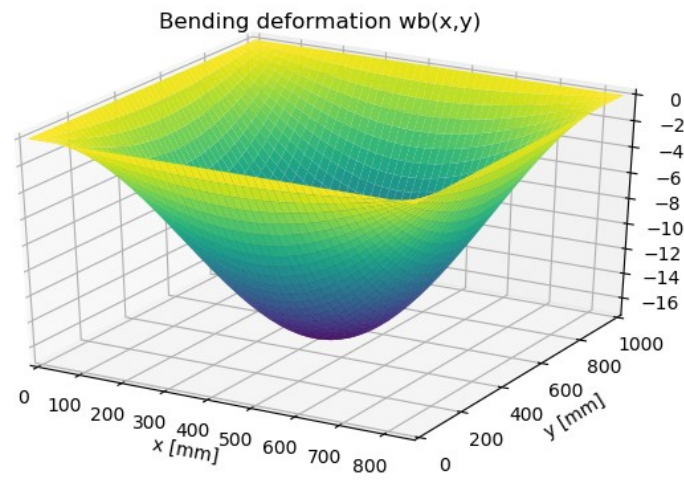
(a) Bending deformation plate [*mm*]
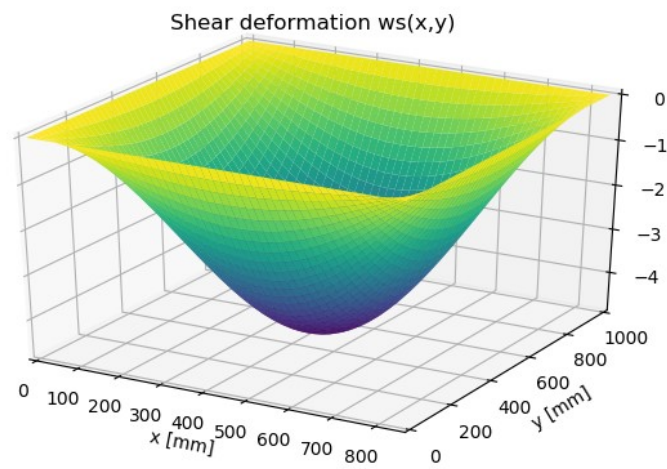


(b) Shear deformation plate [*mm*]

Figure 5.13: Bending and shear deformation plate calculated with orthotropic plate theory [*mm*]
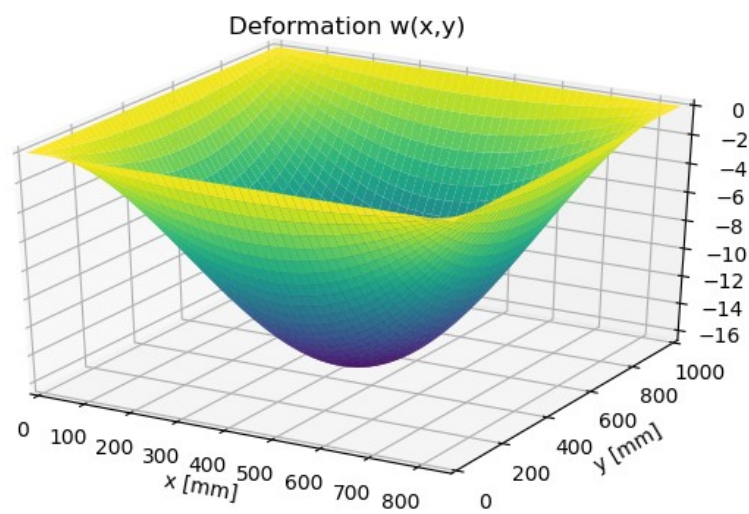


Figure 5.14: Deformation plate calculated with orthotropic plate theory [*mm*]

### 5.3.5. Description of the model with general boundary conditions

A theory without limitations regarding boundary conditions and loads is the theory of an accurate solution method for the static and dynamic deformations of orthotropic plates with general boundary conditions as described by Khov et all. [18]. An overview of the model that is used in this theory is shown in Figure 5.15 and the main formulas are given in Section 2.3.2. This theory is able to give the deformations for an arbitrary load for a combination of all types of boundary conditions by the use of two springs. A translational spring and a rotational spring. Applying different values as a constant for these springs gives a free, simply supported or clamped edge and all options in between. For the different edges, different types of boundary conditions can be used.

A multiple span plate can be represented by clamped edges at two opposite sides. Using this principle, the theory is able to give the deformation for a wheel load on a multiple-span FRP slab. Therefore, the theory can be used to check the deformations of the numerical models. However, the theory has its limitations regarding modeling and computational time. During the thesis, a Python model is made for this theory but unfortunately, this was not successful. When more time is implemented into this model it can be used. However, the calculation time will be even higher than it is for the detailed numerical models and therefore this time is not invested during this thesis.
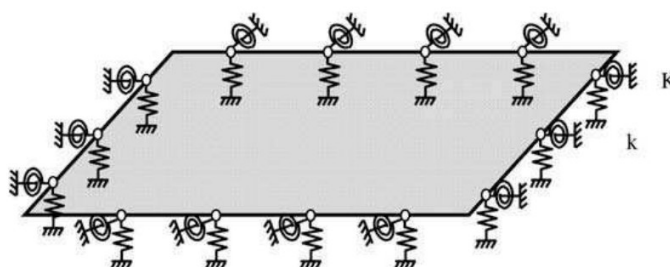


Figure 5.15: Overview model with general boundary conditions [18]

## 5.4. Comparison analytical models

The results of the different analytical methods can be compared to each other. In the Tables 5.3 up to 5.5 the results of the different calculations are given. First, the different beam models are compared to each other. In Table 5.3, a comparison of the deformation for the different load cases is shown. At the bottom of the table, the deformation calculated with the plate model made in ElamX is added to be able to compare the analytical plate and beam models.

It is shown that the deformation calculated with the beam model without springs gives the highest deformation. For load model 2 case 2, the deformation calculated will all the models has the same order of magnitude. The main difference in deformation between the two models is caused by the constraint in deformation due to the springs at the location of the bolts. These springs cause another type of deformation shape and therefore the difference occurs.

Comparing the obtained forces, the table shown in Table 5.4 is made. For the beam model without springs, the forces at the supports are used as bolt forces while for the beam model with springs, the forces occurring in the springs are used. It is observed that both models can give higher and lower forces compared to each other, depending on the load model that is applied.

Table 5.3: Comparison deformation different beam models [$mm$]

| Calculation method | Max deformation [mm] | | |
|---|---|---|---|
| | Load model 1 | Load model 2 case 1 | Load model 2 Case 2 |
| MatrixFrame without springs | 2.4 | 2.0 | 1.8 |
| MatrixFrame with springs | 1.7 | 1.9 | 1.8 |
| ElamX | | | 1.74 |

Table 5.4: Comparison bolt forces different beam models [$kN$]

| Calculation method | Maximum tension bolt force [kN] | | |
|---|---|---|---|
| | Load model 1 | Load model 2 Case 1 | Load model 2 Case 2 |
| MatrixFrame without springs | 8.84 | 21.19 | 12.25 |
| MatrixFrame with springs | 13.15 | 21.42 | 8.57 |

To be able to compare the numerical models with the analytical models, a numerical model is made in Abaqus with the same dimensions, material properties and loads as it is the case for the analytical plate models. Figure 5.16 shows the results calculated with this model for the same boundary conditions as the calculations of the other plate models.
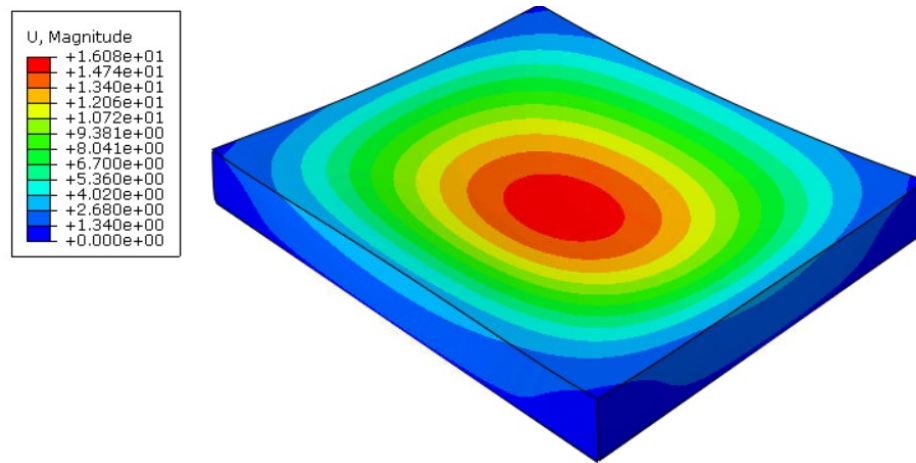


Figure 5.16: Deformation plate calculated with Abaqus [$mm$]

Table 5.5 lists the deformation obtained by the different plate models with the same load and boundary conditions. It is shown that the total deformation is in the same order of magnitude for all models except the model which separates the bending and shear deformation. Considering the Abaqus model as the reference one, it is shown that all other models are on the safe side. Since the deformation is more or less the same for different analytical plate models as for the numerical model, it can be concluded that this model can be used to describe the behavior of an FRP plate. However, since all models use the same material properties, these have to be verified with another method.

Table 5.5: Comparison deformation different plate models with UDL load [$mm$]

| Calculation method | Max deformation [mm] | | |
|---|---|---|---|
| | Bending | Shear | Total |
| ElamX | | | 16.64 |
| CUR | | | 16.42 |
| OPT | 17.09 | 4.79 | 21.88 |
| Abaqus | | | 16.08 |

## 5.5. Discussion analytical models

The beam models can be used to calculate the deformations of the plate. The results depend on the effective width of the beam that is chosen wherefore an assumption is made because it is uncertain how large this width has to be. An initial study on the effective width of the beam that has to be used is described in Section 3.4.2. However, a more in-depth research needs to be performed to obtain the width that needs to be used. Bolt forces can be calculated with the beam model by the use of non-linear springs as supports at the locations of the bolts and the supporting beams. The accuracy of these calculations has to be investigated to be able to

conclude this.

Analytical plate models can be used to describe the deformations of the deck plates for arbitrary load cases depending on the theory that is used. However, calculation of the forces in the bolts cannot be performed with analytical models at the moment. Next to this, the calculation time will be too large for a deck plate with dimensions used in real cases. The first two plate theories described, the CUR model and the orthotropic plate theory, are not useful since these theories are not able to give the deformation for a wheel load and different types of boundary conditions. The last described theory with general boundary conditions is able to give these deformations and therefore, able to verify the numerical models. However, in this research, this theory is not further used due to time limitations and limited applicability.

# 6

# Comparison different models

In the previous three chapters, different models are described to calculate the deformations of FRP slabs and beams and if possible the uplift forces. In this chapter, the different models are compared to each other based on the results and the performance. This comparison is described in the first section. The capacity of the connections in which the bolt forces will occur is determined in the second section. From the comparison of the models and the bolt forces compared to the capacity of the connections, conclusions can be drawn for the second part of the thesis which is described in the last section of this chapter.

## 6.1. Comparison numerical and analytical models

The chapters three, four and five describes all the different models that are made to calculate the uplift forces in the bolted connections between the FRP slabs and the steel structure. An overview of all these models is shown in Figure 6.1.
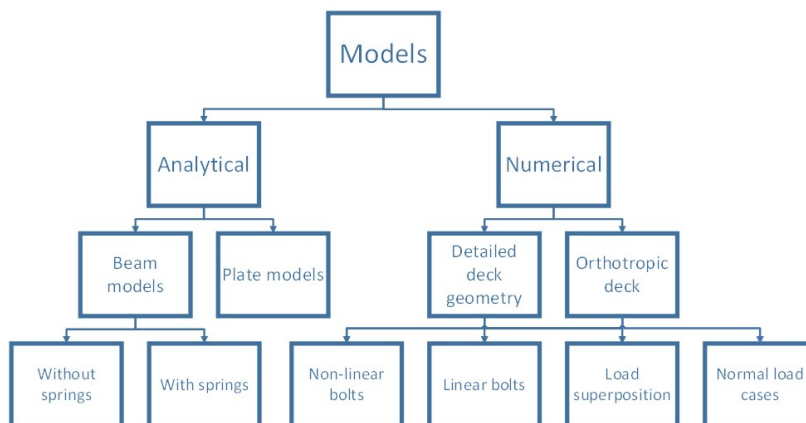


Figure 6.1: Overview of all the numerical and analytical models made in part I of the thesis

The different models are compared based on the fact if it is possible to calculate the bolt forces, the calculation time and the accuracy of the results. Table 6.1 shows the result of the comparison of the maximum bolt forces.

Table 6.1: Overview maximum bolt forces different models

| Model type | Description | Load model 1 Including UDL Max Force [kN] | Load model 1 Excluding UDL Max Force [kN] | Load model 2 Case 1 Max Force [kN] | Load model 2 Case 2 |
|---|---|---|---|---|---|
| Numerical | Detailed model | 0.49 | 0.75 | 2.02 | 4.18 |
| | Load superposition | | | | 4.47 |
| | Linear bolts | 0.52 | 0.68 | 1.61 | 4.17 |
| | Linear bolts & Load superposition | | | | 4.41 |
| | Orthotropic deck | 1.36 | 1.42 | 1.58 | 5.22 |
| | Orthotropic deck & Load superposition | | | | 5.26 |
| | Orthotropic deck & Linear bolts | 1.42 | 1.49 | 1.52 | 5.09 |
| | Orthotropic deck & Linear bolts & Load superposition | | | | 5.08 |
| Analytical | MatrixFrame without springs | 8.84 | | 21.19 | 12.25 |
| | MatrixFrame with springs | 13.15 | | 21.42 | 8.57 |

Next to the result, the models can be compared on the amount of modeling effort that is needed to make the model. All the models made are compared to each other on a scale with low, medium and high relative to the maximum and minimum of the models. The same is done for the accuracy of the results. Next to this, the approximate calculation time needed is listed and shown in Table 6.2.

Table 6.2: Comparison of different models

| Model type | Description | Possible to calculate bolt forces | Calculation time [min] | Modeling effort | Accuracy |
|---|---|---|---|---|---|
| Numerical | Detailed model | Yes | ~20 | High | High |
| | Load superposition | Yes | ~20 | High | Medium |
| | Linear bolts | Yes | ~20 | High | High |
| | Linear bolts & Load superposition | Yes | ~20 | High | Medium |
| | Orthotropic deck | Yes | ~5 | Medium | Low |
| | Orthotropic deck & Load superposition | Yes | ~5 | Medium | Low |
| | Orthotropic deck & Linear bolts | Yes | ~5 | Medium | Low |
| | Orthotropic deck & Linear bolts & Load superposition | Yes | ~5 | Medium | Low |
| Analytical | MatrixFrame without springs | Yes | <1 | Low | Low |
| | MatrixFrame with springs | Yes | <1 | Low | Low |
| | Model CUR96 | No | ~1 | Low | - |
| | Orthotropic plate theory | No | <5 | Medium | - |
| | Orthotropic plate with general boundary conditions | No | >60 | High | - |
| | Model ElamX | No | <1 | Medium | - |

Based on the results listed in Table 6.2, it can be concluded that the analytical beam models are suitable for a quick and rough estimate. The analytical plate models are not useful for calculating the bolt forces. For a more accurate result, a detailed numerical model with linear or non-linear bolts has to be used. Numerical models with an orthotropic deck can be used as a good alternative when a good estimate is found of the equivalent material properties. As long as this is not the case, the accuracy is too low to be useful.

Comparing the bolt forces with the results found in literature, as described in Section 2.4.2, it is shown that the calculated tensile forces are a factor of 5-20 lower than the shear forces in the bolts. Compared to the tensile forces calculated with the fatigue load models by T. Peeters, the obtained forces are a factor of 2-13 lower. In Section 2.4.1, the capacity of the different connections is given. Comparing the obtained uplift forces in the connections to the tensile capacity, it is shown that the magnitude of the forces is only 2.5-5.0 % of the available capacity.

## 6.2. Capacity of the connection used at FCE

The type of connection that is used at the company FiberCore Europe is explained in Section 2.4.1 and shown in Figure 2.17. The capacity of the connections used by FCE is given based on the capacity of the bolts, tensile and shear resistance, the bearing resistance of the clamp plate, the maximum stress in the clamp plate and the strength of the laminates around the bolt [6] [44]. An overview of the parts that determines the capacity is shown in Figure 6.2.
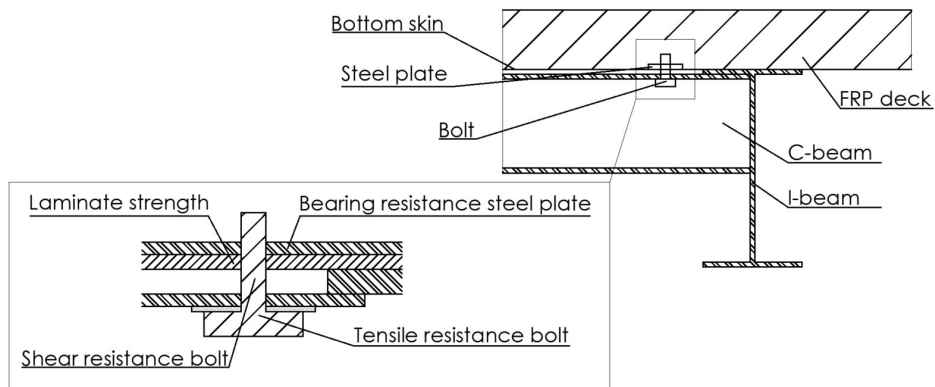


Figure 6.2: Overview of the parts that determines the capacity of the connections

According to EN1993-1-8, the tensile strength of the bolts is given by

$$F_{t.Rd} = \frac{k_2 \cdot f_{ub} \cdot A_s}{\gamma_{M2}}$$
(6.1)

in which $k_2$ is a factor depending on the type of bolts, $f_{ub}$ is the maximum tensile strength of the bolts and $A_s$ is the threaded area of the bolt. $\gamma_{M2}$ is the safety factor for steel connections. The shear resistance of the bolts is given by

$$F_{v.Rd} = \frac{\alpha_v \cdot f_{ub} \cdot A_s}{\gamma_{M2}}$$
(6.2)

using the same parameters as for the tensile strength and $\alpha_v$ as a correction factor depending on the bolt class. For a M20 bolt with a bolt class of 10.9, this gives a capacity of the bolts of

$$k_2 = 0.9$$
$$f_{ub} = 1000 \; MPa$$
$$A_s = 245 \; mm^2$$
$$\gamma_{M2} = 1.25$$
$$F_{t.Rd} = \frac{0.9 \cdot 1000 \cdot 245}{1.25} = 176.4 \; kN \qquad (6.3)$$
$$\alpha_v = 0.5$$
$$F_{v.Rd} = \frac{0.5 \cdot 1000 \cdot 245}{1.25} = 98.0 \; kN$$

Using a steel plate with dimensions of 100 $mm$ by 100 $mm$ with a thickness of 15 $mm$ and an ultimate steel strength of 470 $MPa$, the bearing capacity in longitudinal direction of the plate is given by [44]

$$e_{1.1} = 50 \; mm$$
$$e_{2.1} = 50 \; mm$$
$$k_1 = 1.7$$
$$\alpha_b = \alpha_{d.1} = min\left(\frac{e_{1.1}}{3 \cdot d_0}, 1\right) = 1 \qquad (6.4)$$
$$F_{b.RD.1} = \frac{k_1 \cdot \alpha_b \cdot f_u \cdot d_0 \cdot t_p}{\gamma_{M2}} = \frac{1.7 \cdot 1 \cdot 470 \cdot 20 \cdot 15}{1.25} = 191.8 \; kN$$

In these formulas the bolt hole in the plate is given by $d_0$, $e$ denotes the distance between the center of the hole to the outside of the plate in different directions indicated with different subscripts and $k_1$ is the factor taking the distance between the considered bolt and other bolts into account. Since only one bolt is considered in this case, the minimum value is used. Next to this, $f_u$ is the ultimate strength of the steel plate and $t_p$ the thickness of the steel plate. In transverse direction the bearing strength is given by [44]

$$e_{1.2} = 50 \; mm$$
$$e_{2.2} = 50 \; mm$$
$$k_1 = 1.7$$
$$\alpha_b = \alpha_{d.1} = min\left(\frac{e_{1.2}}{3 \cdot d_0}, 1\right) = 1 \qquad (6.5)$$
$$F_{b.RD.1} = \frac{k_1 \cdot \alpha_b \cdot f_u \cdot d_0 \cdot t_p}{\gamma_{M2}} = \frac{1.7 \cdot 1 \cdot 470 \cdot 20 \cdot 15}{1.25} = 191.8 \; kN$$

Next to the steel parts, the capacity of the connection is dependent on the laminate strength around the bolt hole. These strengths for tensile and compressive stresses in the longitudinal and the transverse direction are given by the formulas below [6]. In these formulas, the correction factors for temperature and moisture are denoted by $\eta_{l.s}$. The strength of the laminates in different directions is denoted by $\sigma$ and the safety factor for the material by $\gamma_{m.s}$.

$$\sigma_{xt.bs} = \frac{\eta_{l.s} \cdot \sigma_{xt.bs}}{\gamma_{m.s}}$$
$$\sigma_{xc.bs} = \frac{\eta_{l.s} \cdot \sigma_{xc.bs}}{\gamma_{m.s}}$$
$$\sigma_{yt.bs} = \frac{\eta_{l.s} \cdot \sigma_{yt.bs}}{\gamma_{m.s}} \qquad (6.6)$$
$$\sigma_{yc.bs} = \frac{\eta_{l.s} \cdot \sigma_{yc.bs}}{\gamma_{m.s}}$$

These maximum strength values are dependent on the layup of the bottomskin. The maximum stress in the bottomskin can be calculated with the use of a stress concentration factor of the CUR96 [6]

$$k_{cc1} = \left(\frac{d_0}{d}\right)^2 \tag{6.7}$$

With $d_0$ the diameter of the hole and $d$ the diameter of the bolt used. Next to this, different correction factors need to be applied for imperfections. The maximum stress values for the longitudinal and the transverse direction for tension and compression are given by the formulas shown below [6]. In these formulas, the different conversion factors are denoted by $k$. $k_{m1}$ and $k_{m2}$ for tilting and geometry respectively and $k_{cc1}$ for the stress concentration around the hole. $F_v$ is the shear strength in the different directions.

$$
\begin{aligned}
\sigma_{bs.x.c} &= \frac{k_{m1} \cdot k_{m2} \cdot k_{cc1} \cdot F_{v.x.Ed}}{d_0 \cdot t_{bs}} \\
\sigma_{bs.x.t} &= \frac{k_{m1} \cdot k_{m2} \cdot k_{cc1} \cdot F_{v.y.Ed}}{d_0 \cdot t_{bs}} \\
\sigma_{bs.y.c} &= \frac{k_{m1} \cdot k_{m2} \cdot k_{cc1} \cdot F_{v.x.Ed}}{d_0 \cdot t_{bs}} \\
\sigma_{bs.y.y} &= \frac{k_{m1} \cdot k_{m2} \cdot k_{cc1} \cdot F_{v.y.Ed}}{d_0 \cdot t_{bs}}
\end{aligned}
\tag{6.8}
$$

As shown in the formulas above, the capacity of the connection is based on the resistance of the steel parts and the resistance of the FRP parts. For all types of slabs, the steel parts will have the same capacity. The capacity of the FRP laminates will depend on the design of the slab.

## 6.3. Connections and optimization

As shown in Table 6.1, the bolt forces are much lower than the capacity of the connection itself, shown in Section 6.2. This means that the number of connections can be reduced. However, when the amount of connections is reduced, the calculations need to be performed for the new case. The calculation procedure stays the same as described in Chapters 3, 4 and 5 of this thesis. Since the number and location of the connections have changed, the force distribution along the bolts can be different and so can the magnitude of the uplift bolt forces.

When the number of connections is reduced, different other problems can occur. For example, clattering of the slab can occur when too few connections are used. Other reasons for placing a minimum number of connections can be the reduction of the capacity of the connections due to mistakes, the loss of pre-loading of the bolts and corrosion. Next to this, a minimum number of connections is advised for the robustness of the construction.

Based on the fact that the magnitude of the uplift forces is such low, the optimization can be performed without taking the connections into account. As argued in Section 6.2, the capacity of the connections is partly based on the steel parts which are independent of the design of the slabs. For the other part, the capacity is based on the ultimate tensile and compression strength of the laminates in the bottomskin. Since the forces in the bolts are much lower compared to the other forces in the deck, all variants that satisfy the strength checks will be able to satisfy the design checks for the connections. Therefore, it can be concluded that the connections do not have to be considered in the optimization procedure.

# PART II

## Optimization

# 7

# Optimization procedure

The second part of the research is about the optimization of FRP traffic decks. For this, in the first section of this chapter, a short background of the optimization is given. In the second section the used optimization procedure is described. After this, the optimization procedure is performed for the same deck that is used in the first part of the thesis and described in the third section. This case is used to show how the optimization procedure works. Section 7.4 gives a discussion about the optimization procedure that is made. After this, the optimization procedure is used to calculate the optimal design for different boundary conditions which is called the standardization of the slabs. This can be found in the fifth section of this chapter. The last section contains a discussion on this standardization.

## 7.1. Background of the optimization procedure

An optimal design is the best or most favorable design [1]. Optimization has to be done with respect to a parameter which is in this case the direct costs of the slab. Direct costs mean the costs which are dependent on the design of the slab. The costs of an FRP traffic deck can be divided into three categories [2]. The first part of the costs is due to material costs, the second part is due to labor costs and the last part are general costs. The first two categories are (partly) variant dependent and therefore taken into account. Costs that are the same for each variant are not considered since the difference is important to compare the variants and not the total costs. Therefore, optimization is the action of making (detecting) the best design with respect to the direct costs [1].

Section 2.5 describes different optimization methods that can be used. However, the disadvantage of all the mathematical optimization methods is the need for a continuous optimization function. Due to the input for this functions is discontinuous, the cost function is also discontinuous. This discontinuity is caused by the fact that an integer number of plies has to be used for the webs and skins. For the different optimization methods that are available and already used in civil engineering applications, the genetic algorithm suits the best for this application. This method can handle the different designs and the computational time needed is acceptable. The design sensitivity analysis cannot be used for multi-variable optimization, only for decision making during the process [31]. The same as for the pure mathematical optimization methods, the simulating annealing method uses a continuous cost function which makes it not useful in this case. The RBDO method can be useful since this method considered both the safety of the design and the costs. Next to this, several limits and/or constraints can be used for different variables. However, due to the need for more evaluations compared to other methods, the computational time needed is relatively high. Another disadvantage is the need for uncertainty values which are not available for most cases in practice [31].

PSOA needs a stop criteria to end the analysis. When such a stop criterion is used, it is possible that the design found is not the most optimal design. The ant colony optimization method uses information from the previous step to calculate the outcome of the next step. This makes the analysis sensitive to local optimal solutions. A problem that is raised for all methods is the need for a check for strength. Since the most optimal design given for costs will be the one with the lowest amount of material for given labour, the strength, stiffness and stability have to be checked. Only methods which work with different variants are able to implement such a check.

A last option for optimization is a special module in Abaqus. This option can be used, however, the com-

putational time will be high since the dimensions of the Abaqus model are quite large. The design can be simplified to a two-dimensional problem which speeds up the calculations. Considering the deck plate as a beam gives also the opportunity to perform the checks with analytical formulas. To conclude, due to the high number of variants compared to the calculation time, not all variants can be considered. Therefore, the method of genetic algorithm is used including a strength check at global level, which is described in Section 7.2.4.

## 7.2. Description of the used optimization method

First, a general explanation of the optimization procedure is given in the first sub-section and the scope of the optimization in the second sub-section. After this, the genetic algorithm that is used for the optimization is explained with the used settings for the algorithm. Sub-section four contains information about the checks that are applied in the procedure and the fifth sub-section contains the calculation of the costs, which is the governing parameter for the optimization. The last sub-section contains some information about the method that is used to control the optimal design that is obtained.

### 7.2.1. General procedure for optimization

An overview of the optimization method used is shown in Figure 7.2. In the optimization procedure, the steps for the genetic algorithm are followed. A more in-depth explanation of the genetic algorithm is given in Section 7.2.3. The first step of the optimization procedure is an initial population that is made based on the different optimization parameters. These parameters are listed below and they cover all variables of the design of the FRP slabs as made by FiberCore Europe. All parameters are independent of each other, however, they can have an effect on which values are possible for another variable.

- Number of times a foam block is wrapped

- Number of z-layers 0/90

- Number of z-layers 45/-45

- Number of UD (unidirectional) plies topskin

- Number of UD plies bottomskin

- Number of UD plies webs

- Number of 45/-45 plies webs

- Overlapping length UD plies topskin

- Overlapping length UD plies bottomskin

- Overlapping length 0/90 plies topskin

- Overlapping length 0/90 plies bottomskin

- Overlapping length 45/-45 plies topskin

- Overlapping length 45/-45 plies bottomskin

- Height of the deck

- Web spacing

The number of times a foam block is wrapped means the amount of 45/-45 plies that are around the foam blocks as is shown in Figure 7.1. Overlapping length means the number of foam blocks the ply is continuing in the skins. A minimum number of foam blocks the plies needs to span is three blocks due to the Infra-Core principle [7]. The maximum number of blocks overlapped is set to nine since otherwise, the thickness becomes too large. For the different types of plies, the overlapping length can differ. For each variant, the design limits need to be checked. These limits are provided by FCE and given in Table 7.1. These boundaries come from limits due to production, type of construction and strength limits. Limits for the layups that can be used are given by the type of design. Due to the z-layers that are used, a limited amount of different layups

are available. A more in depth explanation is given in section 7.2.2. The other design check that needs to be performed is the check if enough fibers are placed in each main direction. According to the CUR96, a minimum amount of 12.5% of the glass fibers needs to be placed in the main directions 0°, 45°, 90° and −45°.

When the variants satisfy the checks on design criteria, each design needs to be checked on strength, stiffness and stability. These checks are done with analytical formulas from the CUR96, which is further described in Section 7.2.4. For the variants which satisfy, the costs are calculated. When the design does not satisfy, the costs are calculated based on the maximum unity check times a penalty. This penalty is a value larger than the maximum costs of the decks that will satisfy. Applying this penalty will make sure that the design that does not satisfy will never be chosen to be optimal. Next to this, when a variant is close to being satisfied, the penalty is the lowest.

For the cases the design checks, either for the design limits or the minimum amount of fibers, do not satisfy, the costs are calculated based on a penalty. This penalty is a high value compared to the other costs, higher than the total variable costs can be for the variants that satisfy the design checks and higher than the penalty applied for the design that not meet the strength checks as well. This makes sure that the design is unfavorable in the optimization procedure and therefore the algorithm is not searching for an optimum in this direction.

As a fitness value for the genetic algorithm, the costs are used. The fitness means how good an individual is with respect to the parameter to which the optimization is performed, which is in this case the direct costs of the slabs. Therefore, the lower the costs, the higher the fitness value of the variant. After calculating this fitness value for each variant within the generation, the end criterion is checked. This end criterion is the maximum number of generations that is applied or a maximum number of generations without improvement of the optimum result. As long as the end criterion is not met, a new generation is made. This new generation contains the best option(s), the elite, of the previous generation and new options based on the best options of the previous generation made by a crossover technique and mutations. For the new generations, the different checks are performed and the fitness values are calculated. This procedure is repeated as long as the end criterion is not met.

When the end criterion is met, the genetic algorithm is stopped. Based on the costs, the designs are ranked to decide on the optimum one. The most optimum design is checked with Abaqus to make sure that the design is safe enough. The procedure is coded and run in Python. The used code is given in Appendix G.
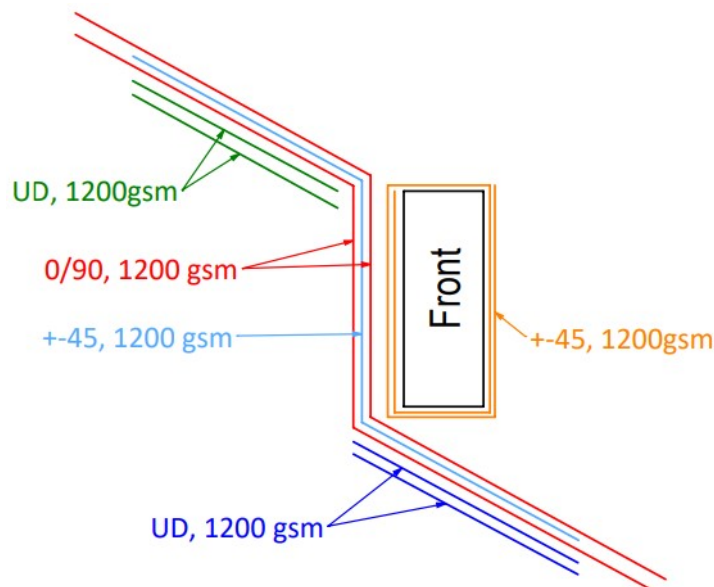


Figure 7.1: Layup traffic decks FCE [9]
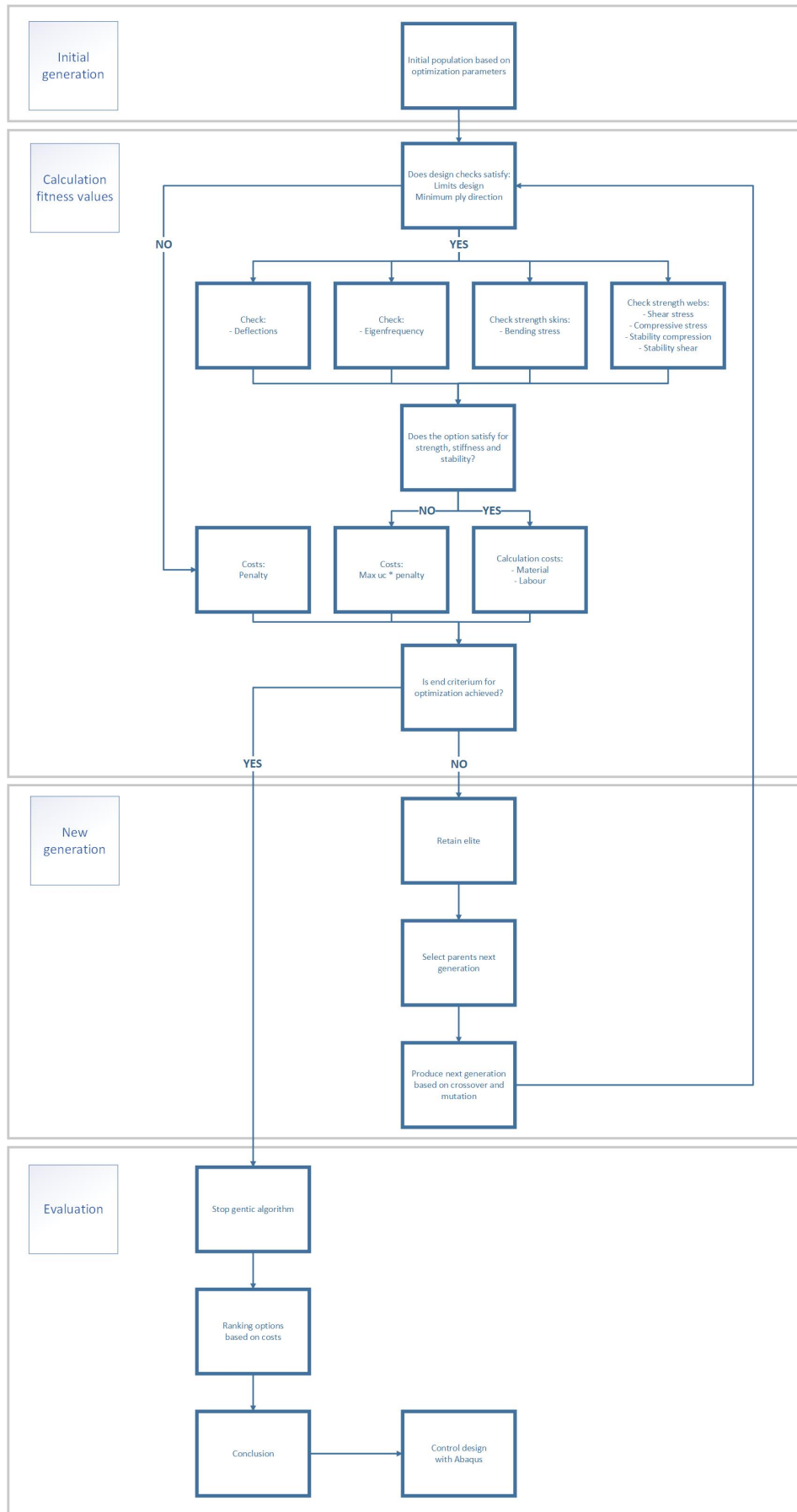
Figure 7.2: Outline optimization procedure

### 7.2.2. Scope of the optimization procedure

For the optimization procedure only the global behavior of the slabs is considered. Therefore, the optimal design that is gained from the optimization cannot be used in practice. More detailed calculations are needed on the local behavior. Options how theses checks can be done are described in Section 7.4.3. Next to this, design limits are provided by the company which are shown in Table 7.1.

Table 7.1: Limits for the optimization [2]

| Parameter | Limits |
|---|---|
| Height deck [$mm$] | 100-200 |
| Spacing webs [$mm$] | 100-400 |
| Thickness skins [$mm$] | 15-30 |
| Thickness webs [$mm$] | 5-15 |
| Minimum overlapping length [$-$] | 3 foam blocks |
| Maximum overlapping length [$-$] | 9 foam blocks |

To be able to compare the obtained optimal design, a reference design is provided by FiberCore Europe. The layups for this design are shown in Figure 7.3. The only things that can be changed on this design are the height and/or web spacing. The chosen values for these parameters are given in Table 7.2. These different reference designs are used for the standardization as described in Section 7.5.
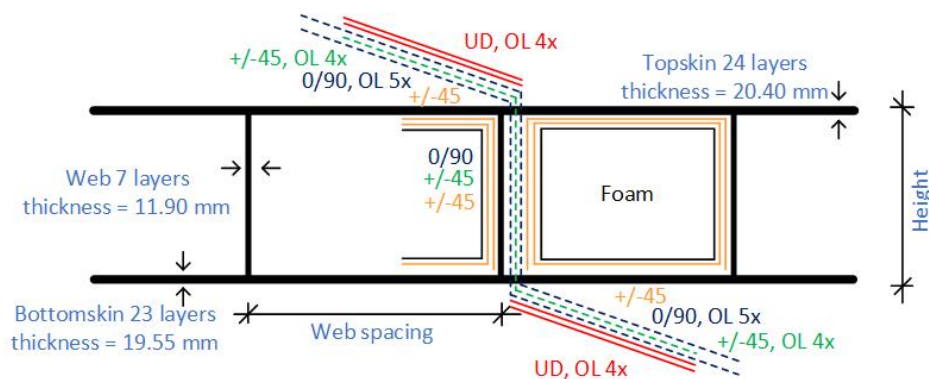


Figure 7.3: Reference design layups traffic decks FCE [2]

Table 7.2: Parameters reference design traffic decks FCE

| Parameter<br>Distance between supports $L_0$ [mm] | Height [mm] | Web spacing [mm] |
|---|---|---|
| 850 (Case deck part I) | 120 | 116 |
| 500 | 110 | 116 |
| 750 | 120 | 116 |
| 1000 | 130 | 116 |
| 1250 | 140 | 116 |
| 1500 | 150 | 116 |
| 500-800 | 110 | 116 |
| 800-1200 | 130 | 116 |
| 1200-1500 | 150 | 116 |

### 7.2.3. Genetic algorithm

An explanation of the theory of the genetic algorithm is provided in Section 2.5. Figure 7.4 shows a schematic overview of the genetic algorithm that is used in this research. A genetic algorithm is a probability-based optimization technique that can process continuous and discontinuous parameters at the same time. The algorithm is based on the principle of evolution and works the same as the natural selection principle. Over

different generations, the fittest individuals survive. When boundary conditions are applied to the optimization, the fittest option out of the possible ones is detected after enough generations [33].

In python, a genetic algorithm package is loaded, which is used for the optimization [45]. This package uses a number of input values to be able to run. These input values are shortly explained below and the chosen values are given in Table 7.3, which are mainly based on research performed by Yihong He and Amjad Aref [46]. In their research, a comparable optimization is performed for an FRP sandwich deck panel but with less variables and with respect to the maximum weight instead of the costs. Discrete and continuous optimization parameters are used and the fitness is calculated based on the weight of the deck. In the paper, a description of the tuning of the settings for the algorithm is given and since the problem is comparable, the same settings are used in this research, unless described below [46].
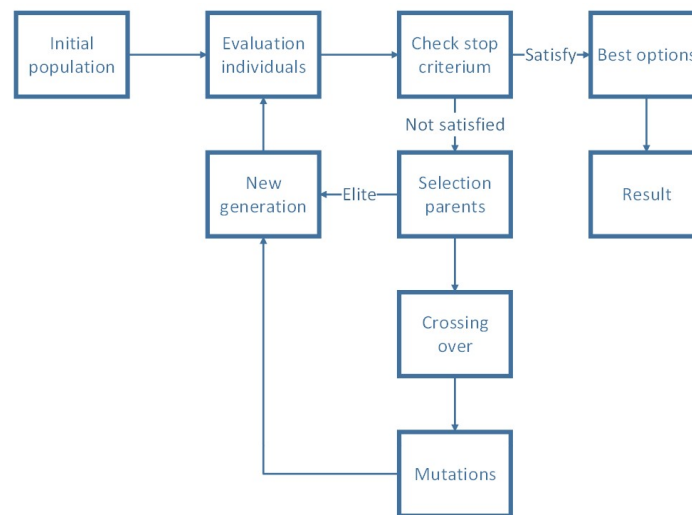
Figure 7.4: Overview process genetic algorithm

### Population size
The first input parameter of the genetic algorithm is the population size. This parameter represents the number of variants that are considered in each generation. In the research of He and Aref, a population size of 10-20 is used [46]. A total of 6-12 variables are used in the design of the slab in their research. Since the amount of variables in this research is higher, namely 15, the number of variants in a generation is increased to 50.

### Mutation probability
Mutation probability is the chance that for a gene of an individual in the generation a mutation occurs. A mutation is the change of one of the variables in the design by a random value (within the design limits). This option makes the optimization procedure less sensitive to local optima. A range of values between 0.003 and 0.3 is used in the research described in the paper of He and Aref [46]. Since more variables are used, the algorithm is more sensitive for local optima. To reduce the higher chance of these local optima an value of 0.5 is used in this thesis.

### Cross-over probability and type
New variants within a generation are not only made based on mutations but also on cross-over of the different genes. For a cross-over type, different options are possible. An uniform type of cross-over uses a number of subsequent variables from one of the best parents which will be changed by the ones for another fit parent. Next to the uniform type, one or two-point type of cross-over can be used. These types work the same way as the uniform type only the number of subsequent variables that are changed are respectively one or two. In this research, two-point cross-over is used. The chance of such a cross-over is given by the cross-over probability. In the paper of He and Aref a range of 0.5 to 0.8 is given. For the optimization in this research, the upper limit of this range of 0.8 is used due to the large number of variables.

### Parents portion

The parents portion is the number of individuals that are used from the current generation for the next generation. Taking a high value for this parameter excludes the change on new variants and therefore the number of variants that needs to be considered will increase. Using a low value, decrease the convergence rate since too much information is lost from the parents. Therefore, a medium value of 0.5 is chosen in this research.

**Elite ratio**
To be sure the next generation will contain a better or at least good enough variant, an elite can be used. These elites are the best options from the previous generation, that stay in the next generation. In this way, the best option will never be lost and the chance of a better variant becomes higher. Since only the best option has to stay, this value is set to 0.1 but can even be smaller when a larger population is used.

**Number of iterations**
For the end criterion, a maximum number of iterations has to be applied. This number of iterations has to be high enough to be able to detect the optimum. However, increasing the number of iterations directly increases the run time. This means that a balance has to be found between the accuracy that is needed and the run time that is acceptable. When a stop criterion is used, the maximum number of iterations has to be high enough so the algorithm is stopped by the stop criterion. Therefore, a maximum number of iterations of 1000 is applied in this case. As a stop criterion, a maximum number of iterations without improvement of the optimum is used. He and Aref use a maximum value of 50 iterations which is kept the same in this research [46].

Table 7.3: Input parameters genetic algorithm

| Input parameter | Value |
|---|---|
| **Population size** | 50 |
| **Mutation probability** | 0.5 |
| **Cross-over probability** | 0.8 |
| **Parents portion** | 0.5 |
| **Elite ratio** | 0.1 |
| **Maximum number of iteration** | 1000 |
| **Stop criteria** | 50 |

### 7.2.4. Checks for strength, stiffness and stability on global level

Before the fitness value of each individual can be calculated, first, each variant has to be checked for strength, stiffness and stability. These checks are performed at the global level with analytical formulas from the CUR96 [6] at the laminate level. Using these formulas is not the most ideal option to check an FRP structure, however, to be able to perform a quick check it is the only available option until now. The formulas that are used are given in Appendix E. Different checks are included namely, check for the maximum bending stress in top- and bottomskin, maximum compression stress and shear stress in the webs, global buckling of the webs and a combination of different stresses in the webs. Next to these global checks, the local behavior of the skins and webs has to be checked, however, this is out of the scope of this thesis. For recommendations about the implementation of the checks for local behavior Section 7.4.3 can be consulted.

The strength values for the laminates are calculated with a laminate failure progression tool of FCE [47]. This tool calculates the laminate strength at last ply failure based on the Tsai-Hill or Hashin Damage criterion. For the optimization, the Tsai-Hill criterion is used since this criterion is the most conservative one. The obtained strength values are checked against the maximum stresses in the laminates which results in unity checks. The highest unity check is the governing one and when one of the unity checks is larger than one, the design does not satisfy the established criteria.

### 7.2.5. Calculation costs

As described in Section 7.1, the costs of the FRP traffic decks are given by a combination of the material and labour costs. The calculation of these costs is described below.

Table 7.4: Price indication used materials [2]

| Material | Price [€/$kg$] |
|----------|----------------|
| Glass    | 3.00           |
| Foam     | 11.40          |
| Resin    | 3.70           |

**Material costs**

The first part is the material costs. An indication of the price for the different materials used are shown in Table 7.4, which came from the suppliers from FCE [2]. Since the price values are property from the company, indicative values are shown instead of the the real values. However, the ratio between the prices of the different materials is kept more or less the same. To be able to show the results without providing private information from the company, the results are shown relative to reference designs. The different reference designs used are shown in Section 7.2.2.

Based on the geometry, the costs for the materials can be calculated. In the different formulas used, the dimensions of the deck are given by $w$ for the width of the deck, $h$ for the height of the deck and $L$ for the length of the deck. The number of plies for the different parts is denoted by $np$ and the number of webs by $n$. Volume is denoted by $V$, density by $\rho$ and the mass by $M$. The price of the different materials is denoted by $p$ and the costs by $Q$. The area of the foam that is used can be calculated as

$$V_{foam} = (w_{deck} - n_{webs} \cdot t_{webs}) \cdot (h_{deck} - t_{topskin} - t_{bottomskin}) \cdot L_{deck} \tag{7.1}$$

The costs for the foam are given by

$$Q_{foam} = V_{foam} \cdot \rho_{foam} \cdot p_{foam} \tag{7.2}$$

Next to the foam, glass is used for the FRP decks. Different types of mats are used as shown in Table 7.5. Since all mats have the same amount of glass, it is assumed that the price for each mat is the same as the most expensive one. This is almost the case, only the price of the UD mats will be a little bit lower. The amount of glass that is used can be calculated as

$$M_{glass} = (w_{deck} \cdot np_{topskin} + w_{deck} \cdot np_{bottomskin} + h_{webs} \cdot np_{webs} \cdot n_{webs}) \cdot L_{deck} \tag{7.3}$$

The costs for the glass are given by

$$Q_{glass} = M_{glass} \cdot p_{glass} \tag{7.4}$$

Table 7.5: Glass mats

| Name | Orientation [°] |
|------|-----------------|
| UD (unidirectional) | [0] |
| Z-0/09 (Z-layer) | [0/90] |
| Z-+/-45 (Z-layer) | [−45/45] |
| Wrap | [−45/45] |

Together with the glass fibers, the resin is used to make the FRP laminates. The volume of the resin that is used in the bridge deck is calculated as the resulting volume. During the vacuum infusion, this empty space will be filled with resin.

$$V_{resin} = V_{deck} - V_{foam} - V_{glass} \tag{7.5}$$

The costs for the resin part are therefore

$$Q_{resin} = V_{resin} \cdot p_{resin} \tag{7.6}$$

The total costs for the part of the materials is given as

$$Q_{material} = Q_{foam} + Q_{glass} + Q_{resin} \tag{7.7}$$

**Labour costs**

The labour costs of the FRP bridge deck can be divided into two types of costs. A part of the labour costs is independent of the geometry of the deck, like

- Setting of the mold

- Installation of the tubes for the resin

- Diffusion of the resin

- Finishing of the deck

And the other part of labour costs is dependent on the geometry of the deck like

- Cutting of the glass

- Wrapping of the foam with glass mats

- Placing of the foam and glass on mold

To determine the total direct costs for the labour part, the hours spent on the geometry dependent tasks are calculated and multiplied by the hourly wage of the employees. First, the costs of the process in the glasshouse are calculated. In the glasshouse, the glass is cut, which depends on the number of webs. The more webs, the more often the glass has to be cut. The number of webs is one of the optimization parameters and therefore these costs need to be taken into account. Next to the cutting of the glass, the foam blocks are wrapped with the glass. For this work, the same holds, the number of foam blocks depends on the web spacing and therefore these costs have to be considered. The costs of the work in the glasshouse are calculated based on the main values of FCE. These values are for a standard spacing of the webs. To make the costs variant depend two factors are introduced, namely

$$\beta_1 = \frac{n_{webs}}{n_{webs.ref}}$$
$$\beta_2 = \frac{n_{foamblocks}}{n_{foamblocks.ref}} \tag{7.8}$$

$n$ denotes the number of webs or foam blocks. The number of foam blocks can be calculated form the number of webs.

$$n_{foamblocks} = n_{webs} - 1 \tag{7.9}$$

The costs for the glasshouse become

$$Q_{glasshouse} = \beta_1 \cdot A_{deck} \cdot s_{glasshouse} \cdot q_{hour} \tag{7.10}$$

In which the area of the deck is denoted by $A$, the amount of work that is done in the different parts of the factory is denoted as a speed $s$ and the hourly wage of the factory workers by $q$. $Q$ are the costs for the different contributions. Next to the glasshouse, the process on the mould is (partly) dependent on the geometry of the bridge deck. On the mould the wrapped foam blocks are placed. The more foam blocks, the higher the costs for this process.

$$Q_{mould} = \beta_2 \cdot A_{deck} \cdot s_{mould} \cdot q_{hour} \tag{7.11}$$

The total variable labour costs are

$$Q_{labour} = Q_{glasshouse} + Q_{mould} \tag{7.12}$$

**General costs**

Next to the geometry dependent costs, general costs occur for each deck. In this part are for example the engineering costs and general company costs. Since these costs are more or less constant for the different decks, the optimization is performed without these costs.

**Total costs**

The total variable costs of the FRP decks are given by

$$Q = Q_{material} + Q_{labour} \tag{7.13}$$

Plotting the costs for a different number of plies looks like the plot shown in Figure 7.5. In this plot, the cost function is plotted for two different numbers of plies in the skins relative to the reference design provided by the company. More information about this reference design can be found in Section 7.2.2. The lowest surface shows the results of the cost function for a case with a minimum number of layers for the laminates and the top surface shows the results for the maximum number of layers for the laminates. In the graph, it is shown that for different options of the geometric parameters, a different layup can have the lowest costs.
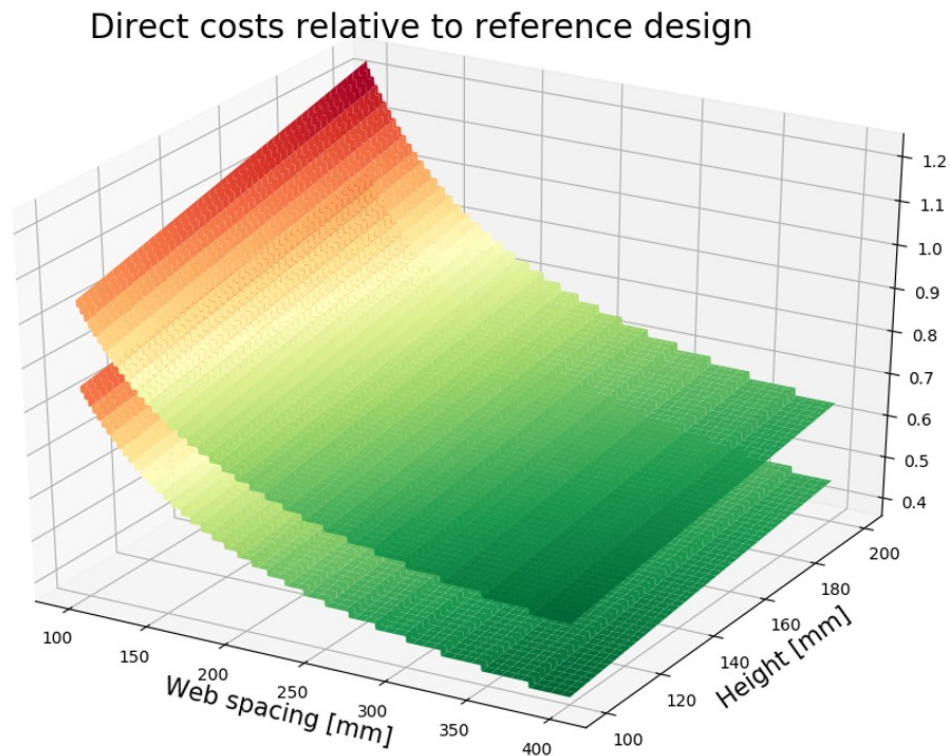


Figure 7.5: Plot of the costs for different parameters

## 7.2.6. Control calculations with numerical model Abaqus

To check if the variant, which is the result of the optimization based on analytical calculations, is safe enough, a control calculation with Abaqus is performed. For this calculation, the same model as described in Chapter 3 is used. To this model, different changes to the material properties are made to make it possible to check for FRP structures. Next to this, shell elements are used to speed up the calculation and improve the mesh quality. The same mesh size of 30 $mm$ is used, which is shown in Figure 7.6. For the loads, the two same load models are considered from the EN1991-2 [4]. However, these loads are placed at the edge of the deck with two cases. In one case the wheel is placed in the midspan between the supporting I-beams, shown in Figure 7.7a and in the other case right above one of the I-beams, shown in Figure 7.7b. Considering these two load cases gives the maximum bending moment (skins) and the maximum shear force (webs). In Abaqus, the Hashin damage parameters are used to check for the strength of the laminates. Values for the two types of fibers that are used at FiberCore Europe are shown in Table 7.6.
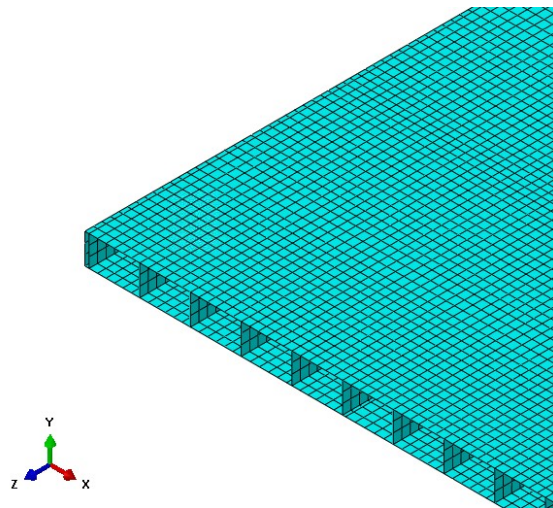
Figure 7.6: Mesh shell model Abaqus (30 mm)
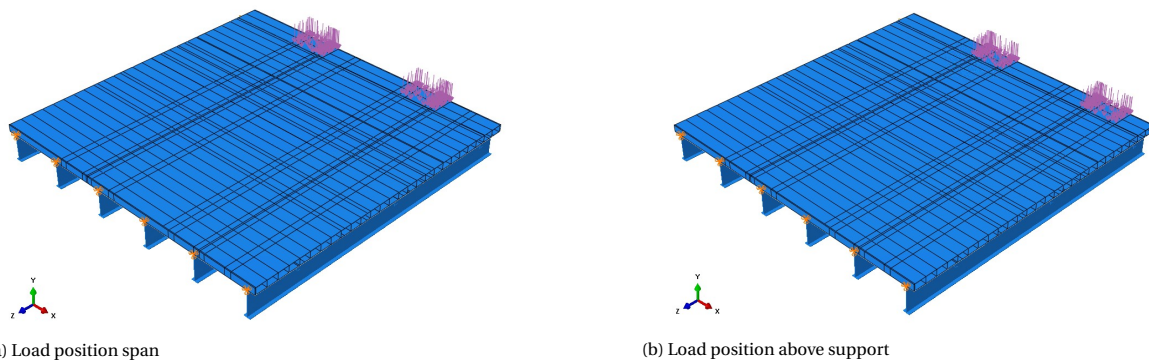


(a) Load position span



(b) Load position above support

Figure 7.7: Load cases load model 2 control model Abaqus

Table 7.6: Material properties Hashin damage [2]

| Material Strength [MPa] | UD vf54 | UD vf27 |
|---|---|---|
| Longitudinal tensile strength | 513.0 | 196.2 |
| Longitudinal compressive strength | 237.0 | 246.0 |
| Transverse tensile strength | 35.4 | 14.4 |
| Transverse compressive strength | 82.8 | 78.0 |
| Longitudinal shear strength | 23.4 | 19.2 |
| Transverse shear strength | 23.4 | 19.2 |

The check in Abaqus using the Hashin damage principle is done according to the following formula's [41]. The maximum fiber tensile strength

$$F_f^t = \left(\frac{\sigma_{11}}{X^T}\right)^2 + \alpha \left(\frac{\tau_{12}}{S^L}\right)^2 \tag{7.14}$$

In which $\sigma$ denotes the occurring stress, $\tau$ the occurring shear stress, $X^T$ the longitudinal tensile strength of the laminate and $S^L$ the longitudinal shear strength. $\alpha$ is a coefficient that determines the contribution of the shear strength. The maximum fiber compressive strength is

$$F_f^c = \left(\frac{\sigma_{11}}{X^C}\right)^2 \tag{7.15}$$

With $\sigma$ the occurring stress and $X^C$ the longitudinal compressive strength of the laminate. The maximum matrix tensile strength is given by

$$F_m^t = \left(\frac{\sigma_{22}}{Y^T}\right)^2 \left(\frac{\tau_{12}}{S^L}\right)^2 \tag{7.16}$$

$\sigma$ is the occurring stress and $\tau$ the occurring shear stress. The capacity of the laminates is given by $Y^T$ as the maximum transverse tensile strength and $S^L$ as the maximum longitudinal shear strength. The maximum matrix compressive strength is described by

$$F_m^c = \left(\frac{\sigma_{22}}{2S^T}\right)^2 + \left[\left(\frac{Y^C}{2S^T}\right)^2 - 1\right]\frac{\sigma_{22}}{Y^C} + \left(\frac{\tau_{12}}{S^L}\right)^2 \tag{7.17}$$

The occurring stress is denoted by $\sigma$ and the occurring shear stres by $\tau$. $S^T$ is the maximum transverse shear strength of the laminate and $S^L$ the maximum longitudinal shear strength of the laminate. The maximum transverse compressive strength is denoted by $Y^C$. The Hashin damage evaluation is dependent on the mesh size. Values, as shown in Table 7.7, are used, which are based on values used for projects at FCE [2]. The values are compared to a study performed by B. Renckens to check if the values are on the safe side [48]. For the damage stabilization, a value of 0.001 is used for the viscosity coefficients in both longitudinal and transverse directions for tension and compression.

Table 7.7: Parameters Hashin Damage evaluation [2]

| Parameter | Fracture energy [N/mm$^2$] |
|---|---|
| **Longitudinal tensile fracture energy** | 12.5 |
| **Longitudinal compressive fracture energy** | 12.5 |
| **Transverse tensile fracture energy** | 0.0 |
| **Transverse compressive fracture energy** | 0.0 |

Next to this, the Tsai-Hill criteria are used in Abaqus to be able to compare to the analytical calculation since this calculation uses the same type of failure criteria.

Table 7.8: Material properties Tsai-Hill [2]

| Material Strength [MPa] | UD vf54 | UD vf27 |
|---|---|---|
| **Longitudinal tensile strength** | 855.0 | 327.0 |
| **Longitudinal compressive strength** | 395.0 | 410.0 |
| **Transverse tensile strength** | 59.0 | 24.0 |
| **Transverse compressive strength** | 138.0 | 130.0 |
| **Longitudinal shear strength** | 39.0 | 32.0 |
| **Transverse shear strength** | 39.0 | 32.0 |

## 7.3. Optimization of the deck of part I thesis

The first optimization process that is performed is for the deck that is considered in part I of the graduation work. As a demonstration, the complete procedure is shown for this deck. For the settings of the genetic algorithm, the values are used as shown in Table 7.3. The python code that is used to perform the optimization is shown in Appendix G.

Using the Python code as given in Appendix G, the first step of the optimization procedure is the creation of an initial population of 50 individuals (slabs). Random different options of geometry for the slabs are created based on the fifteen variables used for the optimization which will function as the genes of the individuals. For each variant within this initial population, the design criteria are checked. These are the minimum and maximum thicknesses of the plies and the minimum amount of fibers in a specific orientation. When the design does not satisfy this check a penalty to the costs of $2 \cdot 10^5$ is given, which is the fitness value of the individual. When the individual does satisfy the design check, the checks for strength, stiffness and stability are performed as given in Appendix E. When the individual does not satisfy these checks a penalty of $2 \cdot 10^4$ times the value of the maximum unity check is applied to the costs. Using this penalty dependent on the maximum unity check ensures that an individual that is almost satisfied will receive a lower fitness value than an individual that does not satisfy at all. This will improve the convergence of the algorithm.

For the individuals that satisfy all checks, the costs are calculated as described in Section 7.2.5. The costs are used as a measure of the fitness value of the individuals. Based on the fittest individuals the next generation of slabs is created using cross-over of the genes of the individuals and mutations as described in Section 7.2.3. After the maximum number of generations (iterations) of 1000, or when the most optimal design stays the same for 50 generations, the optimization procedure is stopped. The results for this optimization are shown in the first sub-section. In the second sub-section, a verification of the obtained result is described and in the last sub-section control calculations with a numerical model are given.

### 7.3.1. Results optimization of deck part I thesis

Since the optimization is based on fifteen different variables, it is not possible to show the variant space in a graph. Therefore, the two main variables are taken namely the height of the slab and the spacing of the webs to plot the variant space for different weights and costs. This graph is shown in Figure 7.8. The graph contains only the variants that satisfy both the design and strength criteria. The graph shows that the genetic algorithm takes different values of the parameters and converges to the optimal design since more variants are considered at that location. It is important that a lot of different variants are checked since otherwise a local optimum can be detected instead of the global optimum.
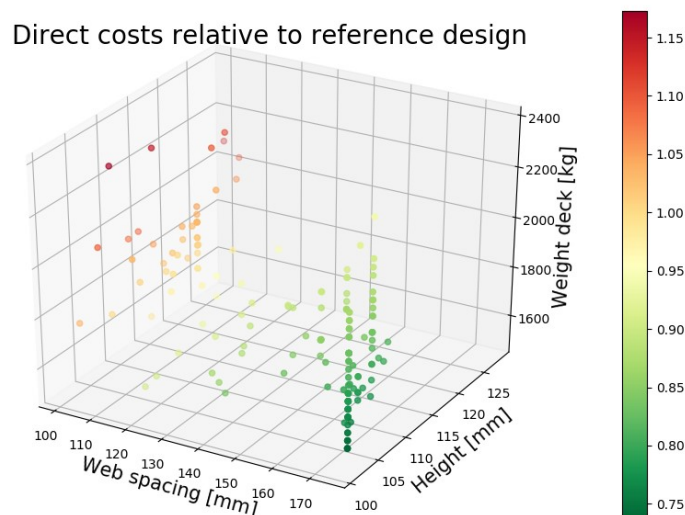


Figure 7.8: Results optimization procedure deck part I

To be able to see how fast the optimization is converging to an optimum, the costs of the most optimal design found relative to the costs of the reference design, can be plotted against the generation that is considered.

This graph is shown in Figure 7.9. It can be seen that the algorithm converges in approximately 25 generations to the area where the global maximum is located. When this area is found, about 100 generations are needed to obtain the optimum. Thereafter, the optimal design does not change for 50 generations and the process is stopped. The black line indicates the costs of the reference design which means that all designs underneath this line are more optimal in terms of costs.
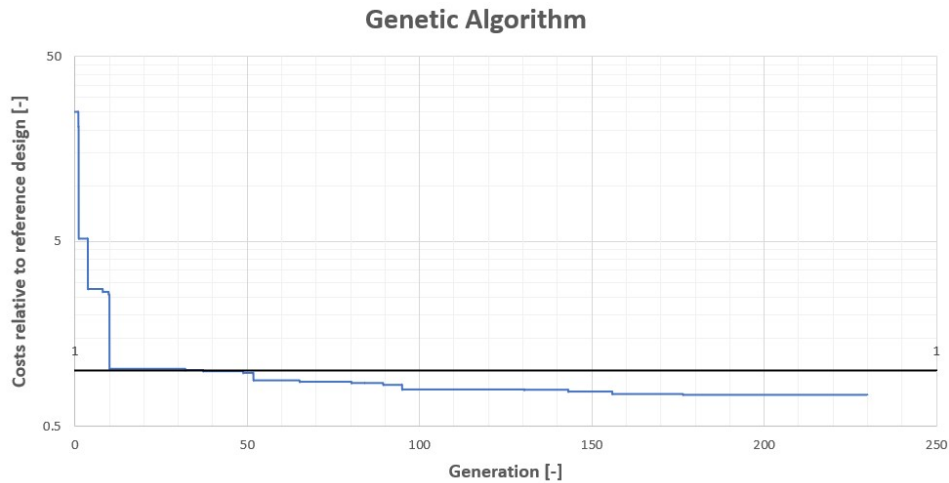


Figure 7.9: Genetic algorithm deck part I

### 7.3.2. Verification optimization of deck part I thesis

To be able to conclude if the described optimization procedure is useful, four things need to be checked. First, it has to be checked if the algorithm is converging every run to the same optimal design. Next to this, it must be checked if this design is the optimal design. When this is the case, the most optimal design has to be checked on strength with a more detailed calculation which is described in the following section. Lastly, it has to be checked if the procedure works for different boundary conditions which is described in Section 7.5.

To check for the first issue, the optimization algorithm is run multiple times with the same input. The results are shown in the graph in Figure 7.10. It is shown that the algorithm converges to options with the same costs within more or less the same amount of generations. The optimal designs found with these runs are given in Table 7.9, for which it is shown that the same optimum is detected.
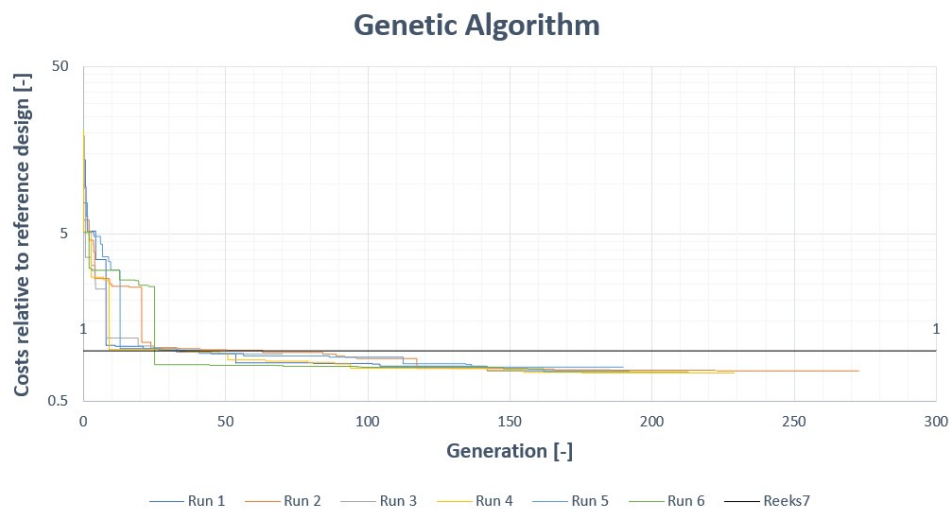


Figure 7.10: Multiple runs genetic algorithm deck part I

Table 7.9: Results of the optimization of the deck form part I

| Parameter | Results | | | | | |
|---|---|---|---|---|---|---|
| | Run 1 | Run 2 | Run 3 | Run 4 | Run 5 | Run 6 |
| **Relative costs [-]** | 0.76 | 0.76 | 0.96 | 0.74 | 0.80 | 0.75 |
| **Height [mm]** | 103.6 | 102.9 | 116.9 | 103.0 | 110.1 | 101.8 |
| **Web spacing [mm]** | 173.8 | 169.6 | 114.8 | 117.4 | 174.7 | 174.1 |
| **Thickness topskin [mm]** | 16.15 | 16.15 | 17.85 | 17.85 | 17.0 | 18.7 |
| **Thickness bottomskin [mm]** | 19.55 | 17.85 | 15.3 | 15.3 | 22.1 | 16.15 |
| **Thickness webs [mm]** | 13.6 | 13.6 | 13.6 | 13.6 | 13.6 | 13.6 |
| **Weight of the deck [kg]** | 1606 | 1547 | 1645 | 1510 | 1749 | 1568 |
| **Max uc ULS** | 0.92 | 0.94 | 0.95 | 0.97 | 1.00 | 0.99 |
| **Max uc SLS** | 0.27 | 0.29 | 0.22 | 0.31 | 0.24 | 0.39 |

To check if the found optimum is the global optimum, the algorithm is run for a population size of 100 individuals for 1500 generations for narrower boundaries for the height of the slab and the web spacing. Decreasing these boundaries to 100-110 for the height of the deck and 150-200 for the web spacing gives the algorithm the opportunity to check more variants close to the found optimum. The result of this calculation is shown in Figures 7.11 and 7.12. In Figure 7.11 it is shown that for this reduced variant space a lot of options are checked with different variables. With the green dots, the area of the optimal designs is clearly visible.
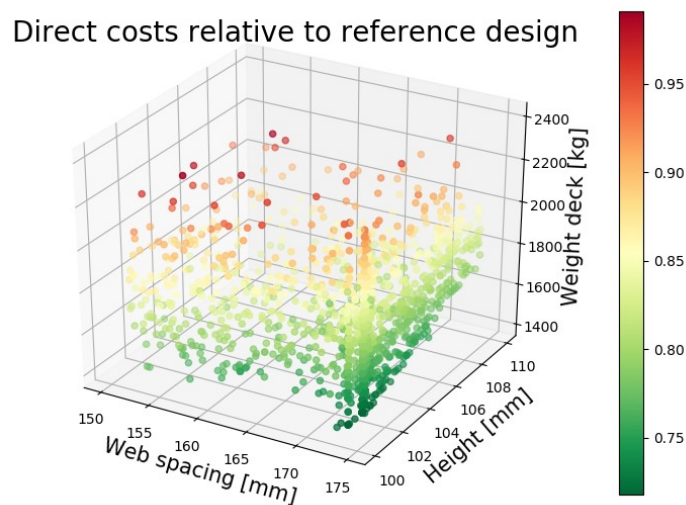


Figure 7.11: Results control calculation optimization procedure deck part I

Figure 7.12 shows that the algorithm converges to an optimum. This optimum design is visualized in Figure 7.13. Comparing the results of the different runs of the algorithm shown in Table 7.9 it is shown that the solutions found are close to the optimum found with the control calculation. Therefore it can be concluded that the algorithm founds the global optimum.
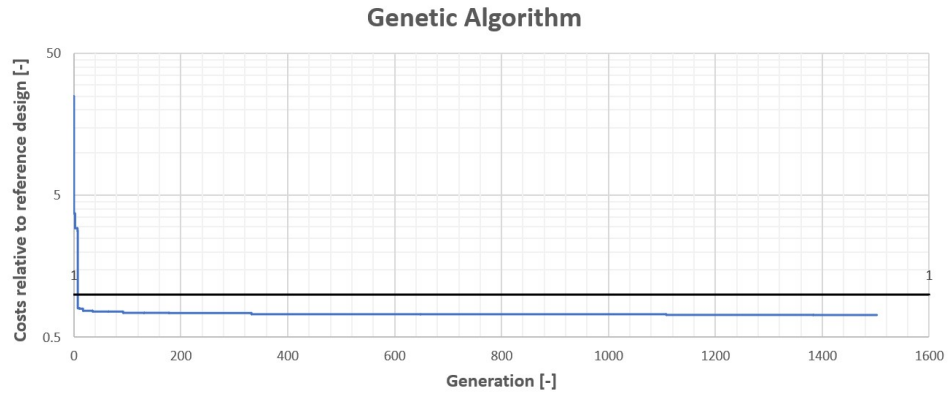
**Genetic Algorithm**



Figure 7.12: Genetic algorithm control calculation deck part I
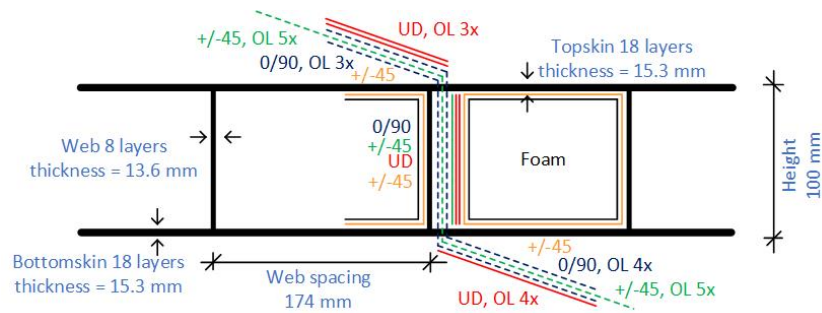


Figure 7.13: Optimal design part I

The layups that are used for the top and bottomskins are shown in Figure 7.14 and for the webs in Figure 7.15.
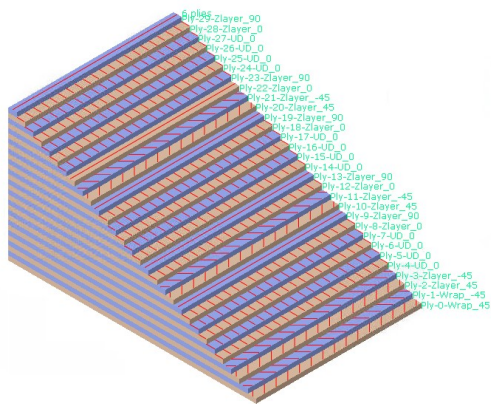


(a) Optimal layup topskin deck part I
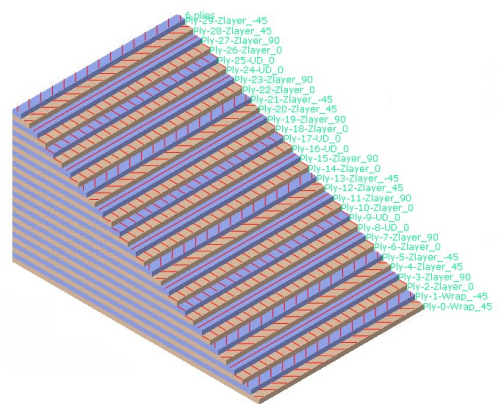


(b) Optimal layup bottomskin deck part I

Figure 7.14: Optimal layup skins deck part I
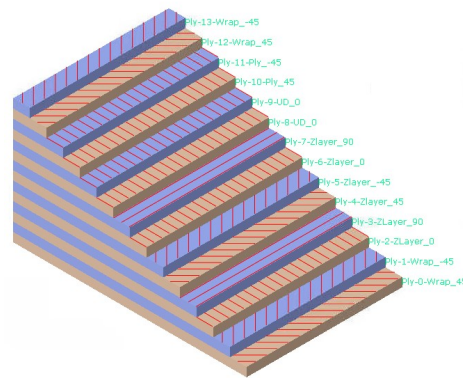
Figure 7.15: Optimal layup webs deck part I

### 7.3.3. Control calculations Abaqus of deck part I thesis

The optimal design, calculated with the analytical formulas, is checked with Abaqus. The results for the two different load models are given in Table 7.11. Since two different calculation models are used, it is difficult to compare them to each other. The analytical model is based on a beam model and the numerical model on a plate model. As shown in Section 3.4.2, using a plate or a beam model will give different results. To be able to make a more reliable comparison, the results are compared to the ones obtained with the reference design of the deck provided by FCE as shown in Section 7.2.2. In Table 7.11 it is shown that the results for both analytical calculations are in the same order of magnitude and the same holds for the numerical calculations.

**Stresses**

The stresses obtained during the optimization process are compared to the stresses obtained during the analytical calculation. Since only the global behavior is checked for the optimization, the same type of stresses is calculated with Abaqus. The average stress over the laminate for shell models is given by SSAVG. However, due to the difference in plate and beam models, the stresses in the average stresses in the skins are relatively low. Therefore, the envelope stresses are checked with Abaqus for the skins. An envelope contour plot shows the maximum ply stress of all the plies in the layup [41].

For the topskin, the maximum bending stresses $S_{11}$ based on the envelope contour plot are considered. Due to the bending of the topskin, compression occurs and therefore the negative stress $S_{11}$ is used. For the bottomskin, the same stress $S_{11}$ based on the envelope contour plot will be critical. However, for the bottomskin it is the positive stress that is considered since tension will occur. Considering the webs, two types of stresses are checked. First the shear stress $S_{12}$ based on the envelope contour plot will be compared with the analytically calculated value. Next to this, the compressive stress in the webs is checked. For the compressive stress in the webs, the average stress SSAVG2 is used since the envelope stress gives a large maximum value in only one of the plies due to a local peak value. Comparing this value to the analytical obtained value will result in an unrealistic comparison.

The analytical calculation gives only an average value of the stress. However, with Abaqus, it is possible to see in which (type of) ply the maximum stress occurs. This is shown for the different stresses in Table 7.10.

Table 7.10: Location maximum stress in Abaqus shell model

| Model Location stress | Reference design | Optimal design |
|---|---|---|
| Maximum tensile stress topskin | UD ply | UD ply |
| Maximum compressive stress bottomskin | UD ply | UD ply |
| Maximum shear stress webs | Z-layer +/-45 | Z-layer +/-45 |
| Maximum compressive stress webs | Z-layer 0/90 | UD ply |

**Results**

Figure 7.16 shows the stresses occurring for the load case where one of the wheels is placed between the I-beams. It is observed that the highest stresses for both the top and bottomskin occur in the middle of the laminate that spans between the I-beams. Therefore, the stresses are plotted at this location along the distance underneath the wheel load. This plot is shown in Figure 7.17 for the topskin and in Figure 7.18 for the bottomskin. The stresses are plotted for both the optimal design and the reference design.
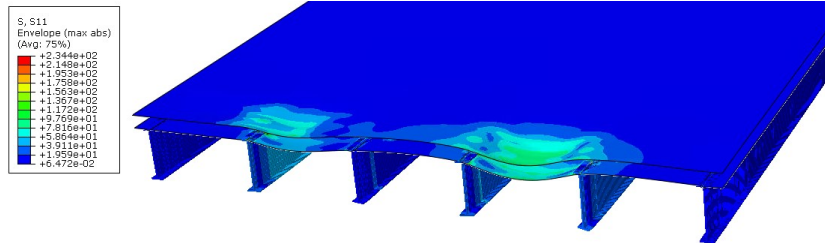


Figure 7.16: Stresses in the skins of the optimal design for the deck of part I [$MPa$]

Observing the graph of the stress $S_{11}$ in the topskin in Figure 7.17, it is shown that the highest stress occurs at the edge of the plate. The plots for the optimal and the reference design show the same shape. The stresses in the laminate for the optimal design are a bit higher at each location since the laminates are better utilized. The same holds for the stresses in the bottomskin as shown in Figure 7.18.
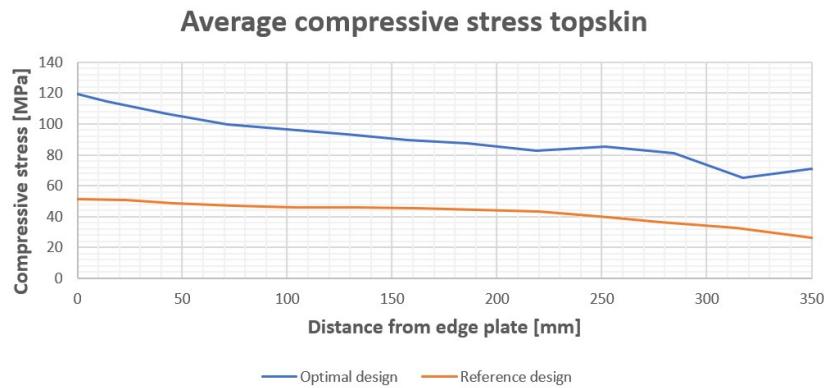


Figure 7.17: Average compressive stress in the topskin for the optimal design for the deck of part I [$MPa$]
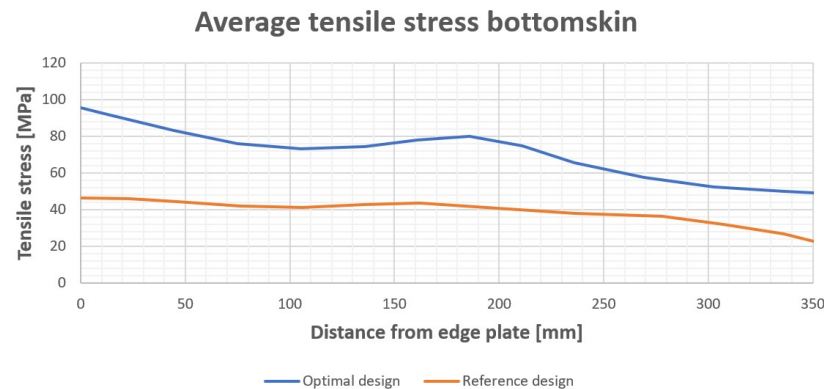


Figure 7.18: Average tensile stress in the bottomskin for the optimal design for the deck of part I [$MPa$]

Next to the stresses in the skins, the stresses in the webs needs to be verified by the numerical calculation. The highest stress in the webs will occur when a wheel is placed above one of the I-beams. Underneath this

wheel, the maximum shear stress occurs as shown in Figure 7.19. The maximum compressive stress in the webs occurs at the same location for the same reason.
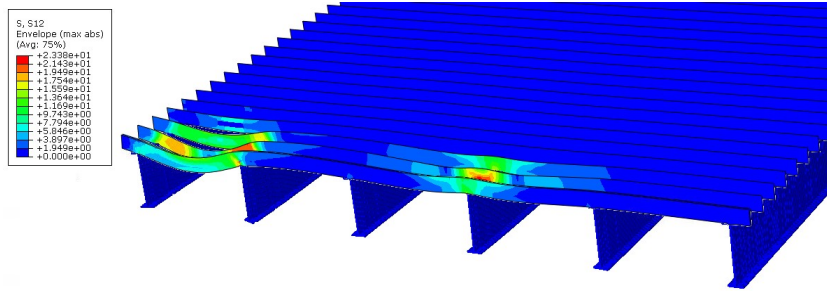


Figure 7.19: Shear stresses in the webs of the optimal design for the deck of part I [$MPa$]

The average shear stresses over the height of the webs underneath the wheel load are plotted and shown in Figure 7.20 for both the optimal and reference design. The height of the webs for the reference design is higher, 120 $mm$, than the height of the webs in the optimal design, 100 $mm$. The maximum shear stress occurs at the bottom of the webs for both cases.
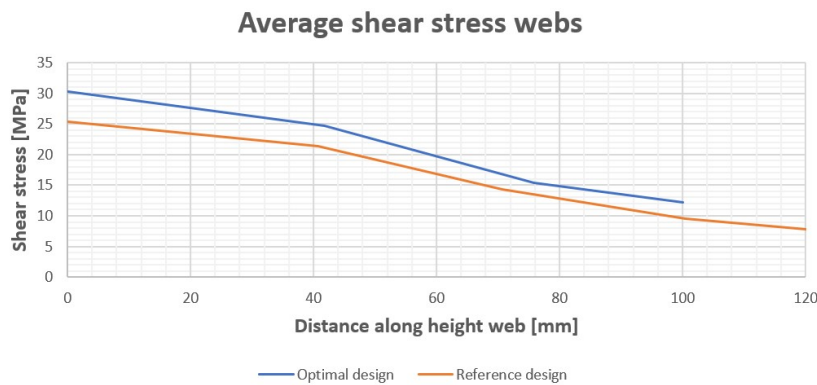


Figure 7.20: Average shear stress in the webs for the optimal design for the deck of part I [$MPa$]

In Figure 7.21 shows the compressive stress in the webs at the same location as for the shear stresses. It is shown that the compressive stress is relative high for the reference design compared to the analytical model. For the optimal design the compressive stress is in the order of magnitude that can be expected based on the applied wheel load.
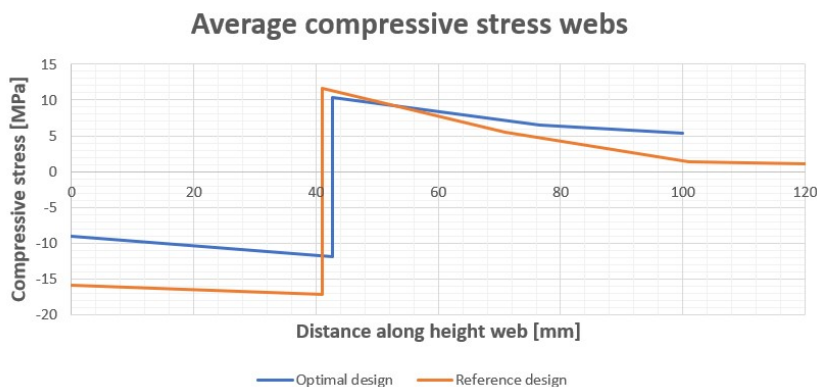


Figure 7.21: Average compressive stress in the webs for the optimal design for the deck of part I [$MPa$]

The comparison of the considered stresses is shown in Table 7.11. It is shown that the stresses for the ana-

lytical calculation are for both models the same amount higher than the ones of the numerical calculations. Therefore, it can be concluded that the analytical formulas can be used since the results are on the safe side. However, some of the stresses can be higher for the numerical calculation. These are peak stresses at the location of the interaction between the slab and the support steel beam underneath. The analytical calculation does not take these stresses into account. Next to this, the local behavior of the slab due to the wheel loads has to be checked in the final design.

Table 7.11: Comparison results calculations deck part I

| Type of loading | Compressive stress topskin [MPa] | Tensile stress bottomskin [MPa] | Shear stress webs [MPa] | Compressive stress webs [MPa] |
|---|---|---|---|---|
| **Numerical model reference design** | 51.2 | 46.2 | 25.4 | 17.2 |
| **Analytical model reference design** | 127.8 | 140.3 | 66.2 | 12.3 |
| **Numerical model optimal design** | 119.5 | 95.5 | 30.3 | 12.0 |
| **Analytical model optimal design** | 202.8 | 207.9 | 102.1 | 16.2 |

Next to the average stresses in the skins and webs, the damage is checked by the numerical calculation as described in Section 7.2.6. First the Tsai-Hill criterion is used since this theory is also used for the analytical strength calculations. The results for one of the loading cases, wheel load placed between the supports, is shown in Figure 7.22 for the optimal design. It is shown that no damage occur in this case. For other cases damage can occur as shown in Table 7.12 since the Tsai-Hill criterion exceeds a value of 1.0. Observing these results, it is shown that the damage will occur at the local spots like the interaction between the plies of the webs and the skins and the interaction between the deck and the supporting structure.
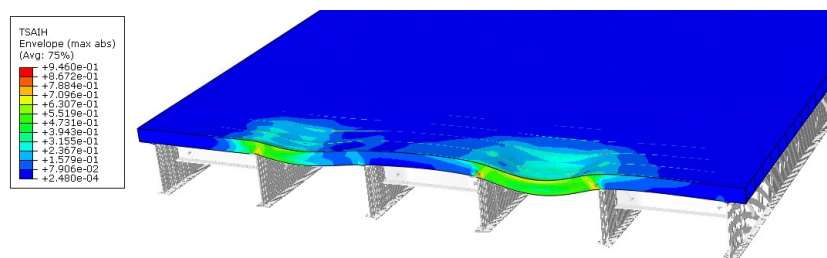


Figure 7.22: Check TsaiHill for the optimal design for the deck of part I

The Hashin damage is checked for the different load cases with the parameters described in Section 7.2.6. For the load case with the wheel load between the supports, the results of the maximum matrix tension are shown in Figure 7.23. Since the maximum value is stated at 1.0, this indicates that damage will occur in the laminates. The locations where this damage most likely will occur are indicated by the red color in the figure. The damage values for the other criteria and load locations are given in Table 7.12. When one of the values is set at 1.0 some damage to the structure occurs. However, due to the redistribution of the stresses, the structure will not collapse. A more in-depth study on the locations where damage will occur is needed. However, this is out of the scope of the research.
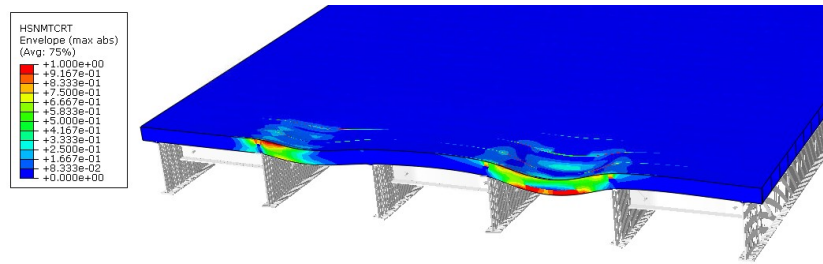
Figure 7.23: Check Hashin damage for the optimal design for the deck of part I

Table 7.12: Hashin damage and Tsai-Hill different models

| Model | Reference design | | Optimal design | |
| Location | Above | Between | Above | Between |
| load | support | supports | support | supports |
|---|---|---|---|---|
| Fiber compression | 1.00 | 0.33 | 1.00 | 1.00 |
| Fiber tension | 0.07 | 0.06 | 0.22 | 0.36 |
| Matrix compression | 1.00 | 0.79 | 1.00 | 1.00 |
| Matrix tension | 1.00 | 1.00 | 1.00 | 1.00 |
| Tsai-Hill | 1.10 | 1.12 | 1.19 | 0.95 |

## 7.4. Discussion optimization procedure

The optimization is done based on analytical formulas. These formulas have a margin due to the difference in plate and beam behavior as shown in Section 3.4.2, therefore not the most optimal design is obtained compared to a case where the calculations are performed with a detailed numerical model. However, this is not possible within a reasonable calculation time.

The optimal design for the deck which is considered in part one of this thesis is given in Figure 7.13. However, since only the global behavior is checked, the design is not safe to be used in practice. The local behavior needs to be checked as well. Considering the formula used to calculate the costs, it is shown that the optimal design is sensitive to the price of the materials compared to the labour costs. A large part of the costs is based on the labour which is done at the mould. However, most of the work that is performed at the mould is constant for all designs like installing the vacuum pump and pipes, placing different layers of plastic sheets and setting the mould. Due to this constant part of the costs, the optimum found can differ from the optimum which is found when the constant part of the costs is excluded. However, there is no data available for the separate activities at the moment.

Considering the results for the different runs shown in Table 7.9, it is shown that the algorithm stops sometimes before the most optimum result is found. Most of the results are close to the optimal one however, almost every run will deviate from it. This is due to the fact that the procedure is based on probabilities, and therefore also less optimum options are tried. This can be solved by increasing the number of generations for which the optimum needs to stay the same which increases the chance of detecting a better option. Next to this, the population size can be increased. Considering a larger population makes sure that more options are considered. Another advantage of a larger (initial) population is that the optimum region is detected earlier which speeds up the procedure.

However, both options will increase the time that is needed for the optimization process. In general, the more generations are considered, the better the result. Therefore, it becomes a balance between accuracy and calculation time needed. To improve the optimization procedure based on this balance, some improvements are suggested in Section 7.4.3. Before this, in the first sub-section, 7.4.1, a comparison between the optimal and the reference design is described and in the second sub-section more information about the local behavior is given.

### 7.4.1. Comparison to reference design

To be able to know if the optimization is successful, the optimal design has to be compared to the reference design which is shown in Section 7.2.2. For the stresses obtained in the different parts of the deck, this is shown in Table 7.11. The costs and weights of the two options are compared to each other in Table 7.13. In

this table, it is shown that the optimized design has 29% lower costs than the initial design.

Next to this, the unity checks are compared for the different parts of the design. These checks are also shown in Table 7.11. It is shown that the unity check for the shear in the webs is too high for the reference design. This is the case since the web spacing and height of the deck are taken from the reference project of FCE. However, the laminate layup is based on a general approach from the company they want to use as a standard for the traffic bridge decks. Therefore, these orientations and the number of plies are used as a reference for the optimization procedure. The other checks are higher for the optimal design which means that this design is more utilized. Since all checks are below one, the design is safe enough according to the global behavior of the slabs.

Table 7.13: Comparison optimal design and reference design deck part I

| Design | Reference | Optimal |
|---|---|---|
| **Weight [kg]** | 1862 | 1407 |
| **Difference in weight [%]** | - | 24.4 |
| **Relative costs [-]** | 1.0 | 0.71 |
| **Difference in costs [%]** | - | 29.0 |
| **Unity check compressive stress bottomskin [-]** | 0.72 | 0.97 |
| **Unity check tensile stress topskin [-]** | 0.45 | 0.61 |
| **Unity check shear stress webs [-]** | 1.35 | 0.89 |
| **Unity check compressive stress webs [-]** | 0.16 | 0.24 |
| **Unity check global buckling webs [-]** | 0.84 | 0.95 |
| **Unity check global shear buckling webs [-]** | 0.06 | 0.05 |
| **Unity check combination shear and compressive stress webs [-]** | 0.84 | 0.96 |

Compared to the reference design the biggest chance in the layups for the skins is the number of overlapping lengths. The reference design is not satisfying the minimum amount of 12.5% of fibers in the main directions according to the CUR96 [6]. Since the optimal design does satisfy this, a larger overlapping length of the $+/-45$ plies is used unless the occurring shear force is low. Another difference is the smaller number of UD plies in the bottomskin. Since the bottomskin does not suffer a lot from the local behavior, a thinner laminate can be used. A minimum amount of plies are used for the 0/90 z-layers from the InfraCore principle and therefore the UD plies can be reduced.

For the webs more changes are made compared to the reference design. For the improvement of the design, it is suggested to put UD plies onto the webs and an extra ply $+/-45$. The goal of this improvement is to get thicker webs that can transfer the shear and compressive stress while increasing the web spacing. Increasing the web spacing is the most effective option to reduce costs. When the web spacing is increased, the applied load on one web is increased as well and the stability of the web is therefore reduced. Since the thickness of the webs only comes from the amount of z-layers and the number of times a foam block is wrapped, another option has to be used. Applying extra UD layers can be possible by continuing the UD layers through the webs into the bottomskin. In this way, z-layers with only fibers in the 0° direction are created. This makes the structure stronger as a whole. Another option is to add separate layers of UD plies to the webs without connecting them to the skins. This can also be done for the $+/-45$ layer. However, another way to add this extra layer is by increasing the number of times the foam block is wrapped and at the same time reducing the overlapping length of the $+/-45$ plies in the top and bottomskin to keep the skin laminates the same.

Since the shear stresses will be the highest in the webs and therefore the governing type of stress, the biggest part of the fibers needs to be in the 45° and $-45°$. However, a minimum amount of fibers is needed in each direction according to the CUR96. Therefore, extra UD layers are suggested to improve the resistance against compressive stress and buckling. The compressive stresses will be quite low compared to the strength of the webs and therefore buckling will not be critical. However, the interaction between shear and compressive stress needs also to be checked which will be governing. Therefore, increasing the compressive strength is also effective.

With critical engineering thinking, the design can be improved even more. Since the algorithm that is used makes only decisions based on probabilities, no engineering-based choices are made. This explains the choice to add more extra UD plies instead of $+/-45$ plies. A way to solve this is to keep the same thickness for the webs but replace one of the UD plies with an $+/-45$ ply and do a recalculation to see if the design satisfies.

### 7.4.2. Local behavior

Since the result of the optimization process is a relatively thin topskin, a check has to be done for the local behavior due to the wheel load. Next to this check, checks have to be performed for other local behavior. For example, the delamination has to be checked. However, this is out of the scope of this graduation work. Some recommendations to include these checks in the optimization procedure are provided in the next subsection.

### 7.4.3. Improvements optimization procedure

To be able to use the optimization process in practice, some improvements need to be made. First, improvements to the genetic algorithm are suggested. To improve the outcome of the algorithm without increasing the run time significantly, the following options can be considered:

1. To reduce the time needed to find the most optimum area, the initial population can be increased without increasing the population size of the next generations. For this, the code of the genetic algorithm needs to be adapted or another code has to be used.

2. Due to the large number of variables that are considered, the number of iterations needed is high. To be able to reduce the area a short calculation of a (large) population with a small number of generations can be used to detect the area where the optimum can be found. When this area is found, the boundaries of the variables can be adapted based on the pre-calculation and a next calculation can be done which needs less generations since the possible options have been reduced. This will reduce the time that is needed for the calculation. However, based on the quality of the pre-calculation a local optimum may be found instead of the global optimum.

Next to the improvements for the algorithm, most of the improvements that need to be made are about the checks for the local behavior of the slabs. Since only the global checks are included in the current optimization procedure, the outcome cannot be used in practice. However, the optimization procedure developed works with analytical formulas which concludes that analytic formulas must also be used with the extension of the procedure. The following local issues have to be checked:

- Delamination

- Local buckling of the webs

- Local buckling of the skins

- Local crushing of the core

- Local stability failure modes like face wrinkling and shear crimping

- Interaction of global and local behavior

One of the options is to split the optimization into two parts. First, the optimization is performed with respect to global behavior. When the optimal design is found for this case, the optimal ratio between height and web spacing can be kept. Then a second optimization can be performed with respect to the local behavior of the slab. This can be done either with an analytical or numerical model. When a numerical model is used, it is recommended to use sub-modeling to limit the calculation time needed. The same model can be used as described in Section 7.2.6. In this model, a sub-model is made for one cell as is shown in Figure 7.24. Instead of modeling the complete skins and webs with one layer, each ply has to be modeled with one cell through the thickness. The cells can be connected to each other using the inter-laminate properties. Using this type of modeling makes it able to control for delamination and local behavior.

Since different designs has to be checked to be able to know the optimal one, a large number of calculations have to be performed. The sub-modeling technique makes it difficult to adapt the dimensions of the slabs and the number and orientation of the plies. Another con for this method is the large time that is needed to run the numerical calculation. The optimization needs to be done with the use of analytical formulas. The numerical option as described can be used as a control calculation for the analytically obtained option in the same way as is done for the global optimization.
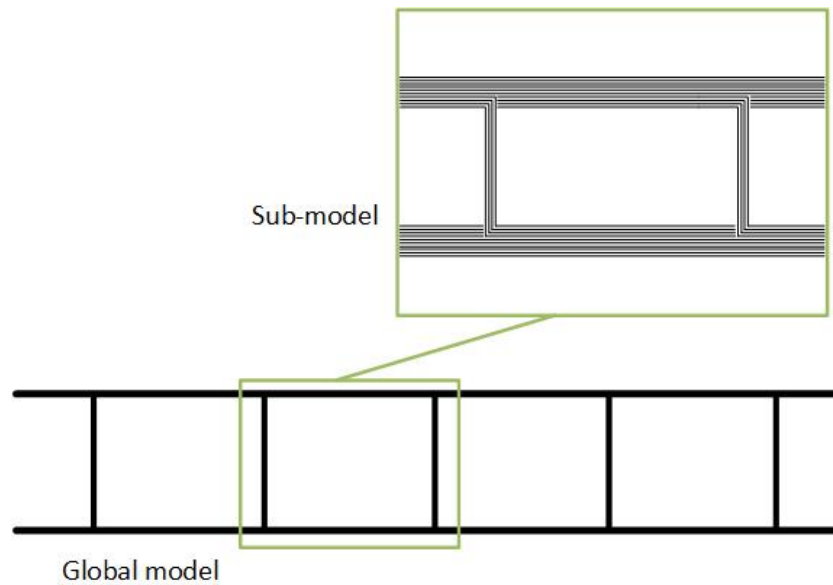
Figure 7.24: Sketch sub-model for checks local behavior

Another, more engineering-based, approach to tackle the problem is to adapt the boundary conditions that are applied for the optimization procedure. Based on the knowledge of engineering practice, minimum thickness for the skins and webs can be applied. Using these minimal thicknesses, the local failure modes are prevented. One way in between is the option to add rough checks in the Python code based on analytical formulas. The outcome of this optimization has to be verified with a numerical calculation to be sure that the design is safe enough. Two main local behaviors has to be checked; The local bending of the topskin and the local buckling of the webs. Analytical formulas which describes this behavior are given below.

**Local bending of the topskin**
Since the applied load is a local load, the topskin has to be checked on local bending due to this load. Figure 7.25 shows on the left side a part of the slab with a wheel load applied on the top. The local bending moments can be calculated with a simplified model shown on the right in Figure 7.25. The two moments occurring due to this distributed load can be calculated by

$$M_{local.support} = \frac{1}{12} \cdot q \cdot L^2$$
$$M_{local.span} = \frac{1}{24} \cdot q \cdot L^2$$

(7.18)

In these formulas, $q$ denotes the load which is the uniform distributed load calculated by the wheel load dived by the length of the wheel. The length $L$ is the distance between the webs. Since the local support moment will always be governing, this moment has to be checked against the strength of the laminate of the topskin. The stress in the topskin caused by this local moment is calculated by

$$\sigma_{loc.ts} = \frac{M_{local.support}}{W_{topskin}}$$

(7.19)

$W$ denotes the section modulus of the topskin which is given by

$$W_{topskin} = \frac{1}{6} \cdot b_{eff} \cdot t^2_{topskin}$$

(7.20)

The thickness of the topskin is denoted by $t$ and the effective width of the topskin which is taken into account by $b_{eff}$. As a safe approach, the width of the wheel can be used. The obtained stress has to be checked against the strength of the topskin laminate.
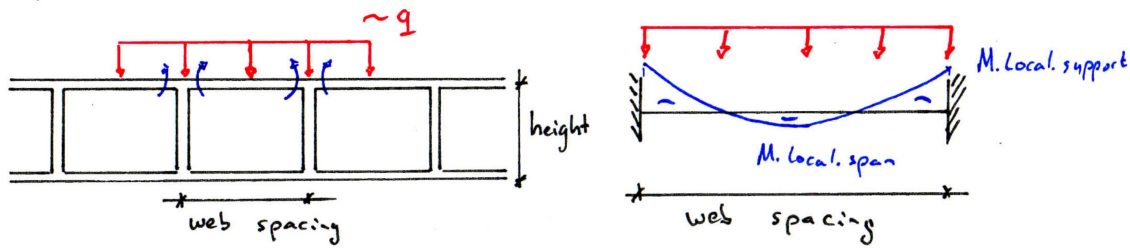
Figure 7.25: Sketches model local bending topskin

**Local buckling of the webs**

The other type of local behavior that needs to be checked is the local buckling of the webs, for which a model is shown in Figure 7.26. To check this, two types of formulas can be used. The first option is the model from the JRC code which is shown in Figure 7.26. In the model, a part of the web above which the wheel load is located is considered as a plate. This plate is simply supported (ss) at both edges because the web will continue. The formula for the maximum buckling load is [49]

$$N_{cr} = \frac{\pi^2}{L_y^2} \cdot \left[ 2 \cdot \sqrt{D_{11} \cdot D_{22}} + 2 \cdot (D_{12} + 2 \cdot D_{66} \right] \tag{7.21}$$

$L_y$ is the width taken into account for the plate as shown in Figure 7.26. As a safe approach, the width of the wheel can be used. The different stiffness parameters can be calculated analytical as well with the following formulas from the JRC code [49]

$$D_{11} = \frac{E_{LC} \cdot t_{web}^3}{12 \cdot (1 - \nu_{LT} \cdot \nu_{TL})}$$
$$D_{12} = \nu_{LT} \cdot D_{22}$$
$$D_{22} = \frac{E_{TC} \cdot t_{web}^3}{12 \cdot (1 - \nu_{LT} \cdot \nu_{TL})} \tag{7.22}$$
$$D_{66} = \frac{G_{LT} \cdot t_{web}^3}{12}$$

In these formulas, the material factors are denoted by $E$ for the bending modulus, $G$ for the shear modulus and $\nu$ for the Poisson's ratio. In the subscripts, the directions are given. $L$ states for longitudinal, $T$ for transverse and $C$ for compression. The maximal stress in the webs is given by the formula below which has to be checked against the strength of the webs.

$$\sigma_{cr} = \frac{N_{cr}}{t_{web}} \tag{7.23}$$

The other option is based on formulas from a book written by Kassapoglou [50]. In this book, the same model is used that is shown in Figure 7.26. The critical stress due to local buckling of the webs is given by

$$\sigma_{cr} = \frac{N_{cr}}{t_{web}} \tag{7.24}$$

The critical buckling load is given by

$$N_{cr} = \frac{\pi^2}{b_{eff}^2} \cdot \sqrt{D_{11} \cdot D_{22}} \cdot K \tag{7.25}$$

The stiffness parameters are the same as for the method from the JRC code and $b_{eff}$ is the width of the plate that is taken into account. The factor $K$ depends on the slenderness factor which is calculated by

$$\lambda = \frac{h_{web}}{b_{eff}} \cdot \left( \frac{D_{22}}{D_{11}} \right)^{1/4} \tag{7.26}$$

Using this slenderness factor $\lambda$, the $K$ factor is given by

$$if \lambda > 1.662$$

$$K = frac{m_b^4 + 8 \cdot m_b^2 + 1}{\lambda^2} \cdot (m_b^2 + 1) + \frac{2 \cdot (D_{12} + 2 \cdot D_{66})}{\sqrt{D_{11} \cdot D_{22}}} + \frac{\lambda^2}{m_b^2 + 1}$$

$$else$$

$$K = \frac{4}{\lambda^2} + \frac{2 \cdot (D_{12} + 2 \cdot D_{66})}{\sqrt{D_{11} \cdot D_{22}}} + \frac{3}{4} \cdot \lambda^2$$

(7.27)

The stiffness parameters $D$ are described by the formulas from the JRC code and $m_b$ is a geometry-based factor that can be assumed to be equal to 1 for the case that is considered.
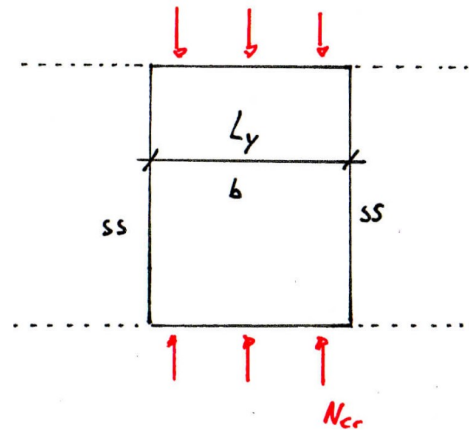


Figure 7.26: Sketch model local buckling of the webs

Different other local behaviors can be checked, however, these will not be critical for the design of the FRP slabs given the occurring load. The different checks that can be added analytically are described and explained below. The analytical formulas are based on the failure mechanisms that can occur. Sketches of some of these failure mechanisms are shown in Figure 7.27.

**Skin failure**
The skin failure is already checked party by the checks for the global behavior. However, horizontal forces are not taken into account which can be caused by breaking vehicles. This failure mode is caused by an insufficient panel or skin strength and thickness. An extra check can be added which is given by [49]

$$\sigma_{Ed.i} = \frac{M_{Ed}}{t_i \cdot h} + \frac{N_{Ed}}{2 \cdot t_i}$$

(7.28)

In this equation, the thickness of the different skins is denoted by $t_i$ and the occurring bending moment and axial force by $M_{Ed}$ and $N_{Ed}$ respectively. The axial load is evaluated per unit width of the panel that is considered. The verification can be done by

$$\sigma_{Ed.i} \le f_{d.ti} \ \ if \ \ \sigma_{Ed.i} \le 0$$
$$\sigma_{Ed.i} \le f_{d.ci} \ \ if \ \ \sigma_{Ed.i} < 0$$

(7.29)

The tensile strength of the skin is given by $f_{d.ti}$ and the compressive strength by $f_{d.ci}$.

**Failure of the core**
During the calculations, it is assumed that the core does not cooperate constructively since the strength of the foam blocks is low and the load transfer will go through the webs. However, this may change in the future. For example, when recycled FRP is used as a core or for special projects. Different checks have to be performed for the strength of the core based on different failure mechanisms like [49]

- Transverse and horizontal shear failure

- Flexural crushing of the core

- Local crushing of the core

**Shear crimping**

When too thin skins are applied in the design, shear crimping can occur as shown in Figure 7.27a. This has to be checked with the critical compressive strength of the skins and the occurring compressive stress. Since the main load will be in the vertical direction, this failure will not be critical. However, due to breaking vehicles, horizontal forces can occur. The topskin can be checked with the formula below in which the compressive stress is denoted by $\sigma_{d.ci}$ and the compressive strength of the laminate by $f_{d.ci}$ [49].

$$\sigma_{d.ci} < f_{d.ci} \tag{7.30}$$

**Skin wrinkling**

Due to the compressive stresses occurring in the topskin, wrinkling can occur. The compressive stress can be caused by horizontal load, due to bending which causes the topskin to be in compression, or a combination of both loading conditions. Two types of wrinkling can occur namely inward and outward as shown in Figure 7.27b. Therefore, the critical strength is given by [49]

$$\sigma_{Rd.wr} = min \left[ 0.5 \cdot \frac{\eta_c}{\gamma_M} \cdot \sqrt[3]{E_i \cdot E_c \cdot G_c}, 0.82 \cdot \frac{\eta_c}{\gamma_M} \cdot E_i \cdot \sqrt{\frac{E_c \cdot t_i}{E_i \cdot t_c}} \right] \tag{7.31}$$

In this formula, $\eta_c$ is the applied conversion factor and $\gamma$ is the applied safety factor. $E$ and $G$ are the bending and shear modulus of the different parts of the sandwich panel. The occurring compressive stress has to be checked against this critical strength.

**Intracell buckling**

Intracell buckling or dimpling is a failure mode that especially can occur by sandwich panels with webs. A sketch of this failure mode is shown in Figure 7.27c. The critical strength of this failure mode is given by

$$\sigma_{Rd.D} = \frac{\eta_c}{\gamma_M} \cdot \bar{k} \cdot \frac{E_i}{\lambda_f} \cdot \left[ \frac{t_f}{\Delta} \right]^2 \tag{7.32}$$

Apart from the same variables for the other failure mechanisms, since a square cell honeycomb is used by the company, the quantity $\Delta$ is the length of the cell and $\bar{k}$ is a factor assumed to be equal to 2.5 [49].

**Delamination of skin and core**

Delamination is a failure mode that has to be checked for structures that are made from FRP. Since this is a complex failure mode, it is recommended to check the laminates with a finite element calculation. However, a quick check can be performed with the formula below based on the failure modes for adhesive joints. In this formula $f_{d.I}$ and $f_{d.II}$ denotes the design values of strength of the adhesive for modes I and II respectively [49].

$$\frac{\sigma_{Ed}}{f_{d.I}} + \frac{\tau_{Ed}}{f_{d.II}} \leq 1 \tag{7.33}$$

(a) Shear crimping



(b) Inward and outward skin wrinkling



(c) Intracell buckling
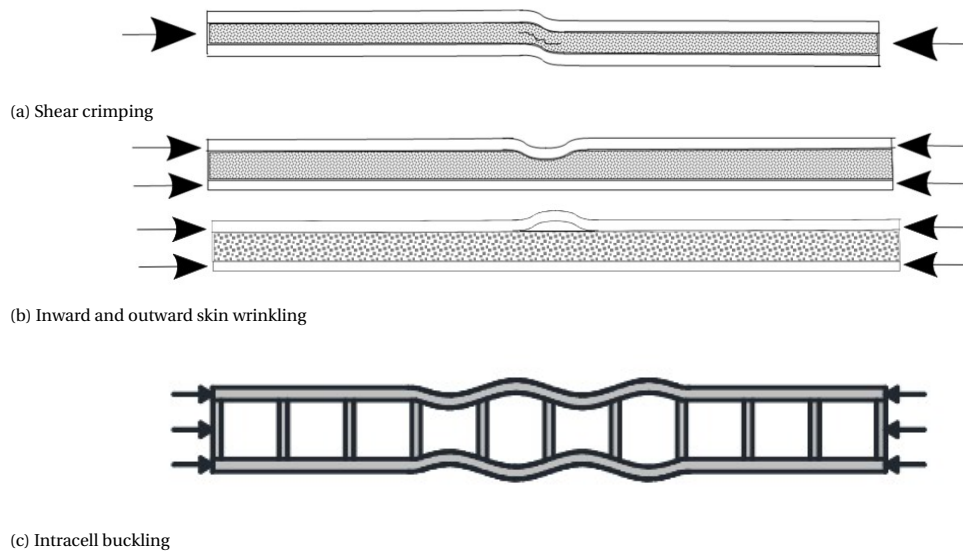
Figure 7.27: Different failure mechanisms FRP plates [49]

## 7.5. Standardization

After developing of the optimization procedure, it can be applied to situations with other boundary conditions. This process is called standardization. In this section, the process of standardization is described and the results are given for a number of situations.

### 7.5.1. Description used method

Two types of standardization can be done. First standardization for the engineering of the slabs. This means that for the boundary conditions that can be applied, a calculation is pre-programmed which founds the optimal design. In this way, a standard can be used to find the optimal design. The next step of this optimization is a table that listed the results for several boundary conditions. In this case, the only boundary condition that varies for the different projects is the distance between the supporting steel beams underneath the deck. This is the distance between the supports (one span) in the calculations. Standardization of the engineering of the slabs is therefore a table with optimal designs for different distances of the supports. This table is shown in Section 7.5.2.

Next to the standardization of the engineering, standardization of the production of the slabs can be done. This type of standardization of the slabs has to be done by using the same type of layups for the slabs with different support distances but different heights and/or web spacing for example. Due to the fact that a range is used for the distance between the supports, the design is not optimal for all distances. This concession needs to be done to make the standardization possible for the production of the slabs.

### 7.5.2. Results standardization

The results for the standardization of the engineering are shown in Table 7.15. These are the results of the optimization procedure described in Section 7 for different distances of the supports. A top ten of the results for the calculations with the different spacing of the supporting beams is given in Appendix F. Comparing the different results, it is shown that some of the parameters are the same for the different cases. These parameters are set constant for all the designs. The remaining parameters are varied for the different ranges that are made. This has to be done since the slabs with a larger span need to have thicker skins to be able to withstand the load. It is chosen to set the number of z-layers constant and have a constant web spacing. This makes it easier to produce the foam blocks. The layups for the webs and the bottomskin stays the same for all the designs. For the topskin the number of UD plies is varied to make the designs for a larger span stronger. Since this gives a difference in the amount of fibers in each direction, the amount of fibers in 45 and -45 direction needs to be increased as well, to satisfy the minimum amount of fibers in the main directions, which is done by increasing the overlapping length of these plies. To make the designs strong enough, the height is increased as well.

The distance between the supports can vary between 0.5 and 1.5 m as given by the experience of the com-

pany [2]. Since the middle of these limits is used the most, this range is made the biggest. Three ranges are made to standardize the results namely, 500 - 800 mm, 800 - 1200 mm and 1200 - 1500 mm. The results for these ranges are given in Table 7.16.

Three of the fifteen variables for the optimization are different for the designs made for the standardization. These variables are the overlapping length of the UD plies in the topskin, the overlapping length of the $+/-45$ plies in the topskin and the height of the deck.

Table 7.15: Results standardization engineering

| Design parameter | $L_0$ | | | | |
|---|---|---|---|---|---|
| | 500 | 750 | 1000 | 1250 | 1500 |
| Number of wraps foam | 1 | 1 | 1 | 1 | 1 |
| Number of z-layers 0/90 | 2 | 2 | 2 | 2 | 2 |
| Number of z-layers 45/-45 | 1 | 1 | 1 | 1 | 1 |
| Number of UD plies topskin | 1 | 1 | 2 | 2 | 2 |
| Number of UD plies bottomskin | 1 | 2 | 1 | 1 | 2 |
| Number of UD plies webs | 2 | 2 | 2 | 2 | 2 |
| Number of 45/-45 plies webs | 1 | 1 | 1 | 1 | 1 |
| Overlapping length UD plies topskin | 4 | 5 | 5 | 6 | 6 |
| Overlapping length UD plies bottomskin | 7 | 4 | 4 | 5 | 4 |
| Overlapping length 0/90 plies topskin | 4 | 4 | 3 | 4 | 5 |
| Overlapping length 0/90 plies bottomskin | 3 | 3 | 3 | 4 | 3 |
| Overlapping length 45/-45 plies topskin | 5 | 4 | 7 | 8 | 8 |
| Overlapping length 45/-45 plies bottomskin | 4 | 4 | 7 | 4 | 4 |
| Height deck [mm] | 100 | 100 | 106 | 102 | 107 |
| Web spacing [mm] | 175 | 174 | 169 | 167 | 174 |
| Relative costs [-] | 0.72 | 0.72 | 0.77 | 0.79 | 0.79 |

Table 7.16: Results standardization production

| Design parameter | Situation | | |
|---|---|---|---|
| | $500 < L_0 < 800$ | $800 < L_0 < 1200$ | $1200 < L_0 < 1500$ |
| **Number of wraps foam** | 1 | 1 | 1 |
| **Number of z-layers 0/90** | 2 | 2 | 2 |
| **Number of z-layers 45/-45** | 1 | 1 | 1 |
| **Number of UD plies topskin** | 2 | 2 | 2 |
| **Number of UD plies bottomskin** | 1 | 1 | 1 |
| **Number of UD plies webs** | 2 | 2 | 2 |
| **Number of 45/-45 plies webs** | 1 | 1 | 1 |
| **Overlapping length UD plies topskin** | 3 | 6 | 7 |
| **Overlapping length UD plies bottomskin** | 6 | 6 | 6 |
| **Overlapping length 0/90 plies topskin** | 4 | 4 | 4 |
| **Overlapping length 0/90 plies bottomskin** | 4 | 4 | 4 |
| **Overlapping length 45/-45 plies topskin** | 5 | 7 | 9 |
| **Overlapping length 45/-45 plies bottomskin** | 4 | 4 | 4 |
| **Height deck [mm]** | 100 | 110 | 114 |
| **Web spacing [mm]** | 175 | 175 | 175 |
| **Relative costs [-]** | 0.74 | 0.80 | 0.81 |

## 7.6. Discussion standardization

For the standardization of the slabs with respect to the production, three intervals are used. This ensures that the slabs are not optimal in all cases. An improvement can be made by increasing the number of intervals. However, this will reduce the effect of the standardization since more different designs need to be produced.

Furthermore, the optimization is sensitive to the different contributions of the costs for the slabs. When the price of one of the elements becomes higher or the hourly wage becomes higher or lower, the optimum can shift to another design. Using the standardized slabs does not anticipate on these changes in prices. Therefore it can be able that more expensive slabs are produced than necessary.

# 8

# Conclusions & Recommendations

This last chapter gives the conclusions of the research described in this report and based on this, some recommendations for further research.

## 8.1. Conclusions

The conclusions are given by answering the research questions which are described in Section 1.3. First, the different sub-questions are answered.

1 Which analytical and (simplified) numerical methods can be used to describe the behavior of FRP bridge slabs, and which one suited best for the calculation of uplift forces in bolted connections?

The different analytical methods that are considered in this thesis are:

- Beam models (MatrixFrame & Formulas of the CUR96)

- Plate model made with ElamX

- Plate model with solution of the CUR96

- Plate model based on an orthotropic plate theory

- Plate model with general boundary conditions

The different numerical models considered in this thesis are:

- Detailed numerical model

- Numerical model with detailed deck geometry and load superposition

- Numerical model with detailed deck geometry and linear bolts

- Numerical model with detailed deck geometry, linear bolts and load superposition

- Numerical model with orthotropic deck

- Numerical model with orthotropic deck and load superposition

- Numerical model with orthotropic deck and linear bolts

- Numerical model with orthotropic deck, linear bolts and load superposition

Analytical plate models cannot be used for the calculation of uplift forces. Analytical beam models can be used for a quick rough estimate of the forces which is on the safe side. For an accurate calculation, a detailed numerical calculation is needed. Simplified numerical models with an orthotropic plate can be used but these models show a deviance from the results of the detailed numerical model.

2 What is the magnitude of the uplift forces in the connections, that connect the FRP traffic decks with a steel structure, calculated with analytical and numerical models for a given load?

Calculated with analytical beam models, the forces are in a range from 8.5 to 21.5 $kN$ for the load models 1 and 2 from EN1991-1. Performing the same calculations with numerical plate models, the bolt forces are in a range of 0.5 to 5.5 $kN$. Since the range of bolt forces is low compared to the capacity of the connections, which is 100 to 200 $kN$, fatigue will not be critical.

3 How can a numerical model, used for calculation of the uplift forces, be simplified and what is the difference in uplift forces between a detailed and simplified numerical calculation?

The numerical model can be simplified by the use of an orthotropic deck with equivalent material properties instead of modeling the skins and webs with laminates. Considering this simplified model, it is shown that the difference in bolt force has a maximum of 2.9 $kN$ compared to the detailed model. However, the calculation time needed is 4-5 times lower for the same mesh size. Since the maximum bolt force is only 5.5 $kN$, the relative difference can be more than 100% which makes the models unusable in practice unless a better description of the equivalent material properties is used.

Other simplifications that can be done are the use of linear bolts and/or load superposition. Using linear bolts gives a maximum difference of 0.5 kN and load superposition a maximum difference of 0.3 kN, both without an improvement of the calculation time. The forces calculated with a linear calculation give higher and lower bolt forces, which means that an error can be introduced on the unsafe side as well. Therefore it can be concluded that the linear calculation can be used when applying a larger safety factor to the calculation.

4 Which are the (main) parameters that influence the design of the FRP slabs and how can the slabs be optimized based on these parameters?

The main parameters are the height of the deck, the spacing of the webs and the layup of the topskin, bottom-skin and webs. The layup of the different elements is dependent on the number of plies, the ply orientation and the overlapping length. The slabs can be optimized using a genetic algorithm driven by a cost function. First, a check has to be done for the strength, stiffness and stability which has to be done based on analytical design formulas from CUR96 at the laminate level.

5 Which method can be used to standardize the FRP bridge slabs and which slabs are optimal to use for a given load and boundary conditions?

For standardization of the engineering of the slabs, the optimization method is used and applied for different cases of the distance between the supports. Standardization for production of the slabs has to be done by using the same type of layups for the slabs with different support distances but different heights and/or web spacing.

Based on these sub-questions, the main research question can be answered, which is

*Which geometry of FRP slabs is optimal to use for a given load and boundary conditions calculated by analytical and (simplified) numerical models taking the uplift forces in the connectors between these slabs and a steel supporting structure into account?*

For the optimization of the FRP slabs, the connectors do not need to be considered due to the low forces obtained, 0.5-21.5 $kN$, compared to the capacity of the connectors, 100-200 $kN$. The optimal geometry for different boundary conditions, considering only the global behavior, is given as a standard design with a variable number of plies for the topskin and a variable height based on intervals for the distance between the supports. The optimal geometry for the deck considered in part one of the graduation work is given in Figure 8.1. However, since global behavior is not considered, the bridge deck is not safe enough and it cannot be built in practice.
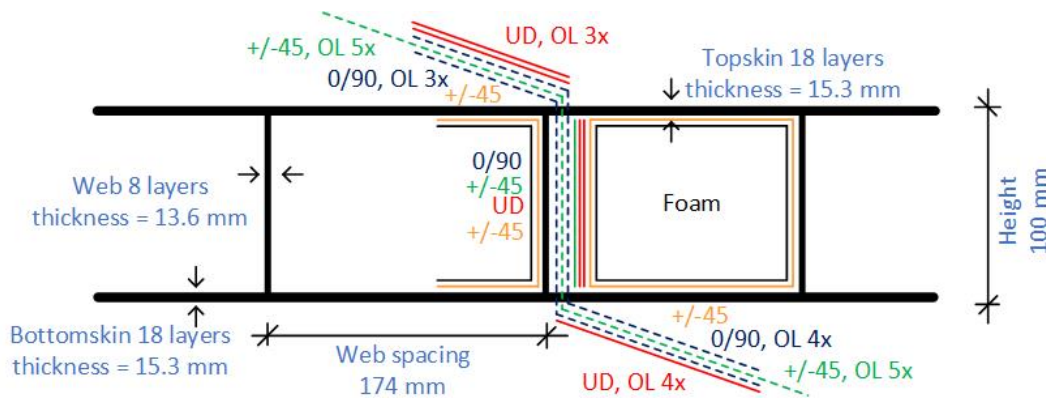
Figure 8.1: Optimal design traffic deck

## 8.2. Recommendations

Two types of recommendations are given. The first recommendations are based on the outcome of the research that is performed. Next to this, recommendations are given for future research based on the gained knowledge and results.

### 8.2.1. Recommendations based on performed work

Based on the performed research some recommendations can be made for others who want to perform the same or similar design calculations.

- For the calculation of uplift forces in the bolted connections between FRP slabs and a steel structure, it is recommended to use a non-linear detailed numerical calculation. When a non-linear calculation is not possible, e.g. due to the program used, a linear calculation can be performed using a larger safety margin to compensate for the error that is made.

- Regarding the design of an FRP bridge slab, it is recommended to use connectors that can transfer both shear and tension forces. Due to the low tension force, there is no need for extra connectors taking only tension forces. When separate connections are used to transfer the tension forces, it is recommended to use the minimum number of connections needed.

- Performing optimization of FRP bridge slabs, it is recommended to use a genetic algorithm with the settings as shown in the research. This optimization technique can handle the large number of variants, which are possible due to the freedom in shape and layups, both with continuous and discontinuous variables.

- When standardization wants to be used for the design and production of FRP slabs, it is recommended to use a constant web spacing and a constant layup for the different elements of the deck. The layup of the topskin can be changed for the different distances between the supports. Different intervals for the distance between the supports can be used for which standard designs are made.

### 8.2.2. Recommendations for future work

After finalizing this research, the following steps can be performed to continue and extend the research.

- Further research on equivalent material properties needs to be done before this can be used in engineering practice. It is recommended based on the performed research to search for a three-layer equivalent model. The top and bottom layers can be thin and stiff while the core layer needs to be large with a low stiffness to represent the web structure.

- Research needs to be done on how large the safety factor needs to be to apply to the different simplified numerical calculations. Since the error is depending on the loading type, geometry of the slab and boundary conditions more calculations need to be done to come up with the error that is made in different cases. Based on this, the range of the safety factors can be determined.

- Since the magnitude of tension forces in the connections is low, it is recommended to use connections that can transfer both tension and shear forces. More research on the interaction of these two types of forces needs to be performed and the performance of the connectors under these two types of loading. In addition, the fatigue forces must be calculated when the magnitude of the bolt forces enters a critical range. The fatigue performance of the different types of connectors needs to be investigated to know which types can be used in practice.

- Experiments need to be performed on the uplift forces in the bolted connections. These experiments need to be used to validate the different models that are made in this research. It is recommended to use specimens of at least 1 $m$ by 2 $m$ with multiple connections.

- To be able to use the results of the optimization procedure in practice, checks for the local bending behavior of the topskin and local buckling of the webs need to be added to the procedure. This can be done with analytical formulas from the JRC code or with the use of an Abaqus shell model with a sub-model when the optimization procedure is divided into two parts, one for global and a second one for local optimization.

# References

[1] U. Oxford, *Oxford English Dictionary*. Oxford university press, 2022.

[2] R. Grefhorst, T. Sharma, and F. Zaaijer, "Data fibercore europe," 2022.

[3] A. Hosseini, "Deck model," 2021.

[4] *En1991-2*, NEN-EN1991-2+C1(nl), CEN, Rue de Stassart 36, B-0150 Brussel, Oktober 2015.

[5] R. Nijssen, *Composieten basiskennis*. VKCN, 2013.

[6] *Crow-cur aanbevelingen 96:2019*, CROW, Nov. 2019.

[7] J. H. A. Peeters, *Method of producing a panel and a core therefor*, US Patent 10,245,765, Apr. 2019.

[8] W. De Corte, A. Jansseune, W. Van Paepegem, and J. Peeters, "Structural behaviour and robustness assessment of an infracore inside bridge deck specimen subjected to static and dynamic local loading," in *Proceedings of the 21st International Conference on Composite Materials, Xi'an*, 2017, pp. 1–8.

[9] J. Dodewaard, "Technical drawing," 2021.

[10] J. M. Lifshitz, "Impact strength of angle ply fiber reinforced materials," *Journal of Composite Materials*, vol. 10, no. 1, pp. 92–101, 1976.

[11] Y.-J. Cheon and H.-G. Kim, "An equivalent plate model for corrugated-core sandwich panels," *Journal of Mechanical Science and Technology*, vol. 29, no. 3, pp. 1217–1223, 2015.

[12] A. Pydah and R. Batra, "Analytical solution for cylindrical bending of two-layered corrugated and web-core sandwich panels," *Thin-Walled Structures*, vol. 123, pp. 509–519, 2018.

[13] H.-X. Wang and S. W. Chung, "Equivalent elastic constants of truss core sandwich plates," *Journal of pressure vessel technology*, vol. 133, no. 4, 2011.

[14] G. Bartolozzi, N. Baldanzini, and M. Pierini, "Equivalent properties for corrugated cores of sandwich structures: A general analytical method," *Composite Structures*, vol. 108, pp. 736–746, 2014.

[15] D. Tumino, T. Ingrassia, V. Nigrelli, G. Pitarresi, and V. U. Miano, "Mechanical behavior of a sandwich with corrugated grp core: Numerical modeling and experimental validation," *Frattura ed Integrità Strutturale*, vol. 8, no. 30, pp. 317–326, 2014.

[16] M. D'Ottavio and O. Polit, "Classical, first order, and advanced theories," in *Stability and vibrations of thin walled composite structures*, Elsevier, 2017, pp. 91–140.

[17] R. Shimpi and H. Patel, "A two variable refined plate theory for orthotropic plate analysis," *International Journal of Solids and Structures*, vol. 43, no. 22-23, pp. 6783–6799, 2006.

[18] H. Khov, W. L. Li, and R. F. Gibson, "An accurate solution method for the static and dynamic deflections of orthotropic plates with general boundary conditions," *Composite Structures*, vol. 90, no. 4, pp. 474–481, 2009.

[19] T. Keller and M. Schollmayer, "Through-thickness performance of adhesive joints between frp bridge decks and steel girders," *Composite Structures*, vol. 87, no. 3, pp. 232–241, 2009.

[20] K. Gradeci, "Upgrading old movable bridges with frp deck application: The case study of wilhelminabrug," 2013.

[21] M. Pavlović, Z. Marković, and M. Veljković, "Resistace of bolted shear connectors in prefabricated steel–concrete composite decks," *Zbornik radova/Društv građevinskih konstruktera Srbije, Simpozijum 2016, 15-17. septembar, Zlatibor*, pp. 64–73, 2016.

[22] F. Csillag, "Demountable deck-to-girder connection of frp-steel hybrid bridges," *Delft: Delft Technical University*, 2018.

[23] G. Olivier, F. Csillag, E. Tromp, and M. Pavlović, "Conventional vs. reinforced resin injected connectors' behaviour in static, fatigue and creep experiments on slip-resistant steel-frp joints," *Engineering Structures*, vol. 236, p. 112 089, 2021.

[24] G. Olivier, F. Csillag, E. Tromp, and M. Pavlovic, "Static, fatigue and creep performance of blind-bolted connectors in shear experiments on steel-frp joints," *Engineering Structures*, vol. 230, p. 111 713, 2021.

[25] F. Csillag and M. Pavlović, "Push-out behaviour of demountable injected vs. blind-bolted connectors in frp decks," *Composite Structures*, vol. 270, p. 114 043, 2021.

[26] Fastener and fixing, *Blind bolt - changing the way for specifiers*, `https://www.fastenerandfixing.com/construction-fixings/blind-bolt-changing-the-way-for-specifiers/`, Accessed: 2022-03-24, 2020.

[27] T. Delft, *Circularity of composite structures*, `https://www.tudelft.nl/citg/over-faculteit/afdelingen/engineering-structures/sections-labs/steel-and-composite-structures/research/research-lines/sustainable-steel-composite-structures/circularity-of-composite-structures`, Accessed: 2022-03-24.

[28] J. ter Kuile, "Case study: Design of gfrp bridge deck & finite element model of shear connection," 2022.

[29] K. Gribnau, "Shear force in bolted connections for hybrid steel-frp bridges: Due to traffic, temperature and fatigue loading," 2021.

[30] T. Peeters, "Design of frp bridge deck and fatigue loading of the connection in a frp-steel composite bridge design," 2021.

[31] Z. K. Awad, T. Aravinthan, Y. Zhuge, and F. Gonzalez, "A review of optimization techniques used in the design of fibre composite structures for civil engineering applications," *Materials & Design*, vol. 33, pp. 534–544, 2012.

[32] D. A. Tortorelli and P. Michaleris, "Design sensitivity analysis: Overview and review," *Inverse problems in Engineering*, vol. 1, no. 1, pp. 71–105, 1994.

[33] D. Whitley, "A genetic algorithm tutorial," *Statistics and computing*, vol. 4, no. 2, pp. 65–85, 1994.

[34] D. Bertsimas and J. Tsitsiklis, "Simulated annealing," *Statistical science*, vol. 8, no. 1, pp. 10–15, 1993.

[35] D. Wang, D. Tan, and L. Liu, "Particle swarm optimization algorithm: An overview," *Soft Computing*, vol. 22, no. 2, pp. 387–408, 2018.

[36] M. Dorigo, M. Birattari, and T. Stutzle, "Ant colony optimization," *IEEE computational intelligence magazine*, vol. 1, no. 4, pp. 28–39, 2006.

[37] I. N. Egorov, G. V. Kretinin, I. A. Leshchenko, and S. V. Kuptzov, "Multi-objective approach for robust design optimization problems," *Inverse Problems in Science and Engineering*, vol. 15, no. 1, pp. 47–59, 2007.

[38] S. Akram and Q. U. Ann, "Newton raphson method," *International Journal of Scientific & Engineering Research*, vol. 6, no. 7, pp. 1748–1752, 2015.

[39] M. A. Schulze, "Linear programming for optimization," *Perspective Scientific Instruments Inc., USA*, 1998.

[40] J. Song, W.-H. Kang, Y.-J. Lee, and J. Chun, "Structural system reliability: Overview of theories and applications to optimization," *ASCE-ASME Journal of Risk and Uncertainty in Engineering Systems, Part A: Civil Engineering*, vol. 7, no. 2, p. 03 121 001, 2021.

[41] *Abaqus 6.11 abaqus/cae user's manual*, Simulia, 2011.

[42] J. W. Welleman, "Force method (hybrid method) with sway degree of freedom," 2017.

[43] T. U. ä. D. Chair of Aircraft Engineering, *Elamx²*, `https://tu-dresden.de/ing/maschinenwesen/ilr/lft/elamx2/elamx?set_language=en`, 2020.

[44] *En1993-1-8*, NEN-EN1993-1-8+C2(nl), CEN, Rue de Stassart 36, B-0150 Brussel, Dec. 2011.

[45] R. M. Solgi, *Geneticalgorithm*, `https://pypi.org/project/geneticalgorithm/`, "Accessed: 2022-06-06", 2020.

[46] Y. He and A. J. Aref, "An optimization design procedure for fiber reinforced polymer web-core sandwich bridge deck systems," *Composite Structures*, vol. 60, no. 2, pp. 183–195, 2003.

[47] F. Zaaijer, "Laminate failure progression tool fibercore europe," 2021.

[48] B. Renckens, "Non-linear buckling analysis of gfrp plates: A numerical approach with progressive failure analysis," 2021.

[49] *Prospect for new guidance in the design of frp structures,* JRC, 2017.

[50] C. Kassapoglou, *Design and analysis of composite structures: with applications to aerospace structures.* John Wiley & Sons, 2013.

# A

# Material properties detailed numerical model

This appendix contains the material properties used for the detailed numerical model. First, the steel properties used are given in Table A.1 which are also used in the simplified numerical models for the supporting structure. Next to this, the material properties used for the FRP are given in Table A.2. These properties are obtained by tests performed by a supplier from FCE [2]. The layups used for the skins are given in Table A.4 and for the webs in Table A.3.

Table A.1: Material properties steel

| Property | Mass density $[kg/m^3]$ | Young's modulus $[MPa]$ | Poisson's ratio $[-]$ |
|---|---|---|---|
| Value | 7800 | 210000 | 0.3 |

Table A.2: Material properties FRP [2]

| Property | Mass density $[kg/m^3]$ | $E_1[MPa]$ | $E_2[-]$ | $v_{12}[-]$ | $G_{12}[MPa]$ | $G_{13}[MPa]$ | $G_{23}[MPa]$ |
|---|---|---|---|---|---|---|---|
| **UD-vf27** | 3539.6 | 21700 | 8000 | 0.27 | 3500 | 3500 | 3400 |
| **UD-vf54** | 3539.6 | 42500 | 8000 | 0.27 | 4200 | 4200 | 3400 |

Table A.3: Ply information web [2]

| Ply | Thickness [mm] | Rotation angle [°] |
|---|---|---|
| Ply-0-Wrap_45 | 0.85 | 45 |
| Ply-1-Wrap_-45 | 0.85 | -45 |
| Ply-2-Wrap_45 | 0.85 | 45 |
| Ply-3-Wrap_-45 | 0.85 | -45 |
| Ply-4-Zlayer_0 | 0.85 | 0 |
| Ply-5-Zlayer_90 | 0.85 | 90 |
| Ply-6-Zlayer_45 | 0.85 | 45 |
| Ply-7-Zlayer_-45 | 0.85 | -45 |
| Ply-8-Zlayer_0 | 0.85 | 0 |
| Ply-9-Zlayer_90 | 0.85 | 90 |
| Ply-10-Wrap_45 | 0.85 | 45 |
| Ply-11-Wrap_-45 | 0.85 | -45 |
| Ply-12-Wrap_45 | 0.85 | 45 |
| Ply-13-Wrap_-45 | 0.85 | -45 |

Table A.4: Ply information top and bottomskin [2]

| Ply | Thickness [mm] | Rotation angle [°] |
| --- | --- | --- |
| Ply-0-UD_0 | 0.85 | 0 |
| Ply-1-UD_0 | 0.85 | 0 |
| Ply-2-UD_0 | 0.85 | 0 |
| Ply-3-UD_0 | 0.85 | 0 |
| Ply-4-UD_0 | 0.85 | 0 |
| Ply-5-UD_0 | 0.85 | 0 |
| Ply-6-UD_0 | 0.85 | 0 |
| Ply-7-UD_0 | 0.85 | 0 |
| Ply-8-Zlayer_45 | 0.425 | 45 |
| Ply-9-Zlayer_-45 | 0.425 | -45 |
| Ply-10-Zlayer_45 | 0.425 | 45 |
| Ply-11-Zlayer_-45 | 0.425 | -45 |
| Ply-12-Zlayer_45 | 0.425 | 45 |
| Ply-13-Zlayer_-45 | 0.425 | -45 |
| Ply-14-Zlayer_45 | 0.425 | 45 |
| Ply-15-Zlayer_-45 | 0.425 | -45 |
| Ply-16-Zlayer_0 | 0.425 | 0 |
| Ply-17-Zlayer_90 | 0.425 | 90 |
| Ply-18-Zlayer_0 | 0.425 | 0 |
| Ply-19-Zlayer_90 | 0.425 | 90 |
| Ply-20-Zlayer_0 | 0.425 | 0 |
| Ply-21-Zlayer_90 | 0.425 | 90 |
| Ply-22-Zlayer_0 | 0.425 | 0 |
| Ply-23-Zlayer_90 | 0.425 | 90 |
| Ply-24-Zlayer_0 | 0.425 | 0 |
| Ply-25-Zlayer_90 | 0.425 | 90 |
| Ply-26-Zlayer_0 | 0.425 | 0 |
| Ply-27-Zlayer_90 | 0.425 | 90 |
| Ply-28-Zlayer_0 | 0.425 | 0 |
| Ply-29-Zlayer_90 | 0.425 | 90 |
| Ply-30-Zlayer_0 | 0.425 | 0 |
| Ply-31-Zlayer_90 | 0.425 | 90 |
| Ply-32-Zlayer_0 | 0.425 | 0 |
| Ply-33-Zlayer_90 | 0.425 | 90 |
| Ply-34-Zlayer_0 | 0.425 | 0 |
| Ply-35-Zlayer_90 | 0.425 | 90 |
| Ply-36-Wrap_45 | 0.425 | 45 |
| Ply-37-Wrap_-45 | 0.425 | -45 |
| Ply-38-Wrap_45 | 0.425 | 45 |
| Ply-39-Wrap_-45 | 0.425 | -45 |

| Ply | Thickness [mm] | Rotation angle [°] |
| --- | --- | --- |
| Ply-0-UD_0 | 0.85 | 0 |
| Ply-1-UD_0 | 0.85 | 0 |
| Ply-2-UD_0 | 0.85 | 0 |
| Ply-3-UD_0 | 0.85 | 0 |
| Ply-4-UD_0 | 0.85 | 0 |
| Ply-5-UD_0 | 0.85 | 0 |
| Ply-6-UD_0 | 0.85 | 0 |
| Ply-7-UD_0 | 0.85 | 0 |
| Ply-8-Zlayer_45 | 0.425 | 45 |
| Ply-9-Zlayer_-45 | 0.425 | -45 |
| Ply-10-Zlayer_45 | 0.425 | 45 |
| Ply-11-Zlayer_-45 | 0.425 | -45 |
| Ply-12-Zlayer_45 | 0.425 | 45 |
| Ply-13-Zlayer_-45 | 0.425 | -45 |
| Ply-14-Zlayer_45 | 0.425 | 45 |
| Ply-15-Zlayer_-45 | 0.425 | -45 |
| Ply-16-Zlayer_0 | 0.425 | 0 |
| Ply-17-Zlayer_90 | 0.425 | 90 |
| Ply-18-Zlayer_0 | 0.425 | 0 |
| Ply-19-Zlayer_90 | 0.425 | 90 |
| Ply-20-Zlayer_0 | 0.425 | 0 |
| Ply-21-Zlayer_90 | 0.425 | 90 |
| Ply-22-Zlayer_0 | 0.425 | 0 |
| Ply-23-Zlayer_90 | 0.425 | 90 |
| Ply-24-Zlayer_0 | 0.425 | 0 |
| Ply-25-Zlayer_90 | 0.425 | 90 |
| Ply-26-Zlayer_0 | 0.425 | 0 |
| Ply-27-Zlayer_90 | 0.425 | 90 |
| Ply-28-Zlayer_0 | 0.425 | 0 |
| Ply-29-Zlayer_90 | 0.425 | 90 |
| Ply-30-Zlayer_0 | 0.425 | 0 |
| Ply-31-Zlayer_90 | 0.425 | 90 |
| Ply-32-Zlayer_0 | 0.425 | 0 |
| Ply-33-Zlayer_90 | 0.425 | 90 |
| Ply-34-Zlayer_0 | 0.425 | 0 |
| Ply-35-Zlayer_90 | 0.425 | 90 |
| Ply-36-Wrap_45 | 0.425 | 45 |
| Ply-37-Wrap_-45 | 0.425 | -45 |

# B

# Study on model assumptions

To verify the model assumptions, a study is performed with a part of the model to check for the influence of these simplifications on the model. The dimensions of the part of the model that is used for this study are shown in Table B.1. Three different small models are considered. The first model is as detailed as possible. Steel beams are modeled with real dimensions and bolts are modeled with solid elements, this model is shown in Figure B.1. The second model that is considered is using rigid surfaces of the I-beams, which cancels the deformations of the I-beams. This model is shown in Figure B.2. The last model that is considered is using beam elements to model the I-beams, which is shown in Figure B.3.

Table B.1: Dimensions small models

| Dimension | Value | Unit |
|---|---|---|
| Length | 1910 | mm |
| Width | 1000 | mm |
| Height | 120 | mm |
| Number of webs | 17 | - |
| Spacing webs | 116 | mm |
| Number of I-beams | 2 | - |
| Number of C-beams | 2 | - |
| Width I-beams | 100 | mm |
| Width C-beams | 50 | mm |
| Number of bolts | 4 | - |
| Length bolts | 60 or 100 | m |
| Radius bolts | 10 | mm |
| Applied concentrated force | 0.675 | $N/mm^2$ |
| Area applied load | 370x400 | $mm^2$ |
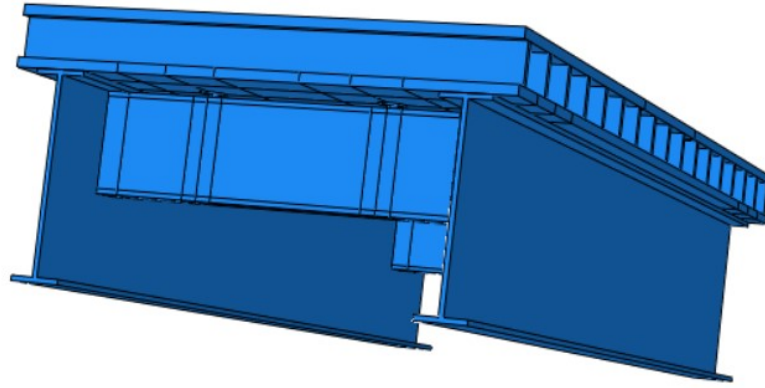
Figure B.1: Small model 1
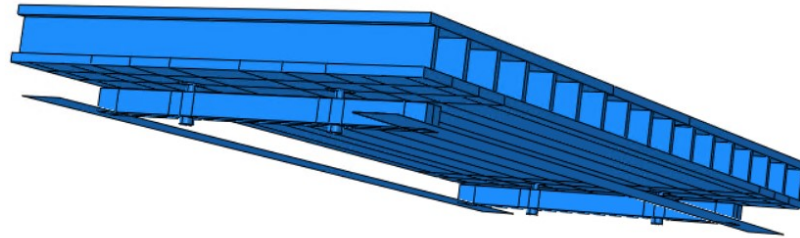


Figure B.2: Small model 2
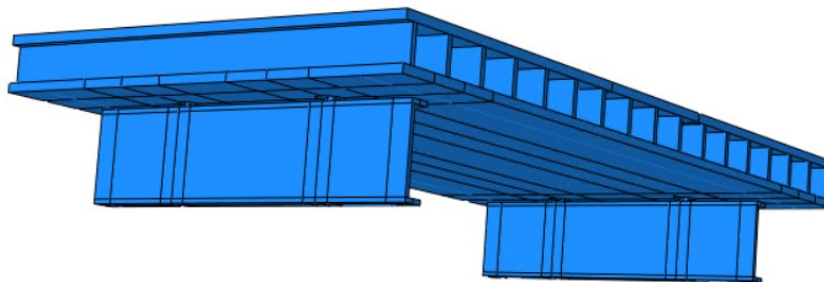


Figure B.3: Small model 3

The results for the given load case which is considered are shown in Tables B.2, B.3 and B.4, which are the maximum stresses in the deck. It is shown that the influence of the modeling with rigid surfaces is quite large. This is due to the rotation of the top flange of the I-beam as is shown in Figure B.4. There are some main differences between the three models:

- Models with modeled beams give small values for the stresses and deformations in the bolts, the other model does not give these forces. This is due to singularities.

- Stresses in the model with the rigid beams are larger compared to the other two models.

- Deformations in the model with rigid beams are smaller compared to the other two models.

Table B.2: Comparison results small models 1 and 2

| | Model 1 (Model with modeling beams continuum shell elements) | Model 2 (Model with simplifications rigid beams) | Difference (%) |
|---|---|---|---|
| **Deformation (mm)** | 1.67 | 0.995 | 51 |
| **S11 (MPa)** | 15.8 | 25.0 | 45 |
| **S22 (MPa)** | 6.17 | 5.98 | 3.1 |
| **S33 (MPa)** | 0.00 | 0.00 | 0.0 |
| **S12 (MPa)** | 2.84 | 2.28 | 22 |

Table B.3: Comparison results small models 2 and 3

| | Model 3 (Model with beam elements) | Model 2 (Model with simplifications rigid beams) | Difference (%) |
|---|---|---|---|
| **Deformation (mm)** | 1.90 | 0.995 | 63 |
| **S11 (MPa)** | 16.2 | 25.0 | 43 |
| **S22 (MPa)** | 6.01 | 5.98 | 0.50 |
| **S33 (MPa)** | 0.00 | 0.00 | 0.0 |
| **S12 (MPa)** | 4.31 | 2.28 | 62 |

Table B.4: Comparison results small models 1 and 3

| | Model 3 (Model with beam elements) | Model 1 (Model with modeling beams continuum shell elements) | Difference (%) |
|---|---|---|---|
| **Deformation (mm)** | 1.90 | 1.67 | 13 |
| **S11 (MPa)** | 16.2 | 15.8 | 2.5 |
| **S22 (MPa)** | 6.01 | 6.17 | 2.6 |
| **S33 (MPa)** | 0.00 | 0.00 | 0.0 |
| **S12 (MPa)** | 4.31 | 2.84 | 41 |

The extra deformation in the models is caused by rotation of the top flange of the I-beam which is shown in Figure B.4. This extra deformation can be calculated with the distance from the middle of the deck to the flange of the I-beam times the rotation of this top flange. The rotation angle of the top flange is

$$\beta = arctan((3.057 \cdot 10^{-2} - -3.178 \cdot 10^{-1})/(100) = 0.00348 rad$$

The extra deformation in the middle of the deck is

$$d = \beta \cdot d = 0.00348 \cdot 405 = 1.4 \ mm$$
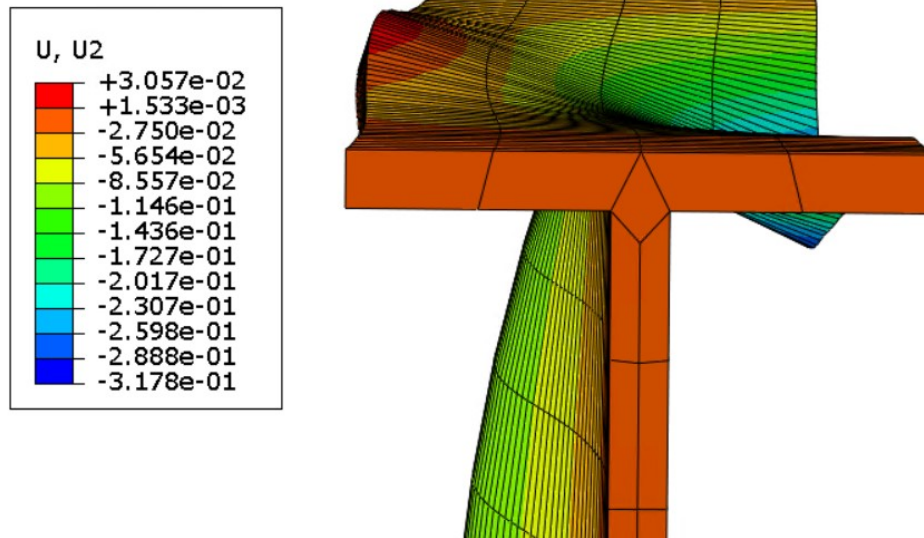
Figure B.4: Rotation top flange I-beam

**Conclusion**

The conclusion is that there is quite a large influence due to the simplification with the rigid surfaces for the stresses and deformations in the deck. Therefore, these types of simplifications cannot be used to accurately calculate the stresses in the deck. The influence of the simplifications on the forces in the bolts has to be checked with a larger model. The model with beam elements can be used as a simplification without adding large errors to the model. Therefore, the I-beams are modeled with beam elements in Abaqus.

# C

# Study equivalent material properties

This appendix contains the study which is performed to determine equivalent properties for an orthotropic plate to represent the detailed geometry as described in Section 4.4. The first section gives an overview of the different formulas that are used to calculate the equivalent material properties. Section C.2 up to and including C.5 gives the results for the different options that are considered to determine the properties. The last section gives a conclusion based on the performed study.

## C.1. Overview formulas to calculate the equivalent material properties

First the different options which are considered for the material properties are described. Dimensions used are shown in Figure C.1.
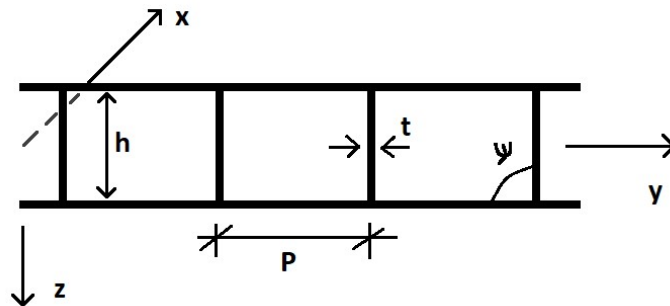


Figure C.1: Dimensions model equivalent properties [$mm$]

$$
\begin{aligned}
t &= 11.9 \; mm \\
h &= 120 \; mm \\
p &= 116 \; mm \\
\phi &= 90°
\end{aligned}
\tag{C.1}
$$

### $E_1$

With $t$ denoting the thickness, $h$ the height, $p$ the web spacing and $\phi$ the angle between the webs and the bottomskin. For E1 of the web, the modulus can be calculated using the approach from a paper written by H.X. Wang and S. W. Chung [13].

$$
E_1 = E \frac{t}{p \cdot \sin\phi} = \frac{11.9}{116 \cdot 1} E \approx 0.1 E
\tag{C.2}
$$

In which $E$ denotes the bending modulus. Using the method of averaging based on volume to calculate the modulus for the complete plate gives

$$E_1 = \frac{E_{1.tf} \cdot h_{tf} + 0.1 \cdot E_{1.w} \cdot h_w + E_{1.bf} \cdot h_{bf}}{h} = \frac{25466 \cdot 20.4 + 0.1 \cdot 11081.1 \cdot 80.05 + 26576 \cdot 19.55}{120} = 9398 \, MPa$$
(C.3)

**$E_2$**

For the core there is (almost) no contribution in the transverse direction. Therefore the bending modulus $E_2$ is set to zero.

$$E_2 = E \frac{t^3 \cdot \cos\phi}{(h^2 - t^2 \cdot \cos\phi)h} = 0$$
(C.4)

Using the method of averaging based on volume to calculate the modulus for the complete plate gives

$$E_2 = \frac{E_{2.tf} \cdot h_{tf} + 0.1 \cdot E_{2.w} \cdot h_w + E_{2.bf} \cdot h_{bf}}{h} = \frac{14276.4 \cdot 20.4 + 0.1 \cdot 1.0 \cdot 80.05 + 14898.6 \cdot 19.55}{120} = 4854 \, MPa$$
(C.5)

**$\nu_{12}$**

For the Poisson ratio, the method of averaging based on volume is used which is described by

$$\nu_{12} = \frac{\nu_{12.tf} \cdot h_{tf} + 0.1 \cdot \nu_{12.w} \cdot h_w + \nu_{12.bf} \cdot h_{bf}}{h} = \frac{0.143 \cdot 20.4 + 0.1 \cdot 0.25 \cdot 80.05 + 0.143 \cdot 19.55}{120} = 0.214$$
(C.6)

**$G_{12}$**

For the in-plane shear modulus $G_{12}$, different options are considered.
Option 1: Assume that only 10% of the part of the webs is contributing due to only 10% of material.

$$G_{12} = \frac{G_{12.tf} \cdot h_{tf} + 0.1 \cdot G_{12.w} \cdot h_w + G_{12.bf} \cdot h_{bf}}{h} = \frac{2910 \cdot 20.4 + 0.1 \cdot 5380.5 \cdot 80.05 + 3036.8 \cdot 19.55}{120} = 1348 \, MPa$$
(C.7)

Option 2: Use approach from the paper of Wang and Chung [13].

$$G_{12} = G \frac{p \cdot t \cdot \sin\phi}{h^2} = \frac{116 \cdot 11.9 \cdot 1}{80.05^2} \approx 0.215G$$
(C.8)

Using the method of averaging based on volume to calculate the modulus for the complete plate gives

$$G_{12} = \frac{G_{12.tf} \cdot h_{tf} + 0.215 \cdot G_{12.w} \cdot h_w + G_{12.bf} \cdot h_{bf}}{h} = \frac{2910 \cdot 20.4 + 0.215 \cdot 5380.5 \cdot 80.05 + 3036.8 \cdot 19.55}{120} = 1761 \, MPa$$
(C.9)

Option 3: The third option is to take no contribution of the webs into account.

$$G_{12} = \frac{G_{12.tf} \cdot h_{tf} + 0.0 \cdot G_{12.w} \cdot h_w + G_{12.bf} \cdot h_{bf}}{h} = \frac{2910 \cdot 20.4 + 0.0 \cdot 5380.5 \cdot 80.05 + 3036.8 \cdot 19.55}{120} = 989 \, MPa$$
(C.10)

**$G_{13}$**

Option 1: For $G_{13}$ of the core, the approach from the work of Wang and Chung is used [13].

$$G_{13} = E \frac{t^3 \cdot \sin\phi}{p^3 - p \cdot t^2 \cdot \sin^2\phi} = \frac{11.9^3 \cdot 1}{116^3 - 116 \cdot 11.9^2 \cdot 1} E \approx 0.103G$$
(C.11)

Using the method of averaging based on volume to calculate the modulus for the complete plate gives

$$G_{13} = \frac{G_{13.tf} \cdot h_{tf} + 0.103 \cdot G_{13.w} \cdot h_w + G_{13.bf} \cdot h_{bf}}{h} = \frac{2910 \cdot 20.4 + 0.103 \cdot 5380.5 \cdot 80.05 + 3036.8 \cdot 19.55}{120} = 1359 \, MPa$$
(C.12)

Option 2: The other option that is considered is when the contribution of webs is neglected.

$$G_{13} = \frac{G_{13.tf} \cdot h_{tf} + 0.0 \cdot G_{13.w} \cdot h_w + G_{13.bf} \cdot h_{bf}}{h} = \frac{2910 \cdot 20.4 + 0.0 \cdot 5380.5 \cdot 80.05 + 3036.8 \cdot 19.55}{120} = 989 \, MPa$$

(C.13)

**$G_{23}$**

For the out-of-plane shear modulus an approach from the work of Hans Welleman as described in Section 4.4 is used.

$$G_{23} = k_e = \frac{Hh}{u} = \frac{12(6hEI_{tf}EI_{bf} - wEI_{bf}EI_W - wEI_{tf}EI_w)EI_w}{w(3EI_{bf}EI_{tf}h^2 - 2EI_{bf}EI_whw - 2EI_{tf}EI_whw + EI_w^2w^2)} = 339 \, MPa$$

(C.14)

## C.2. Model with partly contribution webs

In this section the results are shown for the calculations with different amount of contribution of the webs/core. The calculations are performed for the large scale model, without bolts and load model 2 case 2.
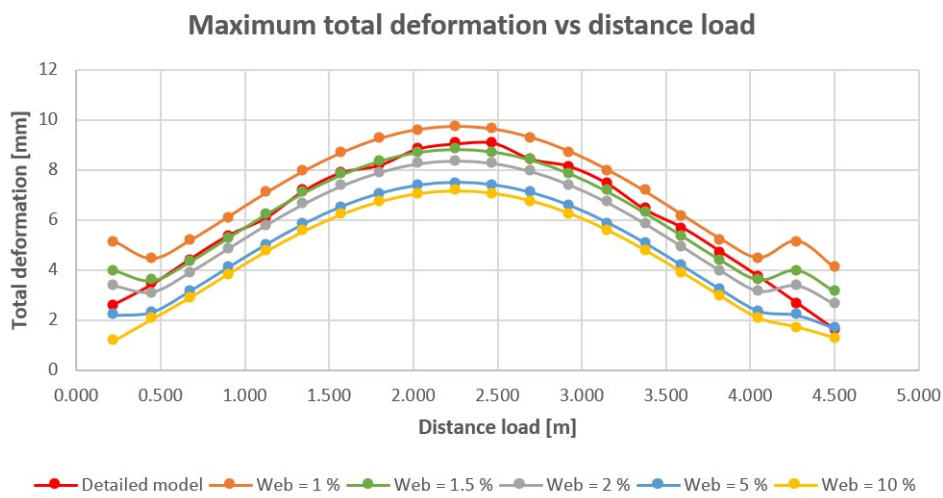


(a) Total deformation model with partly contribution webs *mm*
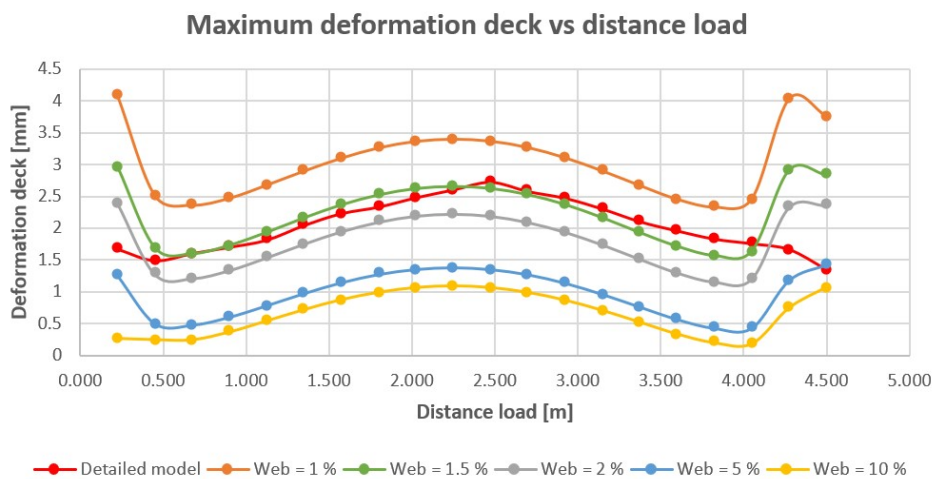


(b) Deformation deck model with partly contribution webs *mm*

Figure C.2: Deformations model with partly contribution webs

## C.3. Model with contribution resin

This section shows the results for calculations performed with the large scale model without bolts for different load models. For the shear stiffness the contribution of the resin is taken instead of the stiffness of the fibers.

**Maximum total deformation vs distance load**
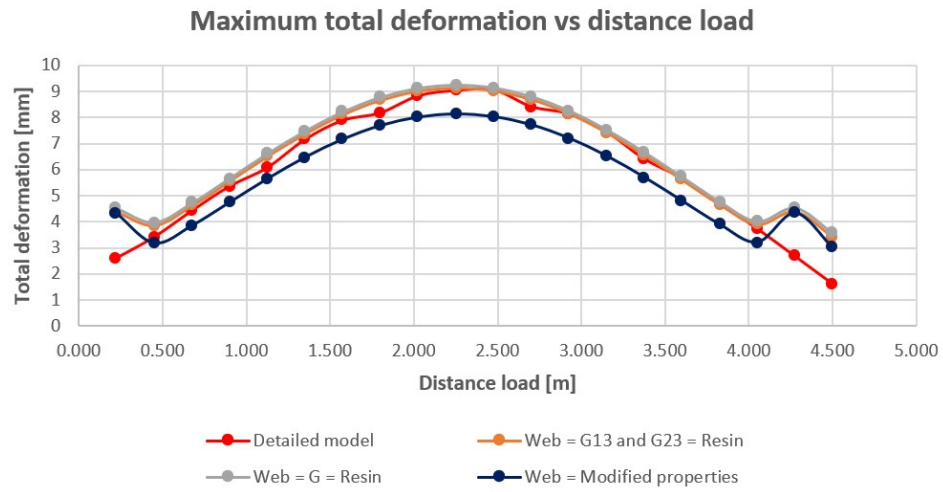
(a) Total deformation model with contribution resin *mm*

**Maximum deformation deck vs distance load**
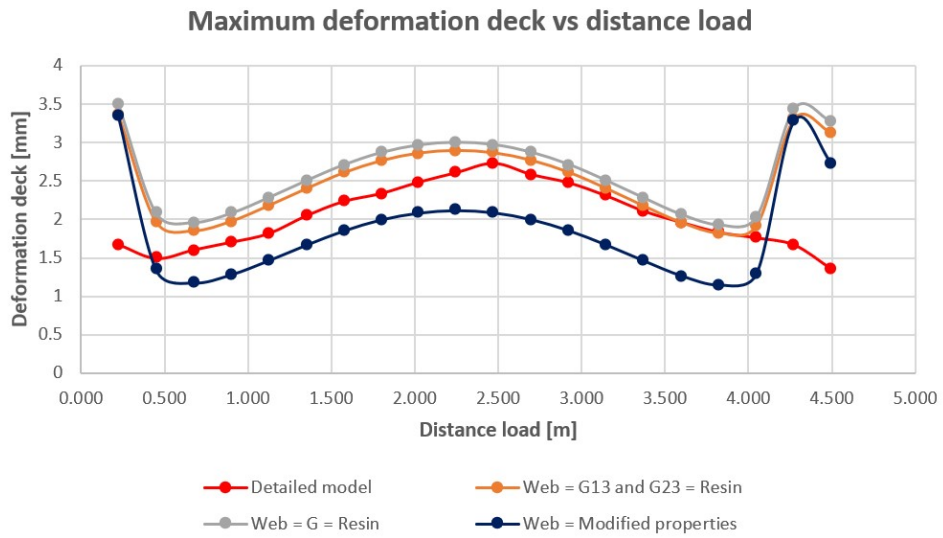
(b) Deformation deck model with contribution resin *mm*

Figure C.3: Deformations model with contribution resin

## C.4. Model based on shear models

In this section the results of the comparison is given between the detailed model and a large scale orthotropic model with properties determined with the shear model as described in Section 4.4 for load model 2 case 2 using different type of elements.

**Maximum total deformation vs distance load**
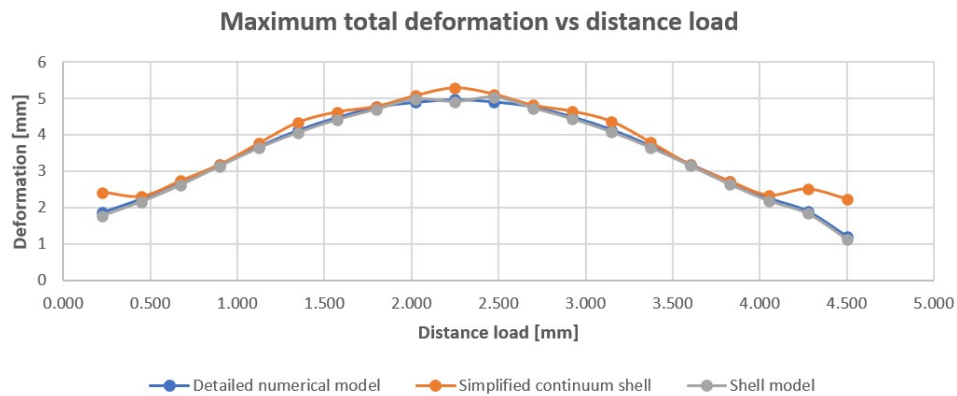


(a) Total deformation model adapted shear stiffness $mm$

**Maximum deformation deck vs distance load**
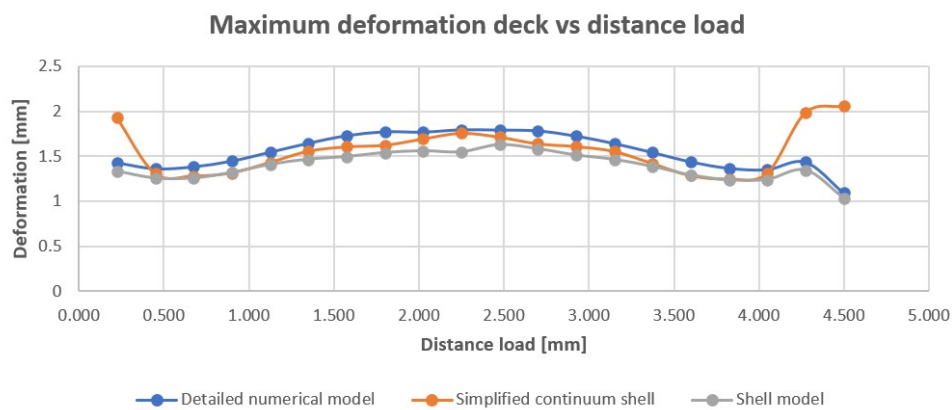


(b) Deformation deck model adapted shear stiffness $mm$

Figure C.4: Deformations model adapted shear stiffness

## C.5. Model with solid elements

In this section the results are given between the detailed model and a large scale orthotropic model calculated with solid elements for load model 2 case 2.



(a) Total deformation model solid elements *mm*



(b) Deformation deck model solid elements *mm*
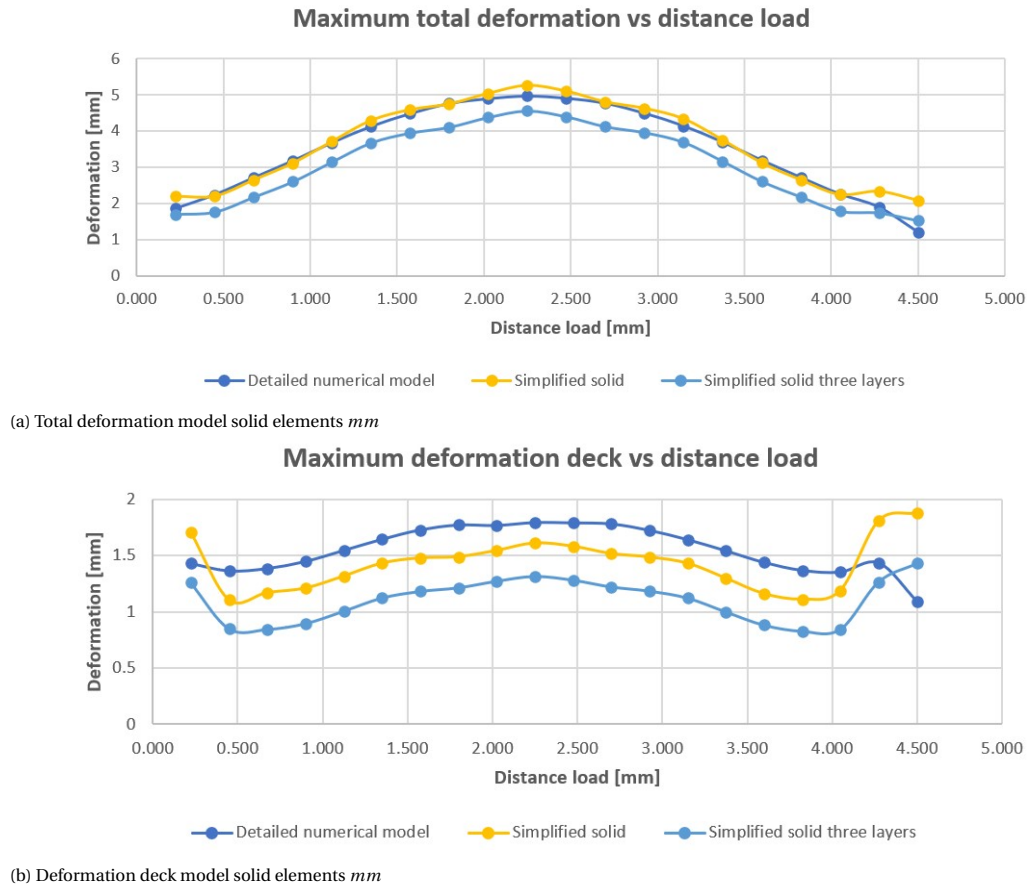
Figure C.5: Deformations model solid elements

## C.6. Conclusion

Based on the study that is performed the following observations are made:

- Deformations are lower for the orthotropic model and bolt forces are higher. Since the bolt forces are related to the deformations this indicates that the E modulus is too high for the orthotropic plate model.

- Deformation pattern looks the same for both models. However, observing the behavior in more detail with small models as described in Section 4.5 shows a different load transfer.

- No (large) buckling or out of plane deformation of the webs, this indicates that there is not much shear stiffness reduction for the webs.

- From the research to the contribution of the webs, 1.5% contribution gives more or less the same results as the detailed model.

- Using the resin properties gives sometimes lower and sometimes larger deformations. Not useful since the resin is not modeled in the detailed model.

The model with the webs transfers the load in one direction due to the webs. For the model where the deck is modeled as an orthotropic plate, the load is spread more due to the fact that more material is available. This can be adapted by reducing the E2 value. An good approximation of the equivalent properties is not found, therefore a safe assumption has to be made. Since the deformations are not taken into account, a safe approach for the bolt forces is used when the equivalent material properties are used as described in Section 4.4.

# Results simplified numerical models

In this appendix, some of the results calculated with the simplified numerical models are given. The results are presented in the same order as the models in Chapter 4.

## D.1. Model with detailed deck geometry and linear bolts
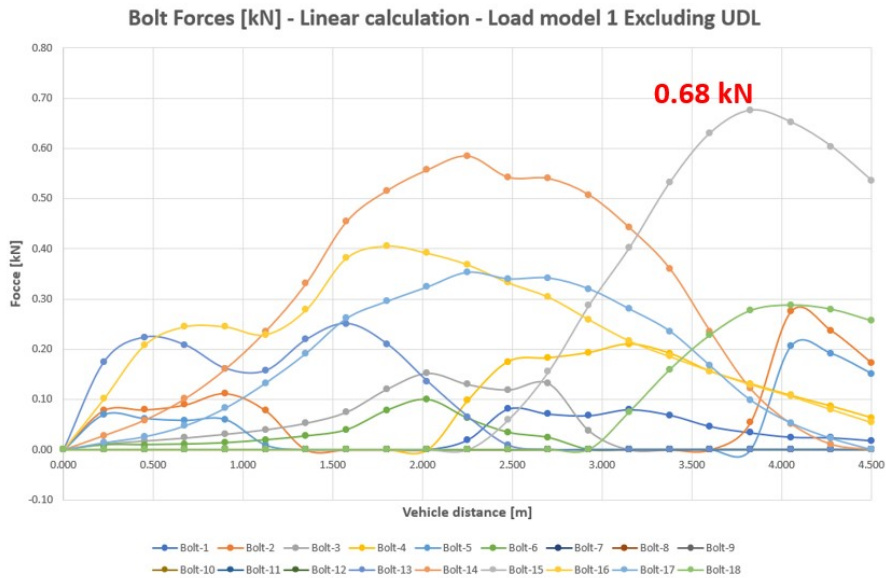


Figure D.1: Bolt forces linear calculation LM1 Excluding UDL [$kN$]
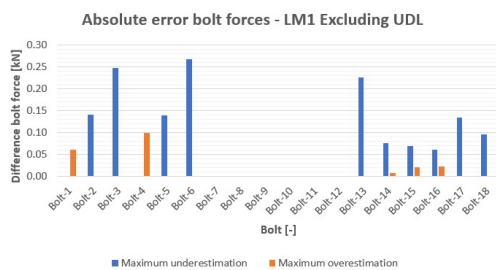


(a) Absolute error bolt forces load model 1 excluding UDL [$kN$]
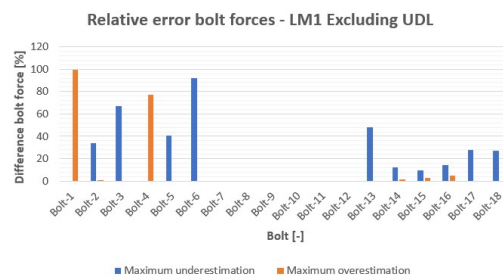


(b) Relative error bolt forces load model 1 excluding UDL [%]

Figure D.2: Difference in bolt forces for model with detailed deck geometry and linear bolts with respect to reference model for load model 1 excluding UDL

139
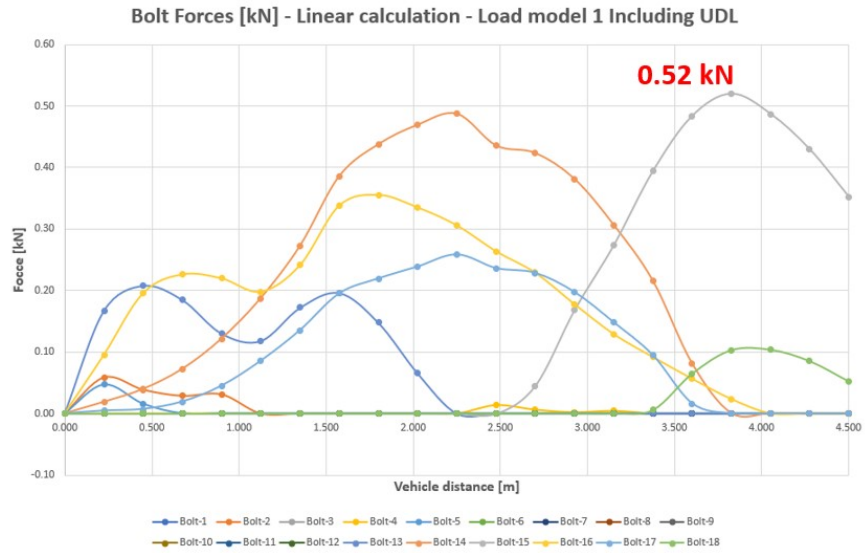
Figure D.3: Bolt forces linear calculation LM1 Including UDL [*kN*]
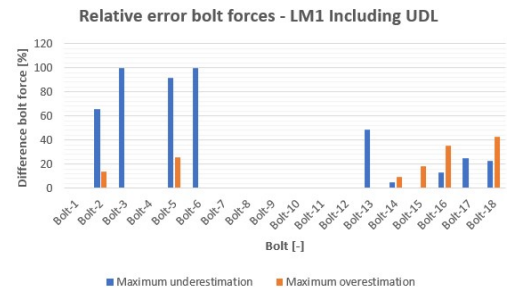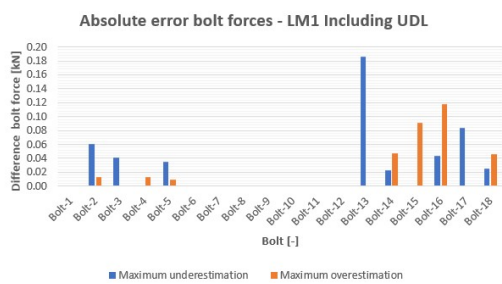


(a) Absolute error bolt forces load model 1 including UDL [*kN*]



(b) Relative error bolt forces load model 1 including UDL [%]

Figure D.4: Difference in bolt forces for model with detailed deck geometry and linear bolts with respect to reference model for load model 1 including UDL
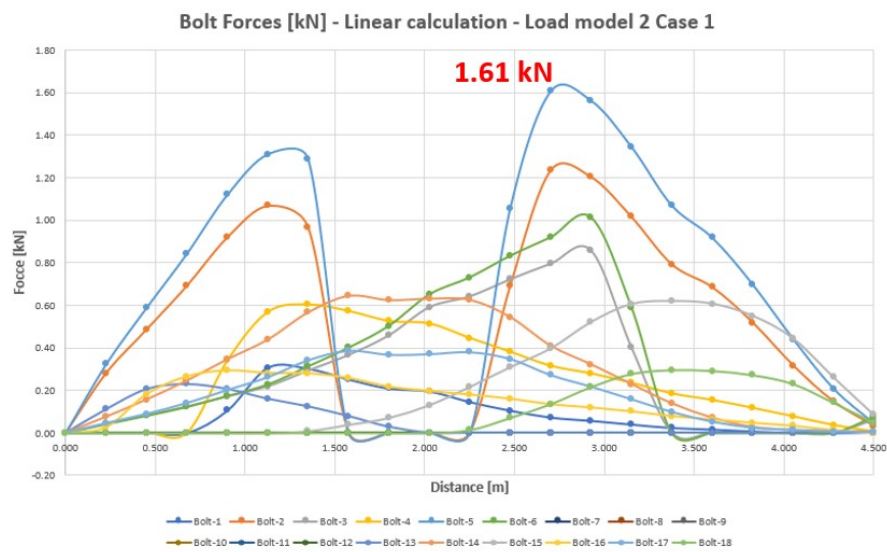


Figure D.5: Bolt forces linear calculation LM2 case 1 [*kN*]
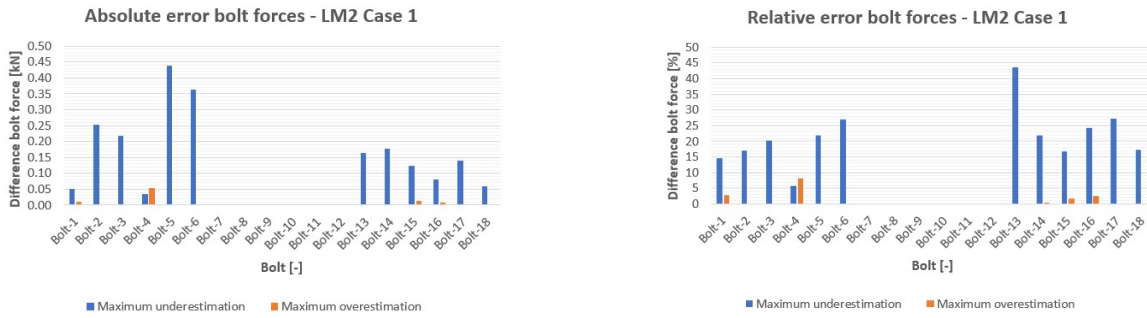
(a) Absolute error bolt forces load model 2 case 1 [$kN$]

(b) Relative error bolt forces load model 2 case 1 [%]

Figure D.6: Difference in bolt forces for model with detailed deck geometry and linear bolts with respect to reference model for load model 2 case 1

## D.2. Model orthotropic deck
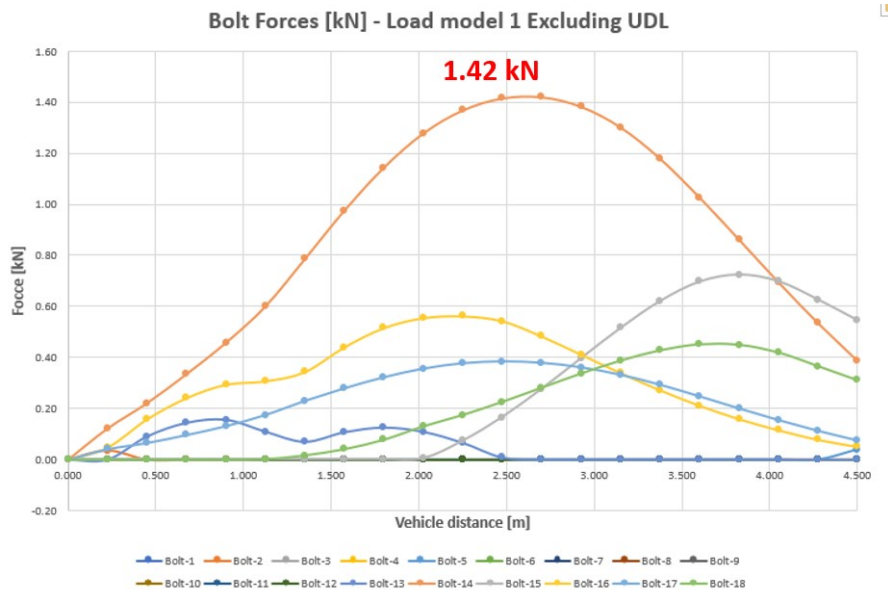


Figure D.7: Bolt forces simplified numerical calculation LM1 excluding UDL [$kN$]
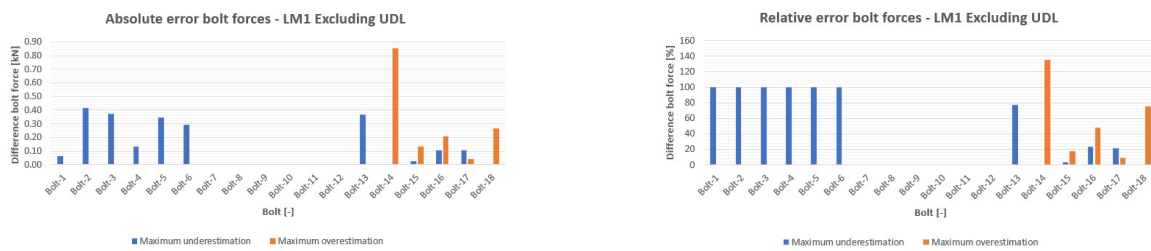


(a) Absolute error bolt forces load model 1 excluding UDL [$kN$]

(b) Relative error bolt forces load model 1 excluding UDL [%]

Figure D.8: Difference in bolt forces for model orthotropic deck with respect to reference model for load model 1 excluding UDL
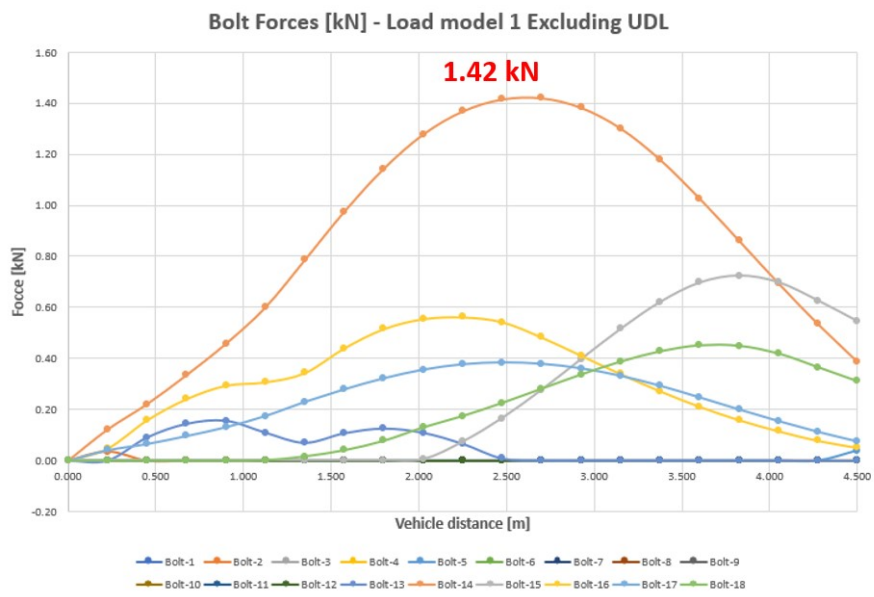
Figure D.9: Bolt forces simplified numerical calculation LM1 excluding UDL [$kN$]
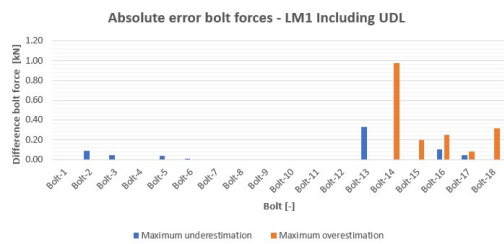


(a) Absolute error bolt forces load model 1 including UDL [$kN$]
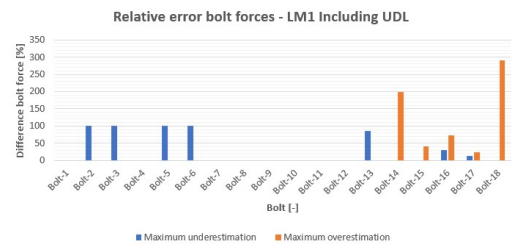


(b) Relative error bolt forces load model 1 including UDL [%]

Figure D.10: Difference in bolt forces for model orthotropic deck with respect to reference model for load model 1 including UDL
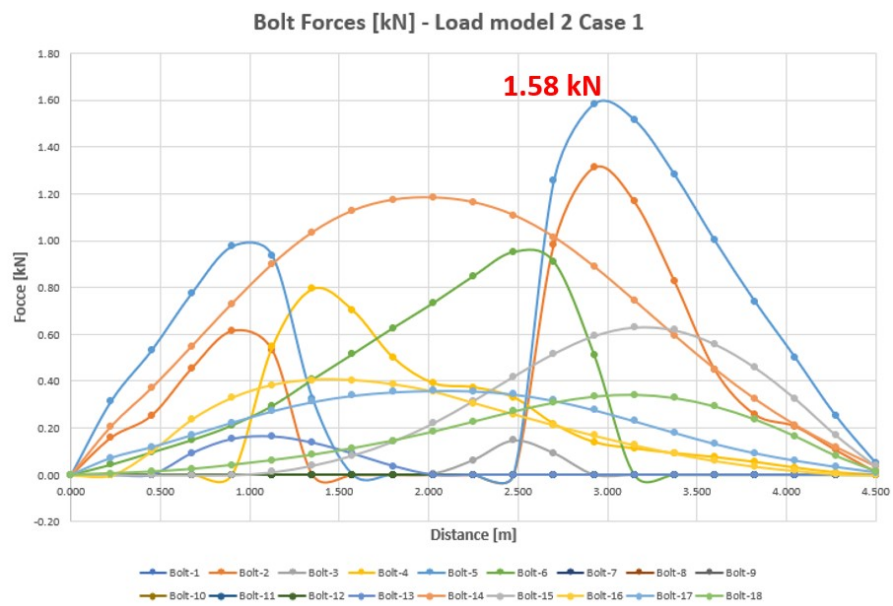


Figure D.11: Bolt forces simplified numerical calculation LM2 case 1 [$kN$]
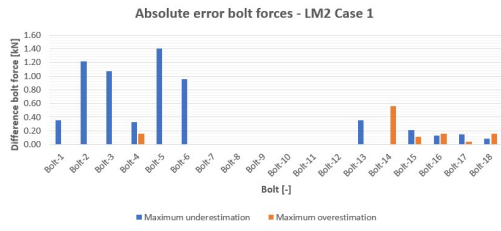
(a) Absolute error bolt forces load model 2 case 1 [*kN*]
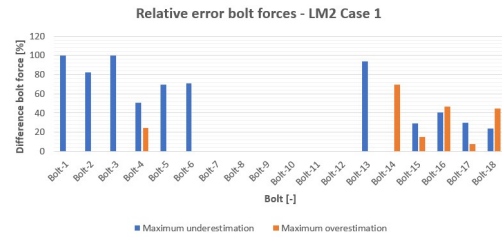


(b) Relative error bolt forces load model 2 case 1 [%]

Figure D.12: Difference in bolt forces for model orthotropic deck with respect to reference model for load model 2 case 1

# D.3. Model with orthotropic deck and linear bolts
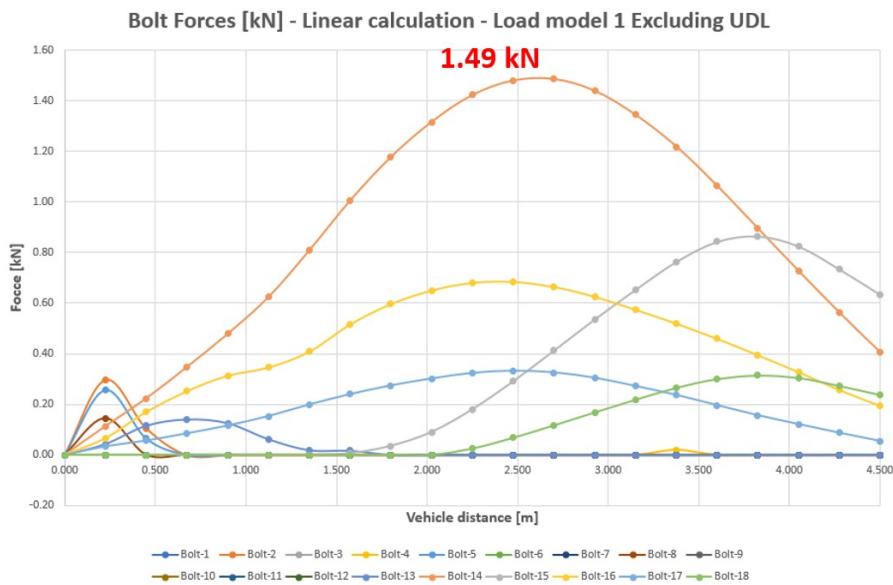


Figure D.13: Bolt forces linear simplified numerical calculation LM1 excluding UDL [*kN*]
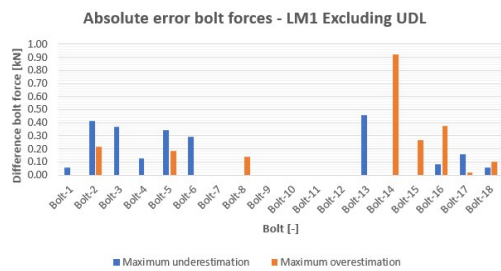


(a) Absolute error bolt forces load model 1 excluding UDL [*kN*]
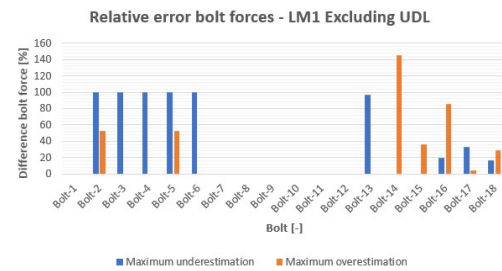


(b) Relative error bolt forces load model 1 excluding UDL [%]

Figure D.14: Difference bolt forces detailed and linear simplified numerical calculation load model 1 excluding UDL
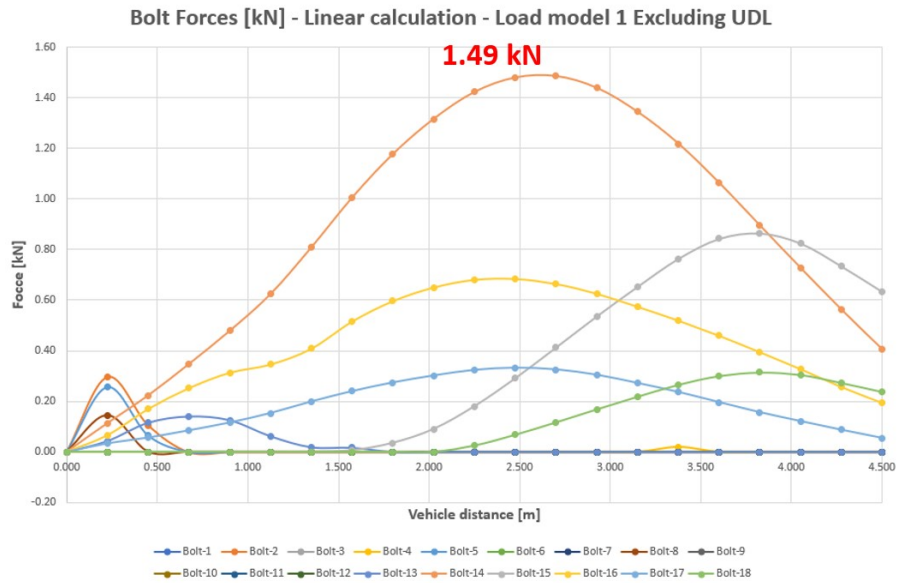
Figure D.15: Bolt forces linear simplified numerical calculation LM1 excluding UDL [$kN$]
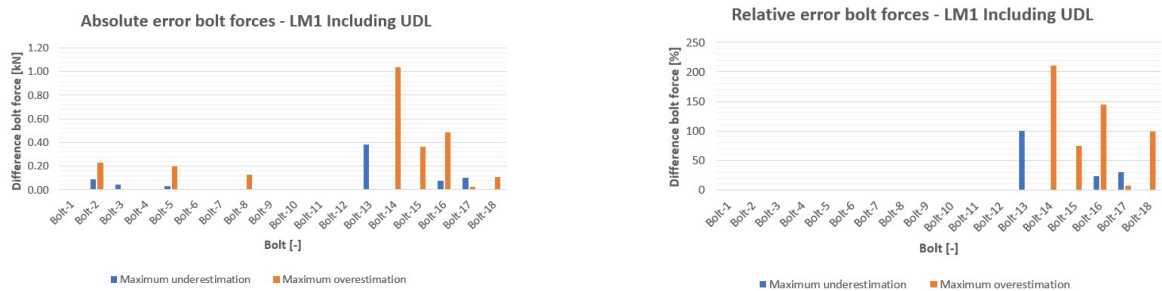


(a) Absolute error bolt forces load model 1 including UDL [$kN$]



(b) Relative error bolt forces load model 1 including UDL [%]

Figure D.16: Difference in bolt forces for model with orthotropic deck and linear bolts with respect to reference model for load model 1 including UDL
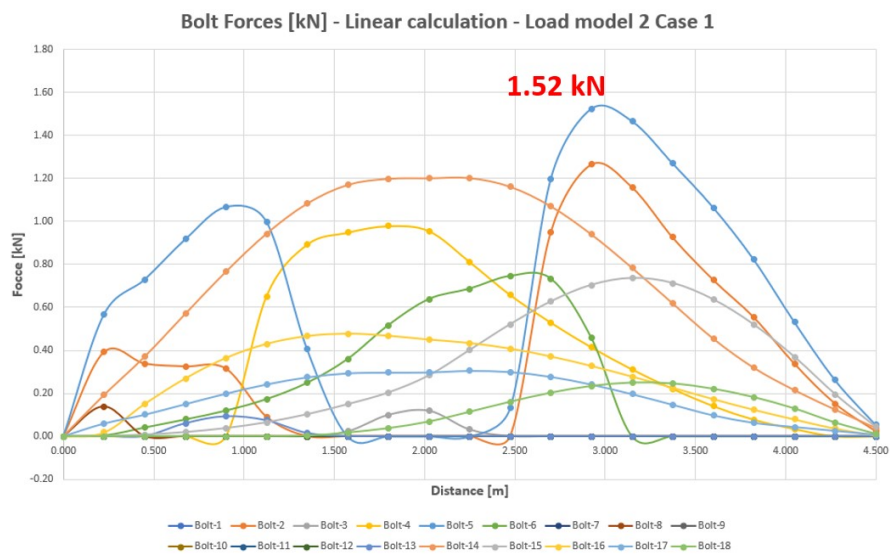


Figure D.17: Bolt forces linear simplified numerical calculation LM2 case 1 [$kN$]
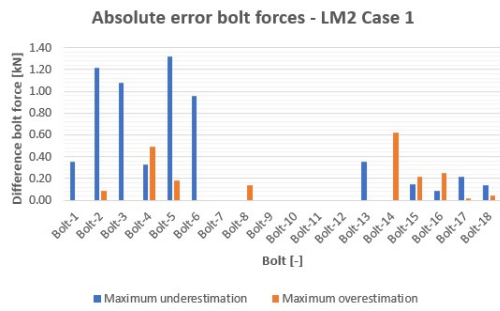
(a) Absolute error bolt forces load model 2 case 1 [$kN$]
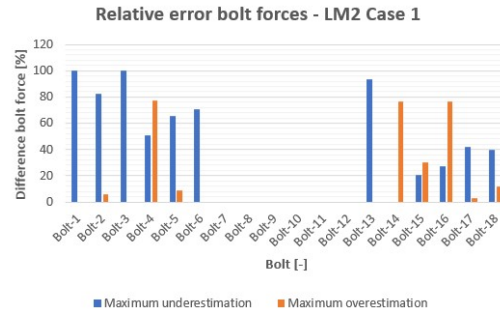


(b) Relative error bolt forces load model 2 case 1 [%]

Figure D.18: Difference in bolt forces for model with orthotropic deck and linear bolts with respect to reference model for load model 2 case 1

# E

# Analytical calculations traffic deck

This appendix contains the analytical calculations that are used for the optimization procedure. The calculations are based on the CUR [6].

## E.1. Serviceability Limit State

**Deformations**

Deformation load model 1

$$w_{LC1.Q} = Q_{1k} \cdot \left[ \frac{L_0^3}{48 \cdot EI_{yy}} + \frac{L_0}{4 \cdot GA_{xz}} \right] \tag{E.1}$$

$$w_{LC1.q} = [q_{1k} \cdot w_{lane} + q_{rk} \cdot w_r] \cdot \left( \frac{5 \cdot L_0^4}{384 \cdot EI_{yy}} + \frac{L_0^2}{8 \cdot GA_{xz}} \right) \tag{E.2}$$

$$w_{LC1} = \frac{\gamma_f \cdot \gamma_m}{\eta_{d.k}} \cdot \left( w_{LC1.Q} + w_{LC1.q} \right) \tag{E.3}$$

Deformation load model 2

$$w_{LC2} = \frac{\gamma_f \cdot \gamma_m}{\eta_{d.k}} \cdot \left( \frac{Q_{2k} \cdot L_0^3}{48 \cdot EI_{yy}} + \frac{Q_{2k} \cdot L_0}{8 \cdot GA_{xz}} \right) \tag{E.4}$$

In these formulas $Q$ is denoting the wheel load, $L_0$ the distance between the supports, $EI$ the bending stiffness and $GA$ the shear stiffness. $\gamma$ is the applied safety factor and $\eta$ the applied conversion factor. To check for the deformations, the maximum value is used

$$uc_{deformation} = \frac{max(w_{LC1}, w_{LC2})}{w_{allowed}} \tag{E.5}$$

**Eigenfrequency**

The eigenfrequency for the unloaded bridge deck

$$f_{unloaded} = \frac{K_n}{2\pi} \cdot \sqrt{\frac{\eta_v \cdot EI_{yy} \cdot g \cdot \gamma_m^{-1}}{q_G \cdot w \cdot L_0^4}} \tag{E.6}$$

The eigenfrequency for the loaded bridge

$$f_{loaded} = \frac{K_m}{2\pi} \cdot \sqrt{\frac{\eta_v \cdot EI_{yy} \cdot g}{Q_{1k} \cdot L_0^3 + K_n \cdot q_G \cdot L_0^4}} \tag{E.7}$$

With $K_n$ denoting a constant based on the boundary conditions and $g$ the gravity constant. The check is performed with the minimum frequency of both cases

$$uc_{frequency} = \frac{min(f_{unloaded}, f_{loaded})}{f_{allowed}} \tag{E.8}$$

## E.2. Ultimate Limit State
### E.2.1. Skins
**Bending stresses**
Equivalent properties are calculated for the effective width which is taken into account based on the length of the loading vehicle

$$EI_{yy.eff} = \frac{EI_{yy}}{w_{tot}} \cdot w_q$$

$$EA_{x.eff} = \frac{EA_x}{w_{tot}} \cdot w_q$$

(E.9)

The width of one lane is denoted by $w_q$ and the total with of the slab by $w_{tot}$. $EA$ is the axial stiffness. The moments occurring in the skins are calculated by

$$M_G = \frac{1}{8} \cdot q_G \cdot w_q \cdot L_0^2$$

$$M_{Q1} = \frac{1}{2} \cdot Q_{1k} \cdot L_0$$

$$M_{q1} = \frac{1}{8} \cdot q_{1k} \cdot w_q \cdot L_0^2$$

$$M_{Q2} = \frac{1}{4} \cdot Q_{2k} \cdot L_0$$

(E.10)

The maximum moment is

$$M_{skin} = \gamma_{m.s} \cdot \left[ \frac{\gamma_G \cdot M_G}{\eta_{s.1}} + \frac{\gamma_{Q1}}{\eta_{s.k} \cdot max(M_{Q1} + M_{q1}, M_{Q2})} \right]$$

(E.11)

Based on this maximum moment, the stresses in the top and bottomskin are

$$\sigma_{ts} = \frac{E_{x.ts}}{\eta_{ts.xc}} \cdot \frac{w_{tot}}{w_q} \cdot \frac{M_{skin} \cdot z_{ts}}{EI_{yy}}$$

$$\sigma_{bs} = \frac{E_{x.bs}}{\eta_{bs.xt}} \cdot \frac{w_{tot}}{w_q} \cdot \frac{M_{skin} \cdot z_{bs}}{EI_{yy}}$$

(E.12)

The checks are given by the formulas below. $E$ is the bending modulus and $z$ denotes the distance between the neutral axis and the outer fibers for the topskin or bottomskin. The compressive and tensile strength of the laminates is denoted by $\sigma_x c$ and $\sigma_x t$ respectively.

$$uc_{ts} = \frac{\sigma_{ts}}{\sigma_{xc.ts}}$$

$$uc_{bs} = \frac{\sigma_{bs}}{\sigma_{xt.bs}}$$

(E.13)

### E.2.2. Webs
**Shear**
The number of webs, $n$, that are activated depends on the width of the wheel which is denoted by $w_{wheel}$.

$$n_{w.LC1} = \frac{w_{wheel.LC1}}{webspacing}$$

$$n_{w.LC2} = \frac{w_{wheel.LC2}}{webspacing}$$

(E.14)

The shear forces occurring in the webs

$$V_G = \frac{1}{2} \cdot q_G \cdot webspacing \cdot L_0$$

$$V_{Q1} = \frac{Q_{1k}}{2 \cdot n_{w.LC1}}$$

$$V_{q1} = \frac{1}{2} \cdot q_{1k} \cdot webspacing \cdot L_0 \qquad \text{(E.15)}$$

$$V_{Q2} = \frac{Q_{2k}}{2 \cdot n_{w.LC2}}$$

The maximum shear force is given by

$$V_{LC1} = \frac{\gamma_{m.s}}{\eta_{web.xy}} \cdot \left[ \frac{\gamma_G \cdot V_G}{\eta_{s.web}} + \frac{\gamma_{Q1} \cdot (V_{Q1} + V_{q1})}{\eta_{s.k}} \right]$$

$$V_{LC2} = \frac{\gamma_{m.s}}{\eta_{web.xy}} \cdot \left[ \frac{\gamma_G \cdot V_G}{\eta_{s.web}} + \frac{\gamma_{Q1} \cdot V_{Q2}}{\eta_{s.k}} \right] \qquad \text{(E.16)}$$

$$V_{max} = max(V_{LC1}, V_{LC2})$$

The area of the webs is calculated based on the thickness of the different elements $t$ and the height of the deck $H$.

$$A_{web} = t_{web} \cdot \left( H_{deck} - \frac{t_{ts} + t_{bs}}{2} \right) \qquad \text{(E.17)}$$

The height of the webs is

$$h_{web} = H_{deck} - (t_{ts} + t_{bs}) \qquad \text{(E.18)}$$

Moment of inertia

$$I_c = \frac{webspacing \cdot H_{deck}^3}{12} - \frac{(webspacing - t_{web}) \cdot h_{web}^3}{12} \qquad \text{(E.19)}$$

First moment of area

$$Q = t_{ts} \cdot webspacing \cdot \left( y_2 - \frac{t_{ts}}{2} \right) + [t_{web} \cdot (y_2 - t_{ts})] \cdot \left[ \frac{y_2 - t_{ts}}{2} \right] \qquad \text{(E.20)}$$

In which the distance between the neutral axis and top of the deck is denoted by $y_2$ and the distance between the neutral axis and the bottom of the deck with $y_1$. The occurring shear stress in the webs is

$$\tau_{max.w} = \frac{Q \cdot V_{max}}{I_c \cdot t_{web}} \qquad \text{(E.21)}$$

The check for the shear stress in the webs is given by the formula below in which the shear strength is denoted as $t\tau_{xy}$

$$uc_{web.\tau} = \frac{\tau_{max.w}}{\tau_{xy.web}} \qquad \text{(E.22)}$$

**Compression**
Maximum compression in the webs

$$\sigma_{web.max} = max\left( \frac{V_{LC1}}{w_{wheel.LC1} \cdot t_{web}}, \frac{V_{LC2}}{w_{wheel.LC2} \cdot t_{web}} \right) \qquad \text{(E.23)}$$

The compressive strength of the laminates is denoted by $\sigma_y c$. The check for compression in the webs is given by

$$uc_{web.sigma} = \frac{\sigma_{web.max}}{\sigma_{yc.web}} \qquad \text{(E.24)}$$

**Stability - Compression**

Effective height for the webs

$$h_{web.eff} = h_{web} + \left( \frac{t_{ts}}{2} + \frac{t_{bs}}{2} \right) \tag{E.25}$$

The buckling length of the webs is assumed to be

$$L_e = \frac{h_{web}}{2} \tag{E.26}$$

The Euler buckling load is

$$N_{cr} = \frac{\pi^2 \cdot D_{11}}{L_e^2} \tag{E.27}$$

In which $L_e$ denotes the buckling length. The Euler critical stress based on this buckling load is

$$\sigma_{cr} = \frac{N_{cr}}{t_{web}} \tag{E.28}$$

The effective width which has to be taken into account is

$$w_{eff} = w_{vehicle} + 2 \cdot \frac{h_{web}}{2} \tag{E.29}$$

The forces occurring are

$$
\begin{aligned}
V_{Q1.stab} &= \frac{Q_{1k}}{2 \cdot n_{w.LC1}} \\
V_{q1.stab} &= q_{1k} \cdot webspacing \cdot t_{web} \\
V_{Q2.stab} &= \frac{Q_{2k}}{2 \cdot n_{w.LC2}} \\
V_{stab} &= \gamma_{Q1} \cdot max(V_{Q1.stab}, V_{q1.stab}, V_{Q2.stab})
\end{aligned}
\tag{E.30}
$$

The stress due to the force is therefore

$$\sigma_{c.stab} = \frac{V_{stab}}{w_{eff} \cdot t_{web}} \tag{E.31}$$

And the unity check for stability due to compression is described by

$$uc_{web.stab.compression} = \frac{\frac{\gamma_{m.web}}{\eta_{c.web}} \cdot \sigma_{c.stab}}{\sigma_{cr}} \tag{E.32}$$

**Stability - shear**

Based on the following factor the allowable shear strength can be calculated

$$K = \frac{2 \cdot D_{66} + D_{12}}{\sqrt{D_{11} \cdot D_{22}}} \tag{E.33}$$

$D$ denotes a part of the stiffness matrix for the laminates and with the different subscripts the location in the matrix is denoted. Based on the factor $K$, the allowable shear strength taking stability into account is

$$
\begin{aligned}
&if\, K < 1.0 \\
&\tau_{xy.stab} = \frac{4}{t_{web} \cdot h_{web.eff}} \cdot \sqrt[4]{D_{11} \cdot D_{22}^3} \cdot (8.125 + 5.045 \cdot K) \\
&if\, K > 1.0 : \\
&\tau_{xy.stab} = \frac{4}{t_{web} \cdot h_{web.eff}} \cdot \sqrt{D_{22} \cdot (D_{12} + 2 \cdot D_{66})} \cdot \left( 18.59 + \frac{3.56}{K^2} \right)
\end{aligned}
\tag{E.34}
$$

The check for the stability of the webs due to shear is given by

$$uc_{web.stab.shear} = \frac{\tau_{max.web}}{\tau_{xy.stab}}$$

(E.35)

**Stability - combination compression and shear**
The webs has to be checked on stability for a combination of compression and shear. This check is given by

$$uc_{web.stab} = \frac{\sigma_{c.stab}}{\sigma_{cr}} + \left(\frac{\tau_{max.web}}{\tau_{xy.stab}}\right)^{1.9+0.1K}$$

(E.36)

# F

# Results standardization

In this appendix, the results of the runs for standardization are given. Each table contains the top 10 results for a different distance $L_0$ between the supports.

Table F.1: Top 10 results optimization $L_0 = 500\ mm$

| Design parameter | Situation | | | | | | | | | |
|---|---|---|---|---|---|---|---|---|---|---|
| | 1 | 2 | 3 | 4 | 5 | 6 | 7 | 8 | 9 | 10 |
| Number of wraps foam | 1 | 1 | 1 | 1 | 1 | 1 | 1 | 1 | 1 | 1 |
| Number of z-layers 0/90 | 2 | 2 | 2 | 2 | 2 | 2 | 2 | 2 | 2 | 2 |
| Number of z-layers 45/-45 | 1 | 1 | 1 | 1 | 1 | 1 | 1 | 1 | 1 | 1 |
| Number of UD plies topskin | 1 | 1 | 1 | 1 | 2 | 1 | 1 | 1 | 1 | 1 |
| Number of UD plies bottomskin | 1 | 1 | 1 | 1 | 1 | 1 | 1 | 1 | 1 | 1 |
| Number of UD plies webs | 2 | 2 | 2 | 2 | 2 | 2 | 2 | 2 | 2 | 2 |
| Number of 45/-45 plies webs | 1 | 1 | 1 | 1 | 1 | 1 | 1 | 1 | 1 | 1 |
| Overlapping length UD plies topskin | 4 | 3 | 5 | 3 | 3 | 4 | 4 | 4 | 4 | 4 |
| Overlapping length UD plies bottomskin | 7 | 7 | 7 | 7 | 7 | 7 | 7 | 7 | 7 | 7 |
| Overlapping length 0/90 plies topskin | 4 | 5 | 4 | 4 | 3 | 4 | 4 | 4 | 4 | 4 |
| Overlapping length 0/90 plies bottomskin | 3 | 3 | 3 | 3 | 3 | 3 | 3 | 3 | 3 | 3 |
| Overlapping length 45/-45 plies topskin | 5 | 4 | 4 | 6 | 5 | 5 | 5 | 5 | 5 | 6 |
| Overlapping length 45/-45 plies bottomskin | 4 | 4 | 4 | 4 | 4 | 4 | 4 | 4 | 4 | 4 |
| Height deck [mm] | 100 | 100 | 100 | 100 | 100 | 100 | 101 | 101 | 101 | 100 |
| Web spacing [mm] | 175 | 175 | 175 | 175 | 174 | 175 | 175 | 175 | 175 | 175 |
| Relative costs [-] | 0.720 | 0.720 | 0.720 | 0.720 | 0.720 | 0.720 | 0.721 | 0.721 | 0.722 | 0.728 |

Table F.2: Top 10 results optimization $L_0 = 750\ mm$

| Design parameter | Situation | | | | | | | | | |
|---|---|---|---|---|---|---|---|---|---|---|
| | **1** | **2** | **3** | **4** | **5** | **6** | **7** | **8** | **9** | **10** |
| **Number of wraps foam** | 1 | 1 | 1 | 1 | 1 | 1 | 1 | 1 | 1 | 1 |
| **Number of z-layers 0/90** | 2 | 2 | 2 | 2 | 2 | 2 | 2 | 2 | 2 | 2 |
| **Number of z-layers 45/-45** | 1 | 1 | 1 | 1 | 1 | 1 | 1 | 1 | 1 | 1 |
| **Number of UD plies topskin** | 1 | 1 | 1 | 1 | 1 | 1 | 1 | 1 | 2 | 1 |
| **Number of UD plies bottomskin** | 2 | 2 | 2 | 1 | 2 | 2 | 2 | 2 | 2 | 2 |
| **Number of UD plies webs** | 2 | 2 | 2 | 2 | 2 | 2 | 2 | 2 | 2 | 2 |
| **Number of 45/-45 plies webs** | 1 | 1 | 1 | 1 | 1 | 1 | 1 | 1 | 1 | 1 |
| **Overlapping length UD plies topskin** | 5 | 5 | 5 | 6 | 5 | 4 | 5 | 6 | 3 | 5 |
| **Overlapping length UD plies bottomskin** | 4 | 4 | 4 | 7 | 4 | 4 | 3 | 4 | 4 | 4 |
| **Overlapping length 0/90 plies topskin** | 4 | 3 | 4 | 4 | 4 | 4 | 4 | 4 | 4 | 4 |
| **Overlapping length 0/90 plies bottomskin** | 3 | 3 | 3 | 3 | 3 | 3 | 4 | 3 | 3 | 3 |
| **Overlapping length 45/-45 plies topskin** | 4 | 6 | 5 | 5 | 4 | 6 | 5 | 4 | 4 | 4 |
| **Overlapping length 45/-45 plies bottomskin** | 4 | 4 | 4 | 4 | 5 | 4 | 4 | 4 | 4 | 5 |
| **Height deck [mm]** | 100 | 100 | 100 | 100 | 100 | 100 | 100 | 100 | 100 | 103 |
| **Web spacing [mm]** | 174 | 174 | 174 | 174 | 174 | 174 | 174 | 174 | 174 | 174 |
| **Relative costs [-]** | 0.718 | 0.718 | 0.726 | 0.726 | 0.726 | 0.726 | 0.726 | 0.726 | 0.726 | 0.730 |

Table F.3: Top 10 results optimization $L_0 = 1000\ mm$

| Design parameter | Situation | | | | | | | | | |
|---|---|---|---|---|---|---|---|---|---|---|
| | **1** | **2** | **3** | **4** | **5** | **6** | **7** | **8** | **9** | **10** |
| **Number of wraps foam** | 1 | 1 | 1 | 1 | 1 | 1 | 1 | 1 | 1 | 1 |
| **Number of z-layers 0/90** | 2 | 2 | 2 | 2 | 2 | 2 | 2 | 2 | 2 | 2 |
| **Number of z-layers 45/-45** | 1 | 1 | 1 | 1 | 1 | 1 | 1 | 1 | 1 | 1 |
| **Number of UD plies topskin** | 2 | 2 | 2 | 2 | 2 | 2 | 2 | 2 | 2 | 2 |
| **Number of UD plies bottomskin** | 1 | 1 | 1 | 1 | 1 | 1 | 1 | 1 | 1 | 1 |
| **Number of UD plies webs** | 2 | 2 | 2 | 2 | 2 | 2 | 2 | 2 | 2 | 2 |
| **Number of 45/-45 plies webs** | 1 | 1 | 1 | 1 | 1 | 1 | 1 | 1 | 1 | 1 |
| **Overlapping length UD plies topskin** | 5 | 5 | 5 | 5 | 5 | 5 | 5 | 5 | 5 | 5 |
| **Overlapping length UD plies bottomskin** | 4 | 5 | 4 | 4 | 7 | 5 | 5 | 4 | 5 | 6 |
| **Overlapping length 0/90 plies topskin** | 3 | 3 | 3 | 3 | 3 | 3 | 3 | 3 | 3 | 3 |
| **Overlapping length 0/90 plies bottomskin** | 3 | 3 | 4 | 3 | 3 | 5 | 3 | 3 | 3 | 3 |
| **Overlapping length 45/-45 plies topskin** | 7 | 7 | 6 | 7 | 7 | 6 | 7 | 7 | 7 | 7 |
| **Overlapping length 45/-45 plies bottomskin** | 7 | 6 | 6 | 7 | 5 | 4 | 7 | 8 | 7 | 6 |
| **Height deck [mm]** | 106 | 106 | 106 | 107 | 102 | 106 | 106 | 106 | 106 | 106 |
| **Web spacing [mm]** | 169 | 169 | 169 | 169 | 169 | 169 | 169 | 169 | 169 | 173 |
| **Relative costs [-]** | 0.767 | 0.767 | 0.768 | 0.768 | 0.770 | 0.774 | 0.774 | 0.774 | 0.774 | 0.775 |

Table F.4: Top 10 results optimization $L_0 = 1250\ mm$

| Design parameter | Situation | | | | | | | | | |
|---|---|---|---|---|---|---|---|---|---|---|
| | 1 | 2 | 3 | 4 | 5 | 6 | 7 | 8 | 9 | 10 |
| Number of wraps foam | 1 | 1 | 1 | 1 | 1 | 1 | 1 | 1 | 1 | 1 |
| Number of z-layers 0/90 | 2 | 2 | 2 | 2 | 2 | 2 | 2 | 2 | 2 | 2 |
| Number of z-layers 45/-45 | 1 | 1 | 1 | 1 | 1 | 1 | 1 | 1 | 1 | 1 |
| Number of UD plies topskin | 2 | 2 | 2 | 2 | 2 | 2 | 2 | 2 | 2 | 2 |
| Number of UD plies bottomskin | 1 | 1 | 1 | 1 | 1 | 1 | 1 | 1 | 1 | 1 |
| Number of UD plies webs | 2 | 2 | 2 | 2 | 2 | 2 | 2 | 2 | 2 | 2 |
| Number of 45/-45 plies webs | 1 | 1 | 1 | 1 | 1 | 1 | 1 | 1 | 1 | 1 |
| Overlapping length UD plies topskin | 6 | 6 | 6 | 6 | 6 | 6 | 7 | 6 | 7 | 7 |
| Overlapping length UD plies bottomskin | 5 | 5 | 5 | 5 | 5 | 5 | 5 | 6 | 5 | 4 |
| Overlapping length 0/90 plies topskin | 4 | 4 | 4 | 4 | 4 | 5 | 4 | 5 | 4 | 4 |
| Overlapping length 0/90 plies bottomskin | 4 | 3 | 4 | 5 | 4 | 4 | 4 | 4 | 4 | 4 |
| Overlapping length 45/-45 plies topskin | 8 | 8 | 8 | 8 | 8 | 8 | 9 | 8 | 9 | 9 |
| Overlapping length 45/-45 plies bottomskin | 4 | 6 | 5 | 5 | 4 | 4 | 4 | 4 | 4 | 5 |
| Height deck [mm] | 102 | 102 | 102 | 102 | 109 | 102 | 102 | 102 | 102 | 102 |
| Web spacing [mm] | 167 | 167 | 167 | 175 | 167 | 167 | 167 | 167 | 167 | 167 |
| Relative costs [-] | 0.789 | 0.789 | 0.796 | 0.798 | 0.798 | 0.804 | 0.811 | 0.811 | 0.811 | 0.811 |

Table F.5: Top 10 results optimization $L_0 = 1500\ mm$

| Design parameter | Situation | | | | | | | | | |
|---|---|---|---|---|---|---|---|---|---|---|
| | **1** | **2** | **3** | **4** | **5** | **6** | **7** | **8** | **9** | **10** |
| **Number of wraps foam** | 1 | 1 | 1 | 1 | 1 | 1 | 1 | 1 | 1 | 1 |
| **Number of z-layers 0/90** | 2 | 2 | 2 | 2 | 2 | 2 | 2 | 2 | 2 | 2 |
| **Number of z-layers 45/-45** | 1 | 1 | 1 | 1 | 1 | 1 | 1 | 1 | 1 | 1 |
| **Number of UD plies topskin** | 2 | 2 | 2 | 2 | 2 | 2 | 2 | 2 | 2 | 2 |
| **Number of UD plies bottomskin** | 2 | 2 | 2 | 2 | 2 | 2 | 2 | 2 | 2 | 2 |
| **Number of UD plies webs** | 2 | 2 | 2 | 2 | 2 | 2 | 2 | 2 | 2 | 2 |
| **Number of 45/-45 plies webs** | 1 | 1 | 1 | 1 | 1 | 1 | 1 | 1 | 1 | 1 |
| **Overlapping length UD plies topskin** | 6 | 6 | 6 | 6 | 6 | 6 | 6 | 6 | 6 | 6 |
| **Overlapping length UD plies bottomskin** | 4 | 4 | 4 | 4 | 4 | 4 | 4 | 4 | 4 | 4 |
| **Overlapping length 0/90 plies topskin** | 5 | 5 | 5 | 5 | 5 | 6 | 5 | 5 | 7 | 6 |
| **Overlapping length 0/90 plies bottomskin** | 3 | 3 | 3 | 3 | 3 | 3 | 3 | 3 | 3 | 3 |
| **Overlapping length 45/-45 plies topskin** | 8 | 8 | 8 | 8 | 8 | 8 | 8 | 8 | 8 | 8 |
| **Overlapping length 45/-45 plies bottomskin** | 4 | 4 | 5 | 5 | 4 | 4 | 6 | 4 | 4 | 4 |
| **Height deck [mm]** | 107 | 107 | 107 | 109 | 107 | 106 | 108 | 107 | 105 | 106 |
| **Web spacing [mm]** | 174 | 174 | 174 | 174 | 167 | 174 | 174 | 163 | 174 | 168 |
| **Relative costs [-]** | 0.793 | 0.793 | 0.800 | 0.803 | 0.807 | 0.807 | 0.810 | 0.820 | 0.821 | 0.821 |

# G

# Python code optimization procedure

```python
# -*- coding: utf-8 -*-
"""
Created on Mon May 30 16:04:09 2022

@author: Lennart Molenaar
"""

###############################################################################
# Import
###############################################################################
import time
import numpy as np
from numpy import linalg as lin
from matplotlib import pyplot as plt
from mpl_toolkits.mplot3d import Axes3D
import itertools
from geneticalgorithm import geneticalgorithm as ga
import pandas as pd

# Import functions FiberCore Europe
from CLT_tool_R15 import Q_calc
from CLT_tool_R15 import ABD_calc
from Failure_Progression_Tool_R15 import Axial_transverse_failure_progression
from Failure_Progression_Tool_R15 import Axial_shear_failure_progression

# Import own functions
from FunctionsOptimization import Materialproperties
from FunctionsOptimization import BuildLayup
from FunctionsOptimization import Layup
from FunctionsOptimization import TestMinPlyDirections
from FunctionsOptimization import TestThicknessPlies
from FunctionsOptimization import Stiffness
from FunctionsOptimization import Engineering_Constants


###############################################################################
# Functions
###############################################################################
def Costs (Width, Height, Length, web_spacing, n_topskin, n_bottomskin, n_web, t_Web, t_topskin, t_bottomskin, rho_foam,
rho_glass, rho_resin, p_foam, p_glass, p_resin, s_glasshouse, s_mould, web_spacing_ref, q_hour):
    n_webs = np.floor(Width / web_spacing)        # Number of webs [int]
    n_webs_ref = np.floor(Width / web_spacing_ref) # Number of reference foamblocks [int]

    t_web = n_web * t_Web            # Thickness webs [mm]
    t_ts = n_topskin * t_topskin      # Thickness top skin [mm]
    t_bs = n_bottomskin * t_bottomskin # Thickness bottom skin [mm]

    V_foam = (Width - n_webs * t_web) * (Height - t_ts - t_bs) * Length                      # Volume foam [mm3]
    M_glass = ((Width * n_topskin / 2 + Width * n_bottomskin / 2 + (Height - t_ts - t_bs) * n_webs * n_web / 4) * Length) * 1200 /
(10**6)   # Mass glass [g]
    V_resin = Width * Height * Length - V_foam - (M_glass / rho_glass) * (10**6)             # Volume resin [mm3]

    Q_foam = V_foam / (10**9) * rho_foam * p_foam      # Price for the foam [€]
    Q_glass = M_glass / (10**3) * p_glass              # Price for the glass [€]
    Q_resin = V_resin / (10**9) * rho_resin * p_resin  # Price for the resin [€]

    Weight = V_foam / (10**9) * rho_foam + M_glass / (10**3) + V_resin / (10**9) * rho_resin

    Q_material = Q_foam + Q_glass + Q_resin       # Total price material [€]

    # Labour costs
    n_foamblocks = n_webs - 1        # Number of foamblocks [int]
    n_foamblocks_ref = n_webs_ref - 1 # Number of reference foamblocks [int]

    A_bridge = (Width * Length) / (10**6) # Area bridge [m2]

    beta_1 = n_webs / n_webs_ref              # Scaling factor reference case [-]
    beta_2 = n_foamblocks / n_foamblocks_ref    # Scaling factor reference case [-]
```

```python
        Q_glasshouse = beta_1 * A_bridge * s_glasshouse * q_hour  # Price for labour glasshouse [€]
        Q_mould = beta_2 * A_bridge * s_mould * q_hour           # Price for labour mould [€]

        Q_labour = Q_glasshouse + Q_mould  # Total labour price [€]

        # Total costs
        Q = Q_material + Q_labour  # Total price [€]
        return Weight, Q


def GA_process (V):  #
# (nwrap,nz_090,nz_45,nUDts,nUDbs,nUDw,n45w,OLts_UD,OLbs_UD,OLts_090,OLbs_090,OLts_45,OLbs_45,Height,web_spacing)
    n.append(1)  # Counting number of variants considered
    # Store data
    Data_row = []
    Data_row.append(V[0])
    Data_row.append(V[1])
    Data_row.append(V[2])
    Data_row.append(V[3])
    Data_row.append(V[4])
    Data_row.append(V[5])
    Data_row.append(V[6])
    Data_row.append(V[7])
    Data_row.append(V[8])
    Data_row.append(V[9])
    Data_row.append(V[10])
    Data_row.append(V[11])
    Data_row.append(V[12])
    Data_row.append(V[13])
    Data_row.append(V[14])
    # Check for requirements layups
    Angles = BuildLayup(V[0], V[1], V[2], V[3], V[4], V[5], V[6], V[7], V[8], V[9], V[10], V[11], V[12])
    Topskin_angle = Angles[0]
    Bottomskin_angle = Angles[1]
    Webs_angle = Angles[2]

    if TestMinPlyDirections (Topskin_angle) == 'satisfy':
        if TestMinPlyDirections (Bottomskin_angle) == 'satisfy':
            if TestMinPlyDirections (Webs_angle) == 'satisfy':
                if TestThicknessPlies (Topskin_angle, t_topskin, min_thickness_topskin, max_thickness_topskin) == 'satisfy':
                    if TestThicknessPlies (Bottomskin_angle, t_bottomskin, min_thickness_bottomskin, max_thickness_bottomskin) ==
'satisfy':
                        if TestThicknessPlies (Webs_angle, t_Web, min_thickness_webs, max_thickness_webs) == 'satisfy':
                            # Thickness web laminate [mm]
                            n_web = len(Webs_angle)
                            t_web = n_web * t_Web        # Thickness webs [mm]
                            Data_row.append(t_web)

                            # Layup webs
                            materialproperties_web = Materialproperties('Kush_UD1200_vf27',27)

                            web_layup = Layup(Webs_angle,materialproperties_web,n_web)

                            # Matrix
                            ABD_web = ABD_calc(web_layup)

                            D11 = ABD_web[2,2]  # Component D-matrix
                            D12 = ABD_web[3,2]  # Component D-matrix
                            D22 = ABD_web[3,3]  # Component D-matrix
                            D66 = ABD_web[5,5]  # Component D-matrix

                            # Allowable stresses
                            for k in range(len(dataframeWebs)):
                                if dataframeWebs.loc[k][0] == V[0] and dataframeWebs.loc[k][1] == V[1] and dataframeWebs.loc[k][2] ==
V[2] \
                                    and dataframeWebs.loc[k][3] == V[5] and dataframeWebs.loc[k][4] == V[6]:
                                    sigma_yc_web = dataframeWebs.loc[k][5]
                                    tau_xy_web = dataframeWebs.loc[k][6]

                            EC_web = Engineering_Constants(ABD_web, t_web)
```

```python
                # Thickness skin laminates [mm]
                n_topskin = len(Topskin_angle)
                t_ts = n_topskin * t_topskin    # Thickness top skin [mm]
                Data_row.append(t_ts)

                # Layup skins
                materialproperties_topskin = Materialproperties('Kush_UD1200_vf54',54)

                topskin_layup = Layup(Topskin_angle,materialproperties_topskin,n_topskin)

                # Matrix
                ABD_topskin = ABD_calc(topskin_layup)

                # Allowable stresses
                for k in range(len(dataframeTopskin)):
                    if dataframeTopskin.loc[k][0] == V[0] and dataframeTopskin.loc[k][1] == V[1] and dataframeTopskin.loc[k][2]
== V[2] \
                        and dataframeTopskin.loc[k][3] == V[3] and dataframeTopskin.loc[k][4] == V[7] and dataframeTopskin.loc[k]
[5] == V[9] and dataframeTopskin.loc[k][6] == V[11]:
                            sigma_xc_ts = dataframeTopskin.loc[k][7]

                EC_ts = Engineering_Constants(ABD_topskin, t_ts)

                Ex_ts = EC_ts[0] # E modulus topskin

                # Thickness skin laminates [mm]
                n_bottomskin = len(Bottomskin_angle)
                t_bs = n_bottomskin * t_bottomskin # Thickness bottom skin [mm]
                Data_row.append(t_bs)

                # Layup skins
                materialproperties_bottomskin = Materialproperties('Kush_UD1200_vf54',54)

                bottomskin_layup = Layup(Bottomskin_angle,materialproperties_bottomskin,n_bottomskin)

                # Matrix
                ABD_bottomskin = ABD_calc(bottomskin_layup)

                # Allowable stresses
                for k in range(len(dataframeBottomskin)):
                    if dataframeBottomskin.loc[k][0] == V[0] and dataframeBottomskin.loc[k][1] == V[1] and
dataframeBottomskin.loc[k][2] == V[2] \
                        and dataframeBottomskin.loc[k][3] == V[4] and dataframeBottomskin.loc[k][4] == V[8] and
dataframeBottomskin.loc[k][5] == V[10] and dataframeBottomskin.loc[k][6] == V[12]:
                            sigma_xt_bs = dataframeBottomskin.loc[k][7]

                EC_bs = Engineering_Constants(ABD_bottomskin, t_bs)

                Ex_bs = EC_bs[0] # E modulus bottomskin

                # Check for strength
                n_webs = np.floor((Width)/V[14])

                EA_x = Stiffness (Width, V[13], EC_ts[0], EC_bs[0], EC_web[0], EC_ts[2], EC_bs[2], EC_web[2], t_ts, t_bs,
t_web, n_webs)[0]
                EI_yy = Stiffness (Width, V[13], EC_ts[0], EC_bs[0], EC_web[0], EC_ts[2], EC_bs[2], EC_web[2], t_ts, t_bs,
t_web, n_webs)[1]
                GA_xz = Stiffness (Width, V[13], EC_ts[0], EC_bs[0], EC_web[0], EC_ts[2], EC_bs[2], EC_web[2], t_ts, t_bs,
t_web, n_webs)[2]

                # Weight deck + material use
                Weight = Costs(Width, V[13], Length, V[14], n_topskin, n_bottomskin, n_web, t_Web, t_topskin, t_bottomskin,
rho_foam, rho_glass, rho_resin, p_foam, p_glass, p_resin, s_glasshouse, s_mould, web_spacing_ref, q_hour)[0]

                Data_row.append(Weight)

                q_G = Weight * 9.81 / (Length * Width) # Own weight of the deck
```

```python
'''SLS - Deflections'''
# Load case 1
w_LC1_Q = Q_1k * ((2 * L_0**3) / (48 * EI_yy) + eta_load * (L_0 / (4 * GA_xz)))
w_LC1_q = (q_1k * w_lane + q_rk * w_r) * ((5 * L_0**4) / (384 * EI_yy) + eta_load * (L_0**2 / (8 * GA_xz)))
w_LC1 = (gamma_f_SLS * gamma_m_SLS) / eta_c_SLS_deflection_short * (w_LC1_Q + w_LC1_q)

# Load case 2
w_LC2 = (gamma_f_SLS * gamma_m_SLS) / eta_c_SLS_deflection_short * ((Q_2k * L_0**3) / (48 * EI_yy) +
eta_load * ((Q_2k * L_0) / (4 * GA_xz)))

# Check deflections
w_max = np.max([w_LC1, w_LC2])
uc_w = w_max / w_all

'''SLS - Frequency'''
f_0_unloaded = (K_n_unloaded / (2 * np.pi)) * np.sqrt((EI_yy * 9.81) / (q_G * L_0**4))
f_0_loaded = (K_m_loaded / (2 * np.pi)) * np.sqrt((EI_yy * 9.81) / (Q_1k * L_0**3 + K_n_loaded * q_G * L_0**4))

# Check frequency
f_min = np.min([f_0_unloaded, f_0_loaded])
uc_f = f_min / f_all
uc_max_SLS = np.max([uc_w, uc_f])
Data_row.append(uc_max_SLS)

'''ULS - Skins'''
'''Moments'''
# Equivalent width due to load spreading
EI_yy_eff = EI_yy / Width * W_eff
EA_x_eff = EA_x / Width * W_eff

# Own weight of the deck
M_G = 1 / 8 * q_G * W_eff * L_0**2
# Load model 1
M_Q1 = 1 / 2 * Q_1k * L_0
M_q1 = 1 / 8 * q_1k * W_eff * L_0**2
# Load model 2
M_Q2 = 1 / 4 * Q_2k * L_0

# Maximum moment
m_max = np.max([M_Q1 + M_q1, M_Q2])
M_max = gamma_m * ((gamma_G_ULS * M_G) / eta_c_ULS_strength_long + (gamma_Q1_ULS /
eta_c_ULS_strength_short) * m_max)

'''Stresses in skins'''
# Neutral axis
y1 = Stiffness (Width, V[13], EC_ts[0], EC_bs[0], EC_web[0], EC_ts[2], EC_bs[2], EC_web[2], t_ts, t_bs, t_web,
n_webs)[3]
y2 = Stiffness (Width, V[13], EC_ts[0], EC_bs[0], EC_web[0], EC_ts[2], EC_bs[2], EC_web[2], t_ts, t_bs, t_web,
n_webs)[4]

sigma_ts = Ex_ts / eta_ts_xc * Width / W_eff * (M_max * y2) / EI_yy
sigma_bs = Ex_bs / eta_bs_xt * Width / W_eff * (M_max * y1) / EI_yy

'''ULS - Webs'''
'''Shear force'''
# Number of contributing webs
n_LC1 = int(l_wheel_LC1 / V[14])
n_LC2 = int(l_wheel_LC2 / V[14])
if n_LC2 < 1:
    n_LC2 = 1
else: n_LC2 = n_LC2

# Own weight
V_G = 1 / 2 * q_G * V[14] * L_0
# Load model 1
V_Q1 = Q_1k / (2 * n_LC1)
V_q1 = 1 / 2 * q_1k * V[14] * L_0
# Load model 2
V_Q2 = Q_2k / (2 * n_LC2)
```

```python
            V_LC1 = gamma_m / eta_webs_xy * ((gamma_G_ULS * V_G) / eta_c_ULS_strength_long + (gamma_Q1_ULS *
(V_Q1 + V_q1)) / eta_c_ULS_strength_short)
            V_LC2 = gamma_m / eta_webs_xy * ((gamma_G_ULS * V_G) / eta_c_ULS_strength_long + (gamma_Q1_ULS *
V_Q2) / eta_c_ULS_strength_short)

            V_max = np.max([V_LC1, V_LC2])

            '''Shear stresses webs'''
            A_web = t_web * (V[13] - (t_bs + t_ts) / 2)
            h_web = V[13] - (t_ts + t_bs)

            # Centroidal moment of inertia
            I_c_webs = (V[14] * (V[13])**3) / 12 - ((V[14] - t_web) * h_web**3) / 12

            # First moment of area
            Q_webs = t_ts * V[14] * (y2 - t_ts / 2) + (t_web * (y2 - t_ts)) * ((y2 - t_ts) / 2)

            # Maximum shear stress
            tau_max_webs = (Q_webs * V_max) / (I_c_webs * t_web)

            '''Compression stesses webs'''
            # Maximum compression stress
            sigma_web = np.max([(V_LC1 / (w_wheel_LC1 * t_web)), (V_LC2 / (w_wheel_LC2 * t_web))])

            '''Stability webs'''
            # Adapted heigth webs
            h_web_eff = h_web + (t_ts / 2 + t_bs / 2)
            # Buckling length
            l_buc = 0.5 * h_web
            # Euler critical load
            N_cr = (np.pi**2 * D11) / (l_buc**2)
            # Euler critical stress
            sigma_cr = N_cr / t_web
            # Effective width
            w_k = l_wheel_LC2 + 2 * h_web / 2

            # Shear forces
            # Load model 1
            V_Q1_stab = Q_1k / (2 * n_LC1)
            V_q1_stab = q_1k * V[14] * t_web
            # Load model 2
            V_Q2_stab = Q_2k / (2 * n_LC2)

            V_max_stab = gamma_Q1_ULS * np.max([V_Q1_stab + V_q1_stab, V_Q2_stab])

            # Stress
            sigma_c_stab = gamma_m_stab / eta_c_ULS_buckling * V_max_stab / (w_k * t_web)

            # Shear
            K = (2 * D66 + D12) / np.sqrt(D11 * D22)
            if K <= 1.5:
                tau_xy_stab = 4 / (t_web * h_web_eff**2) * (D11 * D22**3)**(1/4) * (15.07 + 7.08 * K)
            else:
                tau_xy_stab = 4 / (t_web * h_web_eff**2) * np.sqrt(D22 * (D12 + 2 * D66)) * (18.59 + 3.56 / K**2)

            '''Unity checks'''
            Data_row.append(sigma_ts)
            Data_row.append(sigma_bs)
            Data_row.append(tau_max_webs)
            Data_row.append(sigma_web)
            uc_ts_sigma = sigma_ts / np.abs(sigma_xc_ts)
            uc_bs_sigma = sigma_bs / sigma_xt_bs
            uc_webs_tau = tau_max_webs / tau_xy_web
            uc_webs_sigma = sigma_web / np.abs(sigma_yc_web)
            uc_webs_stability = sigma_c_stab / sigma_cr
            uc_webs_tau_stability = tau_max_webs / tau_xy_stab
            uc_webs_combi_stability = sigma_c_stab / sigma_cr + (tau_max_webs / tau_xy_stab)**(1.9 + 0.1*K)
```

```python
            # Maximum uc
            uc_max_ULS =
np.max([uc_ts_sigma,uc_bs_sigma,uc_webs_tau,uc_webs_sigma,uc_webs_stability,uc_webs_tau_stability,uc_webs_combi_stability])

            uc_max = np.max([uc_max_SLS, uc_max_ULS])
            Data_row.append(uc_max_ULS)

            # Check if option satisfied
            if 0.0 <= uc_max <= 1.0:
                vs.append(1)
                # Calculation costs
                C = Costs(Width, V[13], Length, V[14], n_topskin, n_bottomskin, n_web, t_Web, t_topskin, t_bottomskin,
rho_foam, rho_glass, rho_resin, p_foam, p_glass, p_resin, s_glasshouse, s_mould, web_spacing_ref, q_hour)[1]

                Q = C
                Data_row.append(Q)
            else:
                vns.append(1)
                Q = 2*10**4 * uc_max
                Data_row.append(Q)
        else:
            fd.append(1)
            Q = 2*10**5
            Data_row.append(0)
            Data_row.append(0)
            Data_row.append(0)
            Data_row.append(0)
            Data_row.append(0)
            Data_row.append(0)
            Data_row.append(0)
            Data_row.append(0)
            Data_row.append(0)
            Data_row.append(0)
            Data_row.append(Q)
    else:
        fd.append(1)
        Q = 2*10**5
        Data_row.append(0)
        Data_row.append(0)
        Data_row.append(0)
        Data_row.append(0)
        Data_row.append(0)
        Data_row.append(0)
        Data_row.append(0)
        Data_row.append(0)
        Data_row.append(0)
        Data_row.append(0)
        Data_row.append(Q)
else:
    fd.append(1)
    Q = 2*10**5
    Data_row.append(0)
    Data_row.append(0)
    Data_row.append(0)
    Data_row.append(0)
    Data_row.append(0)
    Data_row.append(0)
    Data_row.append(0)
    Data_row.append(0)
    Data_row.append(0)
    Data_row.append(0)
    Data_row.append(Q)
else:
    fd.append(1)
    Q = 2*10**5
    Data_row.append(0)
    Data_row.append(0)
    Data_row.append(0)
    Data_row.append(0)
```

```python
                Data_row.append(0)
                Data_row.append(0)
                Data_row.append(0)
                Data_row.append(0)
                Data_row.append(0)
                Data_row.append(0)
                Data_row.append(Q)
            else:
                fd.append(1)
                Q = 2*10**5
                Data_row.append(0)
                Data_row.append(0)
                Data_row.append(0)
                Data_row.append(0)
                Data_row.append(0)
                Data_row.append(0)
                Data_row.append(0)
                Data_row.append(0)
                Data_row.append(0)
                Data_row.append(Q)
        else:
            fd.append(1)
            Q = 2*10**5
            Data_row.append(0)
            Data_row.append(0)
            Data_row.append(0)
            Data_row.append(0)
            Data_row.append(0)
            Data_row.append(0)
            Data_row.append(0)
            Data_row.append(0)
            Data_row.append(0)
            Data_row.append(Q)

    Data.append(Data_row)
    return Q

###############################################################################
# Parameters
###############################################################################
# Variables optimization procedure
nwrap_min = 1
nwrap_max = 2
nz_090_min = 1
nz_090_max = 2
nz_45_min = 1
nz_45_max = 2

nUDts_min = 1
nUDts_max = 3
nUDbs_min = 1
nUDbs_max = 3
nUDw_min = 0
nUDw_max = 2
n45w_min = 0
n45w_max = 2

OLts_UD_min = 3
OLts_UD_max = 9
OLbs_UD_min = 3
OLbs_UD_max = 9
OLts_090_min = 3
OLts_090_max = 9
OLbs_090_min = 3
OLbs_090_max = 9
OLts_45_min = 3
OLts_45_max = 9
```

```
OLbs_45_min = 3
OLbs_45_max = 9

Height_min = 100
Height_max = 200
web_spacing_min = 100
web_spacing_max = 400

# Input Genetic Algorithm
max_num_iteration = 1000        # Maximum number of iterations
population_size = 50            # Size of the population
mutation_probability = 0.5      # Probability that a mutation occurs
elit_ratio = 0.1               # Ratio the best option wil be chosen again
crossover_probability = 0.8     # Probability that a cross over will take place in the next generation
parents_portion = 0.5          # Contribution of parents to the next generation
crossover_type = 'two_point'    # Option for crossover type, other options are 'uniform'; 'one_point' or 'two_point'
max_iteration_without_improv = 50   # Maximum number of iterations without improvement of optimum ('none' is also possible)

# Calculation strength values plies
Criterium = 'Tsai-Hill'
#Criterium = 'Hashin'
Ns = 0
Ny = 0
Nx = 0
Degradation_rule = 'no'

# Material
rho_foam = 35       # Density foam [kg/m3]
p_foam_m3 =         # Price foam [€/m3]
p_foam = p_foam_m3 / rho_foam # Price foam [€/kg]
rho_glass = 2620    # Density glass [kg/m3]
p_glass =           # Price glass [€/kg]
rho_resin = 1190    # Density resin [kg/m3]
p_resin =           # Price resin [€/kg]

# Labour
s_glasshouse =      # Factor speed glass house [1/m2]
s_mould =           # Factor speed mould [1/m2]
q_hour =            # Price work per hour [€]

t_topskin = 0.85 / 2     # Thickness of (half) plies in topskin
t_bottomskin = 0.85 / 2  # Thickness of (half) plies in bottomskin
t_Web = 1.7 / 2          # Thickness of (half) plies in web

web_spacing_ref = 211.5  # Reference web spacing scaling labour costs [mm]

# Dimensions deck
Width = 4500     # Width deck [mm]
Length = 4500    # Length deck [mm]
L_0 = 850        # Spacing I-beams [mm]
w_lane = 3000    # Width of a lane [mm]
w_r = Width - w_lane # Remaining widht of the deck [mm]
W_eff = 1000     # Effective width taken into account [mm]

# Requirements
w_all = L_0 / 250 # Maximum allowed deflection [mm]
f_all = 14.6      # Minimum allowed eigenfrequencty [Hz]

min_thickness_topskin = 15
max_thickness_topskin = 30
min_thickness_bottomskin = 15
max_thickness_bottomskin = 30
min_thickness_webs = 5
max_thickness_webs = 15

# Loads
Q_1k = 150*10**3   # Axle load load model 1 [N]
q_1k = 0.009       # Distributed load load model 1 main line [N/mm2]
q_rk = 0.005       # Distributed load load model 1 other lanes [N/mm2]
```

```python
Q_2k = 200*10**3    # Axle load load model 2 [N]
w_wheel_LC1 = 400 # Width wheel load case 1 [mm]
l_wheel_LC1 = 400 # Lenght wheel load case 1 [mm]
w_wheel_LC2 = 600 # Width wheel load case 2 [mm]
l_wheel_LC2 = 350 # Lenght wheel load case 2 [mm]
eta_load = 1.0     # Reduction factor shear deformation

'''Partial material factors'''
gamma_m_SLS = 1.0    # Material factor SLS state
gamma_M1 = 1.15     # Material factor
gamma_M2 = 1.20     # Material factor
gamma_M2_A = 1.00   # Material factor for outstanding load cases
gamma_M2_stab = 1.4 # Material factor for stability cases

gamma_m = gamma_M1 * gamma_M2
gamma_m_stab = gamma_M1 * gamma_M2_stab

'''Partial load factors'''
gamma_f_SLS = 1.0     # Load factor SLS state
gamma_G_ULS = 1.20    # Consequence class 2
gamma_G_ULS_favourable = 0.90 # Consequence class 2
gamma_Q1_ULS = 1.35 # Consequence class 2
gamma_Q2_ULS = 1.50 # Consequence class 2
gamma_A_ULS = 1.00   # Outstanding load case

K_n_unloaded = 9.87 # Constant for eigenfrequentie simply supported beam
K_m_loaded = 6.93    # Constant for eigenfrequentie simply supported beam
K_n_loaded = 0.486   # Constant for eigenfrequentie simply supported beam

'''Conversion factors'''
eta_ts_xc = 0.67     # Reduction factor due to production for top skin
eta_bs_xt = 0.61     # Reduction factor due to production for bottom skin
eta_webs_xy = 1.0    # Reduction factor due to production for webs

eta_ct = 0.9 # Conversion factor temperature
eta_cm = 0.9 # Conversion factor moisture
eta_cv = 0.6 # Conversion factor creep
eta_cf = 0.9 # Conversion factor fatigue

# SLS state
eta_c_SLS_vibrations = eta_ct * eta_cm * eta_cf
eta_c_SLS_deflection_short = eta_ct * eta_cm * eta_cv * eta_cf
eta_c_SLS_deflection_long = eta_ct * eta_cm * eta_cf

# ULS state
eta_c_ULS_strength_short = eta_ct * eta_cm
eta_c_ULS_strength_long = eta_ct * eta_cm * eta_cv
eta_c_ULS_fatigue = eta_ct * eta_cf
eta_c_ULS_buckling = eta_ct * eta_cm * eta_cv

# Imput strength parameters laminates
if Criterium == 'Tsai-Hill':
    DataFileTopskin = 'TopskinLaminateStrength_TsaiHill.csv'
    dataframeTopskin = pd.read_csv(DataFileTopskin, delimiter=',', skiprows=0)
    DataFileBottomskin = 'BottomskinLaminateStrength_TsaiHill.csv'
    dataframeBottomskin = pd.read_csv(DataFileBottomskin, delimiter=',', skiprows=0)
    DataFileWebs = 'WebsLaminateStrength_TsaiHill.csv'
    dataframeWebs = pd.read_csv(DataFileWebs, delimiter=',', skiprows=0)
if Criterium == 'Hashin':
    DataFileTopskin = 'TopskinLaminateStrength_Hashin.csv'
    dataframeTopskin = pd.read_csv(DataFileTopskin, delimiter=',', skiprows=0)
    DataFileBottomskin = 'BottomskinLaminateStrength_Hashin.csv'
    dataframeBottomskin = pd.read_csv(DataFileBottomskin, delimiter=',', skiprows=0)
    DataFileWebs = 'WebsLaminateStrength_Hashin.csv'
    dataframeWebs = pd.read_csv(DataFileWebs, delimiter=',', skiprows=0)

##########################################################################
# Calculations
##########################################################################
```

```python
print('Start optimization process')
Data = []
n = []
fd = []
vns = []
vs = []

algorithm_param = {'max_num_iteration': max_num_iteration,\
            'population_size':population_size,\
            'mutation_probability':mutation_probability,\
            'elit_ratio': elit_ratio,\
            'crossover_probability': crossover_probability,\
            'parents_portion': parents_portion,\
            'crossover_type': crossover_type,\
            'max_iteration_without_improv': max_iteration_without_improv}

varbound=np.array([[nwrap_min,nwrap_max],[nz_090_min,nz_090_max],[nz_45_min,nz_45_max],
            [nUDts_min,nUDts_max],[nUDbs_min,nUDbs_max],[nUDw_min,nUDw_max],[n45w_min,n45w_max],
            [OLts_UD_min,OLts_UD_max],[OLbs_UD_min,OLbs_UD_max],
            [OLts_090_min,OLts_090_max],[OLbs_090_min,OLbs_090_max],
            [OLts_45_min,OLts_45_max],[OLbs_45_min,OLbs_45_max],
            [Height_min,Height_max],[web_spacing_min,web_spacing_max]])
vartype=np.array([['int'],['int'],['int'],
            ['int'],['int'],['int'],['int'],
            ['int'],['int'],
            ['int'],['int'],
            ['int'],['int'],
            ['real'],['real']])

BeginTime = time.time()
OptimizationModel=ga(function=GA_process,\
            dimension=15,\
            variable_type_mixed=vartype,\
            variable_boundaries=varbound,\
            algorithm_parameters=algorithm_param)

OptimizationModel.run()

EndTime = time.time()
print('End optimization process')
print('Caluclation time is ' + str(round((EndTime - BeginTime)/60, 2)) + ' min')
print('')
################################################################################
# Results
################################################################################
# Minimum costs
print('Result:')
l_table = len(Data)
Table = np.zeros((l_table,27))
for i in range(l_table):
    for j in range(26):
        Table[i,j] = Data[i][j]

# Make results relative to initial costs

for k in range(l_table):
    Table[k,26] = Table[k,25] / Costs_initial

Table2 = Table[~np.any(Table >= 2*10**4, axis=1)]

# Minimum costs
Table_sorted = Table2[Table2[:,25].argsort()]

print('Number of variants considered is ' + str(len(n)))
print('Number of variants not allowed is ' + str(len(fd)))
print('Number of variants not satisfy is ' + str(len(vns)))
print('Number of variants satisfy is ' + str(len(vs)))
print('')
```

```python
print('Minimum costs are €' + str(round(Table_sorted[0,25],2)))
print('Minimum costs relative are :' + str(round(Table_sorted[0,22],2)))
print('Height is ' + str(round(Table_sorted[0,13],0)) + ' mm')
print('Web spacing is ' + str(round(Table_sorted[0,14],0)) + ' mm')
print('Thickness topskin : ' + str(round(Table_sorted[0,16],1)) + ' mm')
print('Thickness bottomskin : ' + str(round(Table_sorted[0,17],1)) + ' mm')
print('Thickness webs : ' + str(round(Table_sorted[0,15],1)) + ' mm')
print('Weight of the deck : ' + str(round(Table_sorted[0,18],0)) + ' kg')
print('Max uc SLS: ' + str(round(Table_sorted[0,19],2)))
print('Max uc ULS: ' + str(round(Table_sorted[0,24],2)))

# Plotting 3D
cm = plt.cm.get_cmap('RdYlGn_r')
fig = plt.figure()
ax = plt.axes(projection='3d')
p = ax.scatter3D(xs=Table2[:,14],ys=Table2[:,13],zs=Table2[:,18],c=Table2[:,26],cmap='RdYlGn_r')
ax.set_title('Direct costs relative to reference design', fontsize=20)
ax.set_xlabel('Web spacing [mm]', fontsize=15, rotation=0)
ax.set_ylabel('Height [mm]', fontsize=15, rotation=0)
ax.set_zlabel('Weight deck [kg]', fontsize=15, rotation=0)

fig.colorbar(p,ax=ax)
```

```python
# -*- coding: utf-8 -*-
"""
Created on Fri May 27 10:27:52 2022

@author: Lennart Molenaar
"""

import numpy as np
import itertools
from numpy import linalg as lin

'''Functions'''
def TestMinPlyDirections (layup):
    c_0 = 0
    c_45 = 0
    c_90 = 0
    c_m45 = 0
    for i in range(len(layup)):
        if layup[i] == 0:
            c_0 += 1
        elif layup[i] == 45:
            c_45 += 1
        elif layup[i] == 90:
            c_90 += 1
        if layup[i] == -45:
            c_m45 += 1
    total = len(layup)
    if c_0 / total >= 0.125:
        if c_45 / total >= 0.125:
            if c_90 / total >= 0.125:
                if c_m45 / total >= 0.125:
                    score = 'satisfy'
                else: score = 'not satisfy'
            else: score = 'not satisfy'
        else: score = 'not satisfy'
    else: score = 'not satisfy'

    return score

def TestThicknessPlies (layup, t_ply, min_thickness, max_thickness):
    thickness = len(layup) * t_ply

    if thickness >= min_thickness:
        if thickness <= max_thickness:
            score = 'satisfy'
        else: score = 'not satisfy'
    else: score = 'not satisfy'

    return score


def BuildLayup (nwrap,nz_090,nz_45,nUDts,nUDbs,nUDw,n45w,
            OLts_UD,OLbs_UD,OLts_090,OLbs_090,OLts_45,OLbs_45):
    TopskinLayup = []
    BottomskinLayup = []
    WebLayup = []

    # Wrapping foamblocks
    for i in range(int(nwrap)):
        TopskinLayup.append(45)
        TopskinLayup.append(-45)
        BottomskinLayup.append(45)
        BottomskinLayup.append(-45)
        WebLayup.append(45)
        WebLayup.append(-45)
```

```python
# Plies for the topskin
for i,j,k in itertools.zip_longest(range(int(OLts_090)), range(int(OLts_45)), range(int(OLts_UD))):
    for ii,jj in itertools.zip_longest(range(int(nz_090)), range(int(nz_45))):
        a_090 = np.linspace(1,nz_090,nz_090)
        a_45 = np.linspace(1,nz_45, nz_45)
        a_0 = np.linspace(1,nUDts, nUDts)
        if ii != None and i != None:
            if a_090[ii] <= ii+1:
                TopskinLayup.append(0)
                TopskinLayup.append(90)
        if jj != None and j != None:
            if a_45[jj] <= jj+1:
                TopskinLayup.append(45)
                TopskinLayup.append(-45)
    for kk in range(int(nUDts)):
        if kk != None and k != None:
            if a_0[kk] <= kk+1:
                TopskinLayup.append(0)
                TopskinLayup.append(0)

TopskinLayup = TopskinLayup[::-1]

# Plies for the bottomskin
for i,j,k in itertools.zip_longest(range(int(OLbs_090)), range(int(OLbs_45)), range(int(OLbs_UD))):
    for ii,jj in itertools.zip_longest(range(int(nz_090)), range(int(nz_45))):
        a_090 = np.linspace(1,nz_090,nz_090)
        a_45 = np.linspace(1,nz_45, nz_45)
        a_0 = np.linspace(1,nUDbs, nUDbs)
        if ii != None and i != None:
            if a_090[ii] <= ii+1:
                BottomskinLayup.append(0)
                BottomskinLayup.append(90)
        if jj != None and j != None:
            if a_45[jj] <= jj+1:
                BottomskinLayup.append(45)
                BottomskinLayup.append(-45)
    for kk in range(int(nUDbs)):
        if kk != None and k != None:
            if a_0[kk] <= kk+1:
                BottomskinLayup.append(0)
                BottomskinLayup.append(0)

# BottomskinLayup = BottomskinLayup[::-1]

# Plies for the webs
for i,j in itertools.zip_longest(range(int(nz_090)), range(int(nz_45))):
    a_090 = np.linspace(1,nz_090,nz_090)
    a_45 = np.linspace(1,nz_45, nz_45)
    if i != None:
        if a_090[i] <= i+1:
            WebLayup.append(0)
            WebLayup.append(90)
    if j != None:
        if a_45[j] <= j+1:
            WebLayup.append(45)
            WebLayup.append(-45)
for i in range(int(nUDw)):
    WebLayup.append(0)
    WebLayup.append(0)
for i in range(int(n45w)):
    WebLayup.append(45)
    WebLayup.append(-45)

# Wrapping foamblocks webs
```

```python
    for i in range(int(nwrap)):
        WebLayup.append(45)
        WebLayup.append(-45)

    return TopskinLayup, BottomskinLayup, WebLayup

def Layup(angle, materialproperties, n_plies):
    layup = np.zeros((len(materialproperties)+1, n_plies))
    for i in range(len(materialproperties)):
        for j in range(n_plies):
            layup[0,j] = angle[j]
            layup[i+1,j] = materialproperties[i]
    return layup

def Stiffness (Width, Height, Ex_ts, Ex_bs, Ex_web, G_ts, G_bs, G_web, t_ts, t_bs, t_web, n_webs):
    EAx_ts = Ex_ts * Width * t_ts
    EAx_bs = Ex_bs * Width * t_bs
    EAx_web = Ex_web * (Height - t_ts - t_bs) * t_web * n_webs
    EAx = EAx_ts + EAx_bs + EAx_web

    NA = (t_ts * Width * t_ts / 2 + t_bs * Width * (Height - t_bs / 2) + n_webs * t_web * (Height - t_ts - t_bs) * ((Height - t_ts - t_bs) / 2 + t_ts)) / (t_ts * Width + t_bs * Width + n_webs * t_web * (Height - t_ts - t_bs))
    y2 = NA
    y1 = Height - y2

    EIyy_ts = Ex_ts * (1 / 12 * Width * t_ts**3 + Width * t_ts * (y2 - t_ts/2)**2)
    EIyy_bs = Ex_bs * (1 / 12 * Width * t_bs**3 + Width * t_bs * (y1 - t_bs/2)**2)
    EIyy_web = Ex_web * (1 / 12 * t_web * (Height - t_ts - t_bs)**3 * n_webs + t_web * (Height - t_ts - t_bs) * (y2 - t_ts - (Height - t_ts - t_bs) / 2)**2)
    EIyy = EIyy_ts + EIyy_bs + EIyy_web

    GAxz_ts = G_ts * Width * t_ts
    GAxz_bs = G_bs * Width * t_bs
    GAxz_web = G_web * (Height - t_ts - t_bs) * t_web * n_webs
    GAxz = GAxz_ts + GAxz_bs + GAxz_web

    return EAx, EIyy, GAxz, y1, y2

def Materialproperties(material_name, vf):
    if material_name == 'Kush_UD1200_vf54':
        M     = 1.2      #[kg/m2]
        E1t   = 42.5e3   #[MPa]
        E2t   = 8.0e3    #[MPa]
        E1c   = 40e3     #[MPa]
        E2c   = 13e3     #[MPa]
        G12   = 4.2e3    #[MPa]

        s1t   = 855      #[MPa]
        s2t   = 59       #[MPa]
        e1t   = 2.01     #[%]
        e2t   = 0.41     #[%]
        s1c   = 395      #[MPa]
        s2c   = 138      #[MPa]
        e1c   = 0.93     #[%]
        e2c   = 1.02     #[%]
        t12   = 39.0     #[MPa]
        t23   = 39.0     #[MPa]
        tills = 51       #[MPa]

        v12   = 0.27           #[-]
        v21   = (v12 *E2t)/E1t   #[-]
        alpha1 = 9.22e-6         #[K^-1]
        alpha2 = 35.77e-6        #[K^-1]
        rho   = 1962           #[kg/m3]
        tply  = 0.85/2         #[mm]
```

```python
        beta   = 0
        Glc    = 0
        GIIc   = 0

    elif material_name == 'Kush_UD1200_vf27':
        M      = 1.2       #[kg/m2]
        E1t    = 21.7e3     #[MPa]
        E2t    = 8.0e3      #[MPa]
        E1c    = 24        #[MPa]
        E2c    = 10        #[MPa]
        G12    = 3.5e3      #[MPa]

        s1t    = 327       #[MPa]
        s2t    = 24        #[MPa]
        e1t    = 1.50      #[%]
        e2t    = 0.30      #[%]
        s1c    = 410       #[MPa]
        s2c    = 130       #[MPa]
        e1c    = 1.89      #[%]
        e2c    = 1.25      #[%]
        t12    = 32        #[MPa]
        t23    = 32        #[MPa]
        tills  = 33        #[MPa]

        v12    = 0.27          #[-]
        v21    = (v12 *E2t)/E1t   #[-]
        alpha1 = 0            #[K^-1]
        alpha2 = 0            #[K^-1]
        rho    = 0            #[kg/m3]
        tply   = 1.7/2         #[mm]

        beta   = 0
        Glc    = 0
        GIIc   = 0

    material = [E1t, E2t, E1c, E2c, G12, s1t, s2t, e1t, e2t, s1c, s2c, e1c,\
            e2c, t12, t23, tills, v12, v21, alpha1, alpha2, rho, tply, beta, Glc, GIIc]

    return material

def Engineering_Constants(ABD, Thickness_laminate):
    ABD_inv = lin.inv(ABD)

    E1m    = 1/(Thickness_laminate*ABD_inv[0,0])
    E2m    = 1/(Thickness_laminate*ABD_inv[1,1])
    G12m   = 1/(Thickness_laminate*ABD_inv[2,2])
    v12m   = -ABD_inv[0,1]/ABD_inv[0,0]
    v21m   = -ABD_inv[0,1]/ABD_inv[1,1]

    E1b    = 12/((Thickness_laminate**3)*ABD_inv[3,3])
    E2b    = 12/((Thickness_laminate**3)*ABD_inv[4,4])
    G12b   = 12/((Thickness_laminate**3)*ABD_inv[5,5])
    v12b   = -ABD_inv[3,4]/ABD_inv[3,3]
    v21b   = -ABD_inv[3,4]/ABD_inv[4,4]

    return E1m, E2m, G12m, v12m, v21m, E1b, E2b, G12b, v12b, v21b
```